UNIVERSITÀ DI SIENA 1240

Dipartimento di Biotecnologie, Chimica e Farmacia

Dottorato in Chemical and Pharmaceutical Sciences

XXXVIII° Ciclo

Coordinatore: Prof. Maurizio Taddei

Morita-Baylis-Hillman Adducts: Versatile Tools for Advanced Chemical and Biological Applications

Settore scientifico disciplinare: CHEM-08

Candidato

Jacopo Venditti

Sede di attività

Dipartimento di Biotecnologie, Chimica e Farmacia

Firma digitale del/della candidato/a

JACOPO
VENDITTI
23.03.2026
11:38:57
GMT+01:00

Supervisore

Prof. Andrea Cappelli

Ente di appartenenza

Università degli Studi di Siena

Anno accademico di conseguimento del titolo di Dottore di ricerca

2024/25

Università degli Studi di Siena

Dottorato in Chemical and Pharmaceutical Sciences

XXXVIII° Ciclo

Data dell'esame finale

15-04-2026

Commissione giudicatrice

Prof.ssa Laura Scalvini

Prof. Filippo Samperi

Prof. Gabriele Carullo

Supplenti

Prof.ssa Stephanie Federico

TABLE OF CONTENTS

List of abbreviations

ACN = Acetonitrile

AIE = Aggregation Induced Emission

CD = Circular Dichroism

CEHR = Crown ether-host rotaxane

CuAAC = Copper(I)-Catalyzed Azide-Alkyne Cycloaddition

DABCO = 1,4-Diazabicyclo[2.2.2]octane

DBU = 1,8-diazabicyclo[5.4.0]undecen-7-ene

DCM = Dichloromethane

DIPEA = N,N-Diisopropylethylamine

DLS = Dynamic Light Scattering

DMF = Dimethylformamide

DMPF = 9,9-dimethyl-2-phenyl-9*H*-fluorene

DMSO = Dimethyl sulfoxide

FA = Fatty acid

GFA = Green Fluorescent Albumin

GFP = Green Fluorescent Protein

HSA = Human Serum Albumin

IBCD = Imidazole Binding Cinnamic Derivative

LDT = Ligand-directed tosyl

LRET = Luminescent resonance energy transfer

MA = Methyl acrylate

MBHA = Morita-Baylis-Hillman adduct

MBH = Morita-Baylis-Hillman

MD = Molecular Dynamics

MLM = Monolayer lipid membranes

MS-ESI = Mass spectrometry – Electrospray ionization

NACME = *N*-acetyl-*L*-cysteine methyl ester

NAHME = *N*-acetyl-*L*-histidine methyl ester

NALME = *N*α-acetyl-*L*-lisine methyl ester

NBuA = *n*-Butylamine

NBuPL = *N*-butyl-poly(*L*-lysine)

NMR = Nuclear Magnetic Resonance

OEG = Oligo(ethylene glycol)

PBS = Phosphate-buffered saline

PL = Photoluminescence

PL QY = Photoluminescence Quantum Yield

PLE = Photoluminescence Excitation

POI = Protein of Interest

SDS-PAGE = Sodium Dodecyl Sulphate - PolyAcrylamide Gel Electrophoresis

TCI = Target Covalent Inhibitor

TEA = Triethylamine

TEG = Tri(ethylene glycol)

TFA = Trifluoroacetic acid

THF = Tetrahydrofuran

TLC = Thin Layer Chromatography

TMEDA = N, N, N', N'-tetramethylethylendiamine

TMPDA = N, N, N', N'-tetramethyl-1,3-propanediamine

TPA = Triphenylamine

UV = Ultraviolet

CHAPTER 1

GENERAL INTRODUCTION AND OUTLINE OF THE THESIS

Over the past three years, the research conducted during the Ph.D. period focused on a class of fascinating chemical structures known as Morita–Baylis–Hillman adducts (MBHA). These compounds are generated through the eponymous Morita–Baylis–Hillman (MBH) reaction, a distinctive transformation that has attracted considerable attention within the scientific community. MBHAs are of particular interest due to their versatility, unique chemical properties, and high reactivity, which make them valuable tools in diverse areas of organic and pharmaceutical chemistry. In recent years, the research group coordinated by Professor Cappelli, of which I was a member, has devoted significant effort to the design, synthesis, and characterization of a novel class of MBHA derivatives. Our studies focused on their reactivity with nucleophilic amino groups (i.e., imidazole or *n*-butylamine), which yielded promising results and paved the way for diverse potential applications. In this context, my contribution was primarily dedicated to the synthesis and characterization studies of these compounds, followed by a preliminary evaluation of their potential applications.

This thesis is organized into four chapters, each addressing a specific aspect of the research. In the present **Chapter 1**, a brief overview is provided of the work carried out during the Ph.D. period, summarizing the results obtained and the journal articles published.

Chapter 2 provides a general introduction to the field of organic synthesis, with particular emphasis on the MBH reaction. It also presents the design of a novel MBHA acetyl derivative **9**, bearing a triphenylamine (TPA) moiety. In this context, the Ph.D. candidate's contribution was primarily focused on the synthesis of compound **9**. Photochemical studies revealed that this MBHA acetyl compound exhibited a strong propensity to generate cinnamic structures with favorable optical features. The reactivity behaviors were evaluated towards lysine models such as *n*-butylamine, *N*α-acetyl-*L*-lysine methyl ester, and *N*-butyl-poly(*L*-lysine). The results indicated efficient reactivity with primary amino groups and, most importantly, demonstrated that such reactivity was strictly dependent on the reaction conditions. These findings enabled further investigation into the potential use of the MBHA derivative **9** as a fluorogenic covalent probe in protein labeling experiments.

Chapter 3 describes the investigation of the reaction between MBHA derivative **9** and a biologically relevant macromolecule, such as Human Serum Albumin (**HSA**). Kinetic studies of the reaction were conducted by ^{1}H NMR spectroscopy. Interestingly, the data confirmed the interaction between compound **9** and **HSA**, accompanied by a shift in the

emission properties from blue to green-yellow, leading to the formation of Green Fluorescent Albumin (**GFA**). These results prompted the design of two new fluorescent covalent probes bearing two different electrophilic groups as warheads. Specifically, these probes were obtained by replacing the TPA moiety with a 9,9-dimethyl-2-phenyl-9*H*-fluorene (DMPF) fluorophore. Within this framework, experimental work included the synthesis of the MBHA acetyl derivative **24** and its acrylamide analogue **25**, followed by the evaluation of their reactivity towards different nucleophilic amino acid residues. The analysis provided insight into the distinct behaviors of the two warheads towards the various nucleophilic groups present in the amino acid residues. Differences were also observed in the optical studies, confirming the remarkable properties of the cinnamic fluorophore in a fluorogenic probe. In conclusion, the reaction between **HSA** and the MBHA acetyl derivative **24** was conducted, confirming the ability of MBHAs to interact with complex protein systems.

Chapter 4 presents alternative structural MBHA derivatives with potential applications across a broad range of fields. Specifically, the MBHA scaffold was modified to obtain a tri(ethylene glycol)-linked MBHA dimer (**42a**). This compound was designed to functionalize materials containing reactive basic groups (i. e. amino or imidazole). In this regard, to assess the reactivity of the dimer **42a**, the Ph.D. candidate employed *n*-butylamine as a simple nucleophilic model. The reaction afforded a macrocyclic structure, yielding two distinct isomers, namely (*E*,*Z*)-**43a** and (*E*,*E*)-**43a**. Photochemical studies of compound (*E*,*E*)-**43a** revealed intriguing behavior: upon irradiation of its solution, a competition was observed between the photoisomerization process and the [2+2] photocycloaddition process. Furthermore, a series of related dimers **42b-d** was synthesized by replacing the tri(ethylene glycol) (TEG) linker with longer oligo(ethylene glycol) (OEG) chains. In these cases, as well, the reaction yielded macrocyclic structures **43b-d** as a mixture of two isomers, which could not be separated due to their similar polarity. In conclusion, the biological properties of the entire series of macrocyclic structures were evaluated, revealing remarkable cytotoxicity comparable to that of Doxorubicin.

CHAPTER 2

FROM SYNTHESIS TO REACTIVITY: A TRIPHENYLAMINE-BASED MBHA DERIVATIVE AS A FLUOROGENIC PROBE FOR LYSINE MODELS.

2.1 MORITA-BAYLIS-HILLMAN ADDUCTS

The Morita-Baylis-Hillman (MBH) reaction is a versatile carbon-carbon bond-forming transformation originally developed by Ken-ichi Morita, Anthony B. Baylis, and Melville E. D. Hillman.[1,2] This reaction typically involves three components: the α-position of an activated alkene (or alkyne), an electrophilic substrate, and a catalyst system. According to the extensive literature available, the most commonly employed activated alkenes include alkyl and aryl acrylates,[3,4] β-substituted acrylate derivatives,[5] acrylamides,[6] and nitroalkenes.[7] Conversely, the most common electrophilic partners are alkyl or aryl aldehydes,[8] α,β-unsaturated trifluoromethyl ketones,[9] phosphinamide derivatives,[10] and 2-halo- or 2,3-dihalo-1,4-naphtoquinones.[11] In addition, imines may serve as electrophilic substrates, in which case the process is referred to as the Aza-MBH reaction.[10] With respect to catalysis, a wide range of organic catalysts has been successfully applied, including amines, phosphines, and Lewis acids such as $TiCl_4$.[8] The choice of catalyst is strongly influenced by the type of activated alkene or alkyne, the electrophile counterpart, and the reaction conditions. Among these systems, tertiary amines and diamines represent the most widely used catalysts. Representative examples include TMPDA (*N*, *N*, *N'*, *N'*-tetramethyl-1,3-propanediamine),[12] TMEDA (*N*,*N*, *N'*, *N'*- tetramethylethylendiamine),[13] DBU (1,8-diazabicyclo[5.4.0]undec-7-ene),[14] DABCO (1,4-diazabicyclo[2.2.2]octane),[11] and TEA (triethylamine).[15]

Over the years, the mechanism of the MBH reaction has been the subject of extensive investigations. The earliest studies proposed an addition–elimination reaction mechanism, initiated by a Michael-type addition of the tertiary amine catalyst to the activated alkene. The resulting zwitterionic enolate intermediate undergoes an aldol reaction with the aldehyde, leading to the formation of a new C–C bond. Finally, through a proton transfer step and the elimination of the tertiary amine, the corresponding alcohol product is obtained. In this mechanistic framework, the proton transfer was considered the rate-determining step. Subsequent investigations revealed a significant acceleration of the reaction kinetics in the presence of polar protic solvents such as alcohols, which act as proton shuttles through the formation of a six-membered cyclic transition state.[16-18] In 2015, Plata and Singleton, by means of advanced computational studies supported by experimental evidence, were able to provide a detailed mechanistic description. Specifically, their work focused on the role of methanol in the MBH reaction of *p*-nitrobenzaldehyde **1** and methyl acrylate (MA) in the presence of DABCO (**Scheme 1**). They demonstrated that intermediate **INT-3**, arising from the aldol addition between

zwitterionic enolate **INT-1** and aldehyde **1**, does not engage with methanol through the expected six-membered transition state to form **INT-5**. Instead, methanol was shown to accelerate the process by mediating an acid–base step, converting intermediate **INT-3** into **INT-4**, which is subsequently deprotonated to yield **INT-5**. This latter then furnishes the final product **2** through elimination of DABCO, which is regenerated and re-enters the catalytic cycle.[19] Importantly, their findings also revealed a potential inhibitory effect. Because protonation at the carbon atom of the zwitterionic enolate **INT-1** (thermodynamically favored over protonation at oxygen), excess methanol can deactivate this key intermediate. This observation underscores the necessity of employing methanol only in catalytic amounts, where it functions effectively as a polar protic additive without suppressing the reaction.[19]

Scheme 1. Mechanism of Morita-Baylis-Hillman reaction

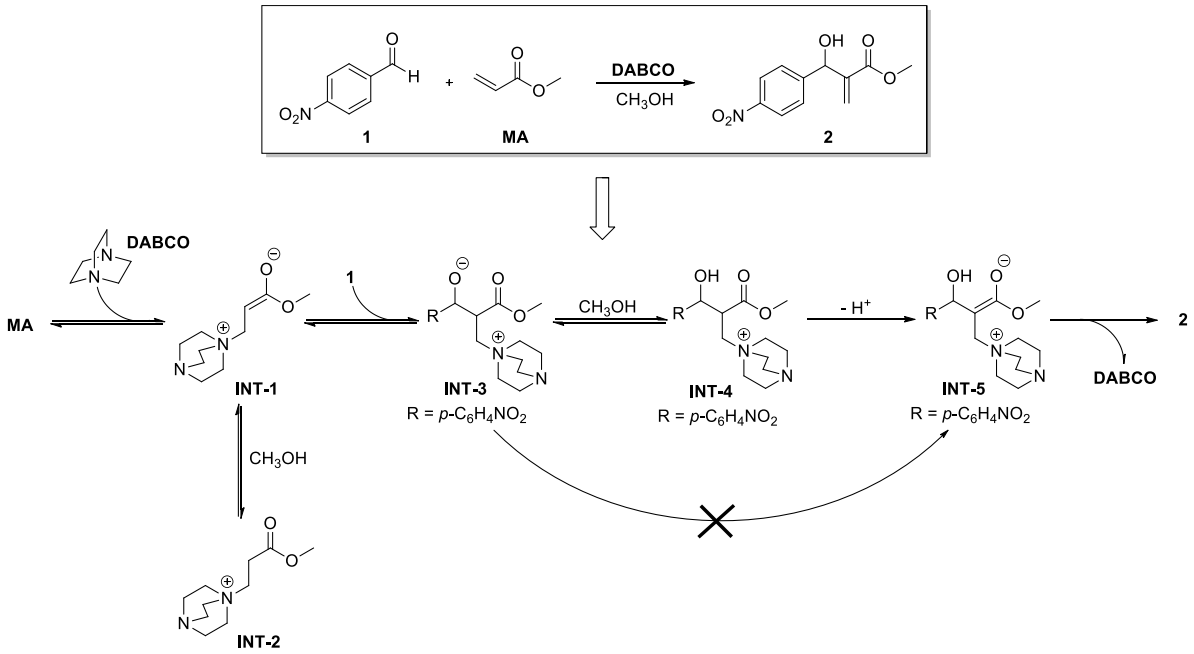

Based on this evidence, the MBH reaction can be classified as an atom-economic transformation, as most atoms from the starting materials are retained in the final product, with only negligible formation of by-products or waste. For this reason, atom economy is considered a fundamental principle of green chemistry, as it provides a direct measure of the efficiency of a synthetic process in terms of material utilization and environmental sustainability.[20] The distinctive features of the MBH reaction have fueled growing interest within the scientific community engaged in organic synthesis. Numerous studies reported in the literature have documented its applications in the synthesis of natural products, the

construction of heterocyclic frameworks, and the preparation of drug intermediates.[21] In recent years, particular attention has also been directed toward MBHAs, which are recognized as promising scaffolds in drug discovery. This interest has been reinforced by several reviews that emphasize the biological properties of MBHA derivatives, summarized in Figure 1, reporting their remarkable antitumoral, antibacterial, antifungal, antimalarial, antileishmanial, and other pharmacologically relevant activities.[21,22]

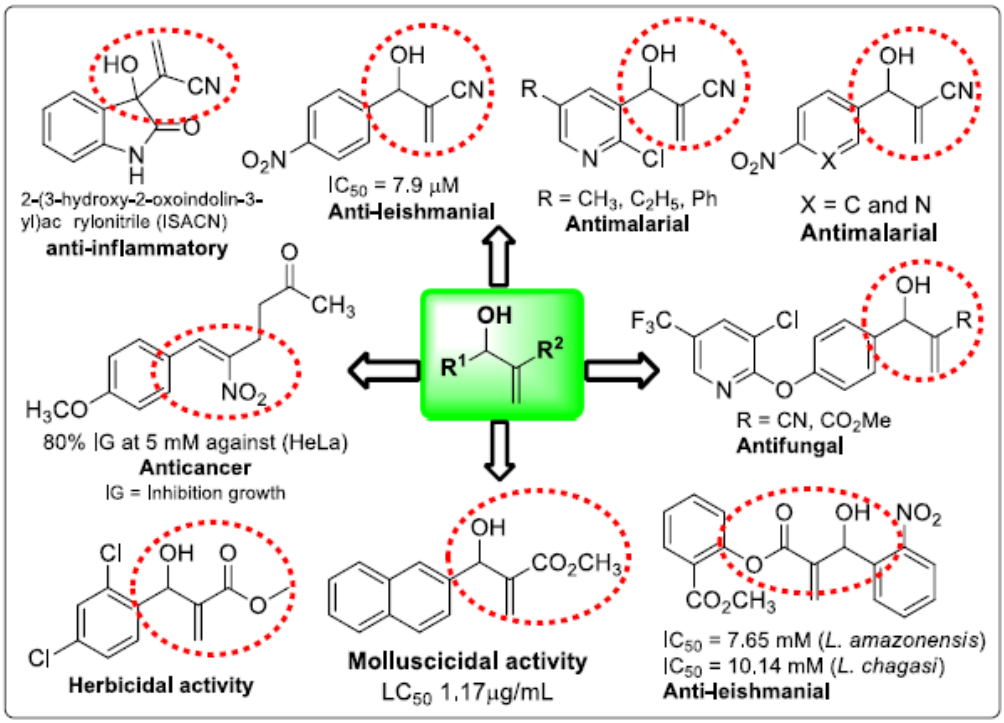

Figure 1. Some literature-reported examples of MBHA derivatives with their pharmacological activities.[21]

2.2 AIMS OF THE CHAPTER

Within the context of the MBHA derivatives, our research group has explored, in recent years, the reactivity of phenyl- and naphthalene-substituted MBHA derivatives **3a-c** and **4a,b** towards imidazole. These interactions afforded Imidazole Binding Cinnamic Derivatives (**IBCDs**), which displayed noteworthy photophysical characteristics, particularly Aggregation Induced Emission (AIE) properties.[23,24] The AIE effect resulted in enhanced emission intensity in the solid state compared to the solution, highlighting their potential as fluorogenic probes. In addition, complementary studies conducted by our research group on poly(benzofulvene) architectures have revealed intriguing

photophysical properties in related cinnamic derivatives **5**, **6**, and **7** with photoluminescence quantum yield (PL QY) in the order of 57-80 % and emission maxima at around 407-540 nm.[25]

These two branches of our research activity converged in identifying cinnamic moiety **8** for the construction of novel potential fluorogenic probes. Specifically, due to the best optical features of the cinnamic derivative **7**, we set ourselves the goal of synthesizing a novel MBHA acetyl derivative **9** bearing a triphenylamine (TPA) moiety (Figure 2). Subsequently, to confirm the outstanding optical behaviors of cinnamic structures, it was necessary to evaluate the photophysical and photochemical features of compound **9**.

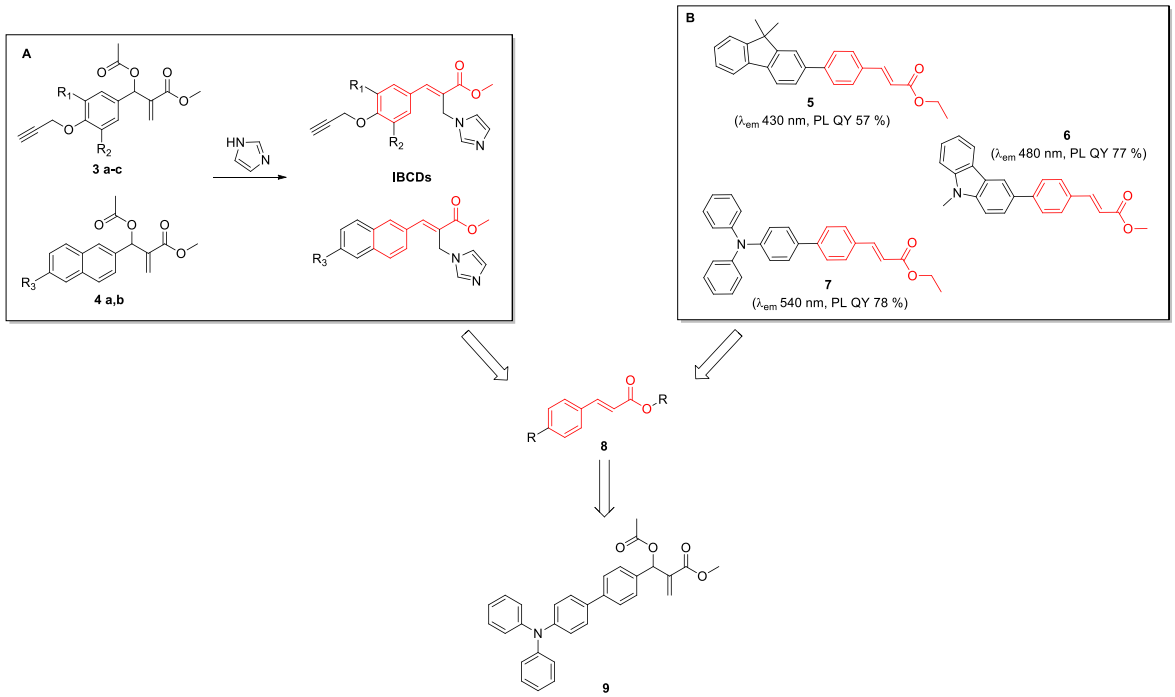

Figure 2. **A)** MBHA acetyl derivatives **3a-c** and **4a,b** leading to **IBCDs**;[23,24] **B)** Cinnamic derivatives with remarkable optical features derived from poly(benzofulvene) architectures.[25]

Finally, as shown in Figure 3, we designed a series of reactivity experiments involving MBHA **9** towards different lysine models, such as *n*-butylamine (**NBuA**), *N*α-acetyl-*L*-lysine methyl ester (**NALME**) hydrochloride, and *N*-butyl-poly(*L*-lysine) (**NBuPL**) hydrochloride. The selection of lysine models was consistent with previous literature, which highlighted the remarkable ability of electrophilic groups, such as the acrylate moiety present in MBHAs, to interact with nucleophilic amino groups within lysine residues or hexahistidine tags.[26-30] It is well established that most lysine residues are located on the protein surface; however, they can also reside within lipophilic pockets or

in active sites buried in the protein structure. The key distinction lies in the different basicity of the amino group depending on its localization. Specifically, lysine residues positioned on the protein surface are fully protonated under physiological conditions, owing to their pKa of approximately 10.8. In contrast, lysine residues located within the protein core exhibit a markedly lower pKa of around 5.7, rendering them highly effective nucleophiles.[31] Accordingly, careful considerations of the protonation state of lysine residues were essential for the rational design and interpretation of reactivity studies.[30]

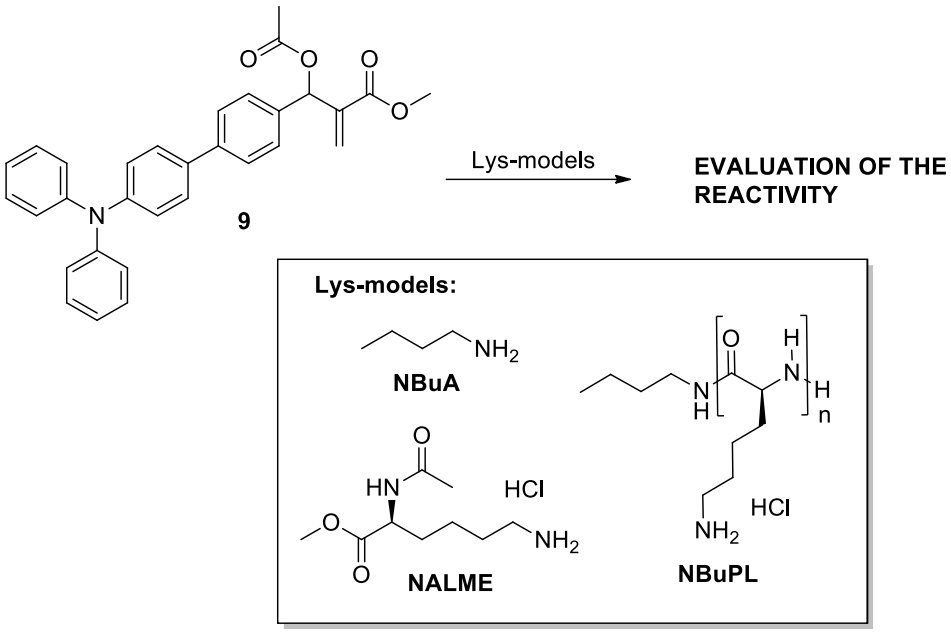

Figure 3. Design of the reactivity studies employing MBHA acetyl derivative **9** with *n*-butylamine (**NBuA**), *N*α-acetyl-*L*-lysine methyl ester (**NALME**) hydrochloride, and *N*-butyl-poly(*L*-lysine) (**NBuPL**) hydrochloride as lysine models.

2.3 SYNTHESIS AND CHARACTERIZATION STUDIES OF NOVEL MBHA BEARING TRIPHENYLAMINE MOIETY

In pursuit of novel reactive molecules targeting basic amino acid residues, MBHA derivative **9** was synthesized through a three-step sequence starting from the commercially available reagents *p*-bromobenzaldehyde **10** and 4-(diphenylamino)phenyl boronic acid pinacol ester (**Scheme 2**). The initial Suzuki-Miyaura coupling reaction between these precursors afforded aldehyde **11**. The key step of the synthetic sequence was the well-established MBH reaction, performed under dark conditions for three days to prevent undesired acrylic polymerization, which successfully delivered alcohol **12** in

acceptable yields. In the final step, compound **12** was converted into the corresponding acetyl derivative **9**.

Scheme 2. Synthesis of MBHA acetyl derivative **9**.

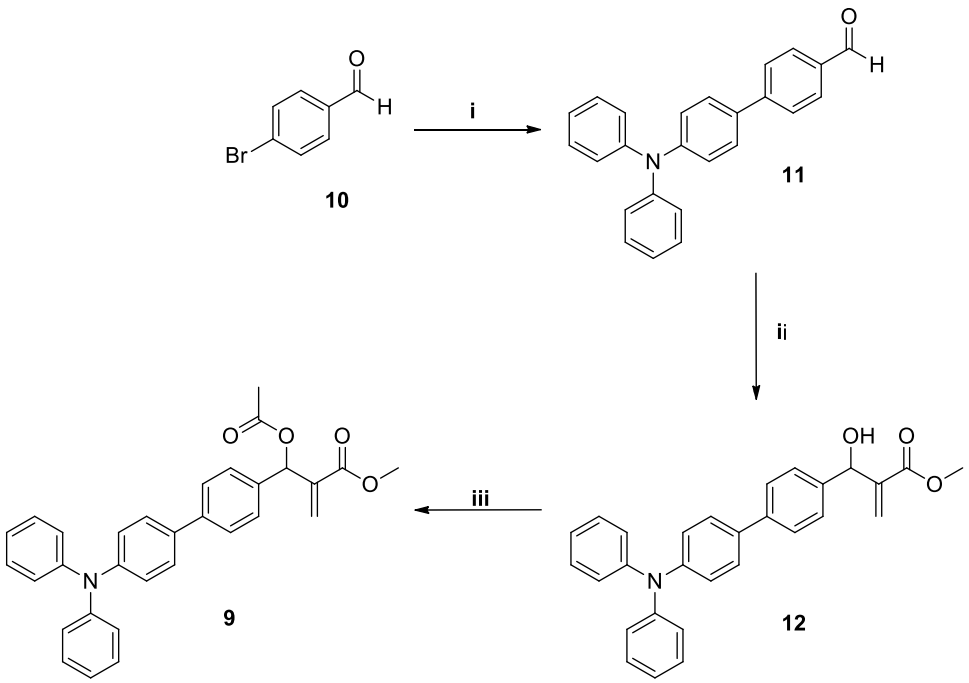

Reagents. (***i***) 4-(diphenylamino)phenyl boronic acid pinacol ester, Cs_2CO_3, $Pd(PPh_3)_2Cl_2$, PPh_3, dry THF, CH_3OH, T = 80 °C, W = 150, P = 250 psi; (***ii***) DABCO, methyl acrylate, CH_3OH; (***iii***) CH_3COCl, TEA, dry CH_2Cl_2. (For more details, see the Research Article in **Paragraph 2.7**)

Subsequently, photophysical and photochemical features of compound **9** were investigated before its application in labelling experiments with the selected lysine models. Interestingly, derivative **9** exhibited an intriguing photochemical activity. Indeed, irradiation of compound **9** in different solvents (i.e. methanol and DCM) with UV-A light afforded three distinct products, depicted in Figure 4.

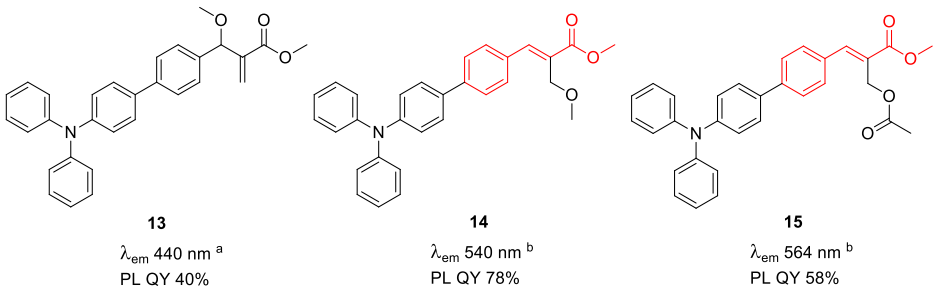

Figure 4. Structures of the obtained compounds **13**, **14**, and **15** after irradiating a solution of compound **9** in different solvents with UV-A light. [a] values were obtained in solid state; [b] values were obtained in solution.

Specifically, irradiating the methanolic solution of **9** yielded compounds **13** and **14**. On the other hand, when DCM was used, cinnamic structure **15** was obtained as the sole product. Compound **13** displayed bright blue emission in the solid state, with AIE properties in solution, which was attributed to facile intramolecular rotation around the acrylate bond. At the same time, compounds **14** and **15** were found to exhibit photophysical behaviors analogous to those of cinnamic derivative **7**, with intense green-yellow emission in solution (PL QY in the range of 58-75%) and emission maxima of 540-564 nm. These findings highlighted the remarkable photophysical properties of the cinnamic fluorophore contained in compound **7**, further supporting the potential of MBHA acetyl derivative **9** as a promising candidate for the fluorogenic labeling of basic amino acid residues.

The data collected in this study have been published in the journal *Dyes and Pigments*. For further details, refer to the Research Article reported in **Paragraph 2.7**.

2.4 REACTIVITY STUDIES TOWARDS DIFFERENT LYSINE MODELS

The remarkable results obtained in the photophysical and photochemical characterization of MBHA acetyl derivative **9** prompted us further to investigate its reactivity towards *n*-butylamine (**NBuA**), *Nα*-acetyl-*L*-lysine methyl ester (**NALME**) hydrochloride, and *N*-butyl-poly(*L*-lysine) (**NBuPL**) hydrochloride. In our hypothesis, **NBuA** was employed as the simplest model, **NALME** as a representative model of lysine residues,[30] and **NBuPL** as a model system mimicking lysine embedded within a homopolymer. The mechanistic

rationale underlying these experiments was based on the addition-elimination pathway. Specifically, the reaction involved an initial nucleophilic attack on the electrophile center of the MBHA scaffold, resulting in the formation of a zwitterionic intermediate characterized by a newly formed C-C bond. Subsequent elimination of the acetyl group from this intermediate facilitated the formation of the cinnamic moiety in the final product.

Specifically, the reaction between compound **9** and **NBuA**, depicted in **Scheme 3**, afforded the corresponding monoadduct **16** and diadduct **17**, respectively. The product distribution was found to depend strongly on the reaction conditions, as summarized in Table 1.

Scheme 3. Reaction between MBHA acetyl derivative **9** with *n*-butylamine (**NBuA**)

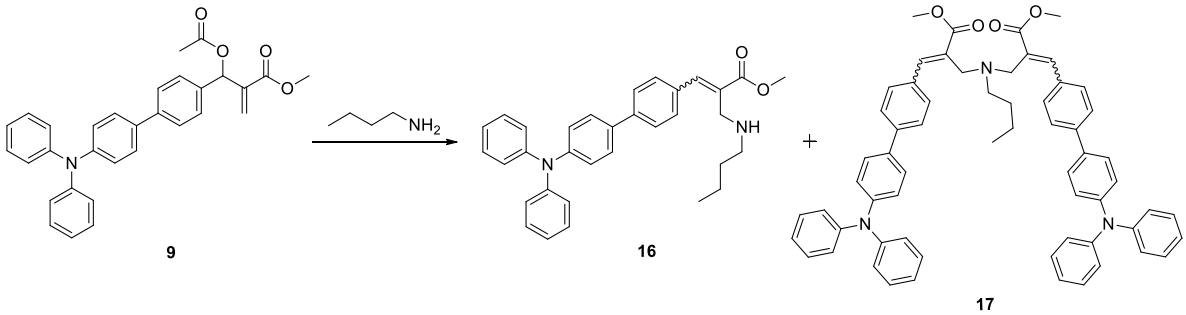

Reagents. **NBuA**, solvents, and temperatures are listed in Table 1.

Overall, under relatively apolar conditions (i. e. chloroform) with a large excess of **NBuA** (entry 1), the reaction yielded primarily the monoadduct **16**. Conversely, the reaction proceeded predominantly toward diadduct **17** under a more polar system, such as acetonitrile-water (ACN-H_2O) mixture containing phosphate-buffered saline (PBS), and employing a slight excess of **NBuA**, (entry 4).

Table 1. Reaction conditions employed in the reaction between compound **9** and **NBuA**.

Entry	eq. NBuA	Solvent	Temperature	Time	16	17
1	5	CH_3Cl	r.t	6 h	66%	13%
2	1.5	CH_3Cl	r.t	48 h	49%	36%
3	5	CH_3CN-H_2O	reflux	24 h	52%	39%
4	1.5	CH_3CN-H_20	reflux	24 h	16%	73%

Regarding the interaction between compound **9** and **NALME** hydrochloride, illustrated in **Scheme 4**, the reaction was conducted in an ACN-H_2O mixture containing PBS with a slight excess (1,5 eq.) of lysine residue in refluxing conditions. The reaction yielded primarily diadduct **19** (77%) and a small amount of monoadduct **18** (14%), as expected.

Scheme 4. Reaction between MBHA acetyl derivative **9** with *N*α-acetyl-*L*-lysine methyl ester (**NALME**) hydrochloride.

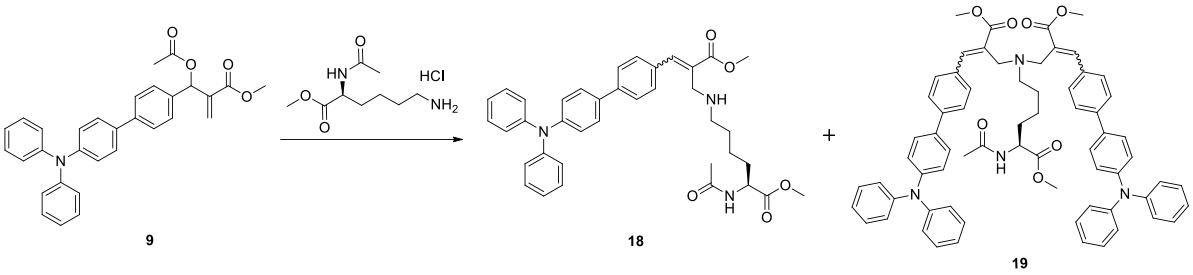

Reagents. **NALME** hydrochloride, CH_3CN, H_2O, PBS, reflux, 24 h.

Finally, the reaction between compound **9** and **NBuPL** hydrochloride was monitored by means of ^{1}H NMR spectroscopy, owing to the structural complexity of the lysine model. Experiments were performed using different excesses of **NBuPL** (approximately 12:1, 6:1, and 3:1), and in the absence or presence of DIPEA. Reaction progress was assessed by monitoring the disappearance of the signal at ~2.10 ppm, corresponding to the methyl group of the acetyl moiety of compound **9**, together with the simultaneous appearance of a singlet at ~1.90 ppm, attributed to the methyl of the acetate released during the addition-elimination process. The results highlighted the critical role of DIPEA, as incomplete conversion was observed in its absence.

In conclusion, these reactivity studies underscored the critical role of the protonation state of lysine models in their interaction with MBHA derivative **9**. Considering that solvent-exposed lysine residues are typically protonated under physiological conditions, compound **9** appears to act as a selective reagent for nucleophilic amino acid residues within lipophilic pockets that remain sufficiently accessible. In fact, within such microenvironments, lysine residue may establish charge-assisted H-bond interactions with suitable counterparts, thereby enhancing their nucleophilicity and, consequently, their reactivity. Furthermore, compound **9** showed the ability to generate both mono- and diadducts. In particular, the formation of the diadduct was more pronounced in a polar solvent system, suggesting that specific interactions between the extended aromatic moieties may serve as the driving force for its formation.

The data collected have been published in the journal *Chemistry-An Asian Journal*. For further details, refer to the Research Article reported in **Paragraph 2.8**

2.5 PHOTOPHYSICAL AND PHOTOSTABILITY OF MONOADDUCTS AND DIADDUCTS

To further assess the potential of compound **9** as a fluorogenic probe, the photophysical and photochemical properties of the mono- and diadducts obtained from its reaction with lysine models were systematically investigated. Interestingly, monoadducts **16** and **18** displayed bright emission features, with maxima at approximately 526 nm and 535 nm, and PL QY in solution of 73% and 51%, respectively. In contrast, diadducts **17** and **19** exhibited two distinct emission bands. The first, centered at 526 nm for compound **17** and 524 nm for compound **19**, closely resembled the emission profiles of the monoadducts and of the cinnamic derivative **7**. The second one, however, appeared as a higher-energy component, centered at 405 nm and 408 nm, respectively. Collectively, these results confirmed the outstanding optical properties of cinnamic derivative **7**, reinforcing the potential application of MBHA acetyl derivative **9** as a fluorogenic probe, while also unveiling a distinctive behavior of the diadducts, indicative of the formation of a novel chemical entity.

Specifically, the presence of two cinnamic moieties within the diadduct structure suggested a [2+2] photocycloaddition process. This hypothesis was supported by ^{1}H NMR spectroscopy and molecular modeling studies, which confirmed the presence of a highly symmetric three-dimensional structure with the two cinnamic moieties adopting a *trans* configuration at the double bond. Additionally, the computational analysis revealed two closely related structures, corresponding to zwitterionic and neutral forms, in which aromatic portions of the two cinnamic fluorophores rearranged in π-π stacking interactions driven by noncovalent forces between the π bonds of the aromatic rings. To validate these hypotheses, irradiation experiments were carried out on diadduct solutions. As illustrated in **Scheme 5**, exposure to monochromatic light at selected wavelengths promoted the conversion of diadducts into the corresponding [2+2] photocycloaddition products **20** and **21**.

Scheme 5. [2+2] photocycloaddition process of diadducts **17** and **19**.

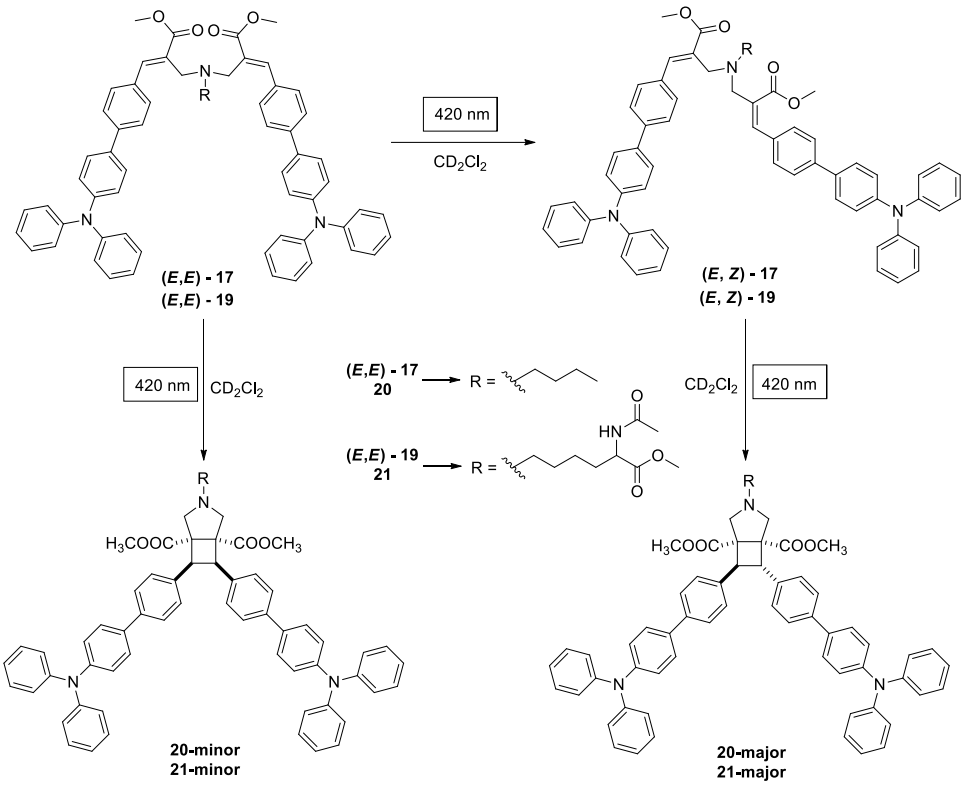

Specifically, the isolated product **20** exhibited an emission maximum centered at around 408 nm with PL QY in solution of 43%, thereby confirming the origin of the higher-energy emission component previously observed in the emission spectrum of compound **17**. Furthermore, compound **20** showed good photostability, whereas compound **21** proved photolabile upon irradiation with high-energy photons (i.e., 365 nm), affording a secondary species **23** (**Scheme 6**). This newly formed compound revealed an emission maximum at around 480 nm, accompanied by a remarkably high PL QY of 69%.

Scheme 6. Photo-lability of compound **21**.

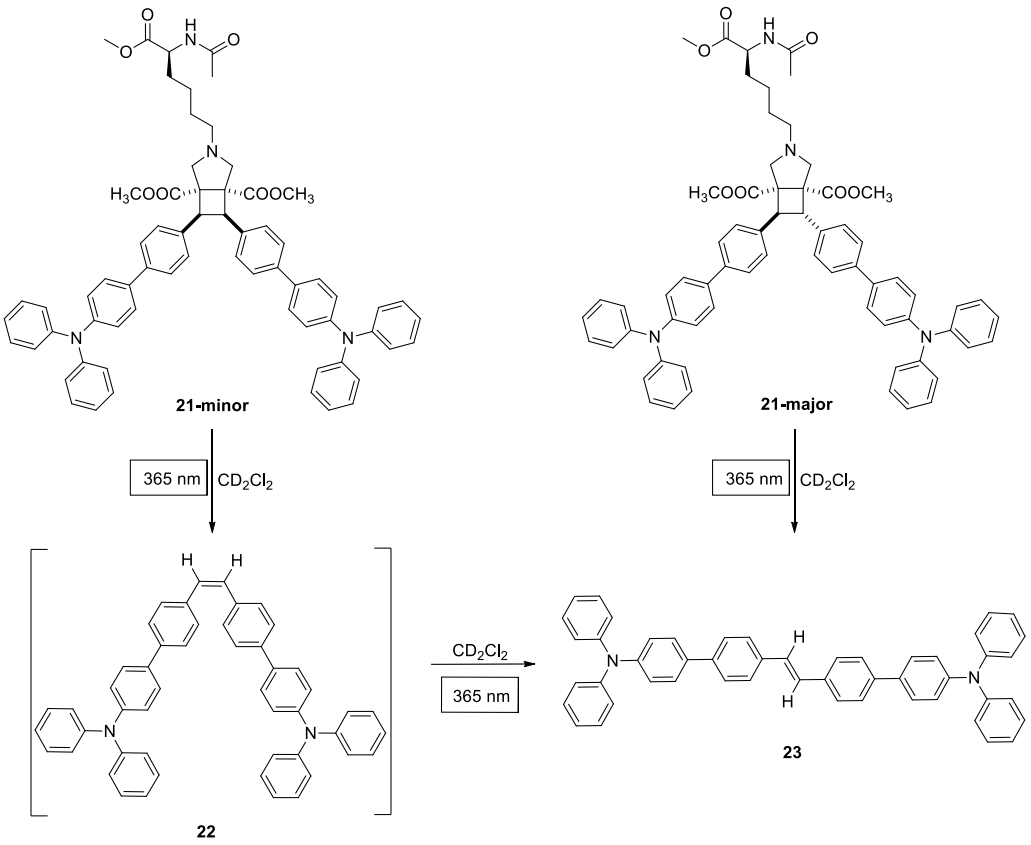

In conclusion, the MBHA acetyl derivative **9** demonstrated significant reactivity toward the selected lysine models, leading to the formation of both monoadducts and diadducts. However, in the context of the reaction of MBHA derivatives with reactive amino acid residues embedded into lipophilic pockets, the propensity for the formation of diadducts should be largely reduced. The photophysical properties of the resulting products confirmed the remarkable optical properties of the cinnamic structure **7**, placing compound **9** as a potential fluorogenic probe for the selective labeling of basic amino acid residues.

The data collected have been published in two journal articles in *Chemistry-An Asian Journal* and *The Journal of Physical Chemistry B*. For further details, refer to the Research Article reported in **Paragraph 2.8** and **Paragraph 2.9**.

2.6 REFERENCES

1. Morita, K.; Suzuki, Z.; Hirose, H. A tertiary phosphine-catalyzed reaction of acrylic compounds with aldehydes. *Bull. Chem. Soc. Jpn.*, **1968**, *41*, 2815-2815.
2. Baylis, A. B.; Hillman, M. E. D. U.S. Patent 3,743,669, **1973**; *Chem. Abstr*. **1972**,*77*, 34174q
3. Drewes, S. E.; Emsile, N. D. Necic acid synthons. Part 1. Total synthesis of integerrinecic acid. *J. Chem. Soc., Perkin Trans. 1*, **1982**, 2079-2083.
4. Kataoka, T.; Kinoshita, S.; Kinoshita, H.; Fujita, M.; Iwamura, T.; Watanabe, S. Self-assisted tandem Micheal-aldol reactions of α,β-unsatured ketones with aldehydes. *Chem. Commun*., **2001**, 1958-1959.
5. Shi, Y.-L.; Xu, Y.-M.; Shi, M. Aza-Baylis-Hillman Reaction of β-Substituted Activated Olefins with *N*-Tosyl Imines. *Adv. Synth. Catal.*, **2004**, *346*, 1220-1230.
6. Yu, C.; Hu, L. Successful Baylis-Hillman Reaction of Acrylamide with Aromatic Aldehydes. *J. Org. Chem.*, **2002**, *67*, 1, 219-223.
7. Rastogi, N.; Namboothiri, I. N. N.; Cojocaru, M. α-Hydroxymethylation of conjugated nitroalkenes va the Morita-Baylis-Hillman reaction. *Tetrahedron Lett*., **2004**, *45*, 4745-4748.
8. Basavaiah, D.; Rao, A. J.; Satyanarayana, T. Recent Advances in the Baylis-Hillman Reaction and Applications. *Chem. Rev*., **2003**, *103*, 3, 811-892.
9. Nenajdenko, V.G.; Druzhinin, S. V.; Balenkova, E. S. Baylis-Hillman reaction for a α,β-unsatured trifluoromethyl ketones. *Mendeleev Commun.*, **2006**, *16*, 273-274.
10. Shi, M.; Zhao, G.-L. Aza-Baylis-Hillman Reactions of N-(Arylmethylene)diphenylphosphinamides with Activated Olefins in the Presence of Various Lewis Bases. *Adv. Synth. Catal.*, **2004**, *346*, 1205-1219.
11. Lee, C. H.; Lee, K.-J. DABCO-Assisted Coupling of Some Activated Olefins and 2,3-Dihalo-1,4-naphtoquinones and Conversion to the Anthraquinone Derivatives. *Synthesis*, **2004**, *12*, 1941-1946.
12. Lee, K. Y.; GowriSankar, S.; Kim, J. N. *N*,*N*,*N*′,*N*′-Tetramethyl-1,3-propanediamine as the catalyst of choice for the Baylis–Hillman reaction of cycloalkenone: rate acceleration by stabilizing the zwitterionic intermediate via the ion–dipole interaction. *Tetrahedron Lett*., **2004**, *45*, 5485-5488.
13. Zhao, S.; Chen, Z. The *N*,*N*,*N*′,*N*′–Tetramethylethylenediamine Mediated Baylis-Hillman Reaction. Synth. Commun., 2005, 35, 121-127.

14. Kumar, K.; Rawal, R. K. CuI/DBU-Mediated MBH Reaction of Isatins: A Convenient Synthesis of 3-Substituted-3-hydroxy-2-oxindole. *ChemistrySelect*, **2020**, *5*, 3048-3051.
15. Sandeep, J.; Durgesh, S.; Tanmay, R.; Avijiti Kumar, P.; Rampal, P. Unveiling Heterogeneous Catalytic Potential of Distinctly Coordinated Polymers Toward Henry and Morita-Baylis-Hillman Reactions. *ChemistrySelect*, **2024**, *9*, e202400247.
16. Price, K. E.; Broadwater, S. J.; Jung, H. M.; McQuade, T. Baylis-Hillman Mechanism: A New Interpretation in Aprotic Solvents. *Org. Lett.*, **2005**, *7*, 1, 147-150.
17. Robiette, R.; Aggarwal, V.; Harvey, J. N. Mechanism of the Morita-Baylis-Hillman Reaction: A Computational Investigation. *J. Am. Chem. Soc*., **2007**, *129*, 50, 15513-15525.
18. Fan, J.-F.; Yang, C.-H.; He, L.-J. DFT study on the role of methanol solvent in Morita-Baylis-Hillman reaction. *Int. J. Quantum Chem.*, **2009**, *109*, 1311-1321.
19. Plata, R. E.; Singleton, D. A. A Case Study of the Mechanism of Alcohol-Mediated Morita Baylis–Hillman Reactions. The Importance of Experimental Observations. *J. Am. Chem. Soc.* **2015**, *137*, 11, 3811-3826.
20. Trost, B. M. On inventing Reactions for Atom Economy. *Acc. Chem. Res.*, **2002**, *35*, 9, 695-705.
21. Devi, N.; Pathania, A. S.; Singh, V.; Sharma, S. Synthesis, biological activities, and structure–activity relationships of Morita–Baylis–Hillman adducts: An update. *Arch. Pharm.*, **2024**, *357*, e2400372.
22. Lima-Junior, C. G.; Vasconcellos, M. L. A. A. Morita-Baylis-Hillman adducts: Biological activities and potentialities to the discovery of new cheaper drugs. *Bioorg. Med. Chem.*, **2012**, *20*, 3954-3971.
23. Razzano, V.; Paolino, M.; Reale, A.; Giuliani, G.; Artusi, R.; Caselli, G.; Visintin, M.; Makovec, F.; Donati, A.; Villafiorita-Monteleone, F.; Botta, C.; Cappelli, A. Development of Imidazole-Reactive Molecules Leading to a New Aggregation-Induced Emission Fluorophore Based on the Cinnamic Scaffold. *ACS Omega*, **2017**, *2*, 9, 5453-5459.
24. Razzano, V.; Paolino, M.; Reale, A.; Giuliani, G.; Donati, A.; Giorgi, G.; Artusi, R.; Caselli, G.; Visintin, M.; Makovec, F.; Battiato, S.; Samperi, F.; Villafiorita-

Monteleone, F.; Botta, C.; Cappelli, A. Ploy-histidine grafting leading to fishbone-like architectures. *RSC Adv.*, **2018**, *8*, 8638-8656.

25. Paolino, M.; Reale, A.; Razzano, V.; Giorgi, G.; Giuliani, G.; Villafiorita-Monteleone, F.; Botta, C.; Coppola, C.; Sinicropi, A.; Cappelli, A. Design, synthesis, structure, and photophysical features of highly emissive cinnamic derivatives. *New J. Chem.*, **2020**, *44*, 13644-13653.
26. Tassone, G.; Paolino, M.; Pozzi, C.; Reale, A.; Salvini, L.; Giorgi, G.; Orlandini, M.; Galvagni, F.; Mangani, S.; Yang, X.; Carlotti, B.; Ortica, F.; Latterini, L.; Olivucci, M.; Cappelli, A. Xanthopsin-Like Systems via Site-Specific Click-Functionalization of a Retinoic Acid Binding Protein. *ChemBioChem*, **2021**, *23*, e202100449.
27. Paolino, M.; Reale, A.; Razzano, V.; Giuliani, G.; Donati, A.; Bonechi, C.; Caselli, G.; Visintin, M.; Makovec, F.; Scialabba, C.; Licciardi, M.; Paccagnini, E.; Gentile, M.; Salvini, L.; Tavanti, F.; Menziani, M. C.; Cappelli, A. Nanoreactors for the multi-functionalization of poly-histidine fragments. *New J. Chem.*, **2019**, *43*, 6834-6837.
28. Paolino, M.; Visintin, M.; Margotti, E.; Visintini, M.; Salvini, L.; Reale, A.; Razzano, V.; Giuliani, G.; Caselli, G.; Tavanti, F.; Menziani, M. C.; Cappelli, A. Functionalization of protein hexahistidine tags by functional nanoreactors. *New J. Chem.*, **2019**, *43*, 17946-17953.
29. Paolino, M.; Tassone, G.; Governa, P.; Saletti, M.; Lami, M.; Carletti, R.; Sacchetta, F.; Pozzi, C.; Orlandini, M.; Manetti, F.; Olivucci, M.; Cappelli, A. Morita–Baylis–Hillman Adduct Chemistry as a Tool for the Design of Lysine-Targeted Covalent Ligands. *ACS Med. Chem. Lett.*, **2025**, *16*, 3, 397-405.
30. Dahal, U. P.; Gilbert, A. M.; Obach, R. S.; Flanagan, M. E.; Chen, J. M.; Garcia-Irizarry, C.; Starr, J. T.; Schuff, B.; Uccello, D. P.; young, J. A. Intrinsic reactivity profile of electrophilic moieties to guide covalent drug design: N-α-acetyl-l-lysine as an amine nucleophile. *Med. Chem. Commun.*, **2016**, *7*, 864-872.
31. Grimsley, G. R.; Scholtz, J. M.; Pace, C. N. A summary of the measured p*K* values of the ionizable groups in folded proteins. *Protein Sci.*, **2008**, *18*, 247-251.

2.7 RESEARCH ARTICLE: **"Synthesis, photophysical and photochemical features of a Morita-Baylis-Hillman adduct derivative bearing a triphenylamine moiety"**

Authors: Mario Saletti, Marco Paolino, **Jacopo Venditti**, Claudia Bonechi, Germano Giuliani, Antonella Caterina Boccia, Chiara Botta, Andrea Cappelli

Publication: Dyes and Pigments

Publisher: Elsevier

DOI: doi.org/10.1016/j.dyepig.2023.111571

Supporting Information available at: doi.org/10.1016/j.dyepig.2023.111571

Reproduced with permission from: Elsevier

Contribution: The Ph.D. candidate contributed to the synthetic pathway of the MBHA derivative bearing a TPA moiety and its preliminary characterization. In particular, the Ph. D. candidate performed ^{1}H NMR spectroscopy analyses (400 MHz), which proved essential for both the structural characterization of the MBHA derivative and the evaluation of the transformations occurring during photochemical studies.

Dyes and Pigments 219 (2023) 111571

Contents lists available at ScienceDirect

Dyes and Pigments

journal homepage: www.elsevier.com/locate/dyepig

Synthesis, photophysical and photochemical features of a Morita-Baylis-Hillman adduct derivative bearing a triphenylamine moiety

Mario Saletti [a], Marco Paolino [a], Jacopo Venditti [a], Claudia Bonechi [a], Germano Giuliani [a], Antonella Boccia [b], Chiara Botta [b], Andrea Cappelli [a,*]

[a] Dipartimento di Biotecnologie, Chimica e Farmacia (Dipartimento di Eccellenza 2018-2022), Università degli Studi di Siena, Via Aldo Moro 2, 53100, Siena, Italy
[b] Istituto di Scienze e Tecnologie Chimiche "G. Natta" - SCITEC (CNR), Via A. Corti 12, 20133, Milano, Italy

ABSTRACT

A new Morita-Baylis-Hillman Adduct (MBHA) derivative **7** was designed and synthesized to obtain a reactive molecule potentially capable of labelling basic amino acid residues. Compound **7** was easily prepared and characterized from the point of view of its photophysical and photochemical features before then to be used in labelling experiments with amino acid.

1. Introduction

In recent years, selectively labeling of proteins at precisely defined positions was developed as a strategy to study their structure–function behavior. Protein labeling strategies usually exploit the interaction of amino acid residues with suitable probes capable of reacting with the amino or thiol groups present in them [1–3].

Fluorescence spectroscopy represents a powerful analytical technique for scrutinizing protein interactions and functions by means of fluorescent dyes. However, more recently, fluorogenic labeling methods (i. e. the fluorescence of the probe is activated by its reaction/attachment to the desired site) have emerged as interesting approaches because of the higher signal-to-noise ratio [4,5]. In fact, when the excess of fluorescent dyes cannot be washed-out in real-time imaging in living systems, fluorogenic probes became the reagents of choice [6]. Fluorogenic probes showing aggregation-induced emission (AIE) properties (i. e. the emission intensities are higher in the solid state than in solution) [7] are particularly interesting because they often feature higher sensitivity and photostability with respect to conventional fluorescence probes, which are generally very emissive in solution, but affected by aggregation caused quenching (ACQ) processes at high concentration [8,9].

Recently, we have developed imidazole-reactive molecules **1a-c** (Fig. 1) leading to Imidazole Binding Cinnamic Derivatives (IBCD) **2a-c** showing fluorogenic properties. Although, **2a-c** displayed very weak emission in solution, methoxy and dimethoxy derivatives **2b** and **2c** showed aggregation-induced emission (AIE). In particular, compound **2c** displayed bright blue emission with photoluminescence (PL) quantum yields (QY) two orders of magnitude higher in the solid state with respect to the corresponding values measured in solution, suggesting the presence of crystallization induced emission (CIE) phenomenon [10].

Owing to these encouraging results, the phenyl group of compounds **1a-c** and **2a-c** was replaced by a naphthalene nucleus as in compounds **3a,b** in order to extend the π electron system. Interestingly, naphthalene derivatives **3a,b** were found to react with imidazole and acetylhistidine with the formation of monoadducts (i. e. **4a-c**) and of the corresponding imidazolium salt diadducts (i. e. **5a-c**). Significant emission features were shown by both monoadducts and imidazolium salt diadducts with PL QY values in the solid state higher than the corresponding values observed in solution (as in AIE phenomenon). Moreover, diadduct **5c** showed a peculiar (i. e. 100 nm) red shift in the solid-state emission up to 520 nm [11].

The characterization of the reactivity of MBHA derivatives **3a,b** with model proteins suggested the interesting potentials of **3a** in the functionalization of lysine residues embedded in molecular cavities [12], and of **3b** in the site-specific PEGylation of engineered proteins bearing poly-histidine tags [13,14].

Very recently, we were successful in the identification and isolation of the chromophores working in π-stacked polybenzofulvene derivatives for optoelectronic applications. These studies led to the discovery of cinnamic derivatives **6a-c** (Fig. 2) showing photophysical features again better than those shown by the corresponding polybenzofulvene derivatives with PL QY values in the order of 57–80% and emission maxima in the range of 407–540nm [15].

* Corresponding author.
E-mail address: andrea.cappelli@unisi.it (A. Cappelli).

https://doi.org/10.1016/j.dyepig.2023.111571
Received 19 April 2023; Received in revised form 12 June 2023; Accepted 24 July 2023
Available online 28 July 2023
0143-7208/

In the present work, the structure of imidazole-reactive molecules **1a-c** was manipulated with the aim of obtaining MBHA derivative **7** potentially useful in the labelling of basic amino acid residues. The introduction of an electron donating group such as triphenylamine (TPA) should lead to the formation, after reaction of **7** with basic amino acid residues, of cinnamic derivatives **8** sharing the most promising fluorophore of compounds **6c**. Thus, the present paper describes the synthesis of MBHA derivative **7** and its characterization from the point of view of its photophysical and photochemical features.

2. Results and discussion

2.1. Chemistry

The preparation of MBHA derivative **7** bearing the electron donating group triphenylamine is described in Scheme 1.

Reagents: (i) 4-(diphenylamino)phenylboronic acid pinacol ester, $Pd(PPh_3)_2Cl_2$, PPh_3, Cs_2CO_3, CH_3OH, THF; (ii) methyl acrylate, DABCO, CH_3OH; (iii) CH_3COCl, TEA, CH_2Cl_2.

4-Bromobenzaldehyde **9** was used as the starting material in Suzuki-Miyaura cross-coupling along with the commercially available 4-(diphenylamino)phenylboronic acid pinacol ester to prepare the required benzaldehyde derivatives **10**. The coupling was carried out in the presence of $Pd(PPh_3)_2Cl_2$ and PPh_3 as catalyst system and Cs_2CO_3 as the base in THF and CH_3OH. Benzaldehyde derivative **10** was then submitted to Morita-Baylis-Hillman reaction with methyl acrylate in the presence of DABCO to provide MBHA alcohol **11**, which was in turn transformed into MBHA acetate **7**. The best overall yields obtained in the synthesis of target triphenylamine MBHA derivative **7** were in the range of 61–63%.

2.2. Photophysical and photochemical features of MBHA derivative 7

We previously reported that the absorption spectrum of model cinnamic derivative **6c** in dichloromethane solutions showed a low energy peak at about 370 nm, with an emission spectrum red-shifted to 540 nm and very remarkable photoluminescence quantum yield (PL QY) of 78% in solution [15]. Moreover, the PL QY of this cinnamic derivative was unaffected by the aggregation in the ordered crystalline state (i. e. PL QY = 80%). These very promising photophysical features were decisive in stimulating the development of MBHA derivative **7**, and immediately after its synthesis and before to be used in labelling experiments with amino acids, it was characterized from the point of view of its photophysical features.

Solutions of **7** display stable properties when stored in dark, however, upon irradiation of the solutions with a UV-A lamp (366 nm, max irradiance 6μw/cm^2/nm), a sharp change in the absorption spectrum is observed for DCM and THF solvents and a slighter one for methanol (see Fig. 3 and Table S1).

In particular, for THF and DCM, the lower energy absorption band of the pristine solutions, centered at about 330–335 nm (with a shoulder at about 310 nm), split into two well-separated bands: one at about 292 nm for both the solvents and one at 349 nm for THF and 364 nm for DCM. The methanol solution displayed slighter variations, with a decrease of the 331 nm main peak absorbance accompanied by the growth of a 305 nm peak and a long wavelength tail at about 380 nm. Interestingly, the absorption spectra of the DCM and THF irradiated solutions resembles those of the cinnamic derivative **6c** [15].

Even more impressive were the variations observed in the emission properties of solutions of **7** after UV-A exposure. In Fig. 4 the pictures of the solutions of Fig. 3 are reported when the samples are exposed to UV-A lamp, before (MeOH) and after irradiation with by the UV-A lamp. As it can be seen, their emission intensity strongly increased with a completely different behaviour according to the solvent. The methanol solution showed a strong intensity enhancement, going from pale to bright blue emission. The THF and DCM solutions showed also a surprising colour change, from blue to green for THF, and from blue to yellow for DCM. In Fig. 5 the PL and PLE spectra of **7** dissolved in THF

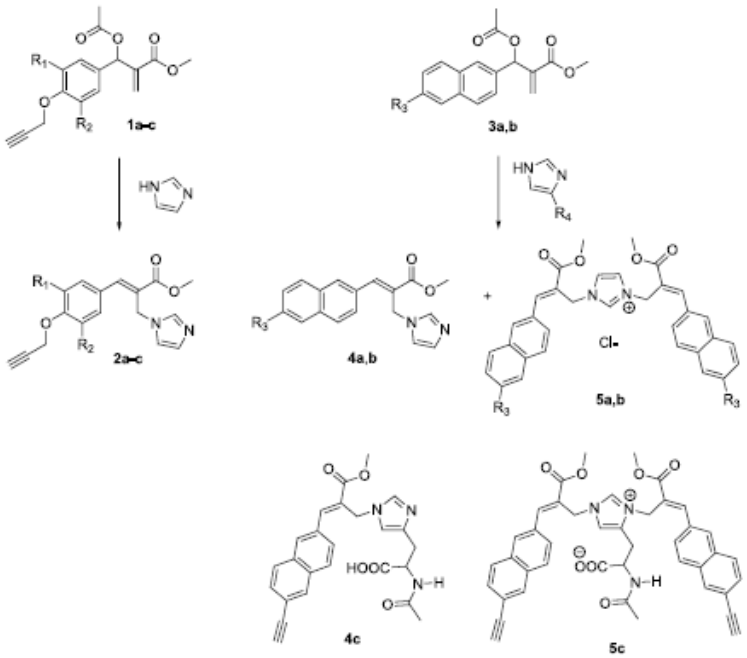

Fig. 1. Structures of imidazole-reactive molecules 1a-c and 3a,b leading to 2a-c, 4a-c, and 5a-c showing fluorogenic properties.

(recorded before and after UV-A exposure for 1 h and 30 min) suggested the presence of a new compound, produced by UV-A irradiation, that emitted in the green and was selectively excited at about 365 nm. The PLQY of the UV-A exposed solution was higher than the pristine one and varied with the excitation wavelength (see Table S1). In particular, when the new green emitting specie was selectively excited its PLQY was maximum (QY = 63% for 365 nm excitation). Moreover, the PL lifetimes were different for the two emission bands, being longer for the green emission (τ_{av} = 0.35 ns at 410 nm; τ_{av} = 3.43 ns at 555 nm; see Fig. S3). The main results of the photophysical characterization of the solutions under UV-A irradiation are summarized in Table S1 (see the Supplementary data).

The results of the photophysical characterization studies suggested that MBHA derivative **7**, upon irradiation with UV-A light, was susceptible of forming reactive excitation states. In order to evaluate this hypothesis, appropriate irradiation studies were performed in different solvents and the progress of the photochemical reactions was followed by ^{1}H NMR spectroscopy.

When a solution of MBHA derivative **7** (3.0 mg) in deuterated methanol (0.5 mL) was irradiated into a 5 mm NMR tube, a quite clean behavior was observed as suggested by the comparison of the ^{1}H NMR spectra shown in Fig. 6.

The purification of the reaction mixture led to the isolation of compound **12-D** as the main reaction product (ca. 80%) and **13-D** as the minor one (ca. 20%) that suggested the interaction of the excited state of **7** with the reaction solvent as depicted in Scheme 2. Similar results were obtained by performing the irradiation experiments with a solution of MBHA derivative **7** (30 mg) in non-deuterated methanol (5.0 mL), and non-deuterated compounds **12** and **13** were obtained (see the Experimental section for details). Moreover, some minor peaks in the ^{1}H NMR spectra supported the presence of small amounts of starting MBHA derivative **7** and of cinnamic derivative **14,** which derived from **7** by the double bond shift in the highly conjugated position as observed in methoxy derivative **13-D**.

Reagents: (i) irradiation with UV-A light, CD_3OD; (ii) irradiation with UV-A light, CH_2Cl_2.

On the other hand, when dichloromethane was used as the solvent in the irradiation experiments, the formation of **12** and **13** was obviously impossible and compound **14** was the only reaction product obtained (see Fig. 7).

After 5 h irradiation, a residual amount (ca. 15%) of MBHA derivative **7** was observed in the reaction mixture, but the irradiation was stopped because significant decomposition signs appeared in the ^{1}H NMR spectrum. Similar results were obtained by using THF as the reaction solvent, but in this solvent the amount of residual MBHA derivative **7** was higher than 30% with respect to compound **14** (ca. 60%) also after 10 h irradiation in a UV-A chamber.

Compounds **12-14** displayed stable absorption/emission properties and did not show relevant variations upon UV light exposure. Therefore, they were photophysically characterized in solution and solid state (see Fig. 8). Their main features are summarized in Table 1 and compared with those of the previously reported model compound **6c** [15].

As expected, the photophysical properties of the DCM solutions of the three compounds **12**,**13,** and **14** resemble those of the UV irradiated MBHA derivative **7** dissolved in methanol, THF, and DCM, respectively (see Table S1). In particular, while compound **12** displays photophysical properties similar to those of pristine compound **7**, the absorption properties of compounds **13** and **14** in solution are very similar to those of model compound **6c**, as expected due to their very similar chemical structure. The DFT and TDDFT theoretical analysis performed on model compound **6c** (see compound **1c** in ref. 15) showed that its absorption spectrum is dominated by the fourth excited state transition, corresponding to an excitation energy of 349 nm. The ground state electron density of the HOMO is mainly localized on the triphenylamine donor group, with the LUMO on the other portion of the molecule, indicating a relevant charge transfer character of the HOMO-LUMO transitions [15]. Going to the solid state (i. e. cast films), the emission of compound **13** is only slightly red-shifted (15 nm) when compared to model compound **6c,** with a PL QY decreased from 80% to 46%. Compound **14** displays a red-shifted (24 nm) emission and a slightly reduced PL QY also in solution, while in the solid state (i. e. cast films) its emission is further red-shifted to 504 nm, with PL QY (43%) similar to **13**. The photophysical properties of compound **12** are sharply different from those of the other two compounds, suggesting AIE properties of this compound. In fact, in solution it displays blue-shifted absorption and emission with a reduced emission efficiency. On the other hand, the cast film of **12**

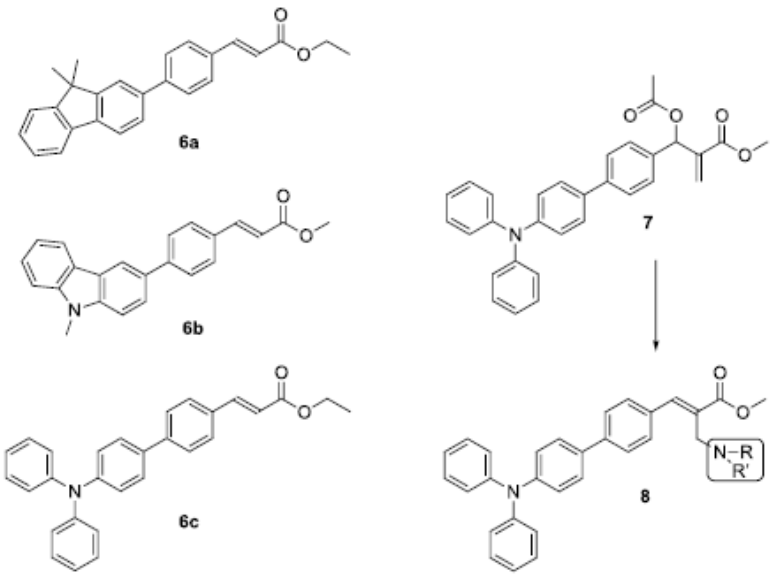

Fig. 2. Development of reactive MBHA derivative **7** potentially capable of reacting with basic amino acid residues and thus leading to cinnamic derivatives **8**.

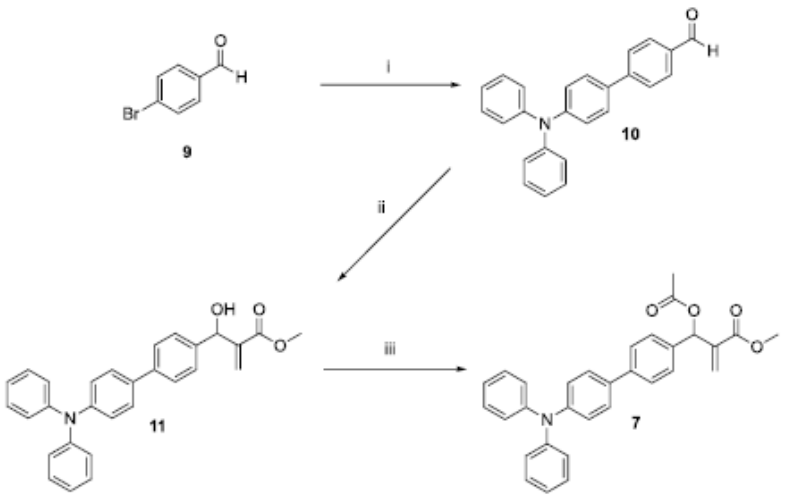

Scheme 1. Preparation of reactive MBHA derivative 7.

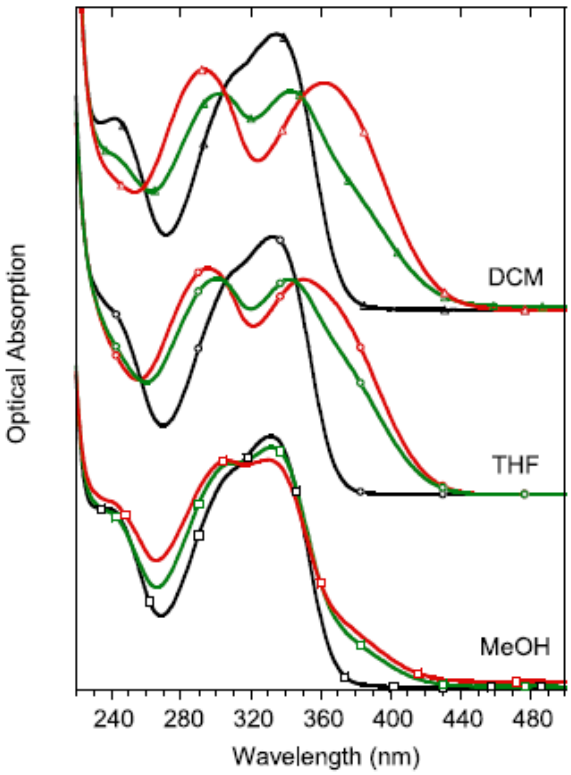

Fig. 3. Normalized optical absorption spectra of solutions of 7 in DCM, THF, and MeOH pristine solutions (black lines) and their evolution with UV-A light exposure: 30 min (green lines) and longer irradiation times (red lines; 1 h and 30 min for THF, 5 h for DCM and 18 h for MeOH). UV-A lamp at 366 nm, max irradiance 6 $\mu w/cm^2/nm$. Solution concentrations of 9 x 10^{-4} M (DCM), 7 x 10^{-4} M (THF), 2 x 10^{-4} M (MeOH).

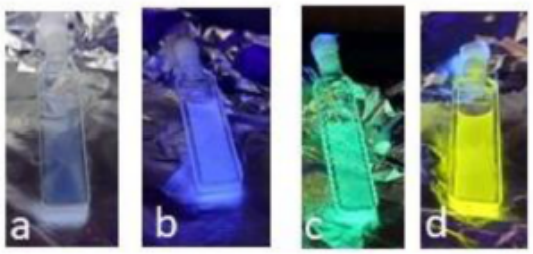

Fig. 4. Picture of the solutions of 7 under UV-A lamp irradiation in different solvents. MeOH pristine solution (a) and after 18 h of irradiation (b); THF solution after 1 h and 30 min of irradiation (c); DCM solution after 5 h irradiation (d).

displays a bright blue emission with an efficiency comparable to that of compounds **13** and **14**. The AIE behavior of compound **12** can be rationalized due to the easy intramolecular rotation around the acrylate bond in solution, that introduces non-radiative deactivation channels [16], in agreement with its sharply reduced lifetime. Its AIE behavior can therefore be attributed to restricted intramolecular motions in the solid state thanks to molecular rigidification [10].

Finally, to evaluate the role of triphenylamine moiety on the peculiar photochemical features of MBHA derivative **7**, similar irradiation experiments were performed on the simplified analogue **15** (Scheme 3) [17].

Reagents: (i) methyl acrylate, DABCO, CH_3OH; (ii) CH_3COCl, TEA, CH_2Cl_2.

This biphenyl derivative was prepared in two steps from the commercially available [1,1′-biphenyl]-4-carbaldehyde **16** (Aldrich) and was used in irradiation experiments in deuterated dichloromethane by using the same experimental conditions used with triphenylamine derivative **7**. The substantial photostability observed for biphenyl derivative **15** supported the key role of triphenylamine moiety in the peculiar photochemical features shown by triphenylamine derivative **7**.

3. Conclusion

In the aim of obtaining new reactive molecules potentially useful in

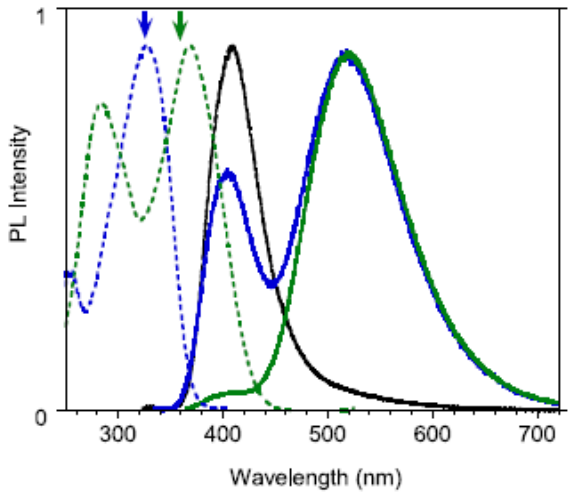

Fig. 5. PL (solid lines) and PLE (dashed lines) spectra of a THF solution of 7 (concentration = $7x10^{-4}$ M) before (black line, λ_{exc} = 300 nm) and after 1 h and 30 min UV lamp irradiation (blue lines, λ_{exc} = 330 nm, λ_{em} = 415 nm; green lines, λ_{exc} = 365 nm, λ_{em} = 527 nm).

basic amino acid labelling, the very promising optical features of previously published cinnamic derivative **6c** stimulated the design of Morita-Baylis–Hillman acetate derivative **7**. This compound was promptly synthesized in three steps from commercially available intermediates and characterized from the point of view of its photophysical and photochemical features before than to be used in labelling experiments with amino acids. Interestingly, derivative **7** displayed an intriguing photochemical activity, which was followed by parallel photophysical and NMR studies in different solvents. Three different compounds (i. e. **12, 13** and **14)** have been isolated and purified from methanol, DCM, and THF solutions of **7** exposed to UV-A light. The so obtained compounds have been fully characterized and compared to the model cinnamic derivative **6c.** Compound **12** displayed AIE behavior attributed to the easy intramolecular rotation around the acrylate bond in solution, with bright blue emission in the solid state. Conversely, compounds **13** and **14** showed photophysical features very similar to those very promising shown by model cinnamic derivative **6c** with very bright (PL QY in the range of 58–75%) green-yellow emission (540–564 nm) in solution that were significantly decreased in the solid state, but however exceeded the 40%. These results consolidated the outstanding photophysical feature of the cinnamic fluorophore contained in compound **6c**, and pave the way for the use of MBHA derivative **7** in the fluorogenic labeling of proteins. Finally, the comparative analysis of the biphenyl derivative **15** supports the role of the triphenylamine moiety in the peculiar photochemical features of **7**.

4. Experimental section

Synthesis. Melting points were determined in open capillaries in a Gallenkamp apparatus and are uncorrected. Merck silica gel 60 (230–400 mesh) was used for column chromatography. Merck TLC plates, silica gel 60 F_{254} were used for TLC. NMR spectra were recorded with a Bruker DRX-400 AVANCE III, a Bruker DRX-500 AVANCE, or a Bruker DRX-600 AVANCE spectrometer in the indicated solvents (TMS as internal standard): the values of the chemical shifts are expressed in ppm and the coupling constants (*J*) in Hz. An Agilent 1100 LC/MSD operating with an electrospray source was used in mass spectrometry measurements, and a Bruker TimsTOF apparatus was used in recording HR-MS spectra (see Supplementary data). UV-A (or -B) irradiations were conducted using a Multyrays chamber equipped with 2 G15T8 Hg UV-A and 2 G15T8 Hg UV-B tubes (2 × 15 Watt) in continuous rotation.

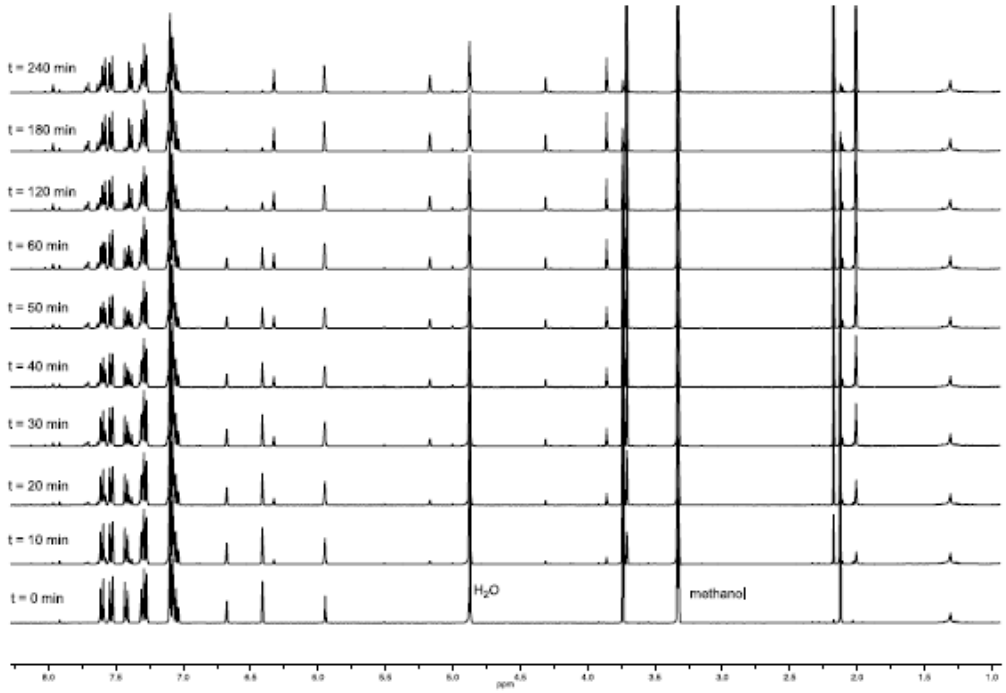

Fig. 6. Comparison of the ^{1}H NMR spectra obtained by irradiating a solution of **7** in deuterated methanol with UV-A for increasing times.

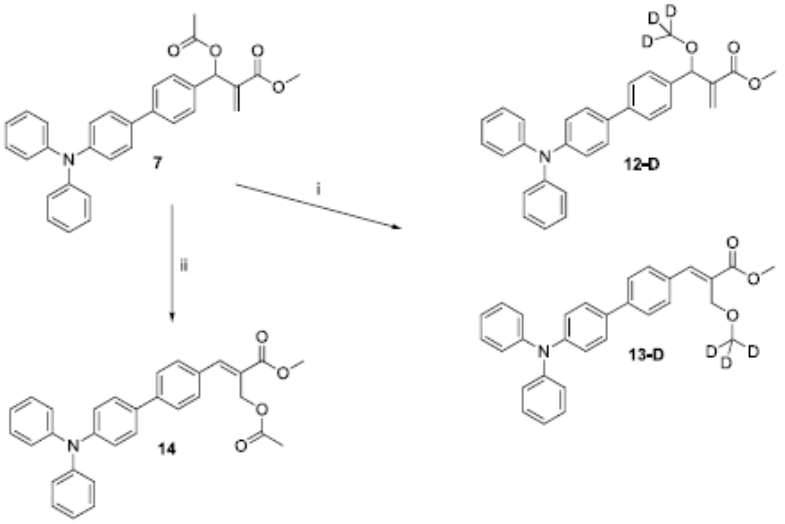

Scheme 2. Photochemical reactions of MBHA derivative 7 in different solvents.

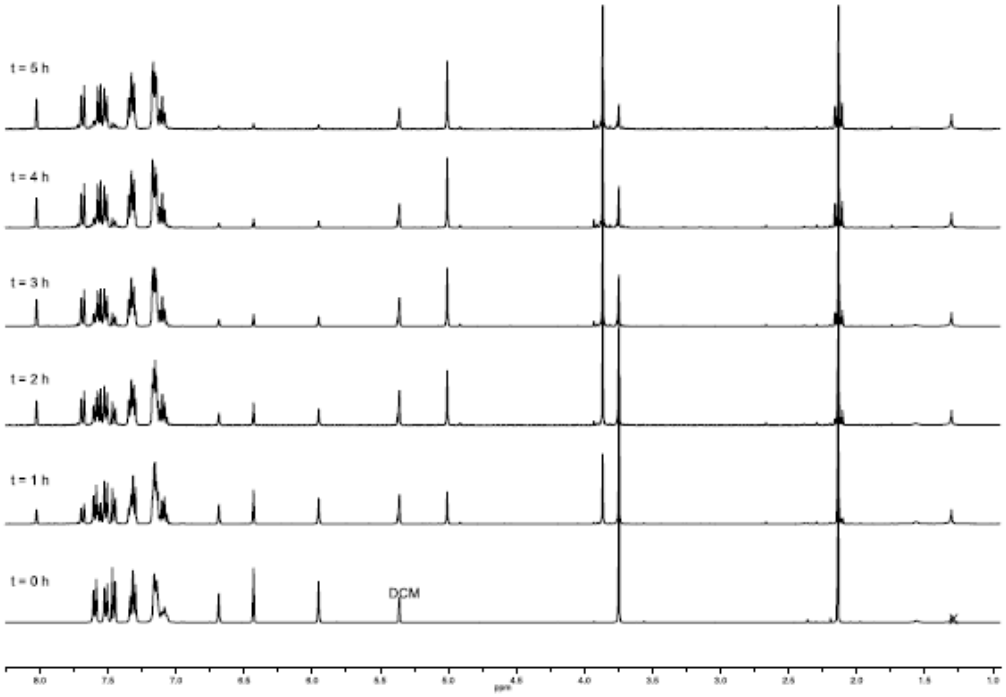

Fig. 7. Comparison of the ^{1}H NMR spectra obtained by irradiating a solution of 7 in deuterated dichloromethane with UV-A for increasing times.

4.1. 4′-(Diphenylamino)-[1,1′-biphenyl]-4-carbaldehyde (10)

In a microwave tube, a mixture of 4-(diphenylamino)phenylboronic acid pinacol ester (Aldrich, 0.40 g, 1.08 mmol) in 4.5 mL of dry THF and 1.0 mL of dry MeOH containing Cs_2CO_3 (1.06 g, 3.25 mmol) was stirred at room temperature for 30 min. To the resulting mixture, $Pd(PPh_3)_2Cl_2$ (0.15 g, 0.214 mmol), PPh_3 (0.28 g, 1.08 mmol), and compound **9** (0.20 g, 1.08 mmol) were added in sequence. The reaction mixture was exposed to microwave irradiation in a CEM Discover apparatus (2–3 cycles of 10 min, T = 80 °C, W = 150, P = 250 psi) and then partitioned between ethyl acetate and water. The organic layer was washed with brine and dried over sodium sulfate and concentrated under reduced pressure. Purification by flash chromatography with petroleum ether-ethyl acetate (9:1) as the eluent afforded **10** (0.29 g, yield 77%) as a yellow solid. An analytical sample was obtained by recrystallization from dichloromethane by slow evaporation (mp 117–119 °C). ^{1}H NMR

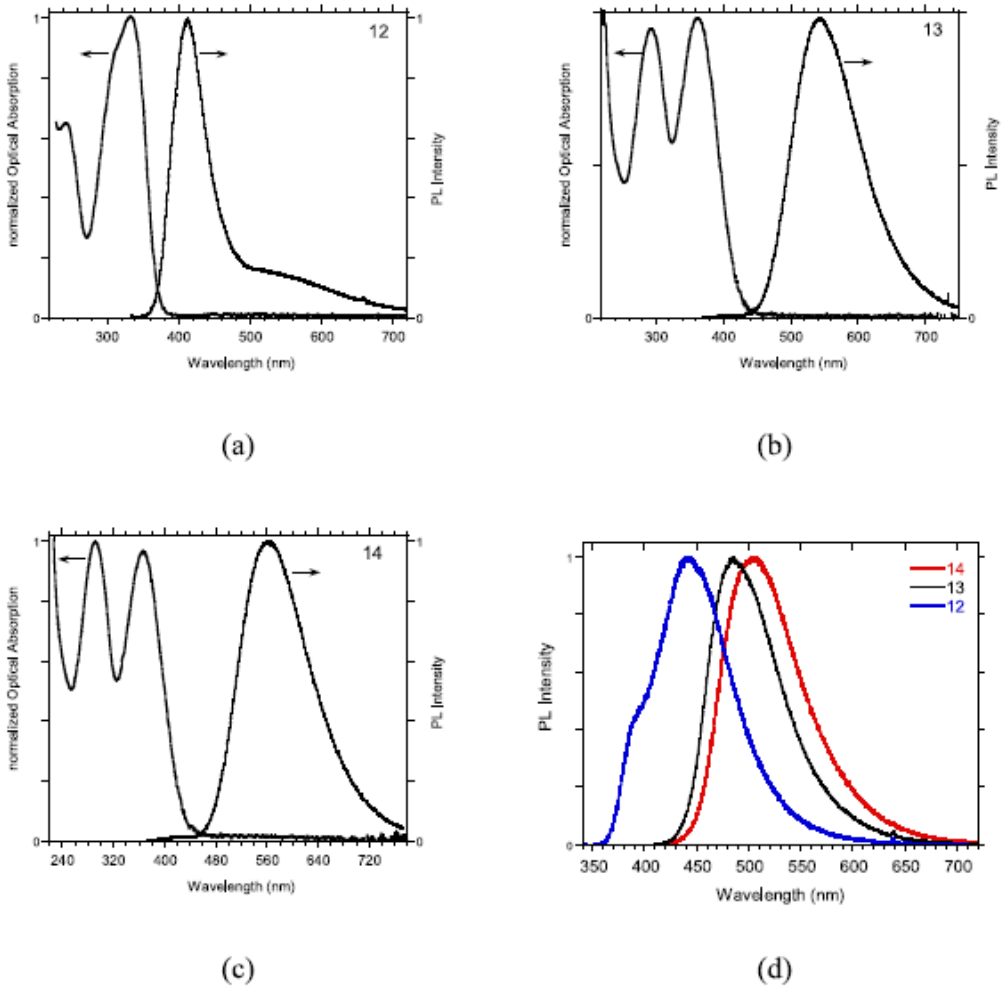

Fig. 8. Normalized optical absorption and emission spectra of DCM solutions ($c = 10^{-5}$M) of **12** (a, $\lambda_{ex} = 330$ nm), **13** (b, $\lambda_{ex} = 365$ nm) and **14** (c, $\lambda_{ex} = 365$ nm). PL spectra of cast films (d) of **12** (blue line), **13** (black line) and **14** (red line), $\lambda_{ex} = 320$ nm.

(400 MHz, $CDCl_3$): 7.06 (t, $J = 7.3$, 2H), 7.10–7.19 (m, 6H), 7.28 (t, $J = 7.8$, 4H), 7.51 (d, $J = 8.3$, 2H), 7.72 (d, $J = 8.4$, 2H), 7.91 (d, $J = 8.4$, 2H), 10.02 (s, 1H). ^{13}C NMR (125 MHz, $CDCl_3$): 123.1, 123.5, 124.9, 126.9, 128.0, 129.4, 130.3, 132.8, 134.7, 146.6, 147.3, 148.4, 191.8. MS (ESI) *m/z*: $[M + H]^+$ Calcd for $C_{25}H_{20}NO$ 350.2; Found 350.0.

4.2. Methyl 2-[[4'-(diphenylamino)-[1,1'-biphenyl]-4-yl](hydroxy) methyl]acrylate (11)

A mixture of aldehyde **10** (0.28 g, 0.80 mmol) with methyl acrylate (0.15 mL, 1.66 mmol), methanol (0.10 mL), and 1,4-diazabicyclo[2.2.2] octane (DABCO) (0.11 g, 0.98 mmol) was stirred at room temperature for 72 h in darkness, and then concentrated under reduced pressure. The resulting residue was dissolved in dichloromethane and washed in sequence with a saturated solution of ammonium chloride. The organic layer was dried over sodium sulfate and concentrated under reduced pressure. Purification of the residue by flash chromatography with petroleum ether-ethyl acetate (7:3) as the eluent gave compound **11** (0.33 g, yield 85%) as a pale-yellow oil. ^{1}H NMR (400 MHz, $CDCl_3$): 2.98 (d, $J = 5.6$, 1H), 3.73 (s, 3H), 5.60 (d, $J = 5.2$, 1H), 5.87 (s, 1H), 6.35 (s, 1H), 7.02 (t, $J = 7.0$, 2H), 7.08–7.17 (m, 6H), 7.21–7.30 (m, 4H), 7.41 (d, $J = 8.1$, 2H), 7.45 (d, $J = 8.5$, 2H), 7.54 (d, $J = 8.2$, 2H). ^{1}H NMR (500 MHz, $CDCl_3$): 2.93 (br, 1H), 3.73 (s, 3H), 5.60 (s, 1H), 5.89 (t, $J = 1.2$, 1H), 6.36 (t, $J = 0.9$, 1H), 7.01-7-03 (m, 2H), 7.10–7.15 (m, 6H), 7.23–7.29 (m, 4H), 7.40–7.43 (m, 2H), 7.44–7.48 (m, 2H), 7.52–7.57 (m, 2H). ^{13}C NMR (125 MHz, $CDCl_3$): 52.0, 73.1, 123.0, 123.8, 124.5, 126.1, 126.7, 127.0, 127.7, 129.2, 134.6, 139.8, 140.2, 141.9, 147.3, 147.6, 166.8. MS (ESI) *m/z*: $[M + Na]^+$ Calcd for $C_{29}H_{25}NNaO_3$ 458.2; Found 458.1.

4.3. Methyl 2-[acetoxy[4'-(diphenylamino)-[1,1'-biphenyl]-4-yl]methyl] acrylate (7)

To a solution of the MBH alcohol **11** (0.34 g, 0.78 mmol) in dry dichloromethane (8.0 mL) containing TEA (0.28 mL, 1.97 mmol), acetyl chloride (0.11 mL, 1.54 mmol) was added dropwise. After stirring at room temperature for 2 h, the reaction mixture was concentrated under reduced pressure and the residue was partitioned between dichloromethane and brine. The organic layer was dried over sodium sulfate and concentrated under reduced pressure. The residue was purified by flash chromatography with petroleum ether-ethyl acetate (8:2) as the eluent

Table 1
Comparison of the optical properties of compounds **12-14** with those of model cinnamic derivative **6c**.

	DCM solution				solid state		
	λ_{ab} (nm)	λ_{em} (nm)	QY[a] (%)	τ_{av}[b] (ns)	λ_{em}[c] (nm)	QY[a] (%)	τ_{av}[b] (ns)
6c	292, 371	540	78	3.32[d]	470	80[e]	3.02
12	242, 332	411	2	0.41[d]	440	41	2.89
13	292, 362	540	75	3.36	485	46	3.00
14	290, 367	564	58	3.52	504	43	2.61

[a] $\lambda_{ex} = 365$ nm
[b] $\lambda_{ex} = 407$ nm
[c] $\lambda_{ex} = 370$ nm
[d] $\lambda_{ex} = 370$ nm
[e] $\lambda_{ex} = 420$ nm, $\tau_{av} = \frac{\sum_{n=1}^{m} A_n t_n^2}{\sum_{n=1}^{m} A_n t_n}$, with bi-exponential (solution) and three-exponential (solid state) fits (see Supplementary data).

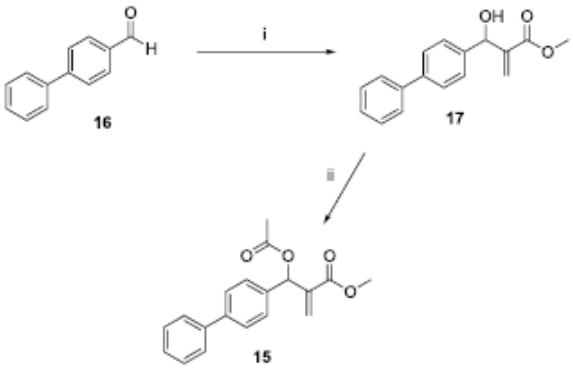

Scheme 3. Preparation of reactive MBHA derivative **15**.

to afford the corresponding Morita-Baylis–Hillman acetate **7** (0.28 g, yield 75%) as a pale-yellow solid. An analytical sample was obtained by recrystallization from dichloromethane by slow evaporation (mp 110–111 °C). ^{1}H NMR (400 MHz, $CDCl_3$): 2.11 (s, 3H), 3.71 (s, 3H), 5.90 (s, 1H), 6.41 (s, 1H), 6.70 (s, 1H), 6.99–7.05 (m, 2H), 7.07–7.16 (m, 6H), 7.20–7.31 (m, 4H), 7.39–7.45 (m, 4H), 7.50–7.55 (m, 2H). ^{1}H NMR (400 MHz, CD_3OD): 2.14 (s, 3H), 3.75 (s, 3H), 5.96 (s, 1H), 6.42 (s, 1H), 6.69 (s, 1H), 7.04–7.14 (m, 8H), 7.27–7.33 (m, 4H), 7.42–7.46 (m, 2H), 7.53–7.57 (m, 2H), 7.60–7.64 (m, 2H). ^{1}H NMR (600 MHz, CD_2Cl_2): 2.14 (s, 3H), 3.75 (s, 3H), 5.96 (s, 1H), 6.44 (s, 1H), 6.69 (s, 1H), 7.09 (t, $J = 7.4$, 2H), 7.12–7.18 (m, 6H), 7.29–7.36 (m, 2H), 7.44–7.49 (m, 2H), 7.50–7.55 (m, 2H), 7.58–7.62 (m, 2H). ^{13}C NMR (150 MHz, CD_2Cl_2): 21.0, 52.0, 72.9, 123.1, 123.7, 124.6, 125.5, 126.6, 127.7, 128.2, 129.3, 134.3, 136.6, 139.7, 140.7, 147.5, 147.7, 165.4, 169.4. MS (ESI) *m/z*: $[M + Na]^+$ Calcd for $C_{31}H_{27}NNaO_4$ 500.2; Found 500.0.

4.4. Irradiation studies of compound 7 in methanol

A solution of compound **7** (30 mg, 0.0628 mmol) in methanol (5.0 mL) was irradiated with UV-A light for 4 h, and the reaction mixture was then concentrated under reduced pressure. The purification of the resulting residue by flash chromatography with petroleum ether-ethyl acetate (98:2) as the eluent led to the isolation of compound **12** as the main reaction product and **13** as the minor one.

4.5. Methyl 2-[[4′-(diphenylamino)-[1,1′-biphenyl]-4-yl](methoxy) methyl]acrylate (12)

Compound **12** (11 mg, yield 39%) was isolated as a less polar fraction of the chromatographic purification described above. ^{1}H NMR (400 MHz, CD_3OD): 3.35 (s, 3H), 3.72 (s, 3H), 5.18 (s, 1H), 5.96 (s, 1H), 6.34 (s, 1H), 7.02–7.12 (m, 8H), 7.28–7.34 (m, 4H), 7.39–7.41 (m, 2H), 7.54–7.56 (m, 2H), 7.59–7.61 (m, 2H). ^{13}C NMR (100 MHz, CD_3OD): 51.8, 56.8, 81.7, 123.7, 124.4, 124.8, 125.1, 127.0, 128.2, 128.8, 129.9, 135.5, 138.8, 141.2, 142.3, 148.3, 146.6, 167.3. MS (ESI) *m/z*: $[M + Na]^+$ Calcd for $C_{30}H_{27}NNaO_3$ 472.2; Found 472.1.

4.6. Methyl (E)-3-[4′-(diphenylamino)-[1,1′-biphenyl]-4-yl]-2-(methoxymethyl)acrylate (13)

Compound **13** (3.0 mg, yield 11%) was isolated as the most polar fraction of the chromatographic purification described above. ^{1}H NMR (400 MHz, CD_3OD): 3.47 (s, 3H), 3.87 (s, 3H), 4.32 (s, 2H), 7.03–7.13 (m, 8H), 7.30–7.34 (m, 4H), 7.60–7.65 (m, 4H), 7.70–7.74 (m, 2H), 7.98 (s, 1H). ^{13}C NMR (100 MHz, CD_3OD): 53.5, 59.4, 68.5, 125.3, 125.4, 126.6, 128.4, 129.6, 130.2, 131.3, 132.6, 135.2, 135.9, 144.0, 146.4, 149.9, 150.1, 170.5. MS (ESI) *m/z*: $[M + Na]^+$ Calcd for $C_{30}H_{27}NNaO_3$ 472.2; Found 472.1.

4.7. Irradiation studies of compound 7 in dichloromethane

A solution of compound **7** (30 mg, 0.0628 mmol) in CH_2Cl_2 (5.0 mL) was irradiated with UV-A light for 5 h, and the reaction mixture was then concentrated under reduced pressure. Purification of the residue by flash chromatography with petroleum ether-ethyl acetate (98:2) as the eluent afforded compound **14** (12 mg, yield 40%) as a yellow solid.

4.8. Methyl (E)-2-(acetoxymethyl)-3-[4′-(diphenylamino)-[1,1′-biphenyl]-4-yl]acrylate (14)

The samples of this compound showed a purity of around 90% being contaminated by ca. 10% of the configurational isomer (*Z*). ^{1}H NMR (400 MHz, CD_2Cl_2): 2.13 (s, 3H), 3.87 (s, 3H), 5.01 (s, 2H), 7.08–7.13 (m, 2H), 7.14–7.19 (m, 6H), 7.28–7.37 (m, 4H), 7.48–7.54 (m, 2H), 7.55–7.59 (m, 2H), 7.66–7.71 (m, 2H), 8.02 (s, 1H).^{1}H NMR (400 MHz, CD_3OD): 2.12 (s, 3H), 3.87 (s, 3H), 5.00 (s, 2H), 7.06–7.12 (m, 8H), 7.28–7.33 (m, 4H), 7.53–7.55 (m, 2H), 7.60–7.62 (m, 2H), 7.72–7.75 (m, 2H), 8.04 (s, 1H). ^{13}C NMR (100 MHz, CD_3OD): 21.6, 53.6, 61.4, 125.3, 125.4, 126.7, 128.2, 128.6, 129.6, 131.3, 132.3, 134.7, 135.7, 144.2, 147.1, 149.8, 150.2, 169.7, 173.3. MS (ESI) *m/z*: $[M + Na]^+$ Calcd for $C_{31}H_{27}NNaO_4$ 500.2; Found 500.1.

4.9. Methyl 2-([1,1′-biphenyl]-4-yl(hydroxy)methyl)acrylate (17)

A mixture of commercially available [1,1′-biphenyl]-4-carbaldehyde **16** (0.20 g, 1.10 mmol) with methyl acrylate (0.20 mL, 2.20 mmol), methanol (7.0 μL), and 1,4-diazabicyclo[2.2.2]octane (DABCO) (0.15 g, 1.34 mmol) was stirred at room temperature for 72 h in darkness, and then concentrated under reduced pressure. The resulting residue was dissolved in dichloromethane and washed with a saturated solution of ammonium chloride. The organic layer was dried over sodium sulfate and then concentrated under reduced pressure. Purification of the residue by flash chromatography with petroleum ether-ethyl acetate (8:2) as the eluent afforded compound **17** (0.16 g, yield 54%) as a white solid (mp 120.9–121.4 °C). ^{1}H NMR (400 MHz, $CDCl_3$): 3.02 (d, $J = 5.7$, 1H), 3.74 (s, 3H), 5.61 (d, $J = 5.3$, 1H), 5.89 (s, 1H), 6.37 (s, 1H), 7.30–7.36 (m, 1H), 7.39–7.47 (m, 4H), 7.55–7.60 (m, 4H). MS (ESI) *m/z*: $[M + Na]^+$ Calcd for $C_{17}H_{16}NaO_3$ 291.1; Found 291.1. Analytical data consistent with that previously published [18–20].

4.10. Methyl 2-([1,1'-biphenyl]-4-yl(acetoxy)methyl)acrylate (15)

To a solution of the previously synthesized MBH alcohol **17** (83 mg, 0.31 mmol) in dry dichloromethane (4.0 mL) containing TEA (106 μL, 0.76 mmol), acetyl chloride (44 μL, 0.61 mmol) was added dropwise. After stirring at room temperature for 2 h, the reaction mixture was concentrated under reduced pressure and the residue was partitioned between dichloromethane and water. The organic layer was dried over sodium sulfate and concentrated under reduced pressure. The residue was purified by flash chromatography with petroleum ether-ethyl acetate (85:15) as the eluent led to the isolation of the corresponding Morita-Baylis–Hillman acetate **15** (65 mg, yield 68%) as a white solid (mp 80.5–82.4 °C). ^{1}H NMR (400 MHz, $CDCl_3$): 2.12 (s, 3H), 3.72 (s, 3H), 5.91 (s, 1H), 6.42 (s, 1H), 6.72 (s, 1H), 7.30–7.37 (m, 1H), 7.39–7.47 (m, 4H), 7.53–7.59 (m, 4H). MS (ESI) *m/z*: $[M + Na]^+$ Calcd for $C_{19}H_{18}NaO_4$ 333.1; Found 333.1.

Photophysical properties. UV–vis absorption spectra are obtained with a Perkin Elmer Lambda 900 spectrometer. PL spectra are obtained with a NanoLog composed by a iH320 spectrograph equipped with a Synapse QExtra charge-coupled device by exciting with a monochromated 450W Xe lamp. The spectra are corrected for the instrument response. PL QY values of solutions were obtained by using quinine sulfate as the reference. PL QY of solid-state samples were measured with a home-made integrating sphere according to the procedure reported elsewhere [21]. Time-resolved TCSPC measurements are obtained with PPD-850 single photon detector module and DeltaTime serie DD-300 DeltaDiode and DD-405L DeltaDiode Laser and analyzed with the instrument software DAS6 by using bi-exponential (solutions) or three-exponential (solid samples) best fits, as reported in the Supplementary data. Irradiation of the solutions has been performed with a UV-A lamp peaked at 366 nm, max irradiance 6μw/cm^2/nm, with bandwidth of about 20 nm.

CRediT authorship contribution statement

Mario Saletti: was involved in the synthesis and the preliminary characterization. **Marco Paolino**: was involved in the synthesis and the preliminary characterization. **Jacopo Vendittri**: was involved in the synthesis and the preliminary characterization. **Germano Giuliani**: was involved in the synthesis and the preliminary characterization. **Claudia Bonechi**: performed the NMR studies. **Antonella Boccia**: performed the NMR studies. **Chiara Botta**: performed the photophysical characterization. **Andrea Cappelli**: designed the compounds and organized the research activities. All authors have approved the final version of the manuscript.

Declaration of competing interest

The authors declare that they have no known competing financial interests or personal relationships that could have appeared to influence the work reported in this paper.

Data availability

Data will be made available on request.

Acknowledgments

The authors are grateful to dr. Samuele Maramai for recording HR-MS spectra.

Appendix A. Supplementary data

Supplementary data to this article can be found online at https://doi.org/10.1016/j.dyepig.2023.111571.

References

[1] Guignet EG, Hovius R, Vogel H. Reversible site-selective labeling of membrane proteins in live cells. Nat Biotechnol 2004;4:440–4. https://doi.org/10.1038/nbt954.
[2] Griffin BA, Adams SR, Tsien RY. Specific covalent labeling of recombinant protein molecules inside live cells. Science 1998;281:269–72. https://doi.org/10.1126/science.281.5374.269.
[3] Krishnan B, Szymanska A, Gierasch LM. Site-specific fluorescent labeling of polyhistidine sequences using metal-chelating cysteine. Chem Biol Drug Des 2007;69:31–40. https://doi.org/10.1111/j.1747-0285.2007.00463.x.
[4] Wang Z, Ding X, Li S, Shi J, Li Y. Engineered fluorescence tags for in vivo protein labeling. RSC Adv 2014;4:7235–45. https://doi.org/10.1039/C3RA46991C.
[5] Rong L, Zhang C, Lei Q, Qin S-Y, Feng J, Zhang X-Z. A two-photon excitation based fluorogenic probe for sialome imaging in living systems. Adv Sci 2016;3:1500211. https://doi.org/10.1002/advs.201500211.
[6] Lavis LD, Chao T-Y, Raines RT. Fluorogenic label for biomolecular imaging. ACS Chem Biol 2006;1:252–60. https://doi.org/10.1021/cb600132m.
[7] Mei J, Leung NLC, Kwok RTK, Lam JWY, Tang BZ. Aggregation-induced emission: together we shine, united we soar. Chem Rev 2015;115:11718–940. https://doi.org/10.1021/acs.chemrev.5b00263.
[8] Ding D, Li K, Liu B, Tang BZ. Bioprobes based on AIE fluorogens. Acc Chem Res 2013;46:2441–53. https://doi.org/10.1021/ar3003464.
[9] Wu WC, Chen CY, Tian Y, Jang SH, Hong Y, Liu Y, Hu R, Tang BZ, Lee YT, Chen CT, Chen WC, Jen AKY. Enhancement of aggregation-induced emission in dye-encapsulating polymeric micelles for bioimaging. Adv Funct Mater 2010;20:1413–23. https://doi.org/10.1002/adfm.200902043.
[10] Razzano V, Paolino M, Reale A, Giuliani G, Artusi R, Caselli G, Visintin M, Makovec F, Donati A, Villafiorita-Monteleone F, Botta C, Cappelli A. Development of imidazole-reactive molecules leading to a new aggregation-induced emission fluorophore based on the cinnamic scaffold. ACS Omega 2017;2:5453–9. https://doi.org/10.1021/acsomega.7b00789.
[11] Razzano V, Paolino M, Reale A, Giuliani G, Donati A, Giorgi G, Artusi R, Caselli G, Visintin M, Makovec F, Battiato S, Samperi F, Villafiorita-Monteleone F, Botta C, Cappelli A. Poly-histidine grafting leading to fishbone-like architectures. RSC Adv 2018;8:8638–56. https://doi.org/10.1039/C8RA00315G.
[12] Tassone G, Paolino M, Pozzi C, Reale A, Salvini L, Giorgi G, Orlandini M, Galvagni F, Mangani S, Yang X, Carlotti B, Ortica F, Latterini L, Olivucci M, Cappelli A. Xanthopsin-like systems via site-specific click-functionalization of a retinoic acid binding protein. Chembiochem 2022:23. https://doi.org/10.1002/cbic.202100449.
[13] Paolino M, Reale A, Razzano V, Giuliani G, Donati A, Bonechi C, Caselli G, Visintin M, Makovec F, Scialabba C, Licciardi M, Paccagnini E, Gentile M, Salvini L, Tavanti F, Menziani MC, Cappelli A. Nanoreactors for the multi-functionalization of poly-histidine fragments. New J Chem 2019;43:6834–7. https://doi.org/10.1039/C9NJ00279K.
[14] Paolino M, Visintin M, Margotti E, Visentini M, Salvini L, Reale A, Razzano V, Giuliani G, Caselli G, Tavanti F, Menziani MC, Cappelli A. Functionalization of protein hexahistidine tags by functional nanoreactors. New J Chem 2019;43:17946. https://doi.org/10.1039/C9NJ03463C.
[15] Paolino M, Reale A, Razzano V, Giorgi G, Giuliani G, Villafiorita-Monteleone F, Botta C, Coppola C, Sinicropi A, Cappelli A. Design, synthesis, structure, and photophysical features of highly emissive cinnamic derivatives. New J Chem 2020;44:13644–53. https://doi.org/10.1039/D0NJ02429E.
[16] Benincori T, Bongiovanni G, Botta C, Cerullo G, Lanzani G, Mura A, Rossi L, Sannicolò F, Tubino R. Tuning of the excited-state lifetime by control of the structural relaxation in oligothiophenes. Phys Rev B 1998;58:9082–6. https://doi.org/10.1103/PhysRevB.58.9082.
[17] Chen W, Ni S, Wang Y, Pan Y. Electrochemical-promoted nickel-catalyzed reductive allylation of aryl halides. Org Lett 2022;24(20):3647–51. https://doi.org/10.1021/acs.orglett.2c01247.
[18] Lin Y-S, Lin C-Y, Liu C-W, Tsai TYR. A highly active ionic liquid catalyst for Morita–Baylis–Hillman reaction. Tetrahedron 2006;62:872–7. https://doi.org/10.1016/j.tet.2005.10.048.
[19] Rasson C, Stouse A, Boreux A, Cirriez V, Riant O. Copper-catalyzed one-pot borylative aldolisation β-fluoride elimination for the formal addition of acrylates to carbonyl moieties. Chem Eur J 2018;24:9234–7. https://doi.org/10.1002/chem.201802023.
[20] Bou Zeid S, Eid S, Najjar F, Macé A, Rivilla I, Cossío FP, Dorcet V, Roisnel T, Carreaux F. Microwave-assisted 1,3-dioxa-[3,3]-sigmatropic rearrangement of substituted allylic carbamates: application to the synthesis of novel 1,3-oxazine-2,4-dione derivatives. Eur J Org Chem 2022:18–29. https://doi.org/10.1002/ejoc.202101100. 2022.
[21] Moreau J, Giovanella U, Bombenger J-P, Porzio W, Vohra V, Spadacini L, Di Silvestro G, Barba L, Arrighetti G, Destri S, Pasini M, Saba M, Quochi F, Mura A, Bongiovanni G, Fiorini M, Uslenghi M, Botta C. Highly emissive nanostructured thin films of organic host–guests for energy conversion. ChemPhysChem 2009;10:647–53. https://doi.org/10.1002/cphc.200800682.

2.8 RESEARCH ARTICLE: **"Reactivity of a Morita-Baylis-Hillman adduct derivative bearing a triphenylamine moiety with lysine models"**

Authors: **Jacopo Venditti**, Mario Saletti, Marco Paolino, Stefano Contena, Claudia Bonechi, Germano Giuliani, Giorgi Gianluca, Antonella Boccia, Chiara Botta, Lluís Blancafort, Andrea Cappelli

Publication: Chemistry – An Asian Journal

Publisher: ACES (Wiley – VCH)

DOI: doi.org/10.1002/asia.202400617

Supporting information: asia202400617-sup-0001-misc_information.pdf

Contribution: The Ph.D. candidate was engaged in the reactivity studies of the MBHA acetate derivative as a fluorogenic probe toward different lysine models. Subsequently, the Ph.D. candidate carried out ^{1}H NMR spectroscopy analyses (400 MHz) of monoadducts and diadducts obtained, as well as kinetics experiments related to the [2+2] photocycloaddition process. In addition, the Ph.D. candidate contributed to the writing of the synthetic procedures included in the "EXPERIMENTAL SECTION".

ACES Asian Chemical Editorial Society
doi.org/10.1002/asia.202400617
CHEMISTRY AN ASIAN JOURNAL Research Article
www.chemasianj.org

Reactivity of a Morita–Baylis–Hillman Adduct Derivative Bearing a Triphenylamine Moiety with Lysine Models

Jacopo Venditti,[a] Mario Saletti,[a] Marco Paolino,[a] Stefano Contena,[a] Claudia Bonechi,[a] Germano Giuliani,[a] Gianluca Giorgi,[a] Antonella Caterina Boccia,[b] Chiara Botta,[b] Lluís Blancafort,[c] and Andrea Cappelli*[a]

The reactivity of Morita–Baylis–Hillman Adduct (MBHA) derivative **7** was studied with different primary amine derivatives such as *n*-butylamine, Nα-acetyl-*L*-lysine methyl ester, and a poly-(*L*-lysine) derivative as lysine models to obtain information about the possible reactions in complex protein environments. MBHA derivative **7** reacted with *n*-butylamine or Nα-acetyl-*L*-lysine methyl ester producing monoadducts **9a** or **9c**, which showed bright emission features in the green region at 526–535 nm with photoluminescence quantum yield values in solutions of 73% and 51%, respectively. Based on these results, MBHA derivative **7** can be considered an interesting new fluorogenic probe potentially useful in the labelling of basic amino acid residues. Furthermore, similar to other MBHA derivatives, compound **7** showed the tendency to produce diadducts especially in polar solvents system where specific interactions between the extended aromatic moieties may play a major role.

Introduction

Protein labeling currently represents one of the topics of increasing interest owing to its many applications including biosensing, diagnostic imaging, drug development, and targeted drug delivery.[1] This is testified also by the numerous papers reporting the functionalization of proteins or antibodies, which could be useful as drugs versus cancer or infections.[2] The techniques of protein labelling are primarily centered around methods involving the reaction of amino group of lysine or thiol groups of cysteine residues.[3–8] Recently, Morita-Baylis-Hillman adduct (MBHA) derivatives were taken into account in protein labelling owing to the presence in their structure of an activated double bond susceptible to attack nucleophilic groups such as amino or thiol groups.[9–18] The design of suitable probes has become a common motif in recent times in order to make them useful in protein labelling even in complex environments.[19–21] For instance, the design of fluorescent labels has been the focus of increasing attention owing to their potential usefulness in performing studies on protein interactions and function.[22] In particular, a growing interest has been dedicated to the considerable advantages that characterize fluorogenic labeling techniques, which are capable of generating higher signal-to-noise ratio relying on fluorescence activation process following reaction/interaction with specific sites in the protein.[22–24]

Another potential benefit of fluorogens can be the phenomenon called aggregation induced emission (AIE), in other words the ability to emit more in the solid state than in solution.[25,26] Thanks to AIE, fluorogens can show greater photostability, accuracy, and sensitivity when compared to traditional probes that have remarkable emissive properties in solution but often suffer aggregation caused quenching (ACQ) processes at high concentration.[27]

In this context, over the past few years, our research group developed some MBHA derivatives (i.e. compound **1**, Figure 1), which were able to react with imidazole[10,11] or *n*-butylamine[14] affording cinnamic derivatives (i.e. compounds **2**) showing fluorogenic characteristics.

With the aim of extending the π electron system, the substituted phenyl ring of MBHA derivatives **1** and **2** was replaced by naphthalene moiety leading to fluorogenic compounds (i.e. **3a**,**b**), which were found to react with imidazole with the formation of monoadducts or diadducts showing AIE features.[11] Furthermore, the reactivity of the newly-designed naphthalene MBHA derivatives **3a**,**b** was investigated in model proteins. The interesting results obtained demonstrated the ability of **3a** to interact and functionalize lysine side chains in lipophilic pockets,[14] while **3b** found applications in the PEGylation of poly-histidine tags of engineered proteins (Figure 1).[12,13]

In the investigations focused on the optical features of polybenzofulvene derivatives,[28–56] we were capable of recognizing cinnamic derivatives **4**, **5**, and **6** (Figure 2) as interesting fluorogenic compounds provided with photoluminescence

[a] J. Venditti, M. Saletti, M. Paolino, S. Contena, C. Bonechi, G. Giuliani, G. Giorgi, A. Cappelli
Dipartimento di Biotecnologie, Chimica e Farmacia, Università degli Studi di Siena, Via Aldo Moro 2, 53100 Siena, Italy
Tel: +39 0577 232416
E-mail: andrea.cappelli@unisi.it
[b] A. C. Boccia, C. Botta
Istituto di Scienze e Tecnologie Chimiche "G. Natta" - SCITEC (CNR), Via A. Corti 12, 20133 Milano, Italy
[c] L. Blancafort
Department of Chemistry, Institute of Computational Chemistry and Catalysis, University of Girona, C/ M. A. Capmany 69, 17003 Girona, Spain
Supporting information for this article is available on the WWW under https://doi.org/10.1002/asia.202400617

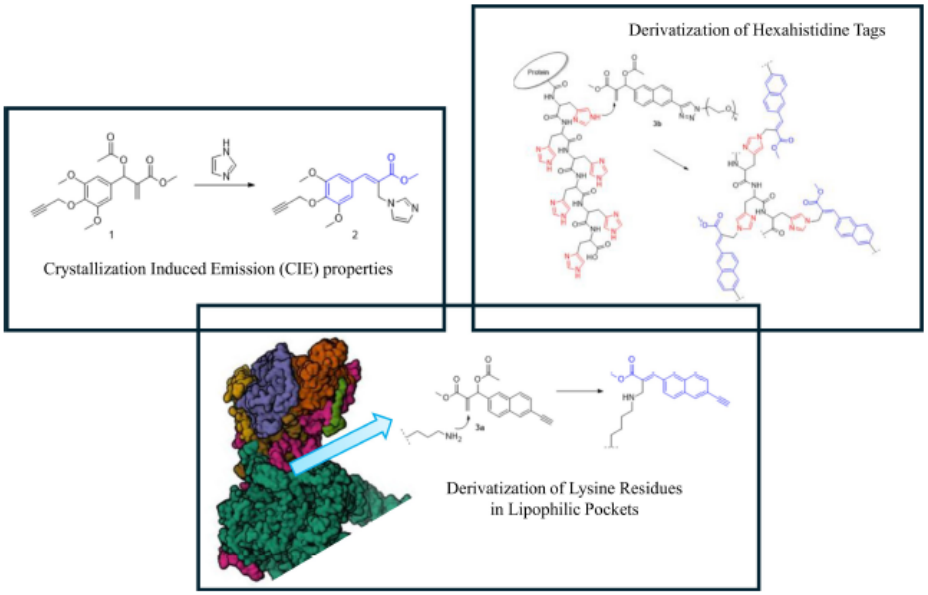

Figure 1. Structures of MBHA derivatives **1** leading to **2**, and MBHA derivatives **3a,b** involved in site-specific protein derivatization.

quantum yield (PL QY) values ranging from 57% to 80% and emission maxima in the range of 407–540 nm.[57]

The promising findings obtained with triphenylamine derivative **6** stimulated the design of MBHA derivative **7**, which was synthesized and characterized from the point of view of its photophysical and photochemical features.[15] Interestingly, the photophysical and photochemical characterization studies confirmed the promising properties of the cinnamic portion present in derivatives **6**, **11** and **12** (Figure 2).[15] It is noteworthy that the shift of the double bond from the acrylic position (i.e. as in compounds **7** and **10**) to the cinnamic one of **6**, **11** and **12** compound produced a significant red-shift in the emission maxima of about 130–150 nm.[15] MBHA derivative **7** was found to show intriguing AIE features since a bright blue emission (478 nm) was observed when its microaggregates were formed in DMSO-water dispersions.[17] Moreover, **7** was found to react with human serum albumin (**HSA**) providing green fluorescent albumin (**GFA**) derivatives and switching its emission from the blue to the green-yellow (525 nm) in **GFA**.[17] Docking studies were performed to evaluate the potential interaction of **7** with the lipophilic pockets present in **HSA** structure, and the obtained results proposed a possible interaction between the acrylic activated moiety with Lys199 driving to the addition-elimination reaction.[17]

Thus, in the present work we investigated on the behaviour of **7** in reacting with *n*-butylamine, Nα-acetyl-*L*-lysine methyl ester, and a poly-(*L*-lysine) derivative as models of the lysine amino acid residues. In our hypothesis, *n*-butylamine represented the simplest model of lysine residues, whereas Nα-acetyl-*L*-lysine methyl ester represented the isolated model of lysine residues, and the poly-(*L*-lysine) derivative represented the model of lysine inserted in the homopolymer.

Results and Discussion

Reactivity of MBHA Derivative 7 with Models of Lysine Residues

First, MBHA derivative **7** was tested in reactivity characterization studies with *n*-butylamine (pKa = 10.8) as the simplest model of the basic amino acid residues lysine and the results are shown in Scheme 1.

Compound **7** reacted quickly with a large (i.e. five-fold) excess of *n*-butylamine in chloroform at room temperature. In particular, the reaction was almost complete after 6 h in agreement with the high nucleophilicity of *n*-butylamine, and provided monoadduct **9a** as the major reaction product (yield 66%) along with significant amount of diadduct **9b** (yield 13%). This result was found to be in full agreement with the ^{1}H NMR spectrum of the reaction mixture (Figure SI-1).

When the amount of butylamine was reduced from the large to a slight excess (i.e. 1.5:1) the reaction was found to slow down (i.e. it was almost complete after stirring at room temperature for 48 h), and the composition of the reaction mixture was found to be relatively different to that obtained in the large excess. In particular, the monoadduct **9a** was isolated in 49% yield, whereas the diadduct **9b** was obtained in 36%

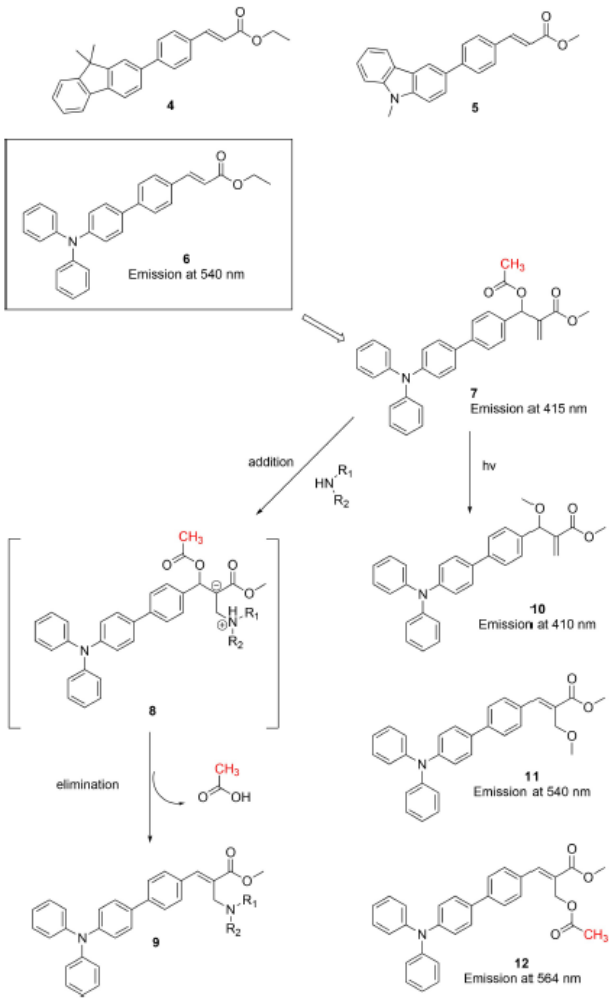

Figure 2. Structure of fluorescent cinnamic derivatives **4–6** and design of reactive MBHA derivative **7** leading to acrylic derivative **10** and cinnamic derivatives **9**, **11**, **12**.

yield, in agreement with the ^{1}H NMR spectrum of the reaction mixture (Figure SI-2).

On the other hand, the reaction of **7** with *n*-butylamine hydrochloride in acetonitrile in the presence of phosphate buffered saline (PBS) solution at room temperature was very slow in agreement with the probable protonation state, which decreased its nucleophilicity. In fact, after stirring at room temperature for 24 h, only negligible amounts of MBHA derivative **7** were reacted. However, the heating of the reaction mixture at refluxing conditions allowed the completion of the reaction in reasonable time.

For example, the reaction of **7** with a large (i.e. five-fold) excess of *n*-butylamine hydrochloride was virtually complete after 24 h, and provided with the monoadduct **9a** in 52% yield and the diadduct **9b** in 39% yield according to the ^{1}H NMR spectrum of the reaction mixture (Figure SI-3).

Similarly, the reaction of **7** with a slight excess (i.e. 1.5:1) of *n*-butylamine hydrochloride was virtually complete after refluxing for 24 h. In this way, monoadduct **9a** was isolated in 16% yield, while diadduct **9b** was isolated as the main reaction product (i.e. yield 73%), in agreement with ^{1}H NMR spectrum of the reaction mixture (Figure SI-4).

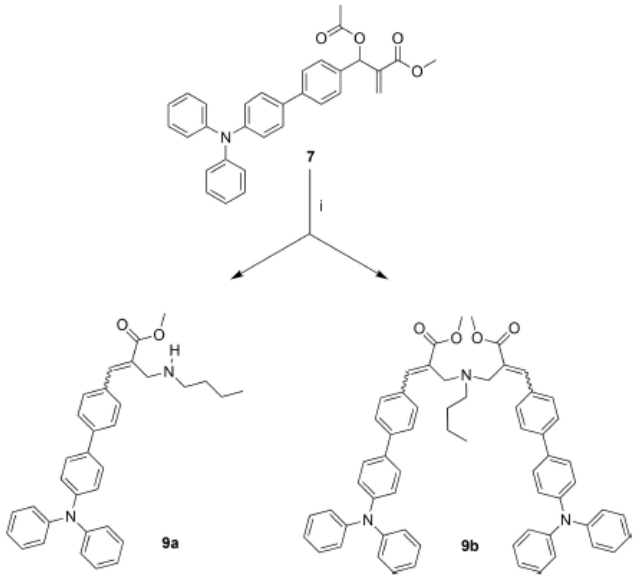

Scheme 1. Reaction of MBHA derivative **7** with *n*-butylamine. Reagents: (i) *n*-butylamine, $CHCl_3$ (or *n*-butylamine hydrochloride, CH_3CN, H_2O, PBS).

Overall, these results confirmed the propensity of MBHA derivatives to produce diadducts.[11,18] It is noteworthy that this propensity appeared more pronounced in polar solvent systems such as acetonitrile-water than in chloroform. This observation led to suspect that the driving force for the diadduct formation could be a specific interaction between the extended aromatic moieties of the fluorophores.

In order to obtain information about the reactivity of compound **7** with a more complex molecular system than *n*-butylamine, Nα-acetyl-*L*-lysine methyl ester was selected as amino acid model (Scheme 2).

As expected, the reaction of compound **7** with a little excess (i.e. 1.5 equivalents) of Nα-acetyl-*L*-lysine methyl ester hydrochloride in acetonitrile in the presence of phosphate buffered saline (PBS) at room temperature was very slow. Therefore, refluxing conditions were applied to carry out the reaction in reasonable times (i.e. 24 h). In this way, monoadduct **9c** was obtained in low yield (i.e. 14%), whereas diadduct **9d** represented the major reaction product and was isolated in 77% yield by flash chromatography separation of the reaction mixture, in agreement with the results obtained in the reaction of **7** with *n*-butylamine hydrochloride in the same conditions.

Finally, the reactivity of MBHA derivative **7** was evaluated by using *n*-butyl-poly-(*L*-lysine) (**BPLL**) hydrochloride (Iris Biotech GMBH) as the most complex model of lysine residues (Scheme 3).

The reaction was performed in deuterated DMSO in 5 mm NMR tubes to allow the reaction kinetics to be followed by ^{1}H NMR spectroscopy, and different excess (i.e. around 12:1, 6:1, and 3:1) of lysine residues were evaluated (Figures SI-5, SI-6, SI-7). The reaction progress was evaluated by monitoring the decrease of the signal (at around 2.10 ppm) attributed to the methyl group of acetyl moiety of MBHA derivative **7**, and the appearance of the signal (at around 1.90 ppm) attributed to acetate, which was liberated during the reaction. The comparative analysis of the results suggested that the reaction was rather slow also at 50 °C and remained incomplete after 24 h also in the large excess of lysine residues.

The same experiments were then repeated in the presence of suitable amounts of DIPEA as the base (Figures SI-8, SI-9, SI-10). As expected, the presence of DIPEA played a crucial role allowing the reaction to go rapidly to completion also in the case of low excess of lysine residues (Figure SI-10) that led to highly conjugated poly-(*L*-lysine) derivatives.

These results highlighted the importance of the protonation state of lysine residues in the reaction with MBHA derivative **7**. Owing to the probable protonation state of the solvent-exposed lysine derivatives, compound **7** could be proposed as a selective reagent for nucleophilic amino acid residues embedded into lipophilic pockets of suitable accessibility. As suggested by the examination of the 3D-structure of water-soluble proteins such as **HSA** obtained by crystallographic studies, the lysine residues located inside the protein structure establish charge assisted H-bond interactions with suitable counterparts, which can produce an increased nucleophilicity and therefore an increased reactivity. Moreover, the initial binding recognition step could be determinant in governing reactivity and selectivity of MBHA derivatives towards proteins. In other words, the suitable binding affinity and orientation in the pocket containing the reactive amino acid residue could

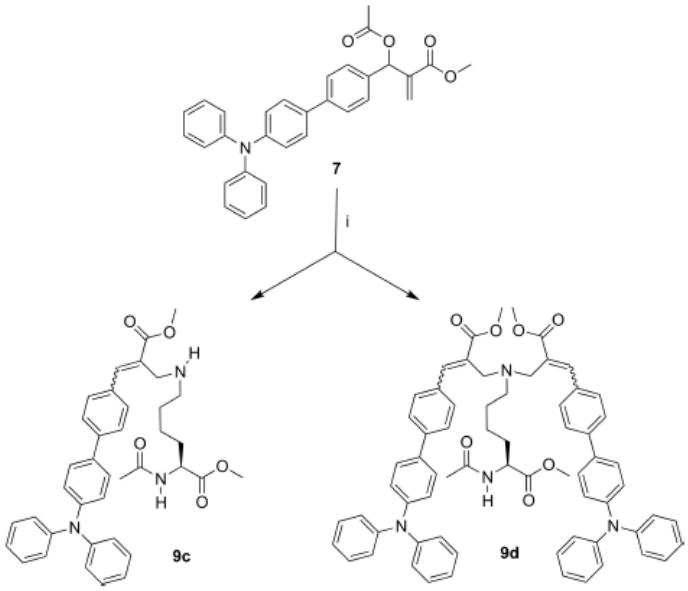

Scheme 2. Reaction of MBHA derivative **7** with Nα-acetyl-*L*-lysine methyl ester. Reagents: (i) Nα-acetyl-*L*-lysine methyl ester hydrochloride, CH_3CN, PBS, H_2O.

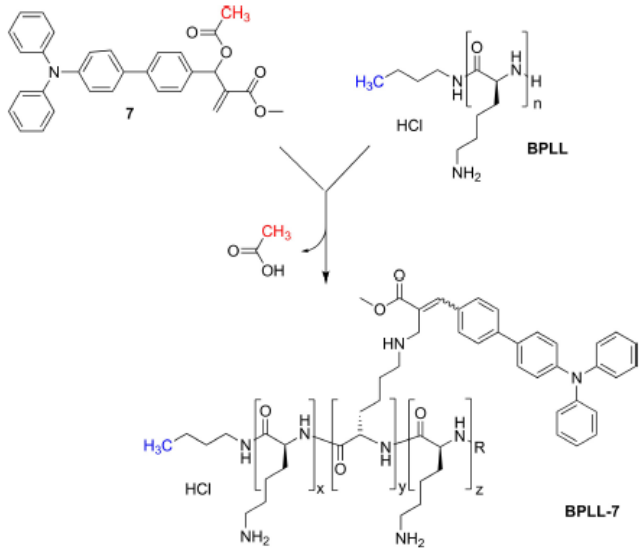

Scheme 3. Reaction of MBHA derivative **7** with *n*-butyl-poly-(*L*-lysine) (**BPLL**). Reagents: (i) DMSO-d_6.

play a key role in producing the desired selectivity. Finally, we assume that in the context of the reaction of MBHA derivatives with reactive amino acid residues embedded into lipophilic pockets, the propensity to the formation of diadducts should be largely reduced.

Structure of of Monoadduct 9a and Diadduct 9b

The structure of the major diastereomer of monoadduct **9a** was studied along with that of the major diastereomer of diadduct **9b** by NMR spectroscopy, molecular modeling, and mass spectrometry techniques.

The purity of the samples used in the structural characterization was evaluated by RP-HPLC with the following experimental set-up: a column ZORBAX eclipse XDB–C8 4.6×150 mm 5 μm; an isocratic elution with a ternary solvent mixture composed by 70% methanol, 20% acetonitrile, and 10% water containing 0.2% formic acid; flow = 1.25 mL/min; analysis time = 10 min.

The purity of monoadduct **9a** was found higher than 94% with the main impurity being the corresponding minor diastereomer, while the purity of diadduct **9b** was around 80% in all the batches synthesized, with the minor diastereomers being the main impurities.

The stability of **9a,b** solutions in DMSO was evaluated by ^{1}H NMR spectroscopy. The ^{1}H NMR spectra performed (in DMSO-d_6) after storage of the solutions at room temperature for one week were perfectly consistent with those performed immediately after the preparation. Similarly, the stability as glassy solids stored in closed vials at room temperature (for more than one month) was confirmed by ^{1}H NMR spectroscopy.

The presence of a cinnamic fluorophore in structure of monoadduct **9a** could lead to the possible existence of two geometric isomers showing (*E*) and (*Z*) configurations. The results of NMR studies suggested for the most abundant isomer **9a** a three-dimensional (3D) structure with the cinnamic moiety showing the trans (*E*) configuration at the double bond, as supported by the chemical shift value of the acrylic proton (D). On the other hand, the presence of two cinnamic fluorophores in structure of diadduct **9b** could lead to the possible existence of three geometric isomers, namely (*E*,*E*), (*E*,*Z*), and (*Z*,*Z*). The NMR spectrum suggested for the most abundant isomer **9b** a highly symmetric three-dimensional (3D) structure, with the two cinnamic moieties showing the trans (*E*) configuration at the double bond, as supported by the chemical shift value of the acrylic proton (D). Owing to both the relative complexity of the NMR spectrum and the relatively low amounts, the minor diastereomers of **9b** were not taken into consideration in the NMR studies.

The structures of (*E*)-**9a** and (*E*,*E*)-**9b** were assigned by NMR experiments and by crossing mono- and two-dimensional data. The characteristic chemical shift values of the carboxylic ester groups [167.9 ppm in (*E*)-**9a** and 168.4 ppm in (*E*,*E*)-**9b**] were used as the starting points in the assignment of the olefinic proton D [signals at 7.70 ppm (140.2 ppm) in (*E*)-**9a** and 7.75 ppm (141.3 ppm) in (*E*,*E*)-**9b**] and the adjacent methylene protons (C) at 3.49 ppm (45.4 ppm) in (*E*)-**9a** and 3.49 ppm (49.8 ppm) in (*E*,*E*)-**9b**, according to the ^{1}H-^{13}C correlations in the HMBC spectrum (Table 1).

Interestingly, the comparison of the chemical shift values shown by diadduct (*E*,*E*)-**9b** with the corresponding ones of monoadduct (*E*)-**9a** showed the existence of up-field shifts in the signals attributed to protons G, J, O, P, N, and K (Figure 3).

Table 1. Assignment of NMR signals of monoadduct (*E*)-**9a** and diadduct (*E*,*E*)-**9b**.

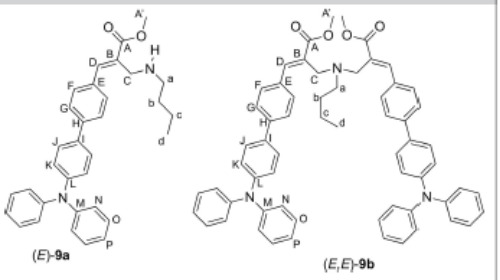

	(*E*)-**9a** DMSO-d_6		(*E*,*E*)-**9b** DMSO-d_6	
	^{1}H (ppm)	^{13}C (ppm)	^{1}H (ppm)	^{13}C (ppm)
b	1.39	31.3	1.39	27.5
c	1.31	19.9	1.15	20.1
d	0.86	13.8	0.77	13.8
a	2.54	48.7	2.39	53.3
C	3.49	45.4	3.49	49.8
A'	3.75	51.9	3.68	51.9
K	7.03	122.9	6.95	122.7
N	7.06	124.3	7.02	124.3
P	7.07	123.4	7.05	123.4
O	7.33	129.6	7.30	129.6
G	7.70	126.0	7.51	125.8
J	7.65	127.6	7.52	127.6
F	7.70	130.5	7.71	131.2
D	7.70	140.2	7.75	141.3
A		167.9		168.4
B		129.6		129.3
E		133.2		133.1
H		140.0		140.0
I		132.8		132.6
L		147.1		147.1
M		146.9		146.8

This observation suggested the existence of specific interactions between the aromatic moieties in the structure of diadduct (*E*,*E*)-**9b**.

This assumption was also evaluated in the light of the dipolar correlations observed in NOESY experiments, which provided us with the information on the dipolar connectivity shown in Table 2.

The most important information from the comparative analysis of NOESY spectra was that an apparent dipolar interaction between the protons F and a was observed in diadduct (*E*,*E*)-**9b**. This observation suggested a possible interaction (in the 3D space) of the butyl sidechain with the cinnamic fluorophore in spite of their apparent distance in the

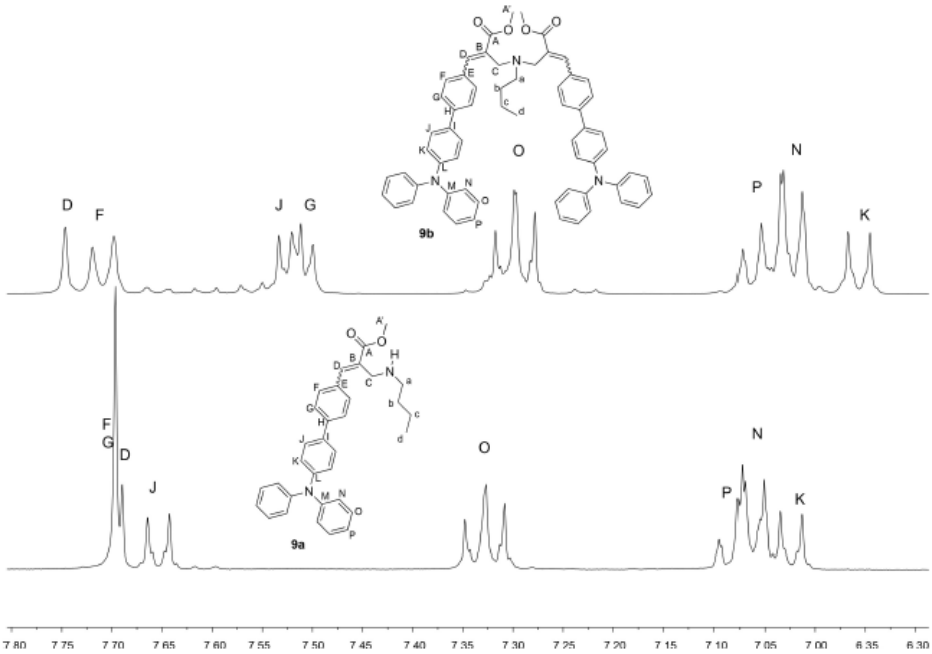

Figure 3. Comparison of the aromatic region of ^{1}H NMR (400 MHz, DMSO-d_6) spectrum of monoadduct **9a** and diadduct **9b**. The up-field shifts observed in the signals attributed to protons G, J, O, P, N, and K support the establishment of specific interactions between the aromatic moieties in the diadduct **9b**.

molecule. On the other hand, only obvious dipolar interactions were observed in the NOESY spectrum of mono adduct **9a**.

Overall, the results of the NMR studies provided evidence on the compactness of the 3D structure of diadduct (*E,E*)-**9b** that was stabilized by the establishment of stacking interactions between its extended aromatic moieties.

Owing to the structural information obtained by the NMR studies, the (*E,E*)-stereoisomer of **9b** was chosen as the starting geometry for the optimizations in DMSO. The results obtained are shown in Figure 4.

The calculations suggested a structure with the aromatic moieties arranged into a π-π stacking due to the non-covalent interactions between the π bonds of the aromatic rings. If we consider the molecular orbitals shown in Figure 5, in addition to the typical π-conjugation on the aromatic substituents, the orbital overlap caused by the stacking of aromatic rings can be easily identified in both ground and excited states.

Once the most probable structure of (*E,E*)-**9b** was determined, we focused our attention on its theoretical spectroscopic features in both DCM and DMSO as implicit solvents.

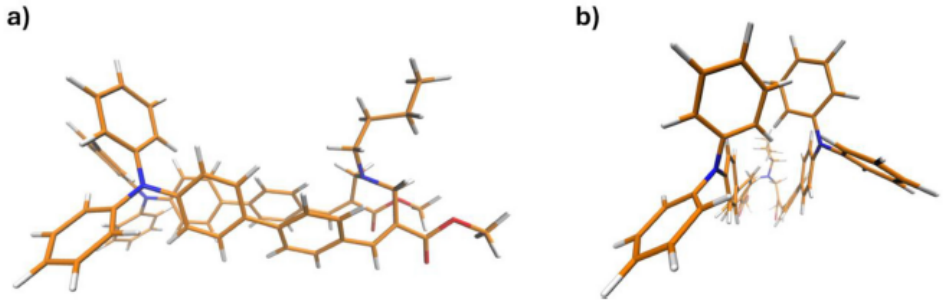

Figure 4. Optimized ground state structure of (*E,E*)-**9b** in DMSO as the solvent. (a) Side view and (b) front view.

Table 2. Dipolar correlations in monoadduct (*E*)-**9a** and diadduct (*E,E*)-**9b** obtained by NOESY experiments performed in DMSO-d_6.

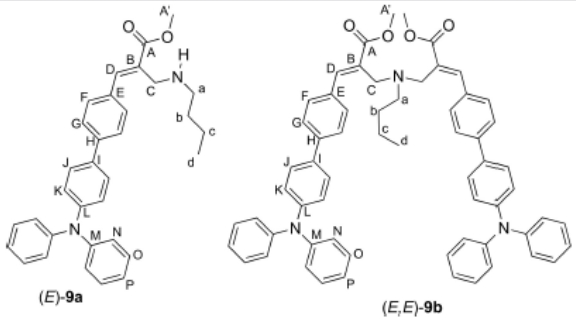

		Cross-peak volume					
		(*E*)-**9a**			(*E,E*)-**9b**		
Proton	Proton	Small	Medium	Large	Small	Medium	Large
D	C					X	
D	a				X		
F	C						x
F	a					X	
F	b				X		
C	a						x
C	d					X	
C	b						x
a	d				X		
a	b			x	X		
c	d			x			
J	C					X	
J	a				X		
J	b				X		
J	K			x			
O	P			x			
O	N			x			

Figure 5 shows the geometries obtained of the ground state (S_0), the Frank-Condon point (FC), the first excited state singlet emitter (S_1), and the distorted ground state after radiative relaxation, in DCM. The simulations of **9b** were also carried out in DMSO and the results are reported in the Supporting Information (Figure SI-11). As can be seen, the change of solvent does not show any effect on the spectroscopic properties of the molecule, and this is likely due to the lipophilicity of its aromatic and aliphatic chains. Indeed, the effects of solvents on the spectroscopic properties of molecules (solvatochromism) are often driven by affinity between solute and solvent, such as the polarity of the solvents and the ability to form hydrogen bonds with the solute.[58,59] In our case, the spectroscopic properties of the strong lipophilic compound **9b** appear to be unaffected by the substitution of polar aprotic solvents (DMSO/DCM).

Anyway, for each structure the HOMO/LUMO molecular orbitals involved in the electronic transition and the relative energy gap are reported. By comparison of the experimental data (see below Table 3) with the calculated ones, a good correlation regarding the absorption energy values can be noted. Specifically, the vertical excitation wavelength computed at the FC point in DCM (3.7 eV or 336 nm) shows a slight blue-shift with respect to the experimentally observed one (3.5 eV or 356 nm).

Starting from the FC structures, adiabatic relaxation on the first excited state S_1 was simulated (red arrows in Figure 5) to obtain geometries and relative wavelengths of the emitting intermediates. Comparing the values of Table 3 and of Figure 5, the calculation shows an emission energy in good agreement with the experimental one (2.35 eV or 528 nm and 2.33 eV or 532 nm). As previously mentioned, in DMSO the calculated

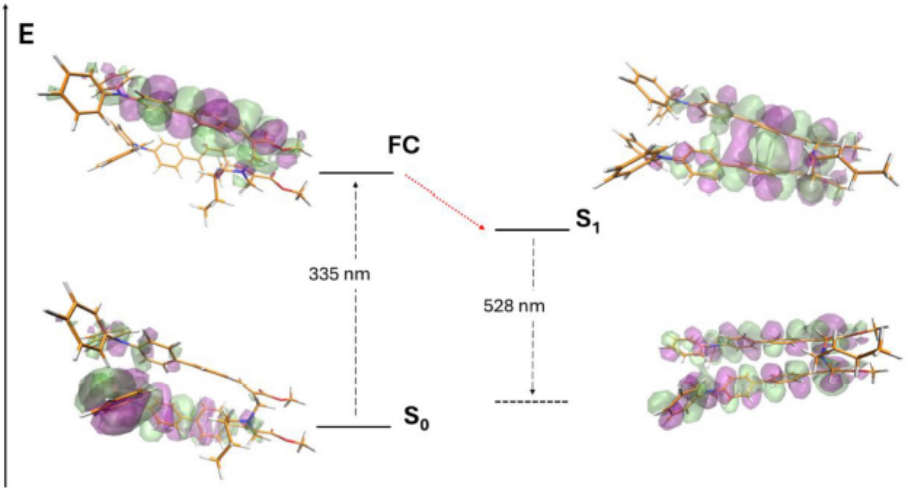

Figure 5. Schematic representations of (*E,E*)-**9b** fluorescence cycle in DCM. The molecular orbital (HOMO/LUMO) involved in electron transitions and relative energies, are shown for vertical excitation (Frank-Condon point, FC) and emission, from the optimized geometries. The red line stands for the adiabatic relaxation pathway on first singlet exited state (S_1).

Table 3. Comparison of the optical properties of compounds **9a–d** and **13** with those of model cinnamic derivative **6**, **11**, and **12** (see reference 15).

	Solution[a]			Solid-state			
	λ_{ab} (nm)	λ_{em} (nm)	QY[b] (%)	τ[c] (ns)	λ_{em} (nm)	QY[d] (%)	τ_{av}[e],[*] (ns)
9a	290, 363	526	73	3.05	485	45	2.05
9b	295, 359	405 526	29[f] 13	1.56[*] 1.42[§,#]	480	16	1.58
9c	296, 357	535	51	3.38[#]	530	5	1.44
9d	296, 356	408 524	43[f] 29	1.6[*] 2.82[§,#]	520	13	2.11
13	331	406	43[f]	1.60	450	39	1.96
6	292, 371	540	78	3.32	470	80	3.02
7	330	415	3	0.35			
10	242, 332	411	2	0.41	440	41	2.89
11	292, 362	540	75	3.36	485	46	3.00
12	290, 367	564	58	3.52	504	43	2.61

[a] dichloromethane, [b]] λ_{ex} = 365 nm; [c] λ_{ex} = 300 nm, [d] λ_{ex} = 390 nm, [e] λ_{ex} = 407 nm, [f] λ_{ex} = 330 nm; τ = lifetime from mono-exponential decay fit; τ_{av} = average lifetime $\tau av = \frac{\sum_{n=1}^{n} A_n \tau_n^2}{\sum_{n=1}^{n} A n \tau_n}$, [#] from bi-exponential fit, [°] from three-exponential fit; [*] λ_{em} = 406 nm; [§] λ_{em} = 526 nm.

spectroscopic results are comparable to those in dichloromethane (see Figure SI-11).

Mass spectrometry studies performed on monoadduct **9a** with a mass spectrometer (Agilent 1100 LC/MSD) equipped with an electrospray source (ESI) revealed the presence of a peak at *m/z* 491 attributed to the protonated molecule (representing the base peak of the spectrum) along with another high intensity peak at *m/z* 418, which was assumed to be produced by a retro-aza-Michael reaction of **9a** protonated molecule (Scheme 4).

This result suggested a certain degree of lability of the bond connecting the cinnamic fluorophore to the butylamine nitrogen owing to the apparent high stability of the fragment showing a mass value of *m/z* 418. It should be noted that the positive charge could be stabilized by resonance over the entire structure of the fragment.

On the other hand, the mass spectrum obtained with diadduct **9b** showed the presence of a peak at *m/z* 908 attributed to the protonated molecule along with some other low intensity peaks, suggesting the higher stability of diadduct

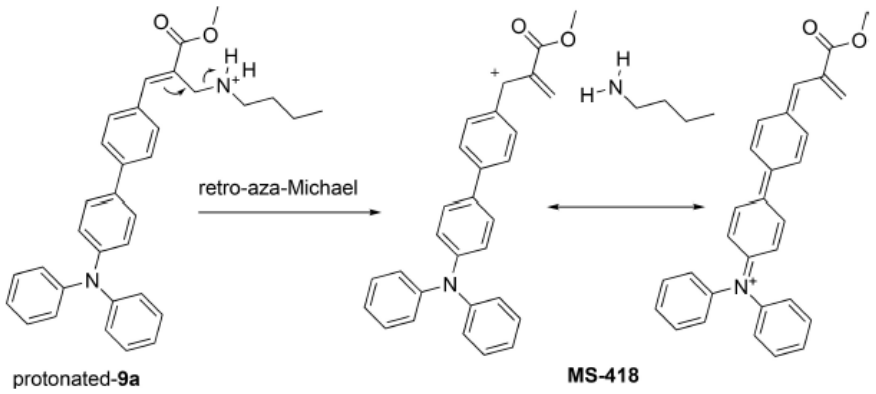

Scheme 4. Mechanistic hypothesis for the fragmentation of compound **9a**.

9b with respect to monoadduct **9a** in the gas phase conditions of the mass spectrometry experiments. Similar results were obtained by the high resolution mass spectrometry measurements performed with a timsTOF spectrometer (Bruker, Bremen, D) equipped with an electrospray source (ESI).

Photophysical Properties of the Newly Synthesized Compounds

We previously reported that cinnamic derivative **6** showed an emission maximum at 540 nm with photoluminescence quantum yield (PL QY) values of 78% in solution and of 80% in the crystalline state.[57] Therefore, these outstanding photophysical properties stimulated the development of MBHA derivative **7**,[16,17] which was very reactive towards *n*-butylamine (see above). Thus, the corresponding cinnamic derivatives **9a**,**b** were characterized from the point of view of their photophysical features.

At first sight, the optical features of monoadduct **9a** in solution were very promising and similar to those shown by models cinnamic derivative **6**, which share the same fluorophore. In particular, compound **9a** showed a significant emission spectrum in dichloromethane solution at low concentration values that was characterized by a large asymmetric peak with a maximum at 526 nm (Figure 6, left) and a PL QY value of 73%.

On the other hand, a double component emission was observed in the PL spectrum of diadduct **9b** (Figure 6, right), suggesting the presence of two emitting species in solution. In fact, the relative intensities of the two components were excitation dependent (see the spectra at three different

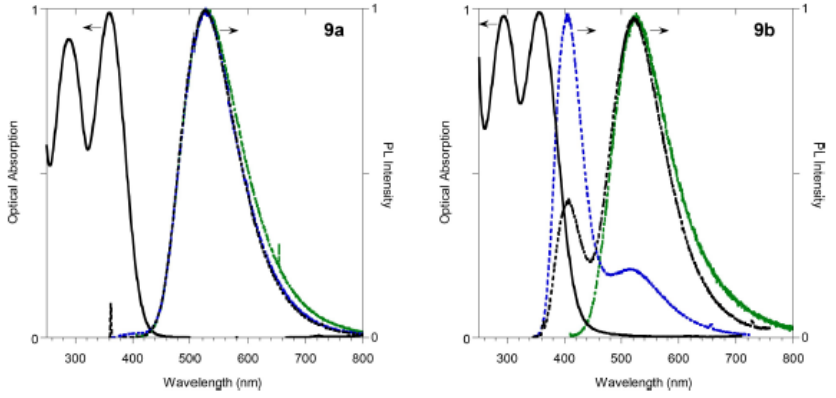

Figure 6. Normalized absorption (black solid line) and PL spectra (dashed lines) of monoadduct **9a** (left) and diadduct **9b** (right) in dichloromethane solutions at different excitation wavelengths (330 nm, blue; 365 nm, black; 408 nm, green). The measurements are performed with freshly prepared solutions at about 10^{-5} M concentrations.

excitation wavelengths in Figure 6, right). In particular, **9b** showed a low energy component at around 526 nm coincident with the emission spectrum of monoadduct **9a** and a high energy component (at around 405 nm), not related with the emission of the **9b** structure (see Figure SI-12), suggesting the possible formation of a new chemical entity responsible for the high energy emission.

Very interestingly a similar behavior was observed in the couple of structurally related monoadduct **9c** and diadduct **9d** (Figure 7).

In fact, the results obtained with the lysine derivatives **9c,d** confirmed the bright emission features of monoadduct derivative **9c** at 535 nm (PL QY = 51 %) in dichloromethane and the double emission of the diadduct derivative **9d** with the low energy component at 524 nm and the high energy component at 408 nm. Also in this case the high energy emission appeared to be not related with the low energy component and with the structure (see the different excitation profiles in Figure SI-13), of **9d** advocating the possible formation of a new chemical entity responsible for the high energy emission. Therefore, we assumed that the high energy peaks at around 405–408 nm could be generated by the products of the [2+2] photocycloaddition promoted by the excitation (see the Photochemical Properties section below).

The photophysical features of compounds **9a–d**, and **13** are summarized in Table 3 for both the solid state (i.e. solid casted films) and the solutions and compared with those of the previously reported model compounds **6**, **7**, **10**, **11**, and **12** (see Table 3).[15]

The comparison of the photophysical properties of the whole series of compounds both in solution and in the solid state allows us to draw some important conclusions. First, the similarity of the emission observed for compounds **9a** and **9c** to that of compound **6** in solution suggests its assignment to the common cinnamic derivative. Secondly, the high energy emission component observed at 405–408 nm for compounds **9b** and **9d** suggests the occurrence of a photochemical reaction leading to similar photoproducts, as discussed in the next section. In the solid state, due to the higher stability of the compounds and the efficient migration processes to the lower energy emitting states, compounds **9a** and **9b**, as well as **9c** and **9d**, display the same emission position at about 480 nm and 520 nm, respectively.

Photostability of Compounds 9 a,b

Further characterization studies were then performed on compounds **9a,b** in order to assess their potential photostability. On the basis of the UV-vis absorption spectra, the solutions of the two compounds in deuterated dichloromethane were irradiated with monochromatic light centered at either 365 nm or 420 nm to probe their reactivity, and this was followed via ^{1}H NMR spectroscopy by recording spectra at regular time intervals (i.e. 0 min, 15 min, 30 min, 1, 2, 4, 8, and 24 h).

First, a solution of **9a** in deuterated dichloromethane (ca. 1.4×10^{-2} M) contained into a 5 mm NMR Pyrex tube was irradiated with monochromatic light centered at either 365 nm or 420 nm until a photo-stationary state was reached. Interestingly, compound **9a** showed a high photostability in these conditions since the irradiation produced only a slight change in the composition of the diastereomeric *E/Z* mixture. In particular, we observed a very small change in the composition of the diastereomeric *E/Z* mixture from (90:10) to (93:7) (Figure SI-14) at 365 nm, and a variation from (90:10) to (80:20) (Figure SI-15) at 420 nm. This *E/Z* ratio was obtained from the integral values of the signals attributed to the same protons in the two diastereomeric species. In particular, the formation of (*Z*)-**9a** was supported by the increase in intensity of the H–D signal at 6.85 ppm, the H–A' signal at 3.73 ppm, and H–C signal at 3.62 ppm.

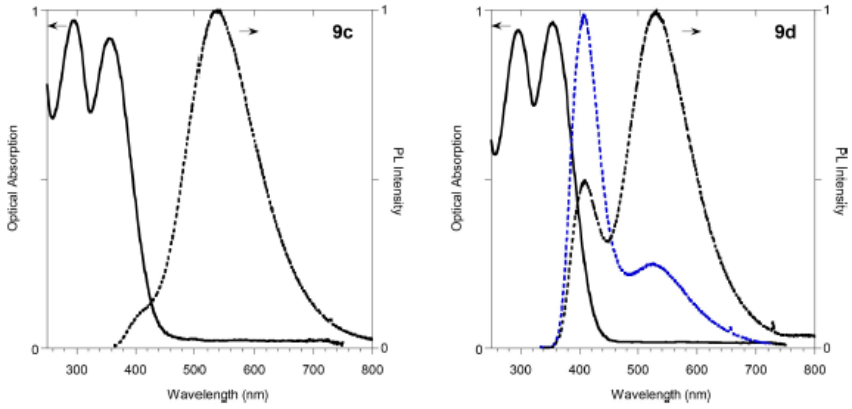

Figure 7. Normalized absorption (black solid line) and PL spectra (dashed lines) of monoadduct **9c** (left) and diadduct **9d** (right) in dichloromethane solutions at different excitation wavelengths (330 nm, blue; 365 nm, black). The measurements are performed with freshly prepared solutions at about 10^{-5} M concentrations.

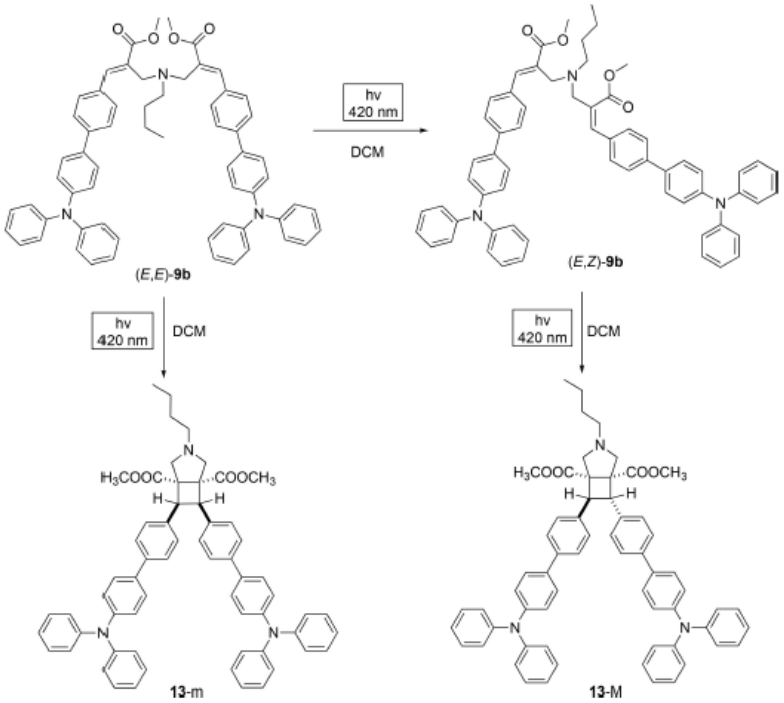

Scheme 5. [2+2] Photocycloaddition of compound **9b** leading to **13**.

Despite the high photostability shown by monoadduct **9a**, the irradiation of diadduct **9b** in the same conditions led to the formation of several chemical species as indicated by the ^{1}H NMR analysis (Figures SI-16 and SI-17). At the preparative scale it was possible to isolate compound **13-M** as the main photoproduct (Scheme 5). This product results from a [2+2] photocycloaddition between the double bonds of the two cinnamic acid groups, leading to a cyclobutane ring. This photochemical process is allowed by the Woodward-Hoffmann rules and has been well studied, for instance, in thymine derivatives.[60] The frontier molecular orbitals of **9b** at the S_1 minimum (right hand side of Figure 5) display antibonding interactions between the orbitals of the two π systems in the HOMO and bonding interactions in the LUMO, which is similar to what is found in a pair of π stacked thymine molecules. This supports our mechanistic assignment.

The characterization of the optical features of **13** confirmed the emission properties this compound (Figure 8) with a very intense band at around 406 nm with a PL QY value of 43% in dichloromethane solutions and a lifetime value of 1.60 ns, in agreement with the results obtained for the high energy emission component of **9b** and **9d** (see Table 3). Interestingly, compound **13** was obtained as a white solid retaining the emission features also in the solid state. For instance, in the film cast from dichloromethane we observed a red shifted emission at 450 nm with a PL QY value of 39%.

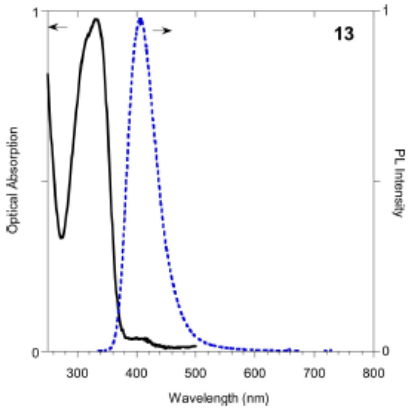

Figure 8. UV-visible absorption (black solid line) and PL spectrum (dashed blue line, excitation at 330 nm) of compound **13** in dichloromethane solution. The concentration values were 10^{-5} M for the absorption spectrum and 10^{-8} M or 10^{-7} M for the emission spectrum.

The comparison of Figure SI-16 with Figure SI-17 suggested that compound **13** appeared to be rather photostable against

irradiation at 420 nm, whereas apparent decomposition signs appeared when irradiated at 365 nm. Notably, the absence of absorption at 420 nm in the spectrum of compound **13** explained the observed photostability against visible irradiation, which can be used to profitably convert diadduct **9b** to compound **13**.

Conclusion

Motivated by the postulated reaction with a lysine residue into a lipophilic pocket of the human serum albumin, the reactivity of MBHA derivative **7** was studied with *n*-butylamine, Nα-acetyl-*L*-lysine methyl ester, and a poly-(*L*-lysine) derivatives as lysine models to obtain information about the possible reactions in complex protein environments.

The results obtained in the present work stressed the importance of the protonation state of lysine residues in the reaction with MBHA derivative **7**. Owing to the probable protonation state of the solvent-exposed lysine derivatives, compound **7** could be proposed as a selective reagent for nucleophilic amino acid residues embedded into lipophilic pockets of suitable accessibility. As suggested by the examination of the 3D-structure of water-soluble proteins such as **HSA** obtained by crystallographic studies, the lysine residues located inside the protein structure establish charge assisted H-bond interactions with suitable counterparts, which can produce an increased nucleophilicity and therefore an increased reactivity. Moreover, the initial binding recognition step could be determinant in governing reactivity and selectivity of MBHA derivatives towards proteins. In other words, the suitable binding affinity and orientation in the pocket containing the reactive amino acid residue could play a key role in producing the desired selectivity.

The reaction of MBHA derivative **7** with *n*-butylamine or Nα-acetyl-*L*-lysine methyl ester produced monoadducts **9a** or **9c**, respectively, both showing bright emission features (526 nm and 535 nm, respectively) in the same range of the one observed with green-fluorescent **HSA** (i.e. 525 nm),[17] and PL QY values in solutions of 73% and 51%, respectively. This result places MBHA derivative **7** in an outstanding position as a new fluorogenic probe potentially useful in the labelling of basic amino acid residues.

Moreover, the peculiar reactivity shown by MBHA derivative **7** confirmed the tendency of MBHA derivatives to produce diadducts, and this tendency appeared more pronounced in polar solvent systems (i.e. acetonitrile-water). This observation led us to consider the specific interactions between the extended aromatic moieties of diadduct (*E*,*E*)-**9b** fluorophores as the driving force for the diadduct formation, and the results of the NMR studies supported the existence of these specific interactions. However, in the context of the reaction of MBHA derivatives with reactive amino acid residues embedded into lipophilic pockets, the propensity to the formation of diadducts should be largely reduced.

Experimental Section

Synthesis

Merck silica gel 60 (230–400 mesh) was used for column chromatography. Merck TLC plates, silica gel 60 F_{254} were used for TLC. NMR spectra were recorded with a Bruker DRX-400 AVANCE III or a Bruker DRX-600 AVANCE III spectrometer in the indicated solvents (residual peak of the solvent as the internal standard): the values of the chemical shifts are expressed in ppm and the coupling constants (*J*) in Hz. An Agilent 1100 LC/MSD operating with an electrospray source (ESI) in positive ion mode was used in mass spectrometry experiments. On the other hand, high resolution mass spectra (HRMS) were obtained by using a timsTOF spectrometer (Bruker, Bremen, D) operating with an electrospray ionization source (ESI) in positive ion mode.

Reaction of MBHA Derivative 7 with n-butylamine in Chloroform

Large Excess of n-butylamine

A mixture of MBH acetate **7** (50 mg, 0.105 mmol) in chloroform (10 mL) containing *n*-butylamine (0.052 mL, 0.525 mmol) was stirred at room temperature for 6 h. The reaction mixture was concentrated under reduced pressure and the resulting residue was purified by flash chromatography with the appropriate eluents to obtain the amine derivatives reported below (**9a**,**b**).

Dimethyl 2,2′-((butylazanediyl)bis(methylene))bis(3-(4′-(diphenylamino)-[1,1′-biphenyl]-4-yl)acrylate) (9b)

Compound **9b** was obtained as a yellow glassy solid (6.0 mg, yield 13%) by using petroleum ether-ethyl acetate (9:1) as the eluent in the above flash chromatography purification. The ^{1}H NMR (400 MHz, DMSO-d_6) spectrum showed that compound **9b** was composed by a mixture of the diastereomers. Samples of major diastereomer (*E*,*E*)-**9b** showing higher purities were obtained by further purification by flash chromatography. ^{1}H NMR (600 MHz, DMSO-d_6): 0.77 (t, J=7.3, 3H), 1.15 (m, 2H), 1.39 (m, 2H), 2.39 (t, J=7.2, 2H), 3.49 (s, 4H), 3.68 (s, 6H), 6.95 (d, J=8.5, 4H), 7.02 (d, J=7.9, 8H), 7.05 (m, 4H), 7.30 (t, J=7.7, 8H), 7.52 (m, 8H), 7.71 (d, J=8.2, 4H), 7.75 (s, 2H). HRMS (timsTOF) *m*/*z*: $[M+H]^+$ Calcd for $C_{62}H_{58}N_3O_4$ 908.44218; Found 908.43915.

Methyl 2-((butylamino)methyl)-3-(4′-(diphenylamino)-[1,1′-biphenyl]-4-yl)acrylate (9a)

Compound **9a** (34 mg, yield 66%) was obtained as a yellow glassy solid as the most polar fraction by using petroleum ether-ethyl acetate (7:3) as the eluent in the above flash chromatography purification. The ^{1}H NMR (400 MHz, DMSO-d_6) spectrum showed that compound **9a** was composed by a mixture of (*E*/*Z*)-diastereomers in the ratio of about (74:26). Samples of major diastereomer (*E*)-**9a** showing higher purities were obtained by further purification by flash chromatography. ^{1}H NMR (400 MHz, DMSO-d_6) 0.86 (t, J=7.2, 3H), 1.24–1.45 (m, 4H), 2.53 (t, J=6.8, 2H), 3.48 (s, 2H), 3.75 (s, 3H), 7.02 (d, J=8.7, 2H), 7.04–7.11 (m, 6H), 7.30–7.35 (m, 4H), 7.63–7.67 (m, 2H), 7.69 (s, 1H), 7.70 (s, 4H). HRMS (timsTOF) *m*/*z*: $[M+H]^+$ Calcd for $C_{33}H_{35}N_2O_2$ 491.26930; Found 491.26850.

Slight Excess of n-butylamine

A mixture of MBH acetate **7** (50 mg, 0.105 mmol) in chloroform (10 mL) containing *n*-butylamine (0.016 mL, 0.162 mmol) was stirred at room temperature for 48 h. The reaction mixture was concentrated under reduced pressure and the resulting residue was purified by flash chromatography with the appropriate eluents to obtain the amine derivatives reported below (**9a**,**b**).

Dimethyl 2,2′-((butylazanediyl)bis(methylene))bis(3-(4′-(diphenylamino)-[1,1′-biphenyl]-4-yl)acrylate) (9b)

Compound **9b** was obtained as a yellow glassy solid (17 mg, yield 36%) by using petroleum ether-ethyl acetate (9:1) as the eluent in the above flash chromatography purification. The ^{1}H NMR (400 MHz, DMSO-d_6) showed that compound **9b** was composed by a mixture of the diastereomers.

Methyl 2-((butylamino)methyl)-3-(4′-(diphenylamino)-[1,1′-biphenyl]-4-yl)acrylate (9a)

Compound **9a** (25 mg, yield 49%) was obtained as a yellow glassy solid as the most polar fraction by using petroleum ether-ethyl acetate (7:3) as the eluent in the above flash chromatography purification. The ^{1}H NMR (400 MHz, DMSO-d_6) showed that compound **9a** was composed by a mixture of (*E*/*Z*)-diastereomers in the ratio of about (74:26).

Reaction of MBHA Derivative 7 with n-butylamine Hydrochloride in Acetonitrile-Water-PBS

Large Excess of n-butylamine Hydrochloride

A mixture of MBH acetate **7** (50 mg, 0.105 mmol) in acetonitrile (12.5 mL), water (3.5 mL) containing solid PBS (Aldrich, 50 mg) and *n*-butylamine hydrochloride (58 mg, 0.529 mmol) was heated to reflux for 24 h. The reaction mixture was concentrated under reduced pressure and the resulting residue was partitioned between ethyl acetate and brine. The organic layer was dried under sodium sulfate and concentrated under reduced pressure. The resulting residue was purified by flash chromatography with the appropriate eluents to obtain the amine derivatives reported below (**9a**,**b**).

Dimethyl 2,2′-((butylazanediyl)bis(methylene))bis(3-(4′-(diphenylamino)-[1,1′-biphenyl]-4-yl)acrylate) (9b)

Compound **9b** was obtained as a yellow glassy solid (25 mg, yield 52%) by using petroleum ether-ethyl acetate (9:1) as the eluent in the above flash chromatography purification. The ^{1}H NMR (400 MHz, DMSO-d_6) showed that compound **9b** was composed by a mixture of the diastereomers.

Methyl 2-((butylamino)methyl)-3-(4′-(diphenylamino)-[1,1′-biphenyl]-4-yl)acrylate (9a)

Compound **9a** (20 mg, yield 39%) was obtained as a yellow glassy solid as the most polar fraction by using petroleum ether-ethyl acetate (7:3) as the eluent in the above flash chromatography purification. The ^{1}H NMR (400 MHz, DMSO-d_6) showed that compound **9a** was composed by a mixture of (*E*/*Z*)-diastereomers in the ratio of about (93:7).

Slight Excess of n-butylamine Hydrochloride

A mixture of MBH acetate **7** (50 mg, 0.105 mmol) in acetonitrile (12.5 mL), water (3.5 mL) containing solid PBS (Aldrich, 50 mg) and *n*-butylamine hydrochloride (17 mg, 0.158 mmol) was heated to reflux for 24 h. The reaction mixture was concentrated under reduced pressure and the resulting residue was partitioned between ethyl acetate and brine. The organic layer was dried under sodium sulfate and concentrated under reduced pressure. The resulting residue was purified by flash chromatography with the appropriate eluents to obtain the amine derivatives reported below (**9a**,**b**).

Dimethyl 2,2′-((butylazanediyl)bis(methylene))bis(3-(4′-(diphenylamino)-[1,1′-biphenyl]-4-yl)acrylate) (9b)

Compound **9b** was obtained as a yellow glassy solid (35 mg, yield 73%) by using petroleum ether-ethyl acetate (9:1) as the eluent in the above flash chromatography purification. The ^{1}H NMR (400 MHz, DMSO-d_6) showed that compound **9b** was composed by a mixture of the diastereomers.

Methyl 2-((butylamino)methyl)-3-(4′-(diphenylamino)-[1,1′-biphenyl]-4-yl)acrylate (9a)

Compound **9a** (8.0 mg, yield 16%) was obtained as a yellow glassy solid as the most polar fraction by using petroleum ether-ethyl acetate (7:3) as the eluent in the above flash chromatography purification. The ^{1}H NMR (400 MHz, DMSO-d_6) showed that compound **9a** was composed by a mixture of (*E*/*Z*)-diastereomers in the ratio of about (90:10).

Reaction of MBHA Derivative 7 with Nα-acetyl-*L*-lysine Methyl Ester Hydrochloride

A mixture of MBHA derivative **7** (67 mg, 0.14 mmol) in acetonitrile (12.5 mL) containing Nα-acetyl-*L*-lysine methyl ester hydrochloride (50 mg, 0.21 mmol), water (3.5 mL), and solid PBS (Aldrich, 25 mg) was refluxed for 24 h. The reaction mixture was concentrated under reduced pressure and the resulting residue partitioned between ethyl acetate and brine. The organic layer was dried over sodium sulfate and concentrated under reduced pressure. The final residue was purified by flash chromatography with the appropriate eluent to obtain the amino acid derivatives reported below (i.e. **9c** and **9d**).

Dimethyl 2,2′-(((5-acetamido-6-methoxy-6-oxohexyl)azanediyl)bis(methylene))(S)-bis(3-(4′-(diphenylamino)-[1,1′-biphenyl]-4-yl)acrylate) (9d)

Compound **9d** was obtained as a yellow glassy solid (53 mg, yield 73%) by using ethyl acetate-petroleum ether (6:4) as the eluent in the above flash chromatography purification. The ^{1}H NMR (400 MHz, DMSO-d_6) spectrum showed that compound **9d** was composed by a mixture of the diastereomers. Samples of major diastereomer (***E*,*E*)-9d** showing higher purities were obtained by further purification by flash chromatography. ^{1}H NMR (400 MHz, DMSO-d_6): 1.14–1.23 (m, 2H), 1.34–1.70 (m, 4H), 1.80 (s, 3H), 2.40 (t, J= 7.2, 2H), 3.50 (s, 4H), 3.53 (s, 3H), 3.70 (s, 6H), 4.12–4.16 (m, 1H), 6.93–7.00 (m, 4H), 7.01–7.12 (m, 12H), 7.28–7.37 (m, 8H), 7.50–7.58 (m, 8H), 7.71 (d, J= 8.3, 4H), 7.76 (s, 2H), 8.16 (d, J= 7.5, 1H). HRMS (timsTOF) *m/z*: $[M+H]^+$ Calcd for $C_{67}H_{65}N_4O_7$ 1037.48478; Found 1037.48146.

Methyl Nα-acetyl-N$^{\varepsilon}$-(3-(4′-(diphenylamino)-[1,1′-biphenyl]-4-yl)-2-(methoxycarbonyl)allyl)-L-lysinate (9c)

Compound **9c** (12 mg, yield 14%) was obtained as a yellow glassy solid as the most polar fraction by using ethyl acetate-methanol (9:1) as the eluent in the above flash chromatography purification. The ^{1}H NMR (400 MHz, DMSO-d_6) spectrum showed that compound **9a** was composed by a mixture of (*E*/*Z*)-diastereomers. Samples of major diastereomer (***E*-9c** showing purity higher than 97% were obtained by further purification by flash chromatography. ^{1}H NMR (400 MHz, DMSO-d_6) 1.28–1.46 (m, 4H), 1.50–1.71 (m, 2H), 1.81 (s, 3H), 2.53 (t, J = 6.6, 2H), 3.47 (s, 2H), 3.58 (s, 3H), 3.75 (s, 3H), 4.14–4.25 (m, 1H), 6.98–7.11 (m, 8H), 7.29–7.37 (m, 4H), 7.63–7.68 (m, 2H), 7.69 (s, 1H), 7.70 (s, 4H), 8.20 (d, J = 7.4, 1H). HRMS (timsTOF) *m/z*: $[M+H]^+$ Calcd for $C_{38}H_{42}N_3O_5$ 620.31190; Found 620.31017.

Reaction of MBHA Derivative 7 with n-butyl-poly-(L-lysine) (BPLL)

Commercially available *n*-butyl-poly-(*L*-lysine) (**BPLL**) hydrochloride (Iris Biotech GMBH) (4.2 mg) was dissolved in deuterated dimethylsulfoxide (0.5 mL) into a 5 mm NMR tube and the appropriate amount of **7** (i.e. 2.0, 4.0, or 8.0 micromol) was added as a (50 mM) solution in DMSO-d_6. The resulting reaction mixture was promptly analyzed by recording a ^{1}H NMR spectrum to obtain the information on the starting conditions (t = 0). The tube was then heated into an oil bath a 50 °C and ^{1}H NMR spectra were recorded at regular time intervals (i.e. 1, 2, 4, 8, 24 h). The obtained spectra were elaborated all in the same manner and staked as shown in Figures SI-5, SI-6, SI-7.

The same experiments were repeated in the presence of suitable amounts (i.e. 2.0, 4.0, or 8.0 micromol) of DIPEA as the base (Figures SI-8, SI-9, SI-10).

Molecular Modelling

Calculations were performed using density functional theory (DFT) within the functional B3LYP with base 6–31 G* from the Gaussian16 package,[61] in DCM and DMSO solutions. The Polarized Continuum Model (PCM) was used to simulate the solvent environment. Ground state geometry of **9b** was fully optimized using B3LYP/6–31 G* and Grimme dispersion D3 correction for long range interactions. Subsequently, absorption spectrum calculations were performed by the time-dependent (TD)DFT procedure, using the Coulomb-attenuated hybrid exchange-correlation functional (CAM–B3LYP) because it well describes structures with charge-transfer excited states.[62,63] The same TD-DFT (CAM–B3LYP/6–31 G*) approach was used to calculate the optimized geometries of the emitting intermediates and the overall scheme of quantum chemical calculations of **9b**.

Photophysical Properties

UV-vis absorption spectra are obtained with a Perkin Elmer Lambda 900 spectrometer. PL spectra are obtained with with NanoLog composed by a iH320 spectrograph equipped with a Synapse QExtra charge-coupled device, by exciting with a monochromate 450 W Xe lamp. The spectra are corrected for the instrument response. PL QY values of solutions were obtained by using quinine sulfate as the reference. PL QY of solid casted films were measured with a home-made integrating sphere according to the procedure reported elsewhere.[64] Time-resolved TCSPC measurements were obtained with PPD-850 single photon detector module by exciting with DD-405 L DeltaDiode Laser or DeltaTime series DD-300 DeltaDiode and analysed with the instrument Software DAS6. Average lifetimes are obtained by multiexponential fittings as $\tau_{av} = \sum_i \frac{A_i \tau_i^2}{A_i \tau_i}$

Photostability of Compounds 9 a,b

The solutions of compounds **9a**,**b** in deuterated dichloromethane contained into 5 mm NMR Pyrex tubes were irradiated with a monochromatic light centered at either 365 nm or 420 nm, and ^{1}H NMR spectra were recorded at regular time intervals (i.e. 0 min, 15 min, 30 min, 1, 2, 4, 8, and 24 h). A tunable light source Zolix (TLS2-X300PU–G, 300 W UV Xenon Light Source with monochromator Omni-λ2047i) was used for the irradiation of the solutions.

Dimethyl 3-butyl-6,7-bis(4′-(diphenylamino)-[1,1′-biphenyl]-4-yl)-3-azabicyclo[3.2.0]heptane-1,5-dicarboxylate (13)

A solution of compound **9b** (25 mg, 27.5 micromol) in dichloromethane (3.75 mL) contained into a vial closed with a screw cap was irradiated with a monochromatic light centered at 420 nm by mean of a tunable light source Zolix (TLS2-X300PU–G, 300 W UV Xenon Light Source with monochromator Omni-λ2047i) at room temperature for 15 h. The reaction mixture was then concentrated under reduced pressure and the resulting residue was purified by flash chromatography with petroleum ether-dichloromethane (2:8) as the eluent to obtain compound **13** (14 mg, yield 56%) as an off-white solid. The ^{1}H NMR spectrum of the solid showed that compound **13** was composed by a mixture of diastereomers. For the sake of simplicity only the major diastereomer (**13-M**, Figure 9) was taken into consideration.^{1}H NMR (600 MHz, $CDCl_3$): 0.91 (t, J = 7.2, 3H), 1.33–1.40 (m, 2H), 1.41–1.51 (m, 2H), 2.39 (d, J = 9.8, 1H), 2.41–2.47 (m, 1H), 2.57–2.63 (m, 1H), 2.73 (d, J = 9.7, 1H), 3.00 (d, J = 9.8, 1H), 3.29 (s, 3H), 3.42 (d, J = 9.6, 1H), 3.72 (s, 3H), 4.47 (d, J = 10.8, 1H), 4.80 (d, J = 10.8, 1H), 7.00–7.04 (m, 4H), 7.07–7.15 (m, 16H), 7.22–7.29 (m, 6H), 7.41–7.44 (m, 2H), 7.45–7.48 (m, 4H), 7.54 (d, J = 8.4, 2H), 7.58 (d, J = 8.4, 2H). ^{13}C NMR (150 MHz, $CDCl_3$): 14.0, 20.5, 30.6, 44.0, 45.1, 51.3, 52.1, 54.5, 56.1, 57.9, 60.3, 63.0, 122.9, 124.0, 124.4, 126.3, 126.6, 127.0, 127.5, 127.7, 128.8, 129.3, 134.8, 135.0, 137.1, 138.3, 138.8, 139.2, 147.1, 147.7, 170.9, 175.0.

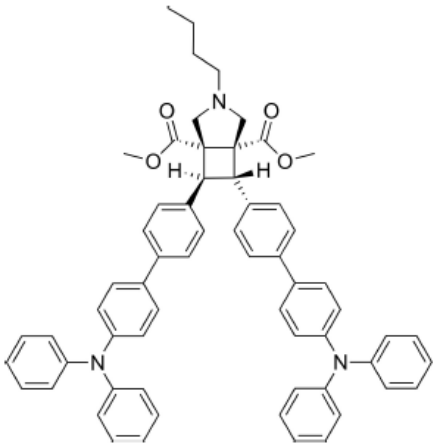

Figure 9. Probable structure of the major diastereomer **13-M** as suggested by NMR analysis. The structure of the corresponding enantiomer was omitted for the sake of simplification.

HRMS (timsTOF) *m/z*: $[M+H]^+$ Calcd for $C_{62}H_{58}N_3O_4$ 908.44218; Found 908.43915.

Acknowledgements

M.P. and A.C. acknowledge the MUR for the financial support under the project CN00000041 – "National Center for Gene Therapy and Drugsbased on RNA Technology" – CUP B63 C2200061 0006 Mission 4 Component 2 (M4 C2) – investment 1.4 [CN3] of the National Recovery and Resilience Plan (PNRR) funded by the European Union "Next Generation EU". M.P. acknowledge the University of Siena for the financial support of the project Chromo-GEnUP through the F-CUR2022 funding line (2265–2022-PM-CONRICMIUR_PC-FCUR2022_003). Open Access publishing facilitated by Università degli Studi di Siena, as part of the Wiley - CRUI-CARE agreement.

Conflict of Interests

The authors declare no conflict of interest.

Data Availability Statement

The data that support the findings of this study are available from the corresponding author upon reasonable request.

Keywords: Protein labeling · Fluorogenic labeling · Lysine · Morita–Baylis–Hillman Adduct · Cinnamic derivatives

[1] V. K. Kadambar, A. Melman, *Adv. Exp. Med. Biol.* **2019**, *1140*, 237–250.
[2] J. Maneesh, N. Kamal, S. K. Batra, *Trends Biotechnol.* **2007**, *25*, 307–316.
[3] C. C. Ward, J. I. Kleinman, D. K. Nomura, *ACS Chem. Biol.* **2017**, *12*, 1478–1483.
[4] P. Rosa-Neto, B. Wängler, L. Iovkova, G. Boening, A. Reader, K. Jurkschat, E. Schirrmacher, *ChemBioChem* **2009**, *10*, 1321–1324.
[5] V. Raindlová, R. Pohl, M. Hocek, *Chem. Eur. J.* **2012**, *18*, 4080–4087.
[6] K. Pagano, M. Paolino, S. Fusi, V. Zanirato, C. Trapella, G. Giuliani, A. Cappelli, S. Zanzoni, H. Molinari, L. Ragona, M. Olivucci, *J. Phys. Chem. Lett.* **2019**, *10*, 2235–2243.
[7] B. D. Smith, J. J. Higgin, R. T. Raines, *Bioorg. Med. Chem. Lett.* **2011**, *21*, 5029–5032.
[8] S. B. Gunnoo, A. Madder, *ChemBioChem* **2016**, *17*, 529–553.
[9] M. H. Mir, S. Parmar, C. Singh, D. Kalia, *Nat. Commun.* **2024**, *15*, 859.
[10] V. Razzano, M. Paolino, A. Reale, G. Giuliani, R. Artusi, G. Caselli, M. Visintin, F. Makovec, A. Donati, F. Villafiorita-Monteleone, C. Botta, A. Cappelli, *ACS Omega* **2017**, *2*, 5453–5459.
[11] V. Razzano, M. Paolino, A. Reale, G. Giuliani, A. Donati, G. Giorgi, R. Artusi, G. Caselli, M. Visintin, F. Makovec, S. Battiato, F. Samperi, F. Villafiorita-Monteleone, C. Botta, A. Cappelli, *RSC Adv.* **2018**, *8*, 8638–8656.
[12] M. Paolino, A. Reale, V. Razzano, G. Giuliani, A. Donati, C. Bonechi, G. Caselli, M. Visintin, F. Makovec, C. Scialabba, M. Licciardi, E. Paccagnini, M. Gentile, L. Salvini, F. Tavanti, M. C. Menziani, A. Cappelli, *New J. Chem.* **2019**, *43*, 6834–6837.
[13] M. Paolino, M. Visintin, E. Margotti, M. Visentini, L. Salvini, A. Reale, V. Razzano, G. Giuliani, G. Caselli, F. Tavanti, M. C. Menziani, A. Cappelli, *New J. Chem.* **2019**, *43*, 17946–17953.
[14] G. Tassone, M. Paolino, C. Pozzi, A. Reale, L. Salvini, G. Giorgi, M. Orlandini, F. Galvagni, S. Mangani, X. Yang, B. Carlotti, F. Ortica, L. Latterini, M. Olivucci, A. Cappelli, *ChemBioChem* **2022**, *23*, e202100449.
[15] M. Saletti, M. Paolino, J. Venditti, C. Bonechi, G. Giuliani, A. Boccia, C. Botta, A. Cappelli, *Dyes Pigm.* **2023**, *219*, 111571.
[16] M. Saletti, J. Venditti, M. Paolino, A. Zacchei, G. Giuliani, G. Giorgi, C. Bonechi, A. Donati, A. Cappelli, *RSC Adv.* **2023**, *13*, 35773–35780.
[17] M. Saletti, M. Paolino, J. Venditti, C. Bonechi, G. Giuliani, S. Lamponi, G. Tassone, A. Boccia, C. Botta, L. Blancafort, F. Poggialini, C. Vagaggini, A. Cappelli, *ChemBioChem* **2024**, *25*, e202300862.
[18] M. Lami, L. Barneschi, M. Saletti, M. Olivucci, A. Cappelli, M. Paolino, *ChemPhotoChem* **2024**, e202400093.
[19] E. G. Guignet, R. Hovius, H. Vogel, *Nat. Biotechnol.* **2004**, *22*, 440–444.
[20] B. A. Griffin, S. R. Adams, R. Y. Tsien, *Science* **1998**, *281*, 269–272.
[21] B. Krishnan, A. Szymanska, L. M. Gierasch, *Chem. Biol. Drug Des.* **2007**, *69*, 31–40.
[22] Z. Wang, X. Ding, S. Li, J. Shi, Y. Li, *RSC Adv.* **2014**, *4*, 7235–7245.
[23] L. Rong, C. Zhang, Q. Lei, S.-. Y. Qin, J. Feng, X.-. Z. Zhang, *Adv. Sci.* **2016**, *3*, 1500211.
[24] L. D. Lavis, T.-Y. Chao, R. T. Raines, *ACS Chem. Biol.* **2006**, *1*, 252–260.
[25] J. Mei, N. L. C. Leung, R. T. K. Kwok, J. W. Y. Lam, B. Z. Tang, *Chem. Rev.* **2015**, *115*, 11718–11940.
[26] D. Ding, K. Li, B. Liu, B. Z. Tang, *Acc. Chem. Res.* **2013**, *46*, 2441–2453.
[27] W. C. Wu, C. Y. Chen, Y. Tian, S. H. Jang, Y. Hong, Y. Liu, R. Hu, B. Z. Tang, Y. T. Lee, C. T. Chen, W. C. Chen, A. K. Y. Jen, *Adv. Funct. Mater.* **2010**, *20*, 1413–1423.
[28] A. Cappelli, G. P. Mohr, M. Anzini, S. Vomero, A. Donati, M. Casolaro, R. Mendichi, G. Giorgi, F. Makovec, *J. Org. Chem.* **2003**, *68*, 9473–9476.
[29] A. Cappelli, M. Anzini, S. Vomero, A. Donati, L. Zetta, R. Mendichi, M. Casolaro, P. Lupetti, P. Salvatici, G. Giorgi, *J. Polym. Sci. Part A* **2005**, *43*, 3289–3304.
[30] A. Cappelli, G. Pericot Mohr, G. Giuliani, S. Galeazzi, M. Anzini, L. Mennuni, F. Ferrari, F. Makovec, E. M. Kleinrath, T. Langer, M. Valoti, G. Giorgi, S. Vomero, . *J. Med. Chem.* **2006**, *49*, 6451–6464.
[31] A. Cappelli, S. Galeazzi, G. Giuliani, M. Anzini, A. Donati, L. Zetta, R. Mendichi, M. Aggravi, G. Giorgi, E. Paccagnini, S. Vomero, *Macromolecules* **2007**, *40*, 3005–3014.
[32] A. Cappelli, S. Galeazzi, G. Giuliani, M. Anzini, M. Aggravi, A. Donati, L. Zetta, A. C. Boccia, R. Mendichi, G. Giorgi, E. Paccagnini, S. Vomero, *Macromolecules* **2008**, *41*, 2324–2334.
[33] A. Cappelli, S. Galeazzi, G. Giuliani, M. Anzini, M. Grassi, R. Lapasin, G. Grassi, R. Farra, B. Dapas, M. Aggravi, A. Donati, L. Zetta, A. C. Boccia, F. Bertini, F. Samperi, S. Vomero, *Macromolecules* **2009**, *42*, 2368–2378.
[34] A. Cappelli, M. Paolino, P. Anzini, G. Giuliani, S. Valenti, M. Aggravi, A. Donati, R. Mendichi, L. Zetta, A. C. Boccia, F. Bertini, F. Samperi, S. Battlato, E. Paccagnini, S. Vomero, *J. Polym. Sci. Part A* **2010**, *48*, 2446–2461.
[35] A. Cappelli, M. Paolino, G. Grisci, G. Giuliani, A. Donati, R. Mendichi, A. C. Boccia, F. Samperi, S. Battiato, E. Paccagnini, E. Giacomello, V. Sorrentino, M. Licciardi, G. Giammona, S. Vomero, *Polym. Chem.* **2011**, *2*, 2518–2527.
[36] A. Cappelli, M. Paolino, G. Grisci, G. Giuliani, A. Donati, R. Mendichi, A. C. Boccia, C. Botta, W. Mróz, F. Samperi, A. Scamporrino, G. Giorgi, S. Vomero, *J. Mater. Chem.* **2012**, *22*, 9611–9623.
[37] A. Cappelli, G. Grisci, M. Paolino, F. Castriconi, G. Giuliani, A. Donati, S. Lamponi, R. Mendichi, A. C. Boccia, F. Samperi, S. Battiato, E. Paccagnini, M. Gentile, M. Licciardi, G. Giammona, S. Vomero, *Chem. Eur. J.* **2013**, *19*, 9710–9721.
[38] A. Cappelli, M. Paolino, G. Grisci, G. Giuliani, A. Donati, A. C. Boccia, F. Samperi, R. Mendichi, S. Vomero, S., In *π-Stacked Polymers and Molecules*. Nakano T. Ed., Springer Japan: Osaka, **2014**, pp 51–149.
[39] A. Cappelli, F. Villafiorita-Monteleone, G. Grisci, M. Paolino, V. Razzano, G. Fabio, G. Giuliani, A. Donati, R. Mendichi, A. C. Boccia, M. Pasini, C. Botta, *J. Mater. Chem. C* **2014**, *2*, 7897–7905.
[40] A. Cappelli, G. Grisci, M. Paolino, V. Razzano, G. Giuliani, A. Donati, C. Bonechi, R. Mendichi, A. C. Boccia, M. Licciardi, C. Scialabba, G. Giammona, S. Vomero, *J. Mater. Chem. B* **2015**, *3*, 361–374.
[41] W. Mróz, F. Villafiorita-Monteleone, M. Pasini, G. Grisci, M. Paolino, V. Razzano, A. Cappelli, C. Botta, *Mater. Lett.* **2015**, *142*, 197–200.
[42] F. Villafiorita-Monteleone, A. Cappelli, M. Paolino, M. Colombo, E. Cariati, A. Mura, G. Bongiovanni, C. Botta, *J. Phys. Chem. C* **2015**, *119*, 18986–18991.
[43] A. Cappelli, V. Razzano, M. Paolino, G. Grisci, G. Giuliani, A. Donati, R. Mendichi, F. Samperi, S. Battiato, A. C. Boccia, A. Mura, G. Bongiovanni, W. Mróz, C. Botta, *Polym. Chem.* **2015**, *6*, 7377–7388.
[44] A. Cappelli, V. Razzano, G. Fabio, M. Paolino, G. Grisci, G. Giuliani, A. Donati, R. Mendichi, W. Mróz, F. Villafiorita-Monteleone, C. Botta, *RSC Adv.* **2015**, *5*, 101377–101385.

[45] A. Cappelli, M. Paolino, G. Grisci, V. Razzano, G. Giuliani, A. Donati, C. Bonechi, R. Mendichi, S. Battiato, F. Samperi, C. Scialabba, G. Giammona, F. Makovec, M. Licciardi, *Polym. Chem.* **2016**, *7*, 6529–6544.
[46] F. Villafiorita-Monteleone, E. Kozma, M. Pasini, M. Paolino, A. Cappelli, G. Bongiovanni, A. Mura, C. Botta, *Appl. Phys. Lett.* **2017**, *110*, 183301.
[47] F. Villafiorita-Monteleone, E. Kozma, U. Giovanella, M. Catellani, M. Paolino, V. Collico, M. Colombo, A. Cappelli, C. Botta, *Dyes Pigm.* **2018**, *149*, 331–335.
[48] F. Fabrizi de Biani, A. Reale, V. Razzano, M. Paolino, G. Giuliani, A. Donati, G. Giorgi, W. Mróz, D. Piovani, C. Botta, A. Cappelli, *RSC Adv.* **2018**, *8*, 10836–10847.
[49] M. Paolino, G. Grisci, A. Reale, V. Razzano, G. Giuliani, A. Donati, R. Mendichi, D. Piovani, A. Boccia, A. Grillo, G. Giorgi, A. Cappelli, *Polymers (Basel).* **2018**, *10*, 752.
[50] M. Paolino, G. Grisci, F. Castriconi, A. Reale, G. Giuliani, A. Donati, C. Bonechi, G. Giorgi, R. Mendichi, D. Piovani, A. C. Boccia, M. Canetti, F. Samperi, S. Dattilo, C. Scialabba, M. Licciardi, E. Paccagnini, M. Gentile, A. Cappelli, *Pharmaceutica* **2018**, *10*, 234.
[51] M. Paolino, A. Reale, V. Razzano, G. Giuliani, A. Donati, G. Giorgi, A. C. Boccia, R. Mendichi, D. Piovani, C. Botta, L. Salvini, F. Samperi, C. Savoca, M. Licciardi, E. Paccagnini, M. Gentile, A. Cappelli, *Pharmaceutica* **2019**, *11*, 444.
[52] M. Paolino, A. Reale, G. Magrini, V. Razzano, G. Giuliani, A. Donati, G. Giorgi, F. Samperi, M. Canetti, M. Mauro, F. Villafiorita-Monteleone, E. Fois, C. Botta, A. Cappelli, *Eur. Polym. J.* **2020**, *137*, 109923.
[53] M. Paolino, A. Reale, G. Magrini, V. Razzano, M. Saletti, G. Giuliani, A. Donati, F. Samperi, A. Scamporrino, M. Canetti, M. Mauro, F. Villafiorita-Monteleone, E. Fois, C. Botta, A. Cappelli, *Eur. Polym. J.* **2021**, *156*, 110597.
[54] M. Paolino, M. Saletti, A. Reale, V. Razzano, G. Giuliani, A. Donati, C. Bonechi, G. Giorgi, A. Atrei, M. Mauro, A. Scamporrino, F. Samperi, E. Fois, G. Tabacchi, C. Botta, A. Cappelli, *Eur. Polym. J.* **2022**, *169*, 111137.
[55] M. Paolino, M. Saletti, A. Reale, M. Licciardi, P. Varvarà, A. Marquette, J. Léonard, C. Bonechi, A. Donati, G. Giorgi, G. Giuliani, B. Carlotti, F. Ortica, L. Latterini, M. Gentile, E. Paccagnini, M. Olivucci, A. Cappelli, *Chem. Eur. J.* **2022**, *28*, e202201477.
[56] M. Paolino, M. Saletti, A. Reale, V. Razzano, G. Giuliani, A. Donati, C. Bonechi, G. Giorgi, G. Mercorillo, F. Samperi, W. Mróz, C. Botta, A. Cappelli, *Eur. Polym. J.* **2023**, *189*, 111957.
[57] M. Paolino, A. Reale, V. Razzano, G. Giorgi, G. Giuliani, F. Villafiorita-Monteleone, C. Botta, C. Coppola, A. Sinicropi, A. Cappelli, *New J. Chem.* **2020**, *44*, 13644–13653.
[58] A. Nangia, G. R. Desiraju, *Chem. Commun.* **1999**, 605–606.
[59] K. J. Kunal, K. Anil, M. Parthapratim, *Cryst. Growth Des.* **2023**, *23*, 2922–2931.
[60] R. Improta, F. Santoro, L. Blancafort, *Chem. Rev.* **2016**, *116*, 3540–3593.
[61] *Gaussian 16*, Revision C.01, M. J. Frisch, G. W. Trucks, H. B. Schlegel, G. E. Scuseria, M. A. Robb, J. R. Cheeseman, G. Scalmani, V. Barone, G. A. Petersson, H. Nakatsuji, X. Li, M. Caricato, A. V. Marenich, J. Bloino, B. G. Janesko, R. Gomperts, B. Mennucci, H. P. Hratchian, J. V. Ortiz, A. F. Izmaylov, J. L. Sonnenberg, D. Williams-Young, F. Ding, F. Lipparini, F. Egidi, J. Goings, B. Peng, A. Petrone, T. Henderson, D. Ranasinghe, V. G. Zakrzewski, J. Gao, N. Rega, G. Zheng, W. Liang, M. Hada, M. Ehara, K. Toyota, R. Fukuda, J. Hasegawa, M. Ishida, T. Nakajima, Y. Honda, O. Kitao, H. Nakai, T. Vreven, K. Throssell, J. A. Montgomery, Jr., J. E. Peralta, F. Ogliaro, M. J. Bearpark, J. J. Heyd, E. N. Brothers, K. N. Kudin, V. N. Staroverov, T. A. Keith, R. Kobayashi, J. Normand, K. Raghavachari, A. P. Rendell, J. C. Burant, S. S. Iyengar, J. Tomasi, M. Cossi, J. M. Millam, M. Klene, C. Adamo, R. Cammi, J. W. Ochterski, R. L. Martin, K. Morokuma, O. Farkas, J. B. Foresman, and D. J. Fox, Gaussian, Inc., Wallingford CT, **2016**.
[62] A. D. Becke, *J. Chem. Phys.* **1993**, *98*, 5648–5652.
[63] C. Lee, W. Yang, R. G. Parr, *Phys. Rev. B* **1988**, *37*, 785–789.
[64] J. Moreau, U. Giovanella, J.-P. Bombenger, W. Porzio, V. Vohra, L. Spadacini, G. Di Silvestro, L. Barba, G. Arrighetti, S. Destri, M. Pasini, M. Saba, F. Quochi, A. Mura, G. Bongiovanni, M. Fiorini, M. Uslenghi, C. Botta, *ChemPhysChem* **2009**, *10*, 647–653.

Manuscript received: May 30, 2024
Revised manuscript received: July 12, 2024
Accepted manuscript online: July 23, 2024
Version of record online: September 21, 2024

2.9 RESEARCH ARTICLE: "Photophysical and Photochemical Features of Lysine Derivatives Bearing Two Triphenylaminocinnamic-Based Fluorophores"

Authors: Mario Saletti, Marco Paolino, **Jacopo Venditti**, Gianluca Giorgi, Claudia Bonechi, Alessandro Donati, Claudio Rossi, Germano Giuliani, Antonella Caterina Boccia, Chiara Boccia, Lluìs Blancafort, Andrea Cappelli.

Publication: The Journal of Physical Chemistry B

Publisher: American Chemical Society

DOI: doi.org/10.1021/acs.jpcb.5c01032

Supporting Information available at: jp5c01032_si_001.pdf

Contribution: The Ph.D. candidate was involved in the photophysical and photochemical studies of the diadducts obtained from the reactions with *n*-butylamine and Nα-acetyl-*L*-lysine methyl ester hydrochloride. The candidate also contributed to the purification of the [2+2] photocycloaddition products by means of flash chromatography and performed the ^{1}H NMR spectroscopy (400 MHz) analyses.

THE JOURNAL OF PHYSICAL CHEMISTRY B
A JOURNAL OF THE AMERICAN CHEMICAL SOCIETY

pubs.acs.org/JPCB

Article

Photophysical and Photochemical Features of Lysine Derivatives Bearing Two Triphenylaminocinnamic-Based Fluorophores

Published as part of The Journal of Physical Chemistry B special issue "Massimo Olivucci Festschrift".

Mario Saletti, Marco Paolino, Jacopo Venditti, Gianluca Giorgi, Claudia Bonechi, Alessandro Donati, Claudio Rossi, Germano Giuliani, Antonella Caterina Boccia, Chiara Botta, Lluís Blancafort, and Andrea Cappelli*

Cite This: J. Phys. Chem. B 2025, 129, 3928−3937

Read Online

ACCESS | Metrics & More | Article Recommendations | Supporting Information

ABSTRACT: A Morita−Baylis−Hillman adduct (MBHA) derivative bearing a triphenylamine (TPA) moiety was previously found to react with Nα-acetyl-L-lysine methyl ester with the formation of the corresponding diadduct derivative as the major reaction product and a monoadduct as the minor one. The characterization of photochemical features of the diadduct bearing two triphenylaminocinnamic (TPAC) fluorophores suggested that this compound shows the tendency to undergo the [2 + 2] photocycloaddition reaction. This hypothesis was evaluated in the present study in both the diadduct derivatives obtained with Nα-acetyl-L-lysine methyl ester and Nα-acetyl-L-lysine. The hypothesis was confirmed in the case of the diadduct derivative obtained from Nα-acetyl-L-lysine methyl ester, whereas the UV-A irradiation of the diadduct derivative obtained from Nα-acetyl-L-lysine led to the formation of a strongly emissive (QY = 69%, λ_{em} = 460 nm) symmetric dimer.

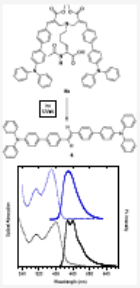

INTRODUCTION

The development of strategies for protein labeling at precisely defined positions is a research topic of great interest owing to the importance in studying their structure−function relationships.[1−3] In general, these strategies are based on the amino acid side chain reactivity where amino or thiol groups play a major role,[4−9] and the derivatization of proteins in complex environments has driven the design of advanced probes.[10−14]

Owing to the importance acquired by fluorescence-based detection techniques in studying protein interactions and functions, the development of suitable fluorescent probes has become a stringent necessity. In this regard, fluorogenic labeling strategies have emerged as promising methods owing to their important advantages (i.e., a higher signal-to-noise ratio) since the fluorescence activation occurs after the reaction/attachment to the desired site.[15] Aggregation-induced emission (AIE) features (i.e., emission intensities higher in the solid state than in solution)[16] represent an interesting added value for fluorescent probes because in this way, they can show higher sensitivity, accuracy, and photostability when compared to conventional fluorescence probes displaying high emissive features in solution, but they often undergo aggregation-caused quenching (ACQ) processes at high concentration.[17,18]

A large variety of Morita−Baylis−Hillman derivatives have been developed in our laboratories to react with imidazole, histidine derivatives, *n*-butylamine, lysine derivatives, and proteins.[19−27] In particular, the reactivity of some MBHA derivatives has been studied in model proteins such as a single-chain Fv antibody, and the results of these studies suggested that MBHA derivative **1a** (Figure 1) could react with the hexahistidine tag leading to the formation of multi-PEGylated species.[21,22]

Furthermore, MBHA derivatives **1b** and **2a,b** (Figure 1) were found to be useful in the functionalization of a lysine residue embedded in a lipophilic pocket of a retinoic acid binding protein.[23] Finally, MBHA derivative **3** bearing a triphenylamine moiety was found to react with human serum albumin (**HSA**) with a significant shift in the emission from blue to green-yellow thus leading to green fluorescent albumin (**GFA**) derivatives.[26] Interestingly, docking studies suggested a possible interaction between the acrylic activated moiety of compound **3** (Figure 1) with Lys199 within a lipophilic pocket in the **HSA** structure, driving the addition−elimination reaction.[26] Thus, the reactivity of MBHA derivative **3** was evaluated with *n*-butylamine, Nα-acetyl-L-lysine methyl ester, and a poly(L-lysine) derivative as models of the lysine amino acid residues.[28]

Received: February 17, 2025
Revised: March 27, 2025
Accepted: March 28, 2025
Published: April 8, 2025

https://doi.org/10.1021/acs.jpcb.5c01032
J. Phys. Chem. B 2025, 129, 3928−3937

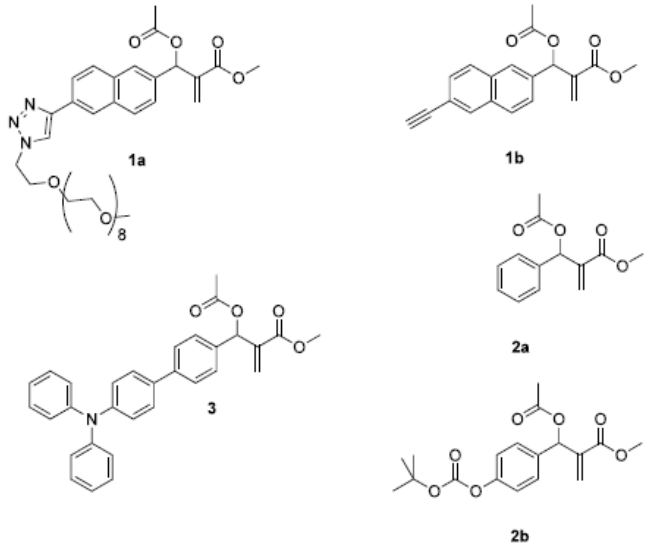

Figure 1. Structure of MBHA derivatives **1a,b**, **2a,b**, and **3**.

Scheme 1. Reaction of MBHA Derivative 3 with Nα-Acetyl-L-lysine Derivatives[a]

[a]Reagents: (i) Nα-acetyl-L-lysine methyl ester hydrochloride (or Nα-acetyl-L-lysine), CH_3CN, PBS, H_2O.

Compound **3** was found to react with Nα-acetyl-L-lysine methyl ester (Scheme 1) showing a peculiar behavior, which was characterized by the formation of diadduct derivative **5a** as the major reaction product and monoadduct **4a** as the minor one.[28]

The study of the photophysical and photochemical features of compounds **4a** and **5a** suggested that diadduct derivative **5a** bearing two triphenylaminocinnamic (TPAC) fluorophores could be prone to undergo the [2 + 2] photocycloaddition reaction.[28] Thus, in the present work, the hypothesis was evaluated in the diadduct derivative **5a** obtained with Nα-acetyl-L-lysine methyl ester and in that (i.e., **5b**) obtained from the reaction of MBHA derivative **3** with Nα-acetyl-L-lysine.

https://doi.org/10.1021/acs.jpcb.5c01032
J. Phys. Chem. B 2025, 129, 3928−3937

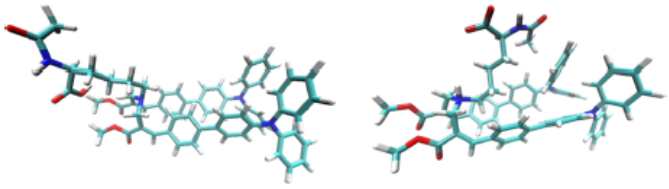

Figure 2. Optimized structure of the neutral isomer of **5b** (left) and comparison with its dipolar form (right) in DMSO as A solvent.

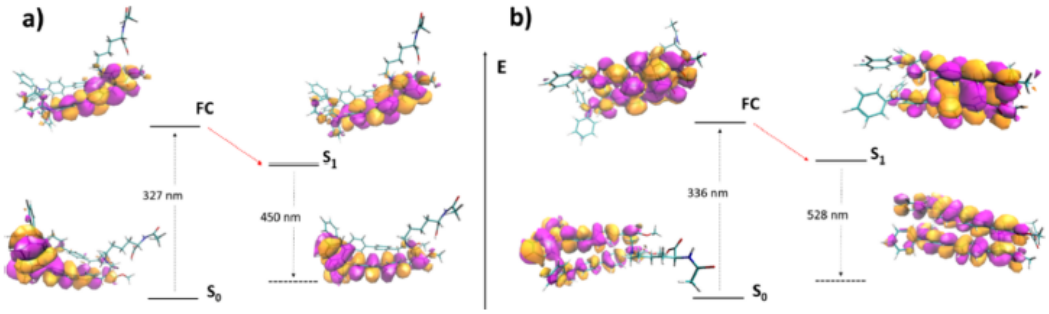

Figure 3. Schematic representations of the **5b** fluorescence cycle in (a) DMSO and (b) DCM. The molecular orbital (HOMO/LUMO) involved in electron transitions and relative energies are shown for vertical excitation (Franck−Condon point, FC) and emission from the optimized geometries. The red line stands for the adiabatic relaxation pathway on first singlet excited state (S_1).

Table 1. Comparison of the Optical Properties of Compound 5b with Those Previously Published for 5a and 4a[j]

	solid state			solution							
compound	λ_{em} (nm)	QY[a] (%)	τ_{av}[b,i] (ns)	solvent	λ_{ab} (nm)	λ_{em} (nm)	Δf	λ_{PLE} blue (nm)	λ_{PLE} green (nm)	QY[c] (%)	τ_{av}[d] (ns)
5b	550	5	1.57	THF	295, 352	395, 502	0.21	330	287, 365	21 (32)	
				DMSO	359	418, 572	0.26	335	295, 367	22 (27)	
				CH_3OH	285, 352	410, 575	0.31	330	295, 360	3	
				DCM	295, 354	410, 535	0.22	327	285, 370	26 (60)	
5a	520	13	2.11		296, 356	408, 524				43[e], 29	1.61[f], 2.822[g,h]
4a	530	5	1.44		296, 357	535				51	3.38[h]

[a]λ_{ex} = 390 nm. [b]λ_{ex} = 407 nm. [c]λ_{ex} = 365 nm; fresh solutions, in parentheses the values obtained after irradiation at 365 nm for about 1 h. [d]λ_{ex} = 300 nm. [e]λ_{ex} = 330 nm. [f]λ_{em} = 406 nm. [g]λ_{em} = 524 nm. τ_{av} = average lifetime, $\tau_{av} = \frac{\sum_{n=1}^{m} A_n \tau_n^2}{\sum_{n=1}^{m} A_n \tau_n}$. [h]From biexponential fit. [i]From three-exponential fit. [j]Adapted from ref 28 available under a CC-BY license. Copyright 2024 Jacopo Venditti, Mario Saletti, Marco Paolino, et al.

EXPERIMENTAL SECTION

Synthesis. Merck silica gel 60 (230−400 mesh) was used for column chromatography. Merck TLC plates and silica gel 60 F_{254} were used for TLC. NMR spectra were recorded with a Bruker DRX-400 AVANCE III or a Bruker DRX-600 AVANCE III spectrometer in the indicated solvents (TMS as an internal standard): the values of the chemical shifts are expressed in ppm and the coupling constants (J) in Hz. The HRMS measurements were performed by the direct infusion (5 μL/min) of sample solutions [methanol−water (9:1) filtered at 0.45 μm] in a heated electrospray ionization (ESI) source and a Q Exactive 240 Orbitrap high-resolution mass spectrometer (ESI-HRMS-Orbitrap, Thermo Fisher Scientific, Waltham, MA, USA). The Orbitrap analyzer was operated in positive mode. The following ion source parameters were used for detection: electrospray voltage, 3.4 kV; capillary temperature, 320 °C; vaporizer temperature, 200 °C; sheath gas flow rate (N_2), 7 arbitrary units (AU); auxiliary gas flow rate (N_2), 5 AU; sweep gas flow rate, 0 AU. The MS parameters were as follows: full mass m/z range from 150 to 1500; mass resolution, 240,000 (at m/z 200); AGC target, standard; maximum injection time, auto; RF lens (%), 70; microscan, 1.

Compound **5a** was resynthesized as previously reported,[28] while compounds **4b** and **5b** were prepared in five different batches as described in the Supporting Information.

Molecular Modeling. Calculations were performed using density functional theory (DFT) within the functional B3LYP with basis set 6-31G* from the Gaussian16 package,[29] in DCM and DMSO solutions. The polarized continuum model (PCM), implemented with the solvent-excluded surface (SES) option, was used to simulate the solvent environment. This method is usually employed to describe the boundary of a large molecular volume (cavity) with respect to a specific implicit solvent. Ground-state geometry of **5b** was fully optimized using B3LYP/6-31G* and Grimme dispersion D3 correction for long-range interactions. Subsequently, absorption spectrum calculations

https://doi.org/10.1021/acs.jpcb.5c01032
J. Phys. Chem. B 2025, 129, 3928−3937

were performed by the time-dependent (TD)DFT procedure, using the Coulomb-attenuated hybrid exchange−correlation functional (CAM-B3LYP) because it well describes structures with charge-transfer excited states. The same TD-DFT (CAM-B3LYP/6-31G*) approach was used to calculate the optimized geometries of the emitting intermediates and the overall scheme of quantum chemical calculations of **5b**.

Photophysical Properties. UV−vis absorption spectra were obtained with a PerkinElmer Lambda 900 spectrometer. PL spectra were obtained with a NanoLog composed by an iH320 spectrograph equipped with a Synapse QExtra charge-coupled device, by exciting with a 450 W Xe lamp monochromated with a double grating Gemini 180. The spectra were corrected for the instrument response. PL QY values of solutions were obtained by using quinine sulfate as the reference. PL QY values of solid powders and cast films were measured with a homemade integrating sphere according to the procedure reported elsewhere.[30] Time-resolved TCSPC measurements were obtained with a PPD-850 single-photon detector module by exciting with a DD-405L DeltaDiode laser or a DeltaTime series DD-300 DeltaDiode and analyzed with instrument software DAS6. Average lifetimes were obtained by multi-exponential fittings as $\tau_{av} = \sum_i \frac{Ai\tau i^2}{Ai\tau i}$.

RESULTS AND DISCUSSION

Reaction of MBHA Derivative 3 with Nα-Acetyl-L-lysine. As already observed in the reaction of MBHA derivative **3** with Nα-acetyl-L-lysine methyl ester hydrochloride, the reaction of **3** with a little excess (i.e., 1.5 equiv) of Nα-acetyl-L-lysine in acetonitrile in the presence of phosphate-buffered saline (PBS) was very slow at room temperature. Therefore, refluxing conditions were applied to accomplish the reaction in a reasonable time (i.e., 24 h). In this way, diadduct **5b** was isolated by flash chromatography separation as the major reaction product (yield 50%), while monoadduct **4b** was obtained in low yield (17%) in agreement with the previously published results concerning corresponding esters **5a** (yield 77%) and **4a** (yield 14%).[28]

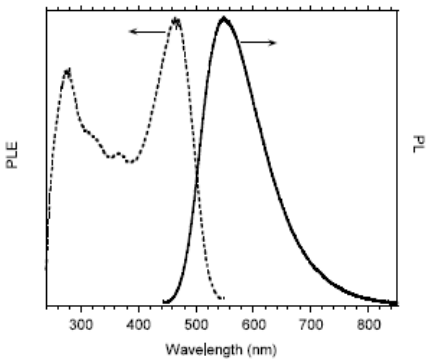

Figure 4. PL spectra (λ_{ex} = 430 nm, solid line) and PL excitation profiles (λ_{em} = 560 nm, dashed line) of diadduct **5b** in the solid state (i.e., crystalline powder).

The results of these experiments confirmed diadduct **5b** as the major reaction product in these reaction conditions, and therefore, it was characterized from the point of view of its structural, photophysical, and photochemical features. Several batches of compound **5b** were synthesized in the context of this investigation, and each one has been assessed for its purity by RP-HPLC in the following conditions: column ZORBAX eclipse XDB-C8 4.6 × 150 mm 5 μm; isocratic elution with a ternary solvent mixture composed of 78% methanol, 13% acetonitrile, and 9% water containing 0.1% formic acid; flow = 1 mL/min; analysis time = 10 min. The purity of the samples was found to be in the range from 89.3 to 97.4%, and that of the samples used in the characterization studies was found to be higher than 95%. The stability in the solid state was evaluated by ^{1}H NMR spectroscopy and RP-HPLC analyses after storage for 4 and 6 months at room temperature. The ^{1}H NMR spectra performed (in DMSO-d_6) after storage were perfectly coincident with those performed immediately after the preparation and purification. RP-HPLC analyses also confirmed suitable stability during the storage in closed glass vials at room temperature in the usual laboratory conditions.

Structure of Diadduct 5b. The structure of diadduct **5b** was studied by ^{1}H NMR spectroscopy and molecular modeling techniques. In particular, the structure of diadduct **5b** was studied by NMR spectroscopy in two different solvent systems. In fact, NMR spectra were recorded by using solutions of **5b** either in DMSO-d_6 as the most polar solvent system or in CD_2Cl_2-DMSO-d_6 (2:1) in order to decrease the polarity. The resulting spectra were assigned by crossing mono- and two-dimensional data, and the assignment of the NMR signals present in the spectra is summarized in the Supporting Information (see Figures S1 and S2).

The structure of diadduct **5b** could be represented by the three possible geometric isomers [namely, (*E*,*E*), (*E*,*Z*), and (*Z*,*Z*)] as a function of the configurations of the double bonds of the two cinnamic fluorophores. A highly symmetric three-dimensional (3D) structure was advocated for **5b** by the NMR spectra, with the two cinnamic moieties showing the trans (i.e., *E*) configuration at the double bond, as suggested by the chemical shift value of the acrylic proton (D).

Extensive dipolar correlation (i.e., NOESY, see for example Figure S5 in the Supporting Information) experiments provided us with information on the dipolar connectivity. In fact, the analysis of NOESY spectra revealed the presence of significant dipolar interactions between the protons F of the cinnamic fluorophore and protons a, b, and c belonging to the amino acid side chain. This observation supported for the existence of a probable interaction (in the 3D space) of the amino acid side chain with the cinnamic fluorophore, suggesting a very compact 3D structure for diadduct **5b**.

Based on the structural information obtained by the NMR studies, the (*E*,*E*)-stereoisomer was employed in the calculations as the starting geometry. Furthermore, under neutral conditions, the amino acid moiety of **5b** can exist in its zwitterion form, where the negative charge comes from the carboxylate ion and the positive charge comes from the ammonium ion. We therefore decided to verify this possibility by performing optimizations of the two molecules in DMSO and determining their relative energies. The results obtained are shown in Figure 2, where the structure of the neutral molecule (left) is compared with the zwitterionic form (right).

The calculations revealed two similar structures with the aromatic moieties of the two cinnamic fluorophores rearranged into a π−π stacking due to the noncovalent interactions between the π bonds of the aromatic rings.[28] When the molecular orbitals shown in Figure 3 are considered, the orbital overlap produced

https://doi.org/10.1021/acs.jpcb.5c01032
J. Phys. Chem. B 2025, 129, 3928−3937

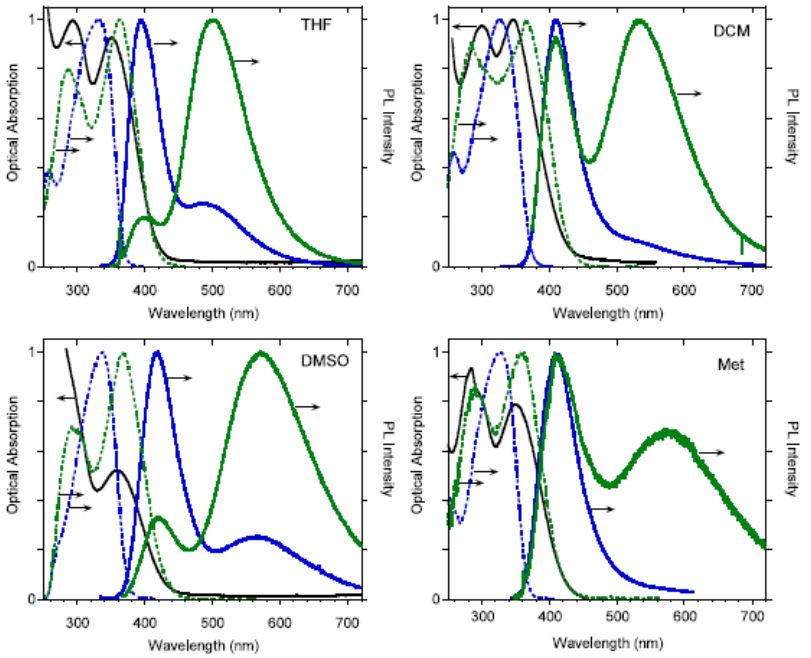

Figure 5. Absorption (black solid line), PL spectra (λ_{ex} = 335 nm; blue solid lines; λ_{ex} = 365 nm, green solid lines) and PL excitation profiles of diadduct **5b** in solution in different organic solvents (blue dashed lines, λ_{em} = 410 nm; green dashed lines λ_{em} = 500 nm, THF; λ_{em} = 535 nm, DCM; λ_{em} = 572 nm, DMSO; λ_{em} = 575 nm, methanol). The measurements are taken for freshly prepared solutions with concentrations of about 10^{-5} M.

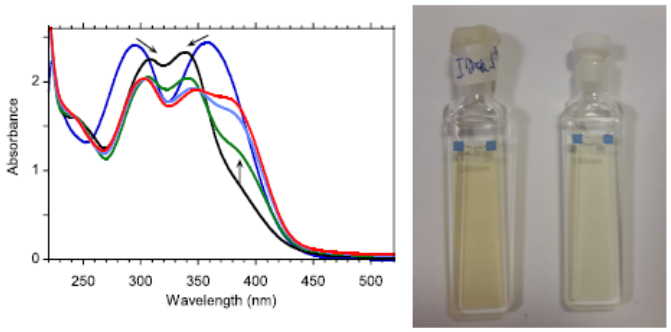

Figure 6. (Left panel) Evolution of the absorbance of diadduct **5b** in a DCM solution (c = 0.7 mg/mL) at different UV-A lamp (366 nm, irradiance 6 μW/cm^2 nm) exposure times (0, blue line; 30 min, black line; 150 min, green line; 270 min, light blue line; 390 min, red line). Arrows show the variation of the absorption by increasing the UV-A irradiation time. (Right panel) Image of the solutions after UV irradiation (left, 480 min; right, 30 min exposure) in ambient light.

by the aromatic stacking can be easily detected in both ground (S_0) and excited (S_1) states in addition to the typical π-conjugation on the aromatic substituents.

Moreover, the neutral form of **5b** seems to be more stable than its ionized counterpart with an energy gap of 0.43 eV (or 10 kcal/mol). Analyzing the Maxwell–Boltzmann distribution between the isomers in the thermal equilibrium condition (25 °C), we obtain the 99.9% possibility to find the molecule in the neutral form.

After the determination of the most probable structure of diadduct derivative **5b**, attention was focused on the theoretical spectroscopic features. As a first step in this direction, we decided to run our simulations considering the neutral isomer of **5b**, in DCM and DMSO as implicit solvents. Thus, the obtained geometries of the ground state (S_0) are shown in Figure 3 along with the Franck–Condon point (FC), the first excited state singlet emitter (S_1), and the distorted ground state after radiative relaxation, in DMSO (Figure 3a) and DCM (Figure 3b). Moreover, the HOMO/LUMO molecular orbitals involved in

https://doi.org/10.1021/acs.jpcb.5c01032
J. Phys. Chem. B 2025, 129, 3928–3937

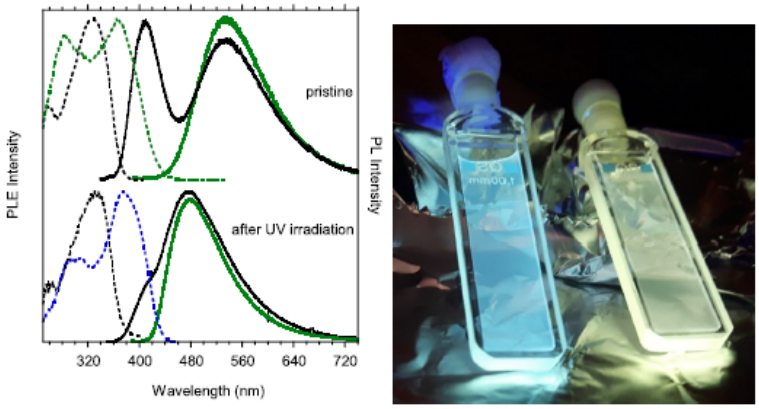

Figure 7. (Left panel) PL (λ_{ex} = 335 nm; black solid lines; λ_{ex} = 390 nm, green solid lines) and PLE (black dashed lines, λ_{em} = 410 nm; green dashed lines λ_{em} = 535 nm; blue dashed line, λ_{em} = 480 nm) spectra of diadduct **5b** in DCM before (top spectra) and after (bottom spectra) UV-A irradiation for 480 min. Solution concentration, 0.7 mg/mL. (Right panel) Picture of the solutions under UV lamp exposure, before (right) and after 480 min of UV-A irradiation (left).

Scheme 2. Formation of Compound 6 by Irradiation of Diadduct 5b with UV-A in Ethanol

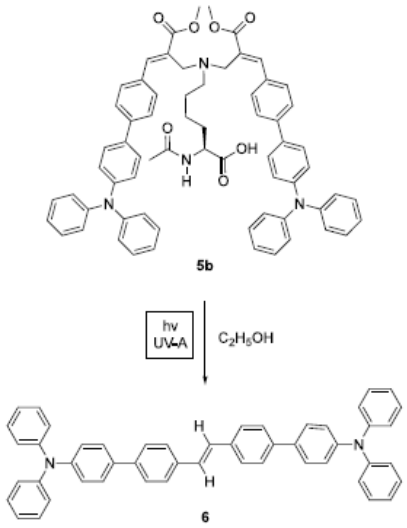

the electronic transition and the relative energy gap are reported for each structure. The comparison of the calculated data with the experimental ones (see below Table 1) showed the existence of a good correlation concerning the absorption energy values. In particular, the vertical excitation wavelength calculated at the FC point in DCM (3.68 eV corresponding to 336 nm) showed a slight blueshift with respect to the experimentally observed (3.5 eV corresponding to 354 nm). In DMSO, the correspondence between calculated (3.78 eV corresponding to 327 nm) and experimental (3.45 eV corresponding to 359 nm) data was maintained, with discrepancies within acceptable values of 0.2–0.3 eV.

Furthermore, the adiabatic relaxation on the first excited state S_1 was simulated starting from the FC structures in both solvents (red arrows in Figure 3) to produce geometries and relative wavelengths of the emitting intermediates. The comparison of the relevant values reported in Table 1 with those reported in Figure 3 showed that the calculation performed in a DCM explicit solvent provided an emission energy (i.e., 2.35 eV corresponding to 528 nm) in good agreement with the experimental one (i.e., 2.33 eV corresponding to 532 nm). On the other hand, more divergent values were obtained in DMSO being the theoretical value of 2.76 eV (corresponding to 450 nm) versus the experimental one of 2.97 eV (corresponding to 418 nm).

Moreover, the oscillator strength at the FC point is 0.6 and increases to 0.8 for the emission. These values are indicative of strong absorption and emission intensities, consistent with a strong radiative $S_1 \rightarrow S_0$ decay (i.e., fluorescence).

Photophysical Properties of Diadduct 5b. We previously reported that monoadduct derivative **4a** showed bright emission features at 535 nm (PL QY = 51%) in dichloromethane, whereas diadduct derivative **5a** showed a double emission spectrum with the low energy component at 524 nm and the high energy component at 408 nm (Table 1).[28]

Very interestingly, the high energy component was absent in the spectrum of **5a** in the solid state (i.e., cast films), so that in the solid state, diadduct **5a** and monoadduct **4a** showed very similar emission features, in agreement with the fact that the same fluorophore is contained in **4a** and **5a** molecules. This observation appeared to support the hypothesis that the excitation of **5a** in solution could lead to the formation of a new chemical entity responsible for the high energy emission at 405–408 nm. In other words, we formulated the hypothesis that the high energy peaks observed only in the spectrum of diadduct **5a** molecularly dissolved in dichloromethane could be generated by the products of the [2 + 2] photocycloaddition promoted by the excitation and occurring in solution.

In the solid state (i.e., cast films), both diadduct **5a** and monoadduct **4a** showed lower photoluminescence quantum yield (PL QY) values, suggesting the existence of aggregation-caused quenching (ACQ) phenomena. Similar results were

https://doi.org/10.1021/acs.jpcb.5c01032
J. Phys. Chem. B 2025, 129, 3928–3937

Scheme 3. Effects of Diadduct 5a Irradiation

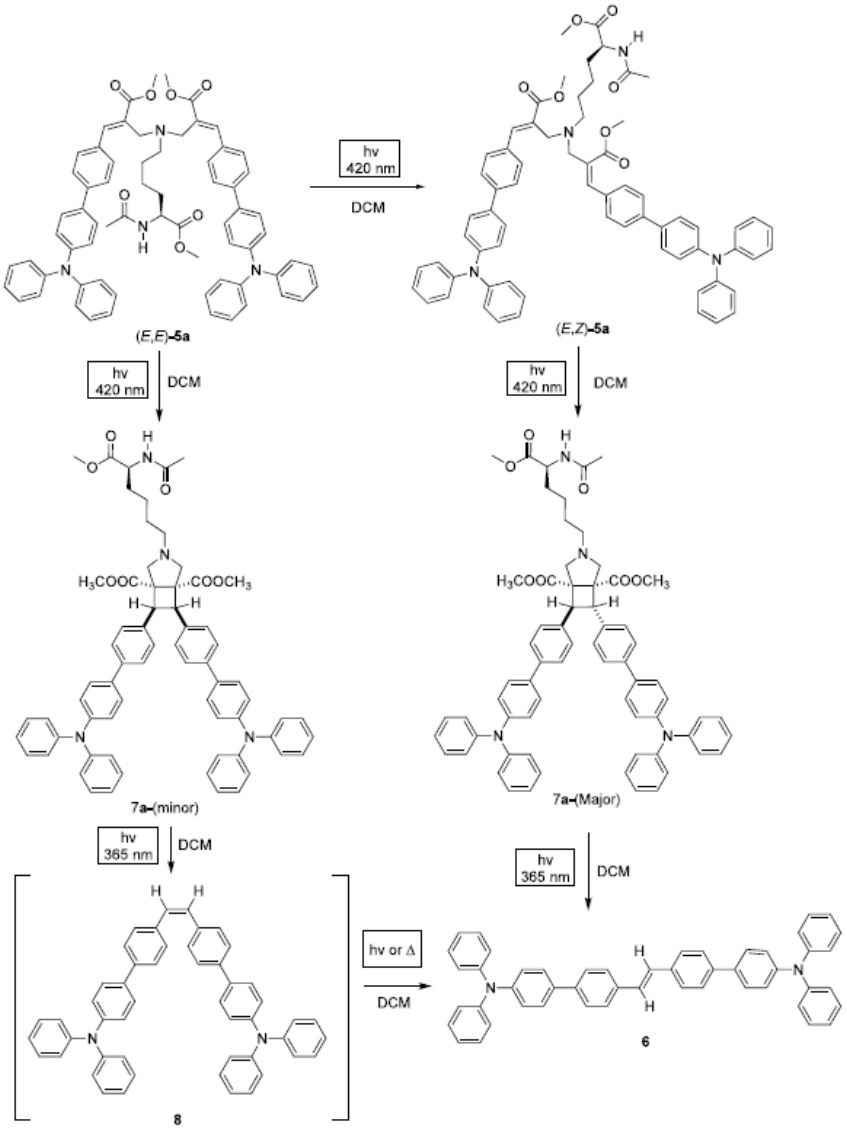

obtained with the newly synthesized diadduct **5b**, which showed in the solid state (i.e., crystalline powder) an emission maximum at around 550 nm (Figure 4) and a PL QY value around 5%.

Afterward, we evaluated the properties of the solutions and the effects of the solvents in the optical features of diadduct **5b** (Figure 5).

In these studies, diadduct **5b** showed a very complex behavior with the presence of distinct emissive species in all the solutions (THF, DCM, DMSO, and methanol) as evidenced by the wavelength-dependent PL spectra shown in Figure 5. In particular, as reported in Table 1, two distinct emissions are resolved by changing the excitation wavelength, one in the blue (peaked in the range 390−420 nm, with an excitation maximum at about 330 nm) and one in the green (500−575 nm). The PL maximum of the green emission displays a redshift for solvents with higher orientation polarizability, Δf, as often observed for polar molecules,[30] and its PLE spectra display two bands well-correlated with the absorption spectra. Differently, the blue emission is less sensitive to the solvent properties and displays a faster decay (see Table 1) and its PLE is not correlated with the absorption. Moreover, its relative intensity is observed to increase in time after the solution preparation and upon light

https://doi.org/10.1021/acs.jpcb.5c01032
J. Phys. Chem. B 2025, 129, 3928−3937

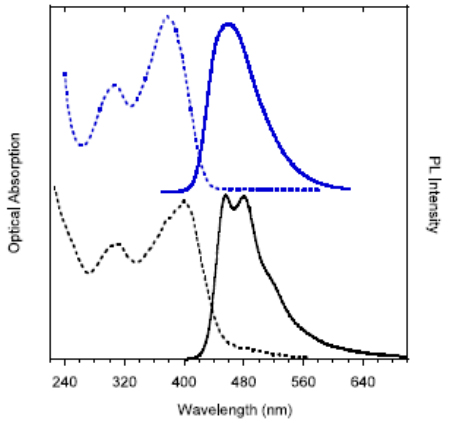

Figure 8. Optical absorption (dashed lines) and PL spectra (solid lines) of compound **6** in dichloromethane solution (top, blue lines, λ_{ex} = 365 nm) and cast films (bottom, black lines, λ_{ex} = 370 nm).

exposure. This behavior supported the hypothesis of the existence of photoinduced degradation phenomena, with the formation of highly emissive compounds with blueshifted emission, in agreement with the results obtained with diadduct derivative **5a**.[28] These processes, particularly evident in dichloromethane and methanol, are faster in diluted solutions with respect to the concentrated ones. As a consequence, their PL QY values could be determined only with low accuracy. In Table 1, both the minimum QY value, measured for freshly prepared solution, and the maximum value measured after about 1 h of excitation at 365 nm are reported. In order to clarify this behavior, we performed a detailed photochemical study of diadduct **5b** by parallel PL and NMR experiments on dichloromethane solutions showing the same concentration.

Photochemical Features of Diadduct 5b. The irradiation with UV-A light (365 nm) of dichloromethane solutions of diadduct **5b** produced a variation in the optical absorption spectra accompanied by a clear-cut blueshift in the emission. The absorption spectrum of the DCM solution slightly changes even after storage in the dark for 2 days, and a shift of the two absorption bands is observed (the 357 nm band blueshifts to 340 nm; the 295 nm band redshifts to 305 nm). The same changes are observed as soon as the solution is exposed to the UV irradiation (up to 30 min exposure), and more relevant changes are observed for prolonged UV irradiation times (see Figure 6) with the appearance and progressive increase of a band at about 390 nm. As a consequence, the light-yellow color of the solution turned to yellow (see Figure 6, right panel).

Even more evident are the variations induced by UV irradiation on the emission properties. As already discussed, before the UV exposure of the solution, the PL analysis reveals the presence of two species emitting at 410 and 535 nm, characterized by distinct PL excitation profiles (PLE) with bands peaked at 325 and 365 nm, respectively (see Figure 5 and Table 1). After UV irradiation, a bright and broad band emission at 480 nm is detected, whose PLE maximum is measured at 378 nm (see Figure 7, left panel, bottom). As a result, the emission color of the solution turns from yellow to blue, when exposed to UV lamp (365 nm) irradiation (see Figure 7, right panel). We noted that the 410 nm blue emission observed in the pristine solution was present also after the irradiation as a shoulder in the spectrum obtained by exciting at 335 nm. Differently, the 535 nm green emission of the pristine solution completely disappeared after irradiation, being shifted to 480 nm. These observations suggested that a new compound was obtained by UV irradiation of the diadduct **5b**, which possesses high emission efficiency in the blue region.

The photolysis reaction process was investigated by ^{1}H NMR spectroscopy studies either in deuterated DCM or DMSO-d_6 by recording spectra at regular time intervals during irradiation at 365 nm. The analysis of the spectra revealed that UV irradiation produced a progressive transformation of diadduct **5b** leading to photolysis reaction mixtures showing very complex compositions. Photolysis experiments were then performed by using ethanol as the solvent. In particular, **5b** solutions in ethanol contained into closed vials were irradiated inside a UV-A chamber for 8 h. After this UV-A exposition, the emission of the ethanolic solution shifted from yellow to cyan (490−520 nm), and the formation of a crystalline solid was observed on the internal surface of the vial. The ethanolic solution was carefully removed from the vial, and the solid was taken up with DCM and purified by flash chromatography to obtain compound **6** as strongly emissive crystals (Scheme 2).

We assumed that the two cinnamic fluorophores of diadduct **5b** are preorganized (see Figure 2) to undergo head-to-head [2 + 2] photocycloaddition leading to the corresponding intermediate, which could interact with another high energy photon leading to the formation of stilbene derivative **6**.

To evaluate this mechanistic hypothesis, the irradiation of **5b** was performed with a less energetic radiation at 420 nm with the aim of isolating the [2 + 2] photocycloaddition intermediate. Thus, a solution of the diadduct derivative **5b** in CD_2Cl_2-DMSO-d_6 (2:1) was irradiated with monochromatic light centered at 420 nm and the reaction progress was followed via ^{1}H NMR spectroscopy by recording spectra at regular time intervals. The analysis of the spectra revealed the formation of some new peaks (see Figure S8), which could be attributed to the product of the [2 + 2] photocycloaddition reaction.

On the bases of the encouraging results obtained, similar experiments were performed on diadduct derivative **5a**, which, in pure DCM, was less aggregated than **5b**. Thus, a solution of the diadduct derivative **5a** in CD_2Cl_2 was irradiated with monochromatic light centered at 420 nm and the reaction progress was followed via ^{1}H NMR spectroscopy by recording spectra at regular time intervals (Figure S9).

This experiment confirmed that in these conditions, compound **5a** underwent the [2 + 2] photocycloaddition reaction leading to compound **7a** (Scheme 3), which was unable to interact with the low energy radiation in the visible range at 420 nm.

On the other hand, when radiations showing higher energy such as those produced by UV-A lamps (i.e., 365 nm) were used, intermediate **7a** was able to generate their excited states capable of evolving in compound **6**.

Interestingly, the characterization of the photophysical features (Figure 8) of compound **6** in solution showed an emission peak at 480 nm with a very remarkable PL QY value (i.e., 69%).

■ CONCLUSIONS

The peculiar reactivity shown by MBHA derivative **3** with Nα-acetyl-L-lysine derivatives led to focusing our attention on diadduct **5b** as the most important reaction product that

https://doi.org/10.1021/acs.jpcb.5c01032
J. Phys. Chem. B 2025, 129, 3928−3937

contains two triphenylaminocinnamic (TPAC) chromophores in its structure. The structure of **5b** was investigated by ^{1}H NMR spectroscopy and molecular modeling. The evaluation of the photophysical features of **5b** in the solid state showed that the presence of two TPAC chromophores in the same molecule of **5b** appeared to redshift the emission and decreased the PL QY as it usually occurs in aggregation quenching phenomena. On the other hand, diadduct **5b** showed in solution a very complex photophysical profile with higher PL QY values, suggesting a possible susceptibility toward the [2 + 2] photocycloaddition reaction. Thus, this liability was evaluated systematically in photolysis experiments monitored by absorption/emission and ^{1}H NMR spectroscopy experiments. These experiments revealed the occurrence of a rather complex pathway of the photolytic reactions but allowed us to isolate (although in low yield) very emissive compound **6**.

■ ASSOCIATED CONTENT

Supporting Information

The Supporting Information is available free of charge at https://pubs.acs.org/doi/10.1021/acs.jpcb.5c01032.

Comparison of the ^{1}H and ^{13}C NMR spectra of diadduct **5b** recorded in DMSO-d_6 or CD_2Cl_2-DMSO-d_6 (2:1) at 600 MHz; COSY, HMBC, and NOESY full spectra of diadduct **5b** in DMSO-d_6 at 600 MHz; experimental details for the synthesis and the characterization of compounds **4b**, **5b**, **6**, and **7a**; experimental details of the photochemical characterization of compounds **5a**,**b**; PL decay of compounds **4a** and **5a**; Cartesian coordinates of the Franck−Condon geometry of neutral **5b** in CH_2Cl_2 and in DMSO; Cartesian coordinates of the neutral emitting intermediate **5b** in CH_2Cl_2 and in DMSO (PDF)

■ AUTHOR INFORMATION

Corresponding Author

Andrea Cappelli − *Dipartimento di Biotecnologie, Chimica e Farmacia, Università degli Studi di Siena, Siena 53100, Italy;* orcid.org/0000-0003-4140-3028; Phone: +39 0577 232416; Email: andrea.cappelli@unisi.it

Authors

Mario Saletti − *Dipartimento di Biotecnologie, Chimica e Farmacia, Università degli Studi di Siena, Siena 53100, Italy;* orcid.org/0000-0002-8414-3134

Marco Paolino − *Dipartimento di Biotecnologie, Chimica e Farmacia, Università degli Studi di Siena, Siena 53100, Italy*

Jacopo Venditti − *Dipartimento di Biotecnologie, Chimica e Farmacia, Università degli Studi di Siena, Siena 53100, Italy*

Gianluca Giorgi − *Dipartimento di Biotecnologie, Chimica e Farmacia, Università degli Studi di Siena, Siena 53100, Italy;* orcid.org/0000-0002-8817-7745

Claudia Bonechi − *Dipartimento di Biotecnologie, Chimica e Farmacia, Università degli Studi di Siena, Siena 53100, Italy*

Alessandro Donati − *Dipartimento di Biotecnologie, Chimica e Farmacia, Università degli Studi di Siena, Siena 53100, Italy*

Claudio Rossi − *Dipartimento di Biotecnologie, Chimica e Farmacia, Università degli Studi di Siena, Siena 53100, Italy*

Germano Giuliani − *Dipartimento di Biotecnologie, Chimica e Farmacia, Università degli Studi di Siena, Siena 53100, Italy;* orcid.org/0000-0001-8111-3776

Antonella Caterina Boccia − *Istituto di Scienze e Tecnologie Chimiche "G. Natta"-SCITEC (CNR), Milano 20133, Italy*

Chiara Botta − *Istituto di Scienze e Tecnologie Chimiche "G. Natta"-SCITEC (CNR), Milano 20133, Italy;* orcid.org/0000-0001-8722-0417

Lluís Blancafort − *Institute of Computational Chemistry and Catalysis and Department of Chemistry, University of Girona, Girona 17003, Spain;* orcid.org/0000-0002-0003-5540

Complete contact information is available at: https://pubs.acs.org/10.1021/acs.jpcb.5c01032

Notes

The authors declare no competing financial interest.

■ ACKNOWLEDGMENTS

The authors thank prof. Massimo Olivucci (Dipartimento di Biotecnologie, Chimica e Farmacia, Università degli Studi di Siena) for the fruitful discussions. M.P. and A.C. acknowledge the MUR for financial support under the project CN00000041−"National Center for Gene Therapy and Drugs based on RNA Technology"−CUP B63C2200061 0006 Mission 4 Component 2 (M4C2)−investment 1.4 [CN3] of the National Recovery and Resilience Plan (PNRR) funded by the European Union "Next Generation EU". M.P. acknowledges the University of Siena for financial support of the project Chromo-GEnUP through the F-CUR2022 funding line (2265-2022-PM-CONRICMIUR_PC-FCUR2022_003).

■ REFERENCES

(1) Kadambar, V. K.; Melman, A. Selective Derivatization of Hexahistidine-Tagged Recombinant Proteins. *Adv. Exp. Med. Biol.* **2019**, *1140*, 237−250.

(2) Jain, M.; Kamal, N.; Batra, S. K. Engineering Antibodies for Clinical Applications. *Trends Biotechnol.* **2007**, *25*, 307−316.

(3) Ward, C. C.; Kleinman, J. I.; Nomura, D. K. NHS-Esters as Versatile Reactivity-Based Probes for Mapping Proteome-Wide Ligandable Hotspots. *ACS Chem. Biol.* **2017**, *12*, 1478−1483.

(4) Rosa-Neto, P.; Wängler, B.; Iovkova, L.; Boening, G.; Reader, A.; Jurkschat, K.; Schirrmacher, E. [^{18}F]SiFA-Isothiocyanate: a New Highly Effective Radioactive Labeling Agent for Lysine-Containing Proteins. *ChemBioChem.* **2009**, *10*, 1321−1324.

(5) Raindlová, V.; Pohl, R.; Hocek, M. Synthesis of Aldehyde-Linked Nucleotides and DNA and Their Bioconjugations with Lysine and Peptides Through Reductive Amination. *Chem. - Eur. J.* **2012**, *18*, 4080−4087.

(6) Pagano, K.; Paolino, M.; Fusi, S.; Zanirato, V.; Trapella, C.; Giuliani, G.; Cappelli, A.; Zanzoni, S.; Molinari, H.; Ragona, L.; et al. Bile Acid Binding Protein Functionalization Leads to a Fully Synthetic Rhodopsin Mimic. *J. Phys. Chem. Lett.* **2019**, *10*, 2235−2243.

(7) Smith, B. D.; Higgin, J. J.; Raines, R. T. Site-Specific Folate Conjugation to Cytotoxic Protein. *Bioorg. Med. Chem. Lett.* **2011**, *21*, 5029−5032.

(8) Gunnoo, S. B.; Madder, A. Chemical Protein Modification Through Cysteine. *ChemBioChem.* **2016**, *17*, 529−553.

(9) Mir, M. H.; Parmar, S.; Singh, C.; Kalia, D. Location-Agnostic Site-Specific Protein Bioconjugation Via Baylis Hillman Adducts. *Nat. Commun.* **2024**, *15*, 859.

(10) Guignet, E. G.; Hovius, R.; Vogel, H. Reversible Site-Selective Labeling of Membrane Proteins in Live Cells. *Nat. Biotechnol.* **2004**, *22*, 440−444.

(11) Griffin, B. A.; Adams, S. R.; Tsien, R. Y. Specific Covalent Labeling of Recombinant Protein Molecules Inside Live Cells. *Science* **1998**, *281*, 269−272.

(12) Krishnan, B.; Szymanska, A.; Gierasch, L. M. Site-Specific Fluorescent Labeling of Poly-Histidine Sequences Using Metal-Chelating Cysteine. *Chem. Biol. Drug Des.* **2007**, *69*, 31−40.

(13) Wang, Z.; Ding, X.; Li, S.; Shi, J.; Li, Y. Engineered Fluorescence Tags for in Vivo Protein Labeling. *RSC Adv.* **2014**, *4*, 7235−7245.

(14) Rong, L.; Zhang, C.; Lei, Q.; Qin, S.; Feng, J.; Zhang, X. A Two-Photon Excitation Based Fluorogenic Probe for Sialome Imaging in Living Systems. *Adv. Sci.* **2016**, *3*, No. 1500211.
(15) Lavis, L. D.; Chao, T.-Y.; Raines, R. T. Fluorogenic Label for Biomolecular Imaging. *ACS Chem. Biol.* **2006**, *1*, 252−260.
(16) Mei, J.; Leung, N. L. C.; Kwok, R. T. K.; Lam, J. W. Y.; Tang, B. Z. Aggregation-Induced Emission: Together we Shine, United We Soar! *Chem. Rev.* **2015**, *115*, 11718−11940.
(17) Ding, D.; Li, K.; Liu, B.; Tang, B. Z. Bioprobes Based on AIE Fluorogens. *Acc. Chem. Res.* **2013**, *46*, 2441−2453.
(18) Wu, W. C.; Chen, C. Y.; Tian, Y.; Jang, S. H.; Hong, Y.; Liu, Y.; Hu, R.; Tang, B. Z.; Lee, Y. T.; Chen, C. T.; et al. Enhancement of Aggregation-Induced Emission in Dye-Encapsulating Polymeric Micelles for Bioimaging. *Adv. Funct. Mater.* **2010**, *20*, 1413−1423.
(19) Razzano, V.; Paolino, M.; Reale, A.; Giuliani, G.; Artusi, R.; Caselli, G.; Visintin, M.; Makovec, F.; Donati, A.; Villafiorita-Monteleone, F.; et al. Development of Imidazole-Reactive Molecules Leading to a New Aggregation-Induced Emission Fluorophore Based on the Cinnamic Scaffold. *ACS Omega* **2017**, *2*, 5453−5459.
(20) Razzano, V.; Paolino, M.; Reale, A.; Giuliani, G.; Donati, A.; Giorgi, G.; Artusi, R.; Caselli, G.; Visintin, M.; Makovec, F.; et al. Poly-Histidine Grafting Leading to Fishbone-Like Architectures. *RSC Adv.* **2018**, *8*, 8638−8656.
(21) Paolino, M.; Reale, A.; Razzano, V.; Giuliani, G.; Donati, A.; Bonechi, C.; Caselli, G.; Visintin, M.; Makovec, F.; Scialabba, C.; et al. Nanoreactors for the Multi-Functionalization of Poly-Histidine Fragments. *New J. Chem.* **2019**, *43*, 6834−6837.
(22) Paolino, M.; Visintin, M.; Margotti, E.; Visentini, M.; Salvini, L.; Reale, A.; Razzano, V.; Giuliani, G.; Caselli, G.; Tavanti, F.; et al. Functionalization of Protein Hexahistidine Tags by Functional Nanoreactors. *New J. Chem.* **2019**, *43*, 17946−17953.
(23) Tassone, G.; Paolino, M.; Pozzi, C.; Reale, A.; Salvini, L.; Giorgi, G.; Orlandini, M.; Galvagni, F.; Mangani, S.; Yang, X.; Carlotti, B.; Ortica, F.; Latterini, L.; Olivucci, M.; Cappelli, A.; et al. Xanthopsin-Like Systems Via Site-Specific Click-Functionalization of a Retinoic Acid Binding Protein. *ChemBioChem.* **2022**, *23*, No. e202100449.
(24) Saletti, M.; Paolino, M.; Venditti, J.; Bonechi, C.; Giuliani, G.; Boccia, A.; Botta, C.; Cappelli, A. Synthesis, Photophysical and Photochemical Features of a Morita-Baylis-Hillman Adduct Derivative Bearing a Triphenylamine Moiety. *Dyes Pigm.* **2023**, *219*, No. 111571.
(25) Saletti, M.; Venditti, J.; Paolino, M.; Zacchei, A.; Giuliani, G.; Giorgi, G.; Bonechi, C.; Donati, A.; Cappelli, A. A tri(ethylene glycol)-tethered Morita-Baylis-Hillman dimer in the formation of macrocyclic crown ether-paracyclophane hybrid structures. *RSC Adv.* **2023**, *13*, 35773−35780.
(26) Saletti, M.; Paolino, M.; Venditti, J.; Bonechi, C.; Giuliani, G.; Lamponi, S.; Tassone, G.; Boccia, A.; Botta, C.; Blancafort, L.; Poggialini, F.; Vagaggini, C.; Cappelli, A.; et al. A Facile Access to Green Fluorescent Albumin Derivatives. *ChemBioChem.* **2024**, *25*, No. e202300862.
(27) Lami, M.; Barneschi, L.; Saletti, M.; Olivucci, M.; Cappelli, A.; Paolino, M. Preparation of Light-Responsive Unnatural RNA Bases Via a Chromogenic Morita-Baylis-Hillman Adduct Path. *ChemPhotoChem.* **2024**, No. e202400093.
(28) Venditti, J.; Saletti, M.; Paolino, M.; Contena, S.; Bonechi, C.; Giuliani, G.; Giorgi, G.; Boccia, A. C.; Botta, C.; Blancafort, L.; Cappelli, A.; et al. Reactivity of a Morita-Baylis-Hillman Adduct Derivative Bearing a Triphenylamine Moiety with Lysine Models. *Chem. - Asian J.* **2024**, No. e202400617.
(29) Frisch, M. J.; Trucks, G. W.; Schlegel, H. B.; Scuseria, G. E.; Robb, M. A.; Cheeseman, J. R.; Scalmani, G.; Barone, V.; Petersson, G. A.; Nakatsuji, H.et al.*Gaussian 16*, Revision C.0; Gaussian, Inc.: Wallingford CT, 2016.
(30) Cariati, E.; Lanzeni, V.; Tordin, E.; Ugo, R.; Botta, C.; Giacometti Schieroni, A.; Sironi, A.; Pasini, D. Efficient Crystallization Induced Emissive Materials Based on a Simple Push−Pull Molecular Structure. *Phys. Chem. Chem. Phys.* **2011**, *13* (40), 18005−18014.

https://doi.org/10.1021/acs.jpcb.5c01032
J. Phys. Chem. B 2025, 129, 3928−3937

CHAPTER 3

SYNTHESIS AND REACTIVITY STUDIES OF DIFFERENT COVALENT PROBES

3.1 PROTEIN LABELLING APPROACHES

Over the past decades, the development of protein labeling techniques has greatly expanded the range of tools available to researchers, spanning from covalent small-molecule probes to advanced biorthogonal strategies. These approaches played a pivotal role in the study of cellular processes and have enabled applications in imaging, proteomics, and the development of both diagnostic and therapeutic platforms.[1] Historically, one of the earliest strategies to monitor protein-protein interactions relied on the use of Green Fluorescent Protein (GFP). Several methodologies have exploited GFP and its chimeras. These included luminescence resonance energy transfer (LRET), which involved the transfer of energy from *Renilla* luciferase to GFP, and fluorescence gel retardation, which takes advantage of the difference in electrophoresis mobility between GFP-tagged proteins alone and their complexes with the protein of interest (POI).[2-4] Despite their utility, GFP-based systems present a major limitation: the relatively large size of the protein tag, which can interfere with the localization and native function of the POI. To overcome these drawbacks, modern strategies increasingly rely on chemical labelling, which offers greater versatility compared to fusion protein approaches, enabling a broader range of functionalities.[5] Current methodologies are generally categorized into three main classes: protein domain recognition strategies, peptide recognition strategies, and endogenous protein labeling strategies.

Protein domain recognition approaches remain conceptually related to GFP-based systems, as they are based on fusing the POI with a second protein that exhibits high affinity for a labeled ligand. While these methods ensure high specificity, the substantial increase in molecular size can still perturb the biological role and localization of the POI.[5] As an alternative, peptide recognition strategies employ smaller affinity tags, which are expected to be less invasive. A representative example is the polyhistidine tag, which exploits the strong Ni^{2+}-*N*-nitrilotriacetic acid interaction for protein recognition.[6] Even in cases requiring the covalent attachment of fluorophores to short peptide tags, the overall tag-fluorophore conjugate remains significantly smaller than GFP, thereby reducing the probability of functional perturbation. Finally, endogenous protein labeling strategies have emerged as the most refined and elegant approaches, as they enable selective recognition of the POI without the need for affinity tags. A notable example is ligand-directed tosyl (LDT) chemistry, in which a tosyl ester-functionalized ligand binds the POI at a specific site through nucleophilic attack from a nearby basic amino acid

residue.[7] These methods minimize structural perturbations while maintaining high labeling specificity, highlighting their growing importance in chemical biology.

For these reasons, the use of chemical probes has recently gained significant attention, and within this context, fluorescent probes have emerged as attractive and versatile tools for optical imaging and analytical sensing due to their rapid response time and remarkable sensitivity. Numerous studies and reviews have focused on the role of fluorescent labeling and on the wide range of fluorescent-based assay and imaging applications, spanning from the investigation of key cellular chemical processes[8,9] to advanced microscopy techniques[10] and various combinatorial strategies.[11] At the same time, another class of probes has been developed, differing slightly from conventional fluorescent probes. These molecules, known as fluorogenic probes, typically exist in a quenched or weakly emissive state and become strongly fluorescent only upon specific conjugation or binding to their target structure at a defined wavelength.[12] Therefore, while fluorescent probes display intrinsic emission when excited by a light source, fluorogenic probes reveal a "switch-on" behavior, emitting light exclusively upon interaction with their target (Figure 1). Because fluorescence arises only upon target recognition, fluorogenic probes offer higher signal-to-noise ratios and are particularly advantageous for biological imaging. In particular, fluorogenic systems that undergo an irreversible switch-on process enable high-contrast images with minimal background signals, making them well-suited for super-resolution microscopy techniques.[13,14]

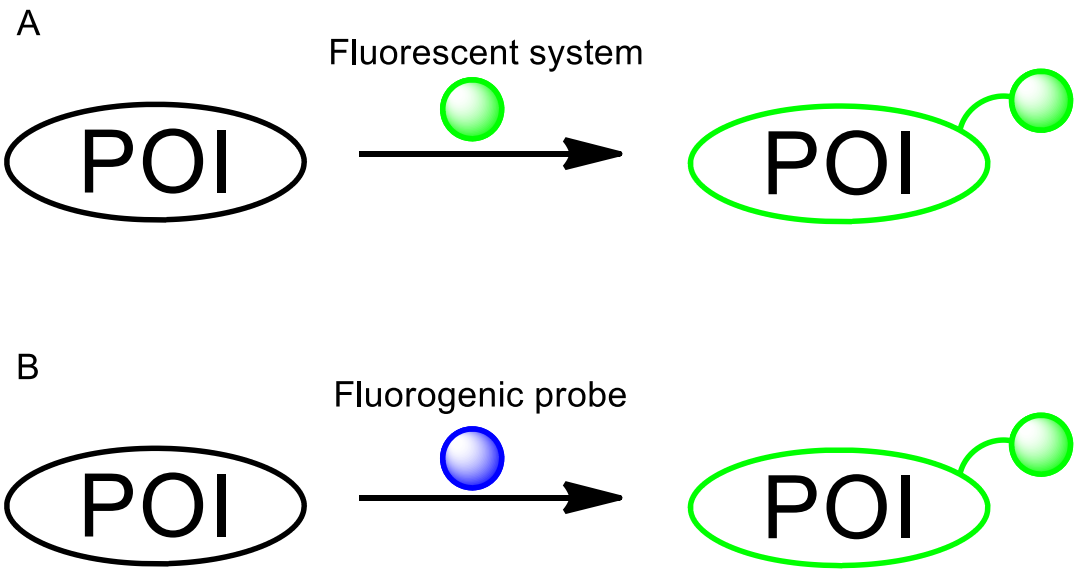

Figure 1. Schematic and simplified illustration highlighting the fundamental difference between protein labeling approaches based on fluorescent systems (**A**) and those employing fluorogenic probes (**B**).

In this regard, the chemical strategies employed for protein labeling must operate under mild, biocompatible conditions, typically at ambient temperature and aqueous environments. Several reactions have been developed to functionalize the side chains of specific amino acids, particularly lysine (Lys), cysteine (Cys), histidine (His), and arginine (Arg), which are among the most common nucleophilic sites in proteins.[15-17] In addition, the side chains of aromatic amino acids such as tyrosine (Tyr) and tryptophan (Trp) can also be modified under appropriate conditions.[18] To efficiently react with these nucleophilic residues, electrophilic moieties are required. Specifically, lysine residues, which often expose on the protein surface, are convenient targets for reactions with relatively hard electrophiles. Conversely, cysteine residues are among the most reactive amino acids owing to the high nucleophilicity of the sulfhydryl group; however, their limited availability, due to their frequent involvement in disulfide bridges, can restrict their accessibility for covalent modification.[19] Despite these challenges, the reactivity of basic and nucleophilic amino acids, such as lysine, cysteine, and sometimes histidine residues, has been exploited in the development of the Target Covalent Inhibitor (TCI) concept. This approach relies on converting reversible inhibitors into covalent probes by introducing weakly electrophilic functional groups, commonly referred to as warheads.[20-21] Representative examples of such warheads include acrylamides,[22-24] *N*-hydroxysuccinimide ester,[25] sulfonyl chloride,[26] isothiocyanates,[27] acrylates,[28] chloroacetamides,[29] and cyanoenone derivatives.[20]

3.2 HUMAN SERUM ALBUMIN

Human Serum Albumin (**HSA**) is the most abundant protein in the circulatory system and performs a wide range of essential physiological functions. The protein consists of 585 amino acid residues, with an approximate molecular weight of 66,5 kDa, and contains a single tryptophan residue (Trp-214) and a free cysteine (Cys-34).[30] All the remaining cysteine residues participate in the formation of eight disulfide bridges, arranged in nine loop-link-loop motifs that contribute to the overall stability of the protein structure.[30] In addition, **HSA** also contains 59 lysine residues, which can be used for the covalent modification of drugs, and 16 histidine residues.[30-32] The crystal structure of **HSA**, depicted in Figure 2 (PDB ID:1AO6),[33] reveals an asymmetric heart-shaped conformation characterized by a predominance of α-helical content (approximately 68%), organized into six helical subdomains.[33,34] The aminoacidic sequence is further arranged into three

homologous domains, called I, II, and III, each comprising two subdomains (A and B) that contribute to the protein's distinctive tertiary organization.[34]

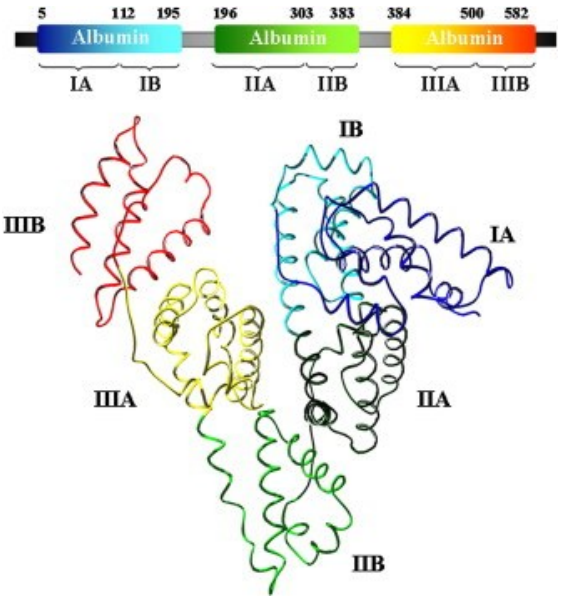

Figure 2. Crystal structure of the Human Serum Albumin.[34] Atomic coordinates were taken from the PDB ID 1AO6.[33] Ribbon representation of HSA was drawn using Swiss-PdbViewer.[35]

HSA performs multiple physiological functions, ranging from maintaining colloid osmotic pressure in blood plasma to serving as the principal transport protein responsible for distributing and metabolizing a wide variety of exogenous and endogenous ligands. These include numerous drugs, peptides, proteins, metal ions such as zinc, calcium, or copper, as well as the heme group, and fatty acids, which all utilize **HSA** as a carrier within the circulatory system.[34] To accommodate this structural versatility, **HSA** possesses several well-defined binding sites within its three-dimensional architecture, among which the fatty acid (FA) binding sites play a crucial role.[34] Among these, the FA1 site, also known as the heme-binding site, is responsible for the interaction and transport of heme groups.[36] Furthermore, FA3 and FA4, located within subdomain IIIA, together form Sudlow's site II,[37,38] commonly referred to as the benzodiazepine site, which represents a major binding region for numerous pharmaceutical compounds, including diazepam and ibuprofen.[39] In addition, the FA7 binding site, positioned within a hydrophobic cavity in subdomain IIA, corresponds to Sudlow site I or the warfarin-binding site.[37,38] This pocket displays a high affinity for drugs such as warfarin, azapropazone, or phenylbutazone, due to the presence of aromatic side chains that promote hydrophobic interaction.[39]

The remarkable potential of **HSA** as a drug delivery system has drawn considerable attention in recent years, owing to its outstanding biodegradability, biocompatibility, non-immunogenic nature, and low toxicity. Its inherent capacity to interact with hydrophobic compounds, coupled with the possibility of surface functionalization and high drug-loading capacity, renders **HSA** an exceptionally versatile and adaptable carrier.[39] This versatility enables the application of **HSA**-based systems not only in the delivery of therapeutic agents[40] but also in biomedical imaging[41] and gene therapy approaches.[42] Furthermore, the specific affinity of albumin for receptors expressed on both endothelial cells and pathological cells facilitates active targeting and site-specific delivery of albumin-based nanocarriers. This property represents one of the distinctive advantages of albumin compared with other nanodelivery systems and has inspired the development of albumin-coated or albumin-corona nanoparticles to enhance biocompatibility and targeting efficiency.[39] With several albumin-derived formulations currently undergoing clinical evaluation, and with the successful approval of Abraxane[43,44] as a pioneering albumin-bound drug delivery system, **HSA** continues to emerge as a promising and clinically relevant nanocarrier for next-generation therapeutic and diagnostic applications.

3.3 AIMS OF THE CHAPTER

In this context, considering the effectiveness of the previously described warheads, it becomes essential to assess the reactivity of well-established MBHA derivatives, particularly in relation to the potential affinity between their acrylic moieties and the nucleophilic side chains embedded within protein structures. The electrophilic portion presented in MBHA derivatives has indeed shown remarkable reactivity properties, deserving significant attention in the design of covalent probes for protein structure modification.[45] Specifically, these covalent probes are potentially capable of interacting with POI through two different steps: an initial non-covalent recognition within a suitable binding pocket in the protein structure, followed by a covalent reaction between the warhead and the appropriate amino acid residue.[45] Building upon the results presented in **Chapter 2,** which demonstrated the outstanding reactivity of MBHA acetyl derivative **9** bearing a TPA moiety toward various lysine models, the focus of **Chapter 3** is on investigating the reactivity of compound **9** toward **HSA**, selected as it represents one of the most relevant and abundant systems in the human body.

Subsequently, to evaluate the contribution of the fluorophore moiety, new covalent probes, **24** and **25**, were designed based on the notable photophysical properties of ethyl (*E*)-3-(4-(9,9-dimethyl-9*H*-fluoren-2-yl)phenyl)acrylate (DMFP) fluorophore **5** (Figure 3). This cinnamic derivative **5** exhibited strong violet emission (430 nm) with high PL QY both in solution (57%) and in the solid state (64%).[46] Moreover, the substitution of the TPA portion to DMFP was expected to influence the initial non-covalent recognition step and, consequently, the overall interaction with the POI. Furthermore, for comparative purposes regarding the warhead functionality, covalent probe **25** was designed by replacing the acrylic moiety of its analogue compound **24** with an acrylamide group, which represents one of the most common warheads in the design of TCIs, and is known for its selective reactivity toward cysteine residues.[20-25]

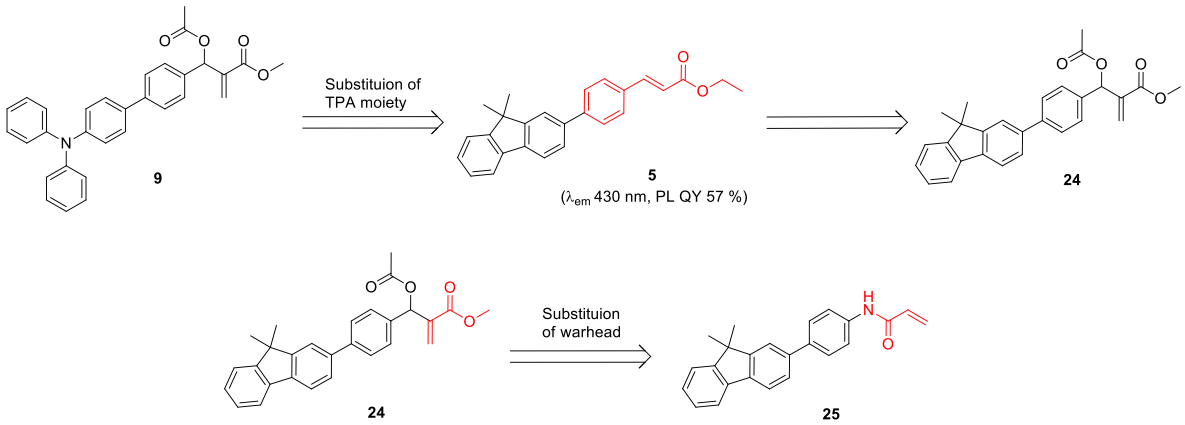

Figure 3. Design approach for the development of two new covalent probes, **24** and **25**, based on the well-described reactivity features of MBHA acetyl **9** (see **Chapter 2**) and the remarkable optical properties of cinnamic derivative **5**.[46]

Therefore, based on the differences in electrophilicity between these two warheads, the reactivity profiles of compounds **24** and **25** were evaluated against different nucleophilic amino acid residues, such as *N*α-acetyl-*L*-lysine methyl ester (**NALME**) hydrochloride, *N*-acetyl-*L*-histidine methyl ester (**NAHME**) acetate, and *N*-acetyl-*L*-cysteine methyl ester (**NACME**).

3.4 INVESTIGATION OF THE INTERACTION BETWEEN MBHA DERIVATIVE 9 AND HUMAN SERUM ALBUMIN.

To evaluate the interaction between MBHA acetyl derivative **9** against **HSA**, multiple techniques, such as computational Molecular Dynamics (MD) simulations, NMR spectroscopy, absorption, and emission spectroscopy, were used.

Concerning NMR spectroscopy, a series of experiments was designed to monitor the addition-elimination mechanism underlying the reaction between compound **9** and the nucleophilic amino acid residues embedded in the **HSA**. Specifically, ^{1}H NMR spectra were recorded at regular time intervals to detect the exit of the acetyl group associated with the elimination step of the reaction, which was conducted at 50 °C. Comparison of the spectra confirmed the good stability of **HSA** under the selected experimental conditions, consistent with its previously reported thermal stability upon prolonged heating at 60 °C.[39] At the same time, a progressive increase in the signal attributed to the protons of the acetate group at 1.88 ppm was observed, indicating the ongoing progress of the addition-elimination reaction.

The most remarkable observation concerned the changes in optical properties during the reaction. In particular, the system exhibited distinctive behavior characterized by pronounced variations in fluorescence emission when the reaction mixture was exposed to a UV lamp (365 nm), typically employed for TLC visualization. Initially, the blue emission of the solution was attributed to the formation of microaggregates of compound **9**, which enhanced its AIE properties. Upon heating at 50 °C, this emission gradually shifted to the green-yellow region, suggesting the formation of cinnamic portions. (Figure 4).

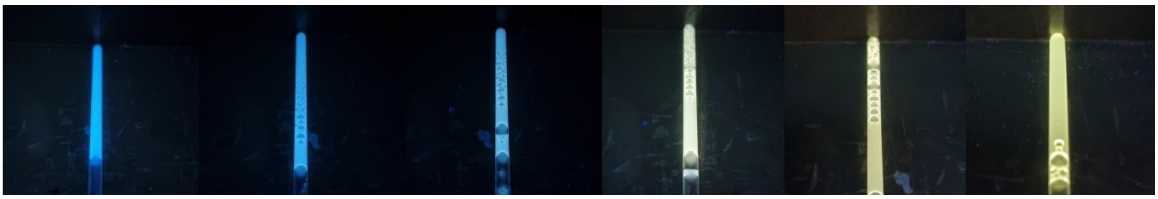

Figure 4. Comparison of the fluorescence emission observed during the reaction between **HSA** and MBHA acetyl **9** in a D_20/DMSO-d_6. The NMR tube was maintained at 50 °C and photographed at regular time intervals (0, 1, 2, 4, 8, and 24 hours from left to right) under UV irradiation at 365 nm.

More interestingly, after thermal treatment, both the photoluminescence (PL) and PL excitation state (PLE) spectra exhibited significant changes. Specifically, PL spectra

showed a progressive red-shift from 480 nm at t = 0 to 525 nm after 8 hours, while PLE spectra revealed a distinctive alteration in profile, displaying a sharp peak at approximately 280 nm, which corresponded to the characteristic absorption of **HSA**. These observations indicated that, within the reaction mixture, **HSA** was capable of transferring energy to the cinnamic structure derived from compound **9** only after thermal activation. The heating process likely facilitated this energy transfer by decreasing the distance between the two chromophores and leading to the formation of a Green Fluorescent Albumin (**GFA**).

The newly formed **GFA** was subsequently characterized through SDS-PAGE, Dynamic Light Scattering (DLS), Molecular Dynamics (MD) simulations, and biological properties. SDS-PAGE analysis confirmed the preservation of **HSA** structural integrity under the reaction conditions, while DLS measurements revealed a marked tendency of **GFA** to form aggregates of defined dimensions, potentially because of conformational changes. Regarding its biological properties, **GFA** was evaluated for its ability to bind drug molecules such as warfarin and diazepam. The results demonstrated that **GFA** retained the essential binding capabilities of native **HSA**, thereby confirming its potential as a drug carrier and a promising candidate for drug delivery applications.

The data collected have been published in the journal *ChemBioChem*. For further details, refer to the Research Article reported in **Paragraph 3.9**.

3.5 SYNTHESIS AND REACTIVITY OF NOVEL DMFP-CONTAINING COVALENT PROBES

To evaluate the different effects induced by two distinct warheads in the design of the novel covalent probes **24** and **25**, both bearing a 9,9-dimethylfluorene (DMFP) moiety, our attention was first focused on their synthesis.

3.5.1 Synthetic procedures to obtain covalent probes 24 and 25

Scheme 1. Preparation of MBHA acetyl derivative **24**.

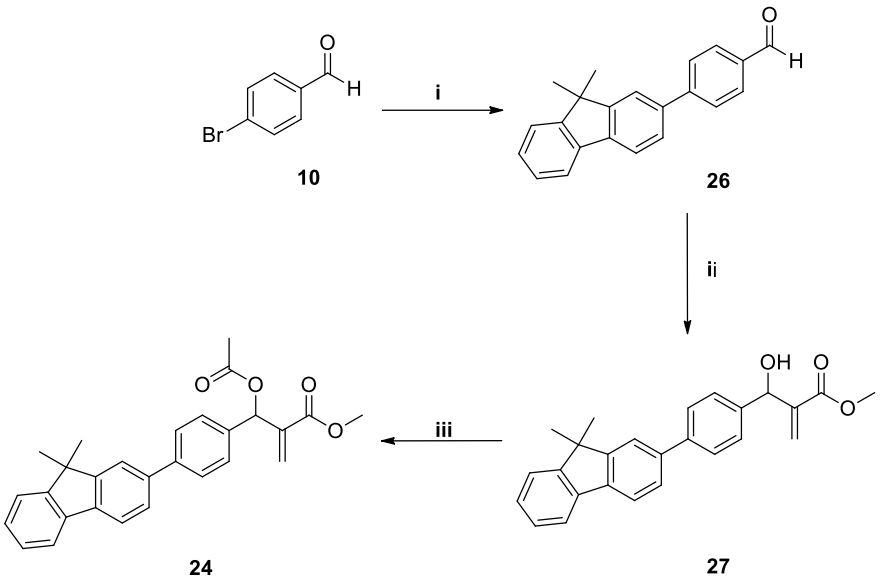

Reagents. (***i***) 9,9-Dimethylfluorene-2-boronic acid pinacol ester, $Pd(PPh_3)_2Cl_2$, PPh_3, Cs_2CO_3, CH_3OH, THF; (***ii***) methyl acrylate, DABCO, CH_3OH; (***iii***) CH_3COCl, TEA, CH_2Cl_2.

Since compound **24** is an analogue of the previously described MBHA acetyl derivative **9**, the same synthetic strategy was employed (**Scheme 1**). Specifically, starting from commercially available 4-bromobenzaldehyde **10**, a Suzuki-Miyaura coupling reaction was carried out with the commercially available 9,9-dimethylfluorene-2-boronic acid pinacol ester in the presence of $Pd(PPh_3)_2Cl_2$ and PPh_3 as the catalytic system, using THF and methanol as solvents. The resulting aldehyde intermediate **26**[47,48] was then subjected to a well-established Morita-Baylis-Hillman reaction with methyl acrylate and DABCO as a tertiary amine, in the presence of catalytic amounts of methanol, affording compound **27**. Finally, acetylation of this intermediate with acetyl chloride in the presence of TEA as base yielded the desired MBHA derivative **24**.

Scheme 2. Synthetic procedures employed to afford the covalent probe **25**.

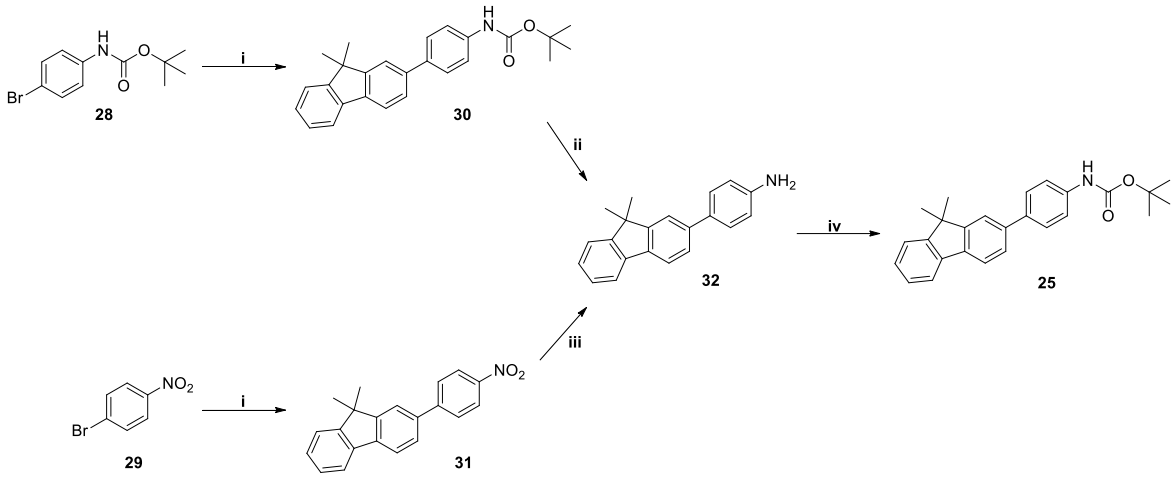

Reagents. (***i***) 9,9-Dimethylfluorene-2-boronic acid pinacol ester, $Pd(PPh_3)_2Cl_2$, PPh_3, Cs_2CO_3, CH_3OH, THF; (***ii***) TFA, CH_2Cl_2; (***iii***) Fe(0), NH_4Cl, HCl, CH_3CH_2OH, H_2O; (***iv***) CH_2=CH-COCl, TEA, CH_2Cl_2.

The analogue covalent probe **25** was designed by substituting the electrophilic moiety of compound **24**, replacing the acrylic group with an acrylamide functionality. To achieve this, two different synthetic routes were explored (**Scheme 2**). Both approaches began with the previous Suzuki-Miyaura coupling reaction, carried out using two different aryl bromide precursors: *tert*-butyl (4-bromophenyl)carbamate **28**[49] and commercially available 4-bromonitrobenzene **29**. In the first case, the reaction afforded the carbamate derivative **30** with an acceptable yield of 50%, whereas the coupling reaction starting from 4-bromonitrobenzene provided compound **31** in a higher yield (88%), probably due to the stronger electron-withdrawing effect of the nitro group compared to the carbamate moiety. Subsequent deprotection of compound **30** with trifluoroacetic acid (TFA) furnished the corresponding amine **32** in good 80% yield. Alternatively, reduction of the nitro group in compound **31** using iron powder under acidic conditions (pH = 3) afforded the same amine intermediate **32** with excellent yields (94%). In the final step, amine **32** reacted with acryloyl chloride in the presence of TEA as a base, leading to the formation of compound **25**. Taken together, these findings indicated that the synthetic pathway originating from 4-bromonitrobenzene **29** was more advantageous, primarily due to its superior overall yields.

3.5.2 Comparative studies of the reactivity profiles of the newly synthesized covalent probes toward different aminoacidic residue models.

The next focus was the evaluation of the reactivity of compounds **24** and **25** towards three different aminoacidic residue models, such as *N*α-acetyl-*L*-lysine methyl ester (**NALME**) hydrochloride, *N*-acetyl-*L*-histidine methyl ester (**NAHME**) acetate, and *N*-acetyl-*L*-cysteine methyl ester (**NACME**). The reactivity profile of the probes was examined in DMSO at 50 °C. DMSO was chosen as the solvent due to its high solubilizing capacity for both the probe and the amino acid derivatives, as well as its proven effectiveness in analogous experimental contexts. Although buffered aqueous media at physiological pH were initially considered, they were ultimately considered unsuitable owing to the pronounced lipophilicity of the probes, which could promote aggregation. Furthermore, it was proposed that the interaction between the probes and amino acid models likely occurs not in a uniform aqueous environment, but rather at hydrophobic interfaces or within nonpolar cavities of the protein architecture. Two different experimental conditions were employed: with and without the addition of DIPEA as a non-nucleophilic base. In this context, DIPEA (pKa = 8.5 in DMSO; 11 in water) was utilized to influence the protonation state of nucleophilic functionalities, such as the ε-amino group of lysine (pKa = 10), the imidazole ring of histidine (pKa = 6), and the thiol group of cysteine (pKa = 8.3), thereby modulating their chemical reactivity.

Scheme 3. Reaction between MBHA acetyl **24** and **NALME** hydrochloride.

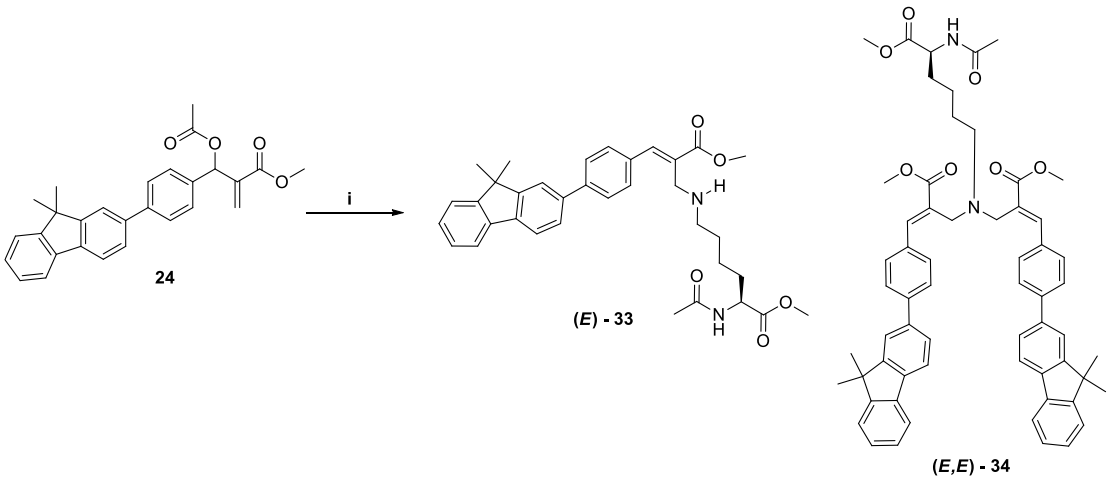

Reagents. (***i***) **NALME** hydrochloride, DIPEA, DMSO.

In this context, MBHA derivative **24** was found to react in DMSO in the presence of **NALME** hydrochloride and one equivalent of DIPEA, affording the monoadduct **(*E*)-33** in 19% yield and the diadduct **(*E,E*)-34** in 56% yield (**Scheme 3**). The reaction was conducted at 50 °C for three hours, and the relatively rapid conversion prompted a further kinetic investigation by means of ^{1}H NMR spectroscopy. The reaction was performed directly into an NMR tube, and ^{1}H NMR spectra were recorded at regular time intervals (Figure 5). Spectral analysis revealed the rapid disappearance of the diagnostic signals of compound **24**, attributed to the acrylate moiety (5.97-6.57 ppm) of the compound.

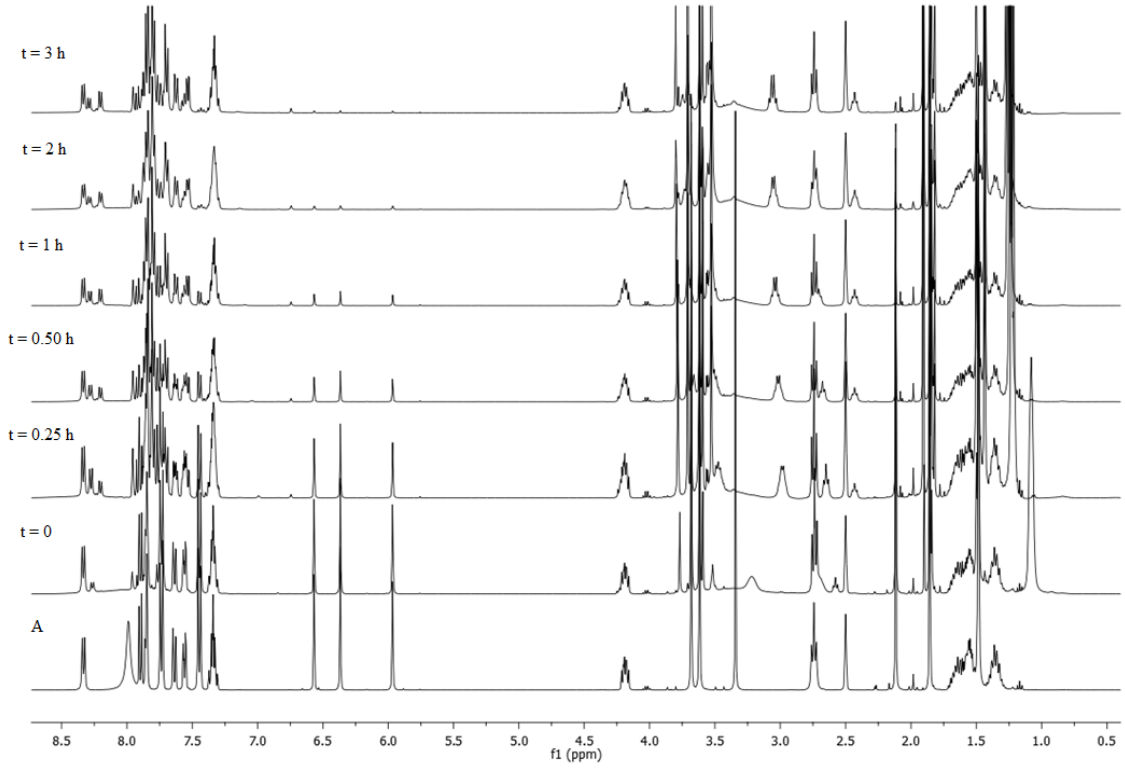

Figure 5. Comparison of ^{1}H NMR spectra (400 MHz) obtained during the kinetic studies of the reaction involving compound **24** (10 mg, 0.020 mmol), **NALME** hydrochloride (5.7 mg, 0.020 mmol), and DIPEA (4.0 µL, 0.020 mmol) in DMSO-d_6 (0.6 mL). The reaction mixture was first analyzed prior to the addition of DIPEA (spectrum A). Subsequently, after the base was added, the NMR tube was heated at 50 °C, and ^{1}H NMR spectra were recorded at regular time intervals (0, 0.25, 0.50, 1, 2, and 3 hours).

The same reaction, when conducted in the absence of DIPEA, resulted in a markedly slower process, affording only the diadduct **(*E,E*)-34** in 28% yield after six days at 50 °C. This outcome clearly demonstrated the crucial role of DIPEA as a base, facilitating the deprotonation of the primary amino group of **NALME**, thereby enhancing its nucleophilicity and overall reactivity. This result confirmed the remarkable findings

reported in **Chapter 2**, highlighting the notable ability of MBHA derivatives to interact with lysine models and form distinct products, corresponding to the mono- and di-attack, respectively.

Furthermore, during these experiments, compound **24** was also found to react with other nucleophilic amino acid models. For instance, the reaction of MBHA acetyl **24** with **NAHME** hydrochloride led to the formation of adduct **35** (**Scheme 4**).

Scheme 4. Reaction between MBHA acetyl **24** and **NAHME** hydrochloride.

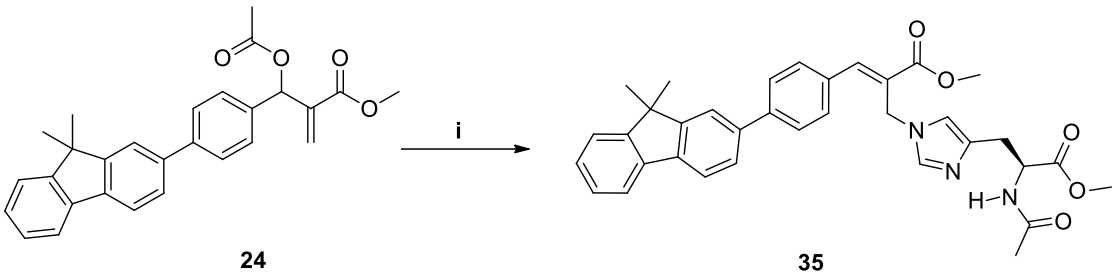

Reagents. (***i***) **NAHME** hydrochloride, DIPEA, DMSO.

In this case, however, the reaction required two equivalents of DIPEA as a base and 24 hours at 50 °C to reach completion. Under these conditions, the corresponding histidine derivative **35** was obtained in 59% yield. This outcome can be rationalized by considering the lower nucleophilicity of the imidazole moiety in the histidine model compared to the primary amino group present in the lysine model.

Finally, the MBHA acetyl derivative **24** reacted with **NACME** in the presence of DIPEA, affording adduct **36** in an excellent 92% isolated yield (**Scheme 5**).

Scheme 5. Reaction between MBHA acetyl **24** and **NACME**.

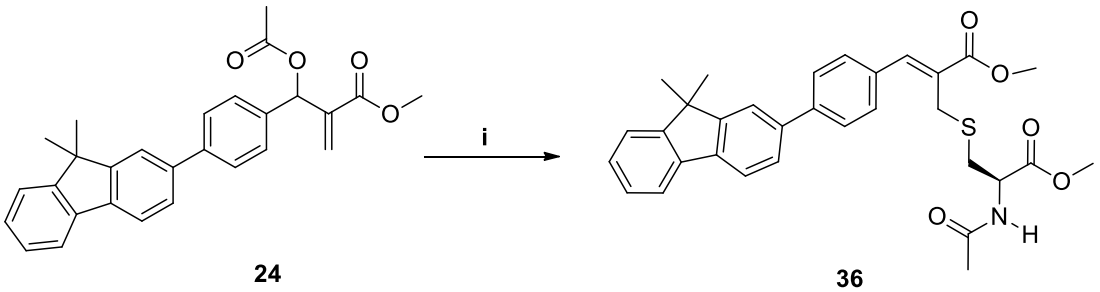

Reagents. (***i***) **NACME**, DIPEA, DMSO.

The reaction proceeded so rapidly that it could not be monitored using standard kinetic measurements using ^{1}H NMR spectroscopy. It was hypothesized that DIPEA (pK_a = 8.5

in DMSO, 11 in water) facilitated the deprotonation of the cysteine sulfhydryl group (pK_a = 8.3), thereby enhancing its nucleophilicity and overall reactivity. To test this assumption, a dedicated kinetic experiment was subsequently carried out by ^{1}H NMR spectroscopy in the absence of DIPEA (Figure 6). Under these conditions, the disappearance of the diagnostic signal corresponding to the acrylic moiety of compound **24** occurred significantly more slowly, thus confirming the pivotal role of DIPEA in accelerating the reaction and promoting the formation of the cysteine-derived adduct **36**.

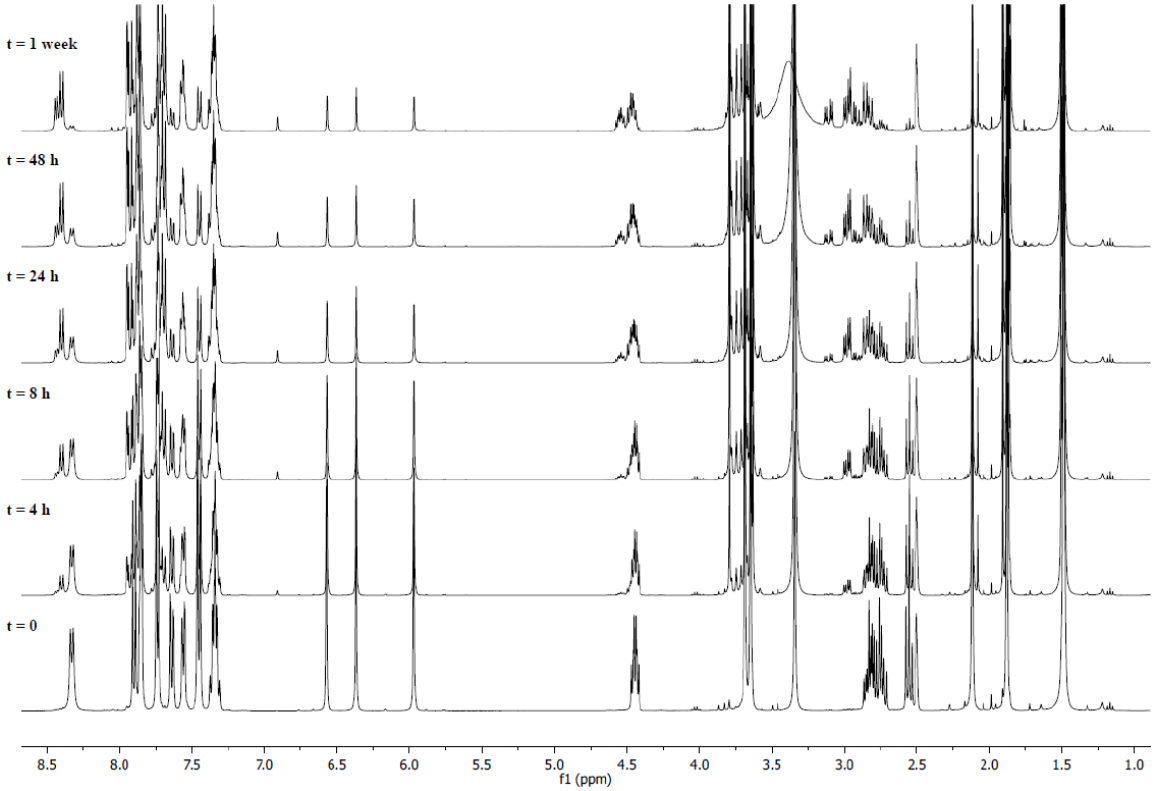

Figure 6. Comparison of ^{1}H NMR spectra (400 MHz) obtained during the kinetic studies of the reaction involving compound **24** (11 mg, 0.026 mmol) and **NACME** (4.6 mg, 0.026 mmol) in DMSO-d_6 (0.6 mL). The reaction mixture was heated at 50 °C, and ^{1}H NMR spectra were recorded at regular time intervals (0, 4, 8, 24, 48 hours, and 1 week).

In contrast to the previously discussed analogue **24**, acrylamide derivative **25** exhibited a markedly different reactivity profile. Specifically, compound **25** was found to react exclusively with the cysteine model **NACME**.

Specifically, the acrylanilide-based covalent probe **25** demonstrated a pronounced reluctance to undergo reaction with **NALME** hydrochloride, both in the absence and presence of DIPEA, and even under elevated thermal conditions (100 °C). Furthermore, considering the inherently lower nucleophilicity of the imidazole moiety in histidine

models compared to the primary amino group of lysine side chain, probe **25** also failed to react with **NAHME** hydrochloride. Conversely, compound **25** was found to react with the cysteine model **NACME**, which proceeded to afford the corresponding adduct **37** (Scheme 6).

Scheme 6. Reaction between acrylanilide covalent probe **25** and **NACME**.

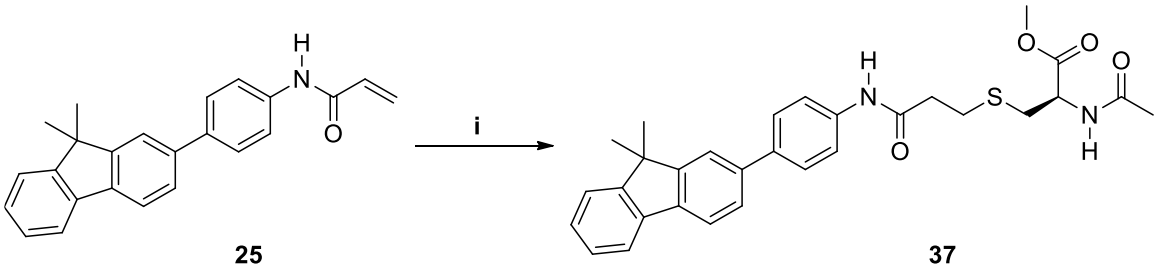

25 **37**

Reagents. (***i***) **NACME**, DIPEA, DMSO

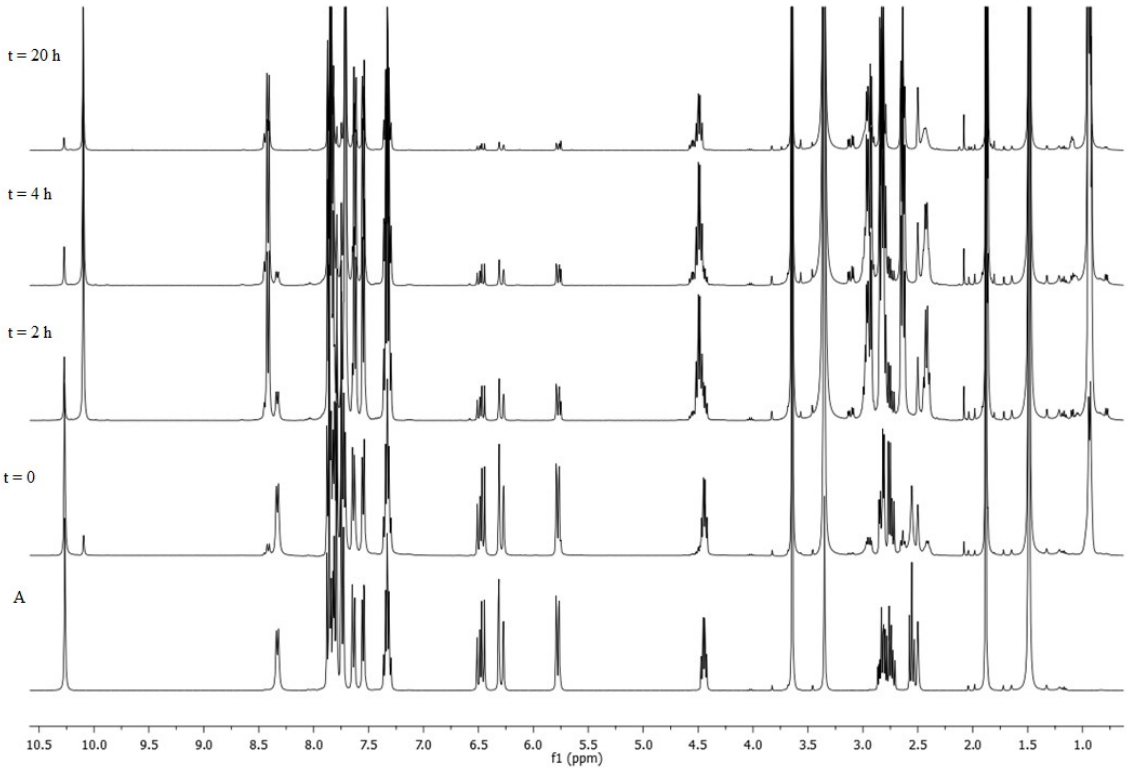

Figure 7. Comparison of ^{1}H NMR spectra (400 MHz) obtained during the kinetic studies of the reaction involving compound **25** (11 mg, 0.030 mmol), **NACME** (5.9 mg, 0.030 mmol), and DIPEA (4.6 µL) in DMSO-d_6 (0.6 mL). The reaction mixture was first analyzed prior to the addition of DIPEA (spectrum A). Subsequently, after the base was added, the NMR tube was heated at 50 °C, and ^{1}H NMR spectra were recorded at regular time intervals (0, 2, 4, and 20 hours).

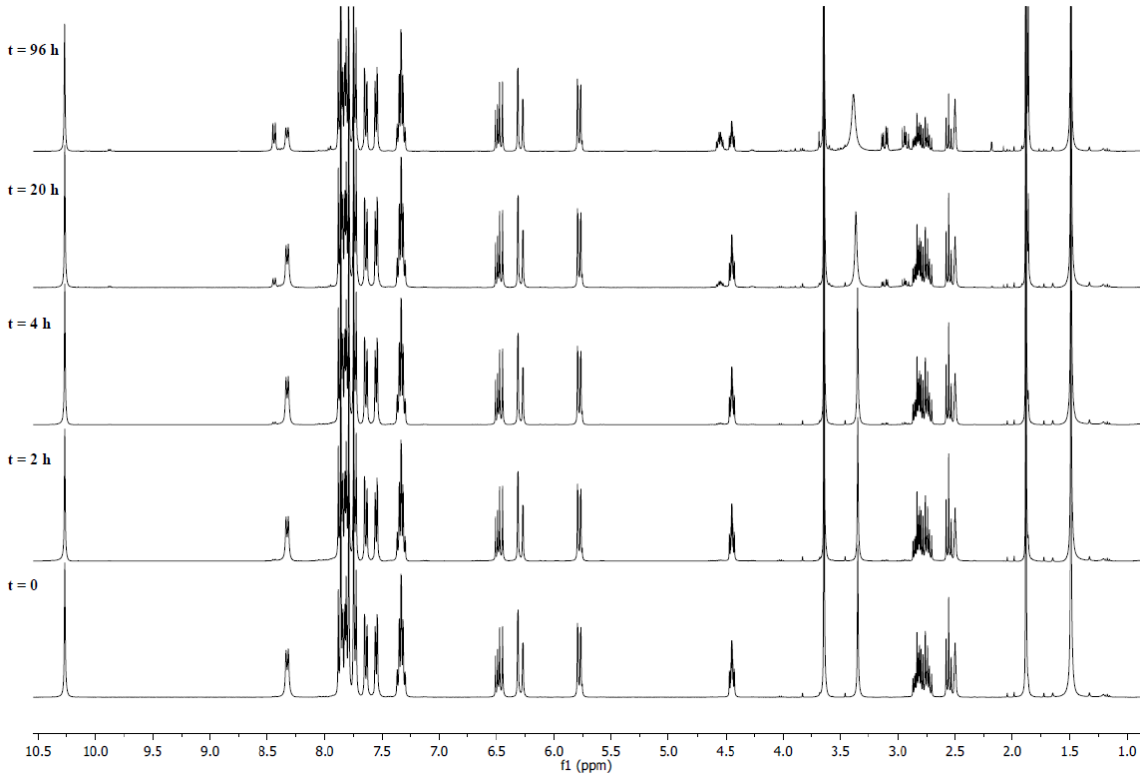

Figure 8. Comparison of ^{1}H NMR spectra (400 MHz) obtained during the kinetic studies of the reaction involving compound **25** (11 mg, 0.030 mmol) and **NACME** (5.9 mg, 0.030 mmol) in DMSO-d_6 (0.6 mL). The reaction mixture was heated at 50 °C, and ^{1}H NMR spectra were recorded at regular time intervals (0, 2, 4, 20, and 96 hours).

As observed previously, DIPEA played a crucial role in enhancing the nucleophilicity of the thiol group in **NACME**, thereby facilitating its relatively rapid reaction with probe **25** at 50 °C to yield the cysteine-derived adduct **37** in an acceptable 67% yield. To validate this hypothesis, kinetic studies were conducted using ^{1}H NMR spectroscopy in both the presence (Figure 7) and absence (Figure 8) of DIPEA. These experiments confirmed the essential role of the base promoting the reaction, as evidenced by the progressive disappearance of the diagnostic signal (5.77-6.48 ppm) attributed to the electrophilic moiety of probe **25**, a phenomenon not observed in the absence of DIPEA.

These results established the lower electrophilic character of the acrylamide moiety in covalent probe **25** relative to the methacrylate group present in compound **24**. Accordingly, the MBHA acetyl scaffold (exemplified by compounds **9** and **24**) can be considered a highly effective platform for the non-selective functionalization of nucleophilic amino acid residues. In contrast, the acrylamide unit in compound **25** exhibited a comparatively selective reactivity toward cysteine residues, thereby highlighting the favorable electrophilic properties of this functional group within the framework of Targeted Covalent Probe (TCI) approaches.[20,21]

3.5.3 Photophysical and photochemical properties

All newly synthesized compounds incorporating the DMPF fluorophore were subjected to the evaluation of their photophysical properties, with the corresponding data summarized in Table 1.

Table 1. Optical properties of the compounds bearing DMPF fluorophore.

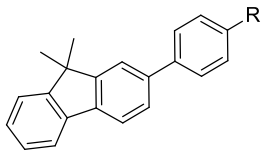

DMPF fluorophore

Compound	R	λ_{ab} (nm)	λ_{em} (nm)	λ_{PLE} (nm)
26	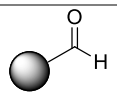	329	414[a]	326
27	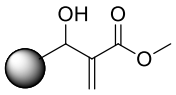	314	357[b]	314
24	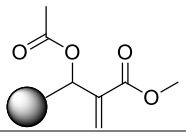	314	357[b]	315
33	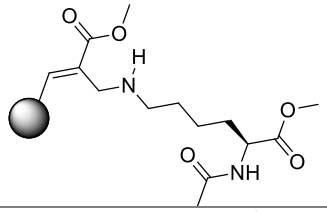	328	438[c]	337
34	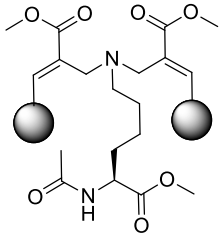	327	361[d]	296
35	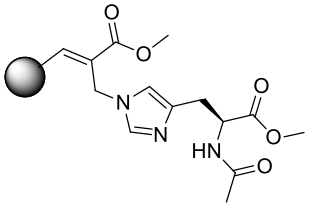	329	444[a]	334
36	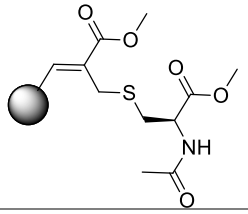	333	439[e]	340

30	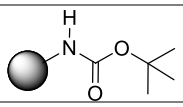	317	368[f]	318
31	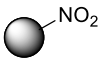	267, 351	535[g]	369
32	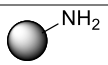	319	389[h]	323
25	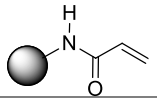	322	371[i]	309
37	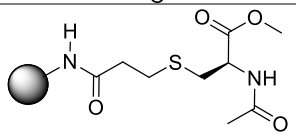	315	368[j]	320

[a] λ_{ex} = 329 nm; [b] λ_{ex} = 314 nm; [c] λ_{ex} = 328 nm; [d] λ_{ex} = 327 nm; [e] λ_{ex} = 333 nm; [f] λ_{ex} = 317 nm; [g] λ_{ex} = 351 nm; [h] λ_{ex} = 319 nm; [i] λ_{ex} = 322 nm; [j] λ_{ex} = 315 nm.

In general, the presence of the DMPF fluorophore resulted in low-energy absorption bands with maxima spanning 314-329 nm. An exception was observed for compound **31**, which, due to the presence of the nitro group, displayed two distinct absorption bands centered at 267 nm and 351 nm. PL spectra revealed emission maxima ranging from 357 to 535 nm across the series. Particular attention was given to the emission behavior of probes **24** and **25** with respect to their respective adducts formed with the amino acid models.

Starting from the MBHA scaffold, acetyl derivative **24** and adducts **33-36** displayed a noteworthy photophysical trend. While the absorption profiles of these compounds remained very similar to each other, their PL spectra exhibited pronounced red-shifts in emission maxima (Figure 9).

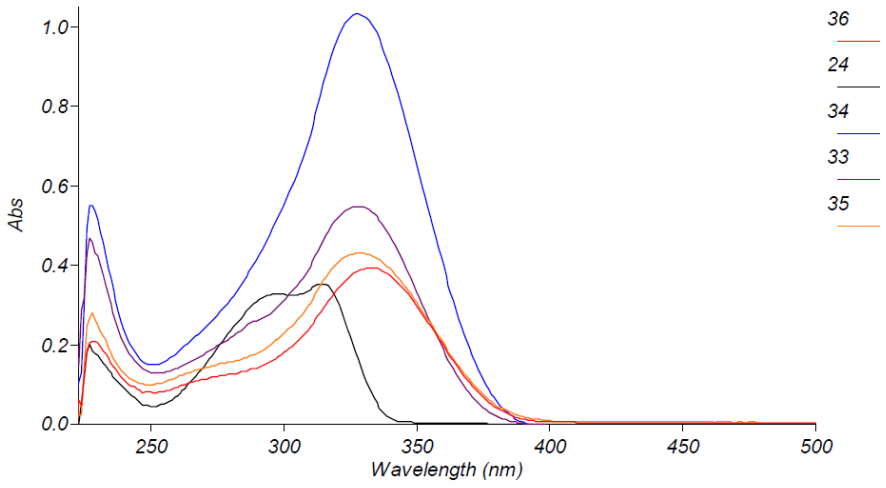

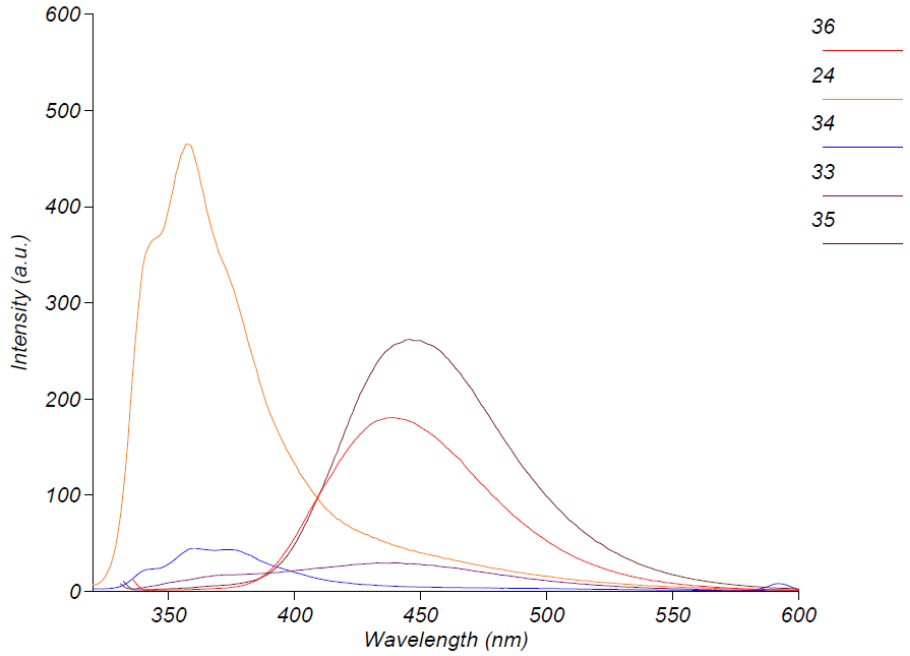

Figure 9. Absorption spectra (top panel) and PL spectra (bottom panel) of the newly synthesized compounds **24**, **33**, **34**, **35**, and **36**. The spectra were recorded using freshly prepared solutions at a concentration of approximately 1 x 10^{-5} M.

This phenomenon was attributed to a structural rearrangement involving the migration of the double bond, resulting in cinnamic-type architecture analogous to the well-characterized cinnamic derivative **5**, known for its outstanding optical properties.[46] This hypothesis was supported by the emission profile of compound **24**, which exhibited a maximum at 357 nm, corresponding solely to the DMFP fluorophore. In contrast, adducts **33**, **35**, and **36** showed emission maxima in the range of 440-446 nm. Moreover, the comparative analysis of the PL spectrum of monoadduct **33** and the related adduct derivatives **35** and **36** revealed only minor variations in their emission maxima, suggesting a slight yet discernible influence employed by the respective amino acid residues. This observation was further substantiated by examining the aromatic region of their ^{1}H NMR spectra (Figure 10), where distinct differences were noted in the signals corresponding to the para-substituted phenyl group, thereby supporting the hypothesis of residue-specific electronic effects on the photophysical behavior of the adducts.

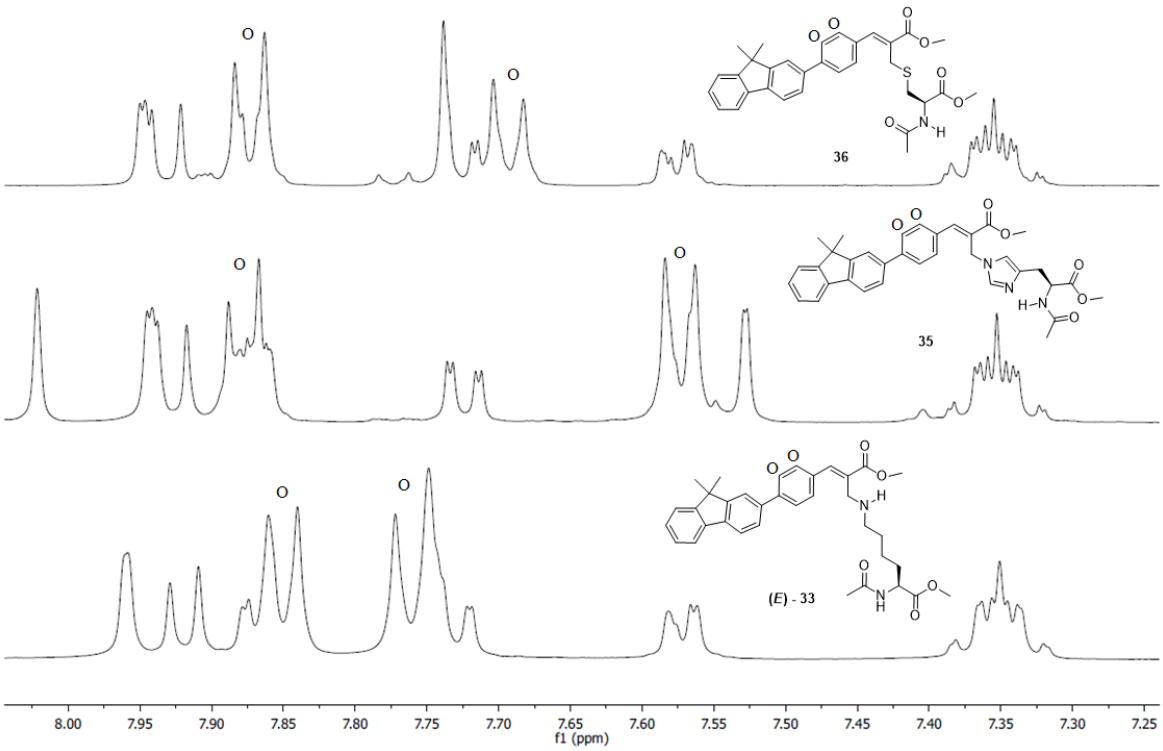

Figure 10. Comparison of the aromatic regions of the ^{1}H NMR (DMSO-d_6, 400 MHz) spectra of the compounds **(*E*)-33**, **35**, and **36**. The open circles indicate the signals attributed to the para-substituted phenyl group.

The only deviation from this trend was observed for diadduct **(*E*,*E*)-34**, which displayed a slightly more intense emission centered at 360 nm, an outcome inconsistent with its strong absorption characteristics. Therefore, it was postulated that this behavior stemmed from a [2+2] photocycloaddition process, facilitated by the presence of two cinnamic double bonds, leading to the formation of a bicyclic derivative **38** (**Scheme 7**). This assumption was substantiated by ^{1}H NMR spectroscopic analysis of a solution of diadduct **(*E*,*E*)-34** irradiated with a monochromatic light centered at 327 nm (Figure 11).

Scheme 7. [2+2] photocycloaddition transformation of diadduct derivative **34**.

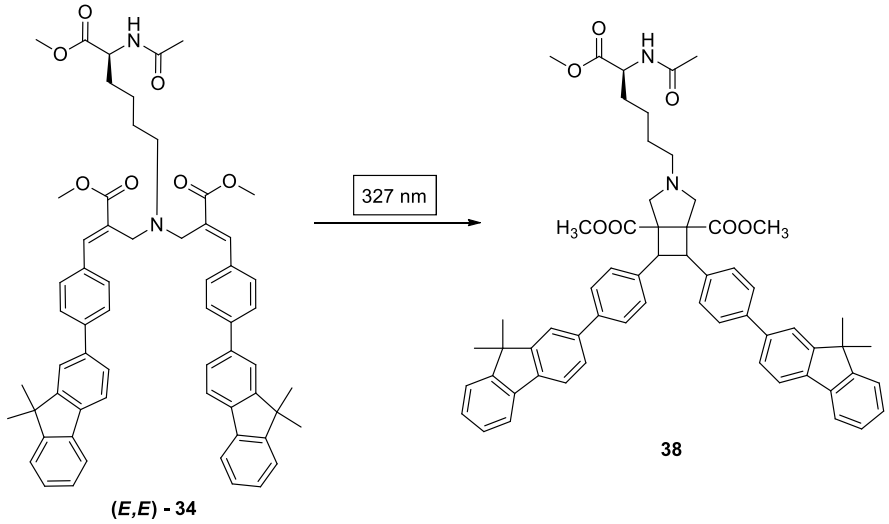

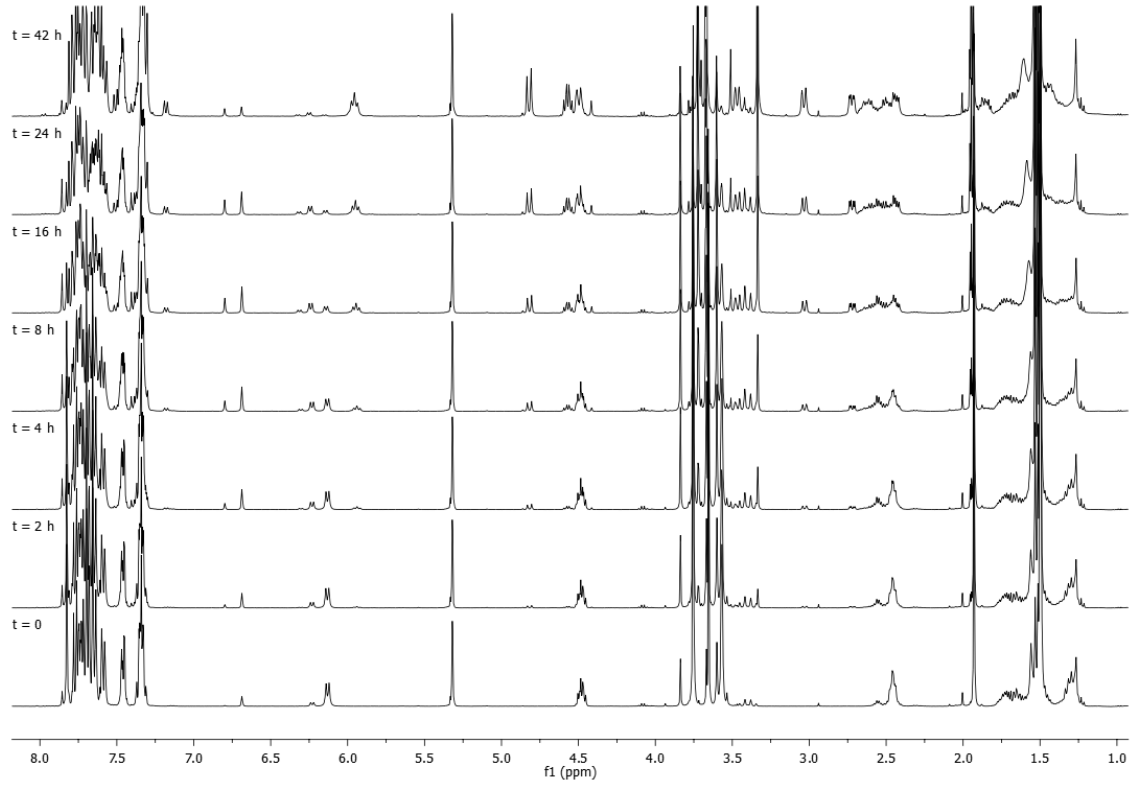

Figure 11. Comparison of ^{1}H NMR spectra (400 MHz) obtained during the kinetic studies of the [2+2] photocycloaddition reaction by irradiating compound **(*E*,*E*)-34** (12 mg, 0.013 mmol) in CD_2Cl_2 (1.0 mL) with a monochromatic light centered at 327 nm at room temperature, registered at regular time intervals (0, 2, 4, 8, 16, 24, and 42 hours).

On the other hand, acrylamide probe **25** showed a broad emission band peaked at 371 nm compared to the respective adduct **37** obtained after the reaction with the **NACME**, which displayed a structured band with a maximum emission centered at 368 nm, but a more

structured profile and with a significant increase in the brightness of the emission (Figure 12).

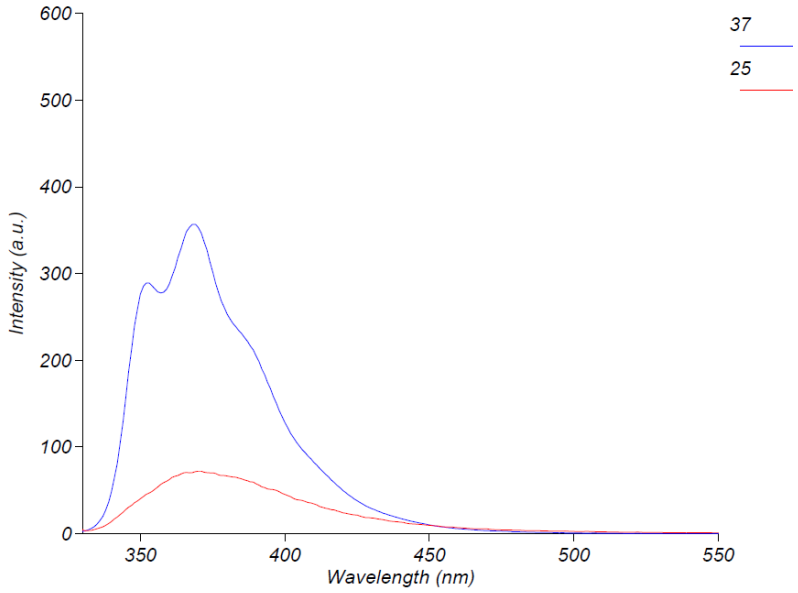

Figure 12. Comparison of PL spectra of the newly synthesized compounds **25** and **37**. The spectra were recorded using freshly prepared solutions at a concentration of approximately 1 x 10^{-5} M.

In conclusion, the obtained results suggested that the MBHA acetyl derivative **24** could represent a promising fluorogenic covalent probe for the detection of nucleophilic amino acid residues, characterized by emission in the blue-violet region of the visible spectrum. Concurrently, acrylamide-based probe **25** also exhibited a distinct photophysical behavior, marked by a significant enhancement in emission intensity when reacted with a cysteine model. This property aligned well with the concept of fluorogenic "turn-on" probes, underscoring the potential of compound **25** within the broader framework of selective and sensitive molecular sensing strategies.[50,51]

3.5.4 Interaction of MBHA acetyl derivative 24 with Human Serum Albumin

The promising interaction profile of compound **9** with **HSA**, as discussed in ***Paragraph 3.4***, prompted further investigation into the reactivity of MBHA acetyl **24**, bearing a DMFP fluorophore, toward the same protein. To gain detailed insights into the interaction between probe **24** and **HSA**, a combination of analytical techniques was employed, including ^{1}H NMR spectroscopy, SDS page, and circular dichroism (CD) spectroscopy. The NMR experiments were designed analogously to those conducted with fluorogenic probe **9**, with the specific aim of monitoring acetate release because of the elimination

step in the addition-elimination reaction mechanism. The reaction was carried out using a solution of **HSA** (67 mg, 1.0 µmol) in deuterium oxide (1.4 mL), buffered with phosphate-buffered saline (PBS, 14 mg, pH 7.4), to which 50 µL (1.0 µmol) of a 20 mM solution of MBHA acetyl derivative **24** (1.47 mg) in DMSO-d_6 was added. The resulting mixture was divided into two 5 mm NMR Pyrex tubes and incubated at 37 °C and 50 °C, respectively. ^{1}H NMR spectra were recorded at regular time intervals to monitor the reaction progress at both thermal conditions. As shown in Figure 13, the signal at 1.88 ppm, attributed to the methyl protons of the liberated acetate, increased progressively during heating, indicating the advancement of the addition-elimination process. This was evaluated relative to the residual DMSO-d_6 peak at 2.66 ppm.

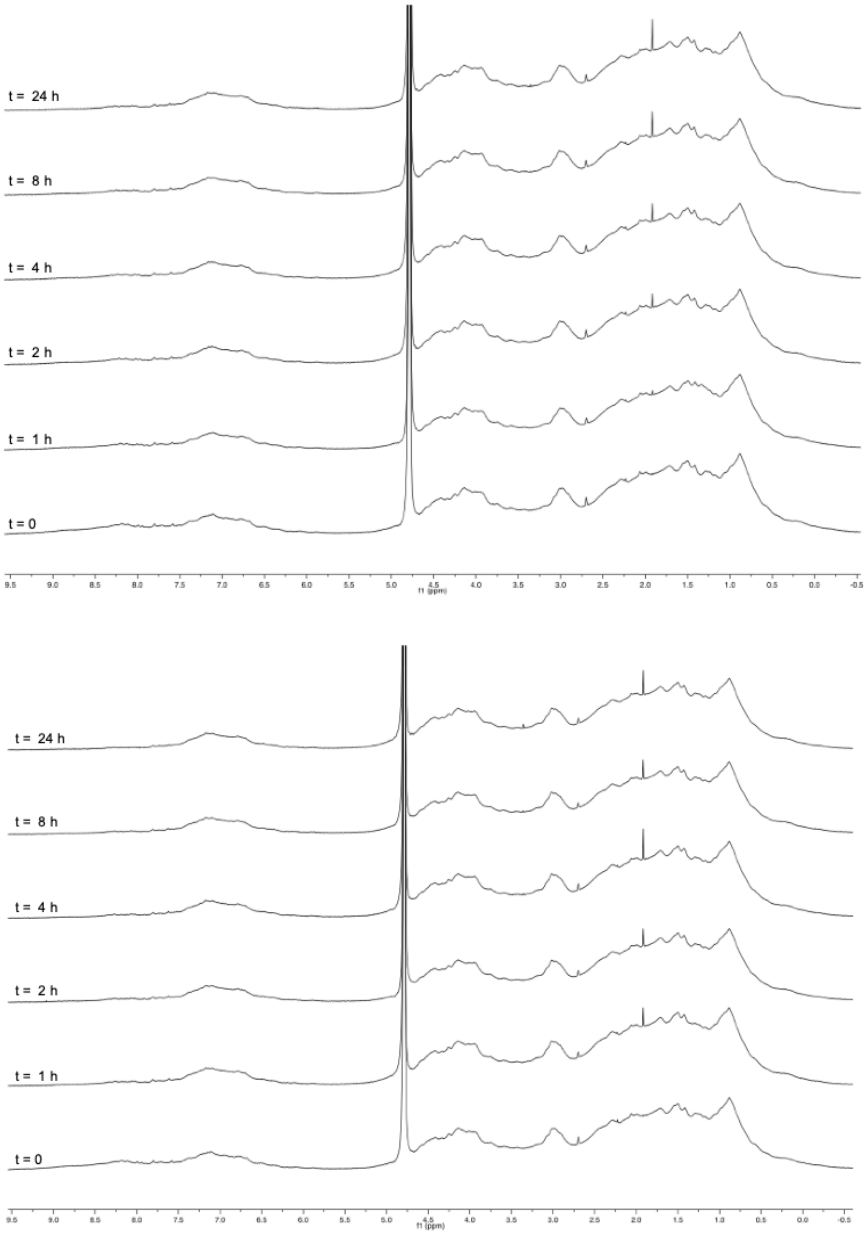

Figure 13. Comparative ^{1}H NMR (400 MHz) spectra of reaction mixtures containing **HSA** (1.0 µmol) in D_2O buffered with PBS at pH 7.4 and compound **24** (1.0 µmol), which was added as a solution in DMSO-d_6. The reaction mixtures were contained in 5 mm NMR tubes and heated at 37 °C (top panel) or 50 °C (bottom panel). ^{1}H NMR spectra were recorded at regular time intervals (0, 1, 2, 4, 8, and 24 h).

Notably, the reaction kinetics were temperature-dependent: at 50 °C, the acetate signal intensified rapidly, reaching an apparent plateau within 4-8 hours, whereas at 37 °C, the increase was more gradual and extended within 24 hours. Moreover, analogous to the behavior observed for compound **9** in its reaction with **HSA**, where a shift in fluorescence from blue to yellow emission led to the formation of **GFA**, the prolonged heating of the reaction mixture containing MBHA **24** with **HSA** also resulted in a distinct change in fluorescence. Specifically, upon exposure of the NMR tube-reactor to a UV lamp (365 nm), the initial (t = 0) deep blue-violet emission gradually shifted to the clear blue over time. These results suggested the formation of Blue Fluorescent Albumin (**BFA**), further supporting the occurrence of covalent modification and associated photophysical transformation (Figure 14).

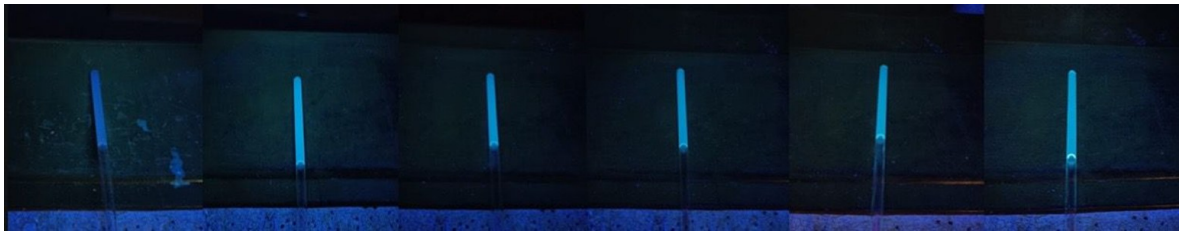

Figure 14. Fluorescence emission comparison of the reaction mixtures containing **HSA** in D_2O, buffered at pH 7.4 with PBS, and compound **24**, added as a solution in DMSO-d_6. The reaction mixtures contained in a 5 mm NMR tube were heated at 37 °C and photographed under excitation at 365 nm at regular time intervals (0, 1, 2, 4, 8, and 24 h, from left to right in the sequence).

Obviously, the experiment conducted at 37 °C was of particular relevance, as it closely approximated physiological conditions. To assess the structural integrity of the protein under the applied experimental conditions, SDS-PAGE analysis was performed on three samples: native **HSA**, and **HSA** derivatized at 37 °C and 50 °C, respectively. All samples exhibited a single protein band, indicating the absence of degradation or aggregation and confirming the preservation of protein structure. A slight variation in electrophoretic mobility was observed in the derivatized samples, suggesting the occurrence of covalent modification. However, this shift may be considered marginal, given the relatively low

molecular weight of probe **24** (426.5 Da) compared to the overall molecular weight of **HSA** (Figure 15, left panel). To further verify the covalent labeling of the protein, a duplicate gel was prepared for fluorescence analysis under UV light (365 nm). A key limitation encountered was the interference caused by post-run staining (SimplyBlue™ SafeStain, Thermo Fisher Scientific), which hindered fluorescent detection. To circumvent this issue, electrophoresis was repeated using duplicate samples: one processed under standard conditions and stained to visualize the protein bands, and the other run without loading buffer and left unstained (Figure 15, right panel). Upon UV exposure (365 nm), the unstained gel revealed clear-blue fluorescent bands corresponding to derivatized protein, whereas no fluorescence was detected in the native, non-derivatized sample. These findings confirmed the successful covalent modification of **HSA** by probe **24** under the tested conditions.

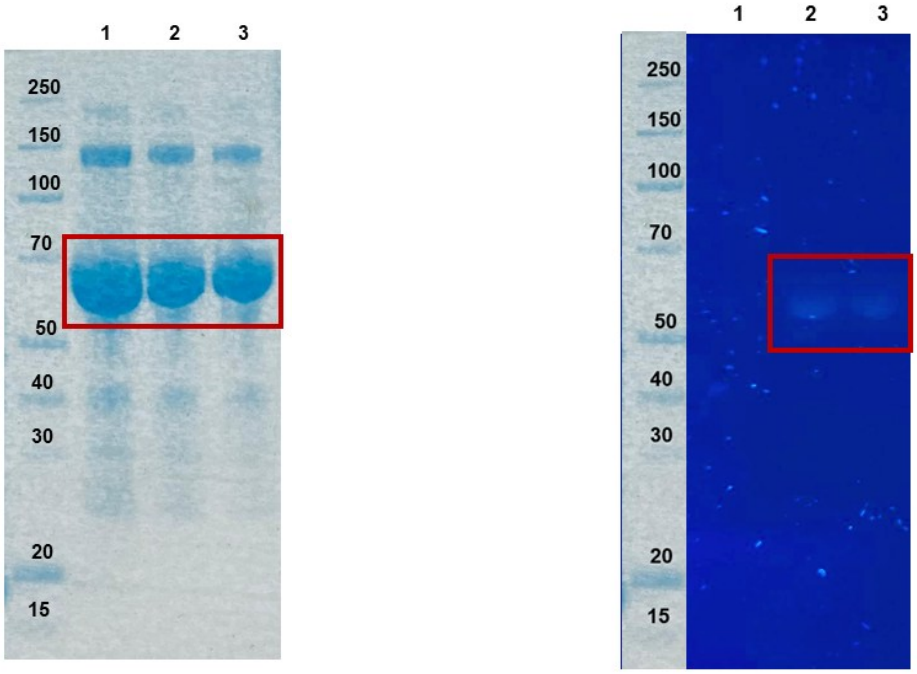

Figure 15. SDS-PAGE analysis (Bis-TRIS gel 4-12% NuPAGE, Thermo Fisher Scientific) of **HSA** (MW 66472 Da, lane 1) and **HSA** derivatized via incubation with MBHA probe **24** (MW 426.50 Da) for 24 hours at 37 °C (lane 2) and 50 °C (lane 3), respectively. The molecular weight marker used was the PageRuler Broad Range Unstained Protein Ladder (Thermo Fisher Scientific, left panel). Protein bands corresponding to each sample are highlighted in red. A duplicate gel, run without post-staining, was exposed to UV light (365 nm, right panel), revealing clear-blue fluorescent bands at the position corresponding to the derivatized **HSA** samples (lanes 2 and 3), confirming the successful covalent modification. No fluorescence was observed for the native **HSA** sample (lane 1).

Moreover, to evaluate the impact of derivatization on the secondary structure of the protein, circular dichroism (CD) spectroscopy was performed on three samples: native **HSA**, **HSA** derivatized at 37 °C, and **HSA** derivatized at 50 °C. The CD spectra, shown in Figure 16, exhibited the typical features of an α-helical protein, characterized by two distinct negative bands centered at approximately 208 and 222 nm.

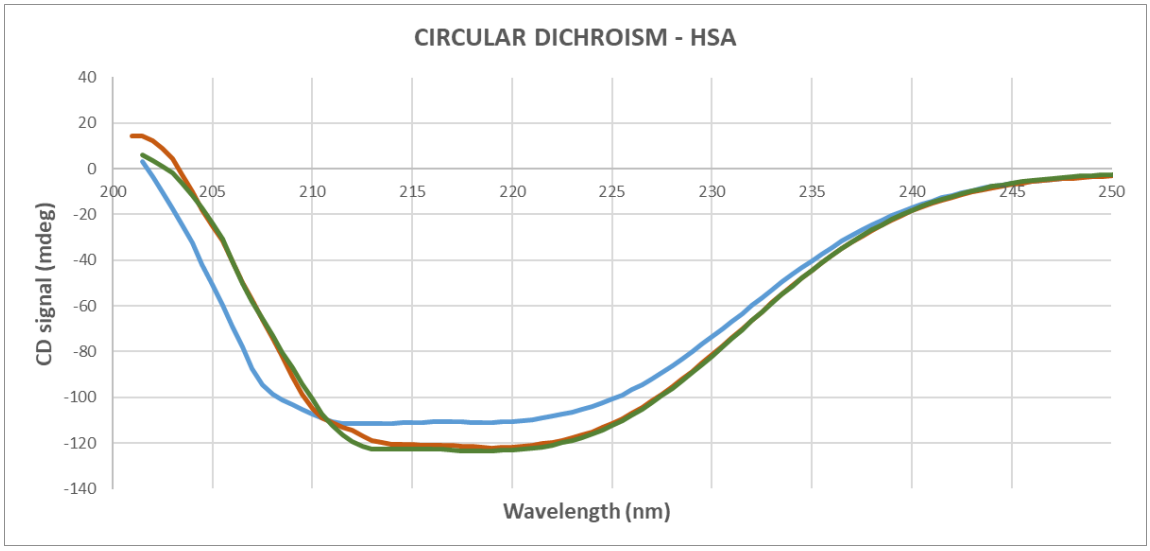

Figure 16. Circular dichroism (CD) spectra of native **HSA** (blue line) and of **HSA** derivatized with MBHA derivative **24** after 24 hours of incubation at 37 °C (orange line) and 50 °C (green line).

These results indicate that the α-helical content of **HSA** was largely retained following derivatization. A slight decrease in ellipticity was observed in the CD spectra of derivatized samples compared to the native protein, suggesting minor conformational adjustments potentially induced by the reaction conditions or by the covalent interaction with the probe **24**. Nonetheless, the overall spectral profile remained consistent, with no evidence of significant structural alteration or unfolding. These findings are in agreement with previous studies, in which **HSA** maintained its native α-helical conformation upon covalent modification with other molecules, as confirmed by CD analysis.[52]

3.6 CONCLUSION

In conclusion, the well-described MBHA fluorogenic probe **9** bearing a triphenylamine moiety exhibited AIE properties with bright blue fluorescence (478 nm) in DMSO-water dispersion. Upon reaction with **HSA**, the emission shifted to green-yellow, forming Green Fluorescent Albumin (**GFA**) derivative. Notably, energy transfer from **HSA** to the newly

formed cinnamic fluorophore was observed only after thermal treatment, suggesting that heating promoted spatial proximity between the fluorophore and aromatic residues within the protein. Structural analyses (SDS-PAGE and DLS) confirmed the stability of **HSA** and revealed an increased tendency of **GFA** to form defined aggregates. In addition, biological evaluation demonstrated that **GFA** retained the drug-binding properties of native **HSA**, supporting its potential as a drug delivery platform. Moreover, to evaluate the effect of the fluorophore, two covalent fluorescent probes were developed by functionalizing the 9,9-dimethyl-2-phenyl-9*H*-fluorene (DMPF) fluorophore with distinct electrophilic warheads: a methylacrylate moiety (compound **24**) and an acrylamide group (compound **25**). These warheads were selected for their differing reactivity profiles toward nucleophilic amino acid residues. Reactivity studies revealed that MBHA-based probe **24** exhibited broader, less selective reactivity, while acrylamide-based probe **25** showed expected chemoselectivity toward the cysteine model. This highlighted the greater versatility of the acrylate moiety, including in the MBHA scaffold, which may be advantageous for targeting diverse protein environments, though it requires careful structural design to avoid off-target effects. Furthermore, photophysical characterization of the resulting adducts showed that compound **24** displayed fluorogenic behavior sensitive to the identity of the bound amino acid, whereas compound **25** primarily exhibited enhanced emission upon reaction. Finally, the ability of MBHA acetyl probe **24** to covalently modify **HSA** was supported by NMR, absorption, and emission spectroscopy, CD analysis, and the SDS-PAGE technique.

3.7 EXPERIMENTAL SECTION

3.7.1 Synthesis

Merck silica gel 60 (230-400 mesh) was used for column chromatography. Merck TLC plates, silica gel 60 F_{254} were used for TLC. NMR spectra were recorded with a Bruker DRX-400 AVANCE III, a Bruker DRX-500 AVANCE, and a Bruker DRX-600 AVANCE III spectrometer in the indicated solvents (TMS as internal standard): the values of the chemical shifts are expressed in ppm and the coupling constants (*J*) in Hz. An Agilent 1100 LC/MSD operating with an electrospray source was used in mass spectrometry experiments. Melting points were determined in open capillaries in a Cole-Parmer Stuart apparatus and are uncorrected.

4-(9,9-Dimethyl-9*H*-fluoren-2-yl)benzaldehyde (26).[46,47]

The commercially available 9,9-dimethylfluorene-2-boronic acid pinacol ester (616 mg, 1.9 mmol) was dissolved in dry THF (8.0 mL) and CH_3OH (2.0 mL) in a microwave tube. After the addition of Cs_2CO_3 (1.9 g, 5.8 mmol), the reaction mixture was stirred for 30 min at room temperature. After this time, $Pd(PPh_3)_2Cl_2$ (267 mg, 0.38 mmol), PPh_3 (498 mg, 1.9 mmol), and 4-bromobenzaldehyde **10** (352 mg, 1.9 mmol) were added in sequence. The resulting mixture was exposed to microwave irradiation in a CEM Discovery apparatus for two cycles of 10 min (T = 80 °C, W = 150, P = 250 psi). Subsequently, the reaction mixture was partitioned between brine and ethyl acetate, the organic layer was dried over sodium sulfate, filtered, and concentrated under vacuum. The organic residue was purified by flash chromatography using petroleum ether-ethyl acetate (95:5) as eluent to yield benzaldehyde **26** (460 mg, yield 81%) as an off-white solid (mp 126-128 °C). ^{1}H NMR (400 MHz, $CDCl_3$): 1.54 (s, 6H), 7.32-7.40 (m, 2H), 7.43-7.48 (m, 1H), 7.62 (dd, *J* = 7.9, 1.6, 1H), 7.68 (d, *J* = 1.2, 1H), 7.73-7.78 (m, 1H), 7.79–7.84 (m, 3H), 7.97 (d, *J* = 8.2, 2H), 10.06 (s, 1H). ^{13}C NMR (125 MHz, $CDCl_3$): 27.2, 47.0, 120.3, 120.5, 121.6, 122.7, 126.5, 127.1, 127.7, 130.3, 135.0, 138.4, 138.7, 139.7, 147.6, 154.0, 154.5, 191.9. MS (ESI): m/z 321.2 [M + Na^+].

Methyl 2-[[4-(9,9-dimethyl-9*H*-fluoren-2-yl)phenyl](hydroxy)methyl]acrylate (27).

Compound **26** (454 mg, 1.5 mmol) reacted with methyl acrylate (0.27 mL, 3.0 mmol) in the presence of DABCO (202 mg, 1.8 mmol), and catalytic amounts of CH_3OH (10 µL). The resulting mixture was stirred in the darkness for 72 hours at room temperature. After concentration under reduced pressure, the resulting residue was dissolved in DCM. The organic layer was washed with a saturated solution of NH_4Cl, separated, dried over sodium sulfate, filtered, and concentrated under vacuum. The resulting residue was purified by flash chromatography on silica gel (petroleum ether-ethyl acetate 6:4), yielding MBHA alcohol **27** (489 mg, yield 84%) as a colorless oil, which crystallized in a white crystalline solid (mp 110-112 °C) upon standing. ^{1}H NMR (400 MHz, $CDCl_3$): 1.52 (s, 6H), 3.04 (d, *J* = 5.7, 1H), 3.75 (s, 3H), 5.63 (d, *J* = 5.7, 1H), 5.90 (s, 1H), 6.37 (s, 1H), 7.29-7.38 (m, 2H), 7.42–7.49 (m, 3H), 7.56 (dd, *J* = 7.8, 1.6, 1H), 7.62-7.66 (m, 3H), 7.72-7.75 (m, 1H), 7.77 (d, *J* = 7.8, 1H). MS (ESI): m/z 407.1 [M + Na^+].

Methyl 2-[acetoxy[4-(9,9-dimethyl-9*H*-fluoren-2-yl)phenyl]methyl]acrylate (24).

In a two-neck round-bottom flask, compound **27** (472 mg, 1.2 mmol) was dissolved in dry DCM (7.0 mL), followed by the sequential addition of TEA (0.42 mL) and acetyl chloride (0.17 mL, 2.4 mmol). The resulting mixture was stirred under an inert nitrogen atmosphere at room temperature for one hour. After quenching with brine, the organic layer was separated, dried over sodium sulfate, filtered, and concentrated under reduced pressure. The crude product was purified by flash chromatography eluting with a petroleum ether-ethyl acetate (8:2) mixture. The MBHA acetate derivative **24** (338 mg, yield 66%) was obtained as an off-white solid (mp 113-114 °C).

^{1}H NMR (400 MHz, $CDCl_3$): 1.52 (s, 6H), 2.13 (s, 3H), 3.73 (s, 3H), 5.93 (s, 1H), 6.43 (s, 1H), 6.73 (s, 1H), 7.29-7.37 (m, 2H), 7.43-7.48 (m, 3H), 7.54 (dd, *J* = 7.9, 1.7, 1H), 7.59-7.64 (m, 3H), 7.73 (dd, *J* = 7.4, 1.5, 1H), 7.76 (d, *J* = 7.9, 1H).

^{1}H NMR (600 MHz, DMSO-d_6): 1.49 (s, 6H), 2.12 (s, 3H), 3.69 (s, 3H), 5.97 (s, 1H), 6.37 (s, 1H), 6.57 (s, 1H), 7.31-7.37 (m, 2H), 7.45 (d, *J* = 8.1, 2H), 7.55-7.58 (m, 1H), 7.64 (dd, *J* = 7.9, 1.3, 1H), 7.74 (d, *J* = 8.3, 2H), 7.85-7.87 (m, 2H), 7.90 (d, *J* = 7.9, 1H).

^{13}C NMR (150 MHz, $CDCl_3$): 20.7, 26.8, 46.6, 52.1, 72.3, 120.2, 120.5, 121.3, 122.7, 125.8, 126.1, 126.9, 127.0, 127.4, 128.0, 136.5, 138.1, 138.8, 139.0, 140.6, 153.6, 154.1, 164.9, 169.2.

MS (ESI): m/z 449.0 [M+Na^+].

***tert*-Butyl [4-(9,9-dimethyl-9*H*-fluoren-2-yl)phenyl]carbamate (30).**

The commercially available 9,9-dimethylfluorene-2-boronic acid pinacol ester (101 mg, 0.32 mmol) was dissolved in dry THF (4.0 mL) and CH_3OH (1.0 mL) in a microwave tube. After the addition of Cs_2CO_3 (313 g, 0.96 mmol), the reaction mixture was stirred for 30 min at room temperature. Subsequently, $Pd(PPh_3)_2Cl_2$ (45 mg, 0.064 mmol), PPh_3 (84 mg, 0.32 mmol), and *tert*-butyl (4-bromophenyl)carbamate **28**[48] (87 mg, 0.32 mmol) were added in sequence. The resulting mixture was exposed to microwave irradiation in a CEM Discovery apparatus for two cycles of 30 min (T = 80 °C, W = 150, P = 250 psi). Subsequently, the reaction mixture was quenched with brine, and the organic layer was extracted with DCM. The organic layers were combined, dried over sodium sulfate, filtered, and concentrated under vacuum. The organic residue was purified by flash chromatography using petroleum ether-ethyl acetate (95:5) as the eluent to afford compound **30** (61 mg, yield 50%) as a white solid (mp 205-207 °C). ^{1}H NMR (400 MHz, $CDCl_3$): 1.52 (s, 6H), 1.53 (s, 9H), 6.52 (s, 1H), 7.28-7.36 (m, 2H), 7.41-7.46 (m, 3H),

7.53 (dd, *J* = 7.9, 1.2, 1H), 7.58 (d, *J* = 8.4, 3H), 7.71-7.76 (m, 2H). MS (ESI): m/z 408.0 [M+Na^+].

9,9-Dimethyl-2-(4-nitrophenyl)-9*H*-fluorene (31).

The commercially available 9,9-dimethylfluorene-2-boronic acid pinacol ester (324 mg, 1.0 mmol) was dissolved in dry THF (4.0 mL) and CH_3OH (1.0 mL) in a microwave tube. After the addition of Cs_2CO_3 (977 g, 3.0 mmol), the reaction mixture was stirred for 30 min at room temperature. Successively, $Pd(PPh_3)_2Cl_2$ (140 mg, 0.20 mmol), PPh_3 (262 mg, 1.0 mmol), and the commercially available 4-bromonitrobenzene **29** (202 mg, 1.0 mmol) were added in sequence. The resulting mixture was exposed to microwave irradiation in a CEM Discovery apparatus for one cycle of 10 min (T = 80 °C, W = 150, P = 250 psi). After that, the reaction mixture was quenched with brine, and the organic layer was extracted with DCM. The organic layers were combined, dried over sodium sulfate, filtered, and concentrated under vacuum. The organic residue was purified by flash chromatography using petroleum ether-ethyl acetate (95:5) as the eluent to afford compound **31** (290 mg, yield 92%) as a pale-yellow solid (mp 159-161 °C). ^{1}H NMR (400 MHz, $CDCl_3$): 1.54 (s, 6H), 7.33-7.39 (m, 2H), 7.45-7.48 (m, 1H), 7.61 (dd, *J* = 7.9, 1.3, 1H), 7.66 (s, 1H), 7.75-7.83 (m, 4H), 8.31 (d, *J* = 8.7, 2H). MS (ESI): m/z 337.5 [M+Na^+].

4-(9,9-Dimethyl-9*H*-fluoren-2-yl)aniline (32).

Compound **30** (110 mg, 0.29 mmol) was dissolved in DCM (10 mL) in the presence of TFA (2.0 mL), and the solution was stirred at room temperature for one hour. After quenching the reaction mixture with a saturated solution of $NaHCO_3$, the organic layer was separated, dried over sodium sulfate, filtered, and concentrated under reduced pressure. The crude product was purified by flash chromatography by means of petroleum ether-ethyl acetate (7:3) as the eluent to obtain amine derivative **32** (68 mg, yield 83%) as a pale-yellow solid (mp 116-117 °C). ^{1}H NMR (400 MHz, $CDCl_3$): 1.52 (s, 6H), 6.80 (d, *J* = 8.4, 2H), 7.28-7.35 (m, 2H), 7.42-7.44 (m, 1H), 7.47-7.52 (m, 3H), 7.58 (d, *J* = 1.4, 1H), 7.71-7.75 (m, 2H). MS (ESI): m/z 286.1 [M+H^+].

Alternatively, compound **31** (290 mg, 0.92 mmol) was dissolved in ethanol (12 mL) in the presence of NH_4Cl (59 mg, 1.1 mmol) and acidified to pH = 3 using a 1N solution of HCl (80 µL). The reaction mixture was stirred under a nitrogen atmosphere at reflux conditions for three hours. After completion, the reaction mixture was concentrated under

pressure to remove the ethanol, and the resulting residue was purified by flash chromatography using petroleum ether-ethyl acetate (7:3) as eluent to yield amine **32** (255 mg, yield 97%) as a pale-yellow solid.

***N*-[4-(9,9-Dimethyl-9*H*-fluoren-2-yl)phenyl]acrylamide (25).**

Amine derivative **32** (202 mg, 0.71 mmol) was dissolved in dry DCM (10 mL) in a two-neck round-bottom flask and cooled at 0 °C. TEA (0.20 mL, 1.4 mmol) and acryloyl chloride (57 µL, 0.71 mmol) were added sequentially, and the resulting mixture was stirred under a nitrogen atmosphere at room temperature for two hours. Subsequently, a 1N solution of HCl was added, and the organic layer was separated, dried over sodium sulfate, filtered, and concentrated under reduced pressure. Purification of the organic residue by flash chromatography (petroleum ether-ethyl acetate 7:3) yielded compound **25** (199 mg, yield 83%) as a white solid (mp 183-184 °C).

^{1}H NMR (400 MHz, $CDCl_3$): 1.53 (s, 6H), 5.80 (dd, *J* = 10.2, 1.3, 1H), 6.27 (dd, *J* = 16.8, 10.2, 1H), 6.47 (dd, *J* = 16.8, 1.3, 1H), 7.28-7.39 (m, 3H), 7.41-7.48 (m, 1H), 7.55 (dd, *J* = 7.9, 1.7, 1H), 7.62-7.71 (m, 5H), 7.71-7.78 (m, 2H).

^{1}H NMR (400 MHz, DMSO-d_6): 1.48 (s, 6H), 5.77 (dd, *J* = 10.1, 2.0, 1H), 6.28 (dd, *J* = 17.0, 2.1, 1H), 6.46 (dd, *J* = 17.0, 10.1, 1H), 7.28-7.38 (m, 2H), 7.53-7.57 (m, 1H), 7.63 (dd, *J* = 7.9, 1.7, 1H), 7.73 (d, *J* = 8.8, 2H), 7.78 (d, *J* = 8.8, 2H), 7.81-7.85 (m, 2H), 7.87 (d, *J* = 78.4, 1H), 10.24 (s, 1H).

MS (ESI): m/z 362.1 [$M+Na^+$].

Reaction of MBHA derivative 24 with *Nα*-acetyl-*L*-lysine methyl ester (NALME) hydrochloride.

A solution of MBHA derivative **24** (51 mg, 0.12 mmol) in DMSO (3.0 mL) was added to **NALME** hydrochloride (29 mg, 0.12 mmol) and DIPEA (21 µL, 0.12 mmol). The reaction mixture was stirred at 50 °C for three hours. After completion, brine (3 x 50 mL) was added to the reaction mixture. The organic layers were extracted with ethyl acetate, combined, dried over sodium sulfate, filtered, and concentrated under reduced pressure. The crude product was purified by flash chromatography using the appropriate eluent.

Methyl (*E*)-N^2-acetyl-N^6-[3-[4-[9,9-dimethyl-9*H*-fluoren-2-yl)phenyl]-2-(methoxycarbonyl)allyl-*L*-lisinate (*E*-33).

The above flash chromatography purification using ethyl acetate-methanol (95:5) as the eluent afforded compound **(*E*)-33** (13 mg, yield 19%) as a colorless glassy solid.

^{1}H NMR (600 MHz, DMSO-d$_6$): 1.31-1.48 (m, 4H), 1.50 (s, 6H), 1.57-1.73 (m, 2H), 1.84 (s, 3H), 2.57 (t, *J* = 6.8, 2H), 3.51 (s, 2H), 3.60 (s, 3H), 3.77 (s, 3H), 4.21-4.24 (m, 1H), 7.33-7.38 (m, 2H), 7.55-7.60 (m, 1H), 7.73 (dd, *J* = 8.0, 1.7, 1H), 7.74 (s, 1H), 7.76 (d, *J* = 8.4, 2H), 7.85 (d, *J* = 8.3, 2H), 7.86-7.88 (m, 1H), 7.92 (d, *J* = 8.0, 1H), 7.96 (d, *J* = 1.7, 1H), 8.23 (d, *J* = 7.5, 1H).

^{13}C NMR (150 MHz, DMSO-d$_6$): 22.2, 23.2, 26.8, 28.7, 30.9, 45.5, 46.6, 48.8, 51.7, 51.9, 120.3, 120.6, 121.2, 122.8, 125.7, 126.7, 127.1, 127.5, 130.5, 133.7, 138.1, 138.3, 138.4, 140.4, 140.9, 153.7, 154.2, 167.9, 169.4, 172.8.

MS (ESI): m/z 569.2 [M+H$^+$].

Dimethyl 2,2'-[[((*S*)-5-acetamido-6-methoxy-6-oxohexyl)azanediyl]bis(methylene)](2*E*,2'*E*)-bis[3-[4-(9,9-dimethyl-9*H*-fluoren-2-yl)phenyl]acrylate] (*E*,*E*-34)

The above flash chromatography purification using ethyl acetate-methanol (95:5) as the eluent afforded compound **(*E*,*E*)-34** (32 mg, yield 57%) as a white solid (mp 91-93 °C).

^{1}H NMR (600 MHz, DMSO-d$_6$): 1.19-1.25 (m, 2H), 1.42-1.48 (m, 14H), 1.52-1.64 (m, 2H), 1.82 (s, 3H), 2.43 (t, *J* = 7.4, 2H), 3.50-3.55 (m, 7H), 3.71 (s, 6H), 4.15-4.21 (m, 1H), 7.31-7.36 (m, 4H), 7.52-7.56 (m, 2H), 7.63 (dd, *J* = 7.9, 1.8, 2H), 7.70 (d, *J* = 7.9, 4H), 7.77-7.88 (m, 12H), 8.17 (d, *J* = 7.8, 1H).

^{13}C NMR (150 MHz, DMSO-d$_6$): 22.2, 23.4, 25.1, 26.7, 30.8, 46.5, 49.8, 51.6, 51.8, 52.0, 53.5, 120.2, 120.6, 121.0, 122.7, 125.7, 126.5, 127.0, 127.5, 129.6, 131.1, 133.5, 138.0, 138.2, 138.3, 140.9, 141.4, 153.6, 154.1, 168.4, 169.3, 172.8.

MS (ESI): m/z 957.4 [M+Na$^+$].

Reaction of MBHA derivative 24 with N-acetyl-*L*-histidine methyl ester (NAHME) acetate.

Methyl (*S*,*E*)-2-[(4-(2-acetamido-3-methoxy-3-oxopropyl)-1*H*-imidazol-1-yl)methyl]-3-[4-(9,9-dimethyl-9*H*-fluoren-2-yl)phenyl]acrylate (35).

A solution of MBHA derivative 24 (30 mg, 0.071 mmol) in DMSO (3.0 mL) was added to NAHME acetate (15 mg, 0.071 mmol) and DIPEA (24 µL, 0.14 mmol). The reaction mixture was stirred at 50 °C for 24 hours. After completion, brine (3 x 50 mL) was added to the reaction mixture. The organic layers were extracted with ethyl acetate, combined, dried over sodium sulfate, filtered, and concentrated under reduced pressure. The purification by flash chromatography using ethyl acetate-petroleum ether (9:1) yielded compound 35 (24 mg, yield 59%) as an off-white solid (mp 81-84 °C).

^{1}H NMR (600 MHz, DMSO-d_6): 1.50 (s, 6H), 1.78 (s, 3H), 2.76 (dd, *J* = 14.6, 8.5, 1H), 2.85 (dd, *J* = 14.6, 5.4, 1H), 3.56 (s, 3H), 3.77 (s, 3H), 4.37-4.50 (m, 1H), 4.99 (s, 2H), 6.81 (s, 1H), 7.29-7.39 (m, 2H), 7.53 (s, 1H), 7.56-7.60 (m, 3H), 7.72 (dd, *J* = 8.0, 1.7, 1H), 7.86-7.89 (m, 3H), 7.93 (d, *J* = 8.0, 1H), 7.94 (s, 1H), 8.02 (s, 1H), 8.19 (d, *J* = 7.5, 1H).

^{13}C NMR (150 MHz, DMSO-d_6): 22.2, 26.8, 30.0, 42.7, 46.6, 51.6, 52.3, 115.9, 120.3, 120.7, 121.2, 122.8, 125.8, 126.2, 127.1, 127.5, 130.0, 132.4, 136.5, 137.1, 138.0, 138.1, 138.5, 141.6, 143.4, 153.7, 154.2, 166.7, 169.1, 172.3.

MS (ESI): m/z 578.1 [M+H$^+$].

Reaction of MBHA derivative 24 with N-acetyl-*L*-cysteine methyl ester (NACME)

Methyl (*R*,*Z*)-2-[[(2-acetamido-3-methoxy-3-oxopropryl)thio]methyl]-3-[4-(9,9-dimethyl-9*H*-fluoren-2-yl)phenyl]acrylate (36).

A solution of MBHA derivative **24** (52 mg, 0.12 mmol) in DMSO (3.0 mL) was added to **NACME** (21 mg, 0.12 mmol) and DIPEA (21 µL, 0.12 mmol). The reaction mixture was stirred at 50 °C for 20 minutes. After completion, brine (3 x 50 mL) was added to the reaction mixture. The organic layers were extracted with ethyl acetate, combined, dried over sodium sulfate, filtered, and concentrated under reduced pressure. The crude product was purified by flash chromatography using the mixture containing ethyl acetate-methanol (98:2) as the eluent to afford **36** (62 mg, yield 95%) as an off-white solid (mp 68-71 °C).

^{1}H NMR (600 MHz, DMSO-d_6): 1.50 (s, 6H), 1.87 (s, 3H), 2.84 (dd, *J* = 13.8, 8.6, 1H), 2.98 (dd, *J* = 13.8, 5.4, 1H), 3.63 (s, 3H), 3.70 (d, *J* = 12.4, 1H), 3.76 (d, *J* = 12.4, 1H), 3.79 (s, 3H), 4.45-4.48 (m, 1H), 7.31-7.41 (m, 2H), 7.55-7.60 (m, 1H), 7.69 (d, *J* = 8.1, 2H), 7.71-7.75 (m, 2H), 7.84-7.90 (m, 3H), 7.93 (d, *J* = 7.9, 1H), 7.95 (d, *J* = 1.7, 1H), 8.39 (d, *J* = 7.8, 1H).
MS (ESI): m/z 566.1 [M+H$^+$].

Reaction of acrylanilide derivative 25 with N-acetyl-*L*-cysteine methyl ester (NACME)

(*S*)-Methyl 2-acetamido-3-[[3-[[4-(9,9-dimethyl-9*H*-fluoren-2-yl)phenyl]amino]-3-oxopropyl]thio]propanoate (37).
A solution of acrylanilide derivative **25** (52 mg, 0.15 mmol) in DMSO (3.0 mL) was added to **NACME** (53 mg, 0.30 mmol) and DIPEA (52 µL, 0.30 mmol). The reaction mixture was stirred at 50 °C for three days. After completion, brine (3 x 50 mL) was added to the reaction mixture. The organic layers were extracted with ethyl acetate, combined, dried over sodium sulfate, filtered, and concentrated under reduced pressure. The resulting organic residue was purified by flash chromatography using ethyl acetate as eluent to obtain compound **37** (54 mg, yield 68%) as an off-white solid (mp 129-132 °C).
^{1}H NMR (600 MHz, DMSO-d_6): 1.49 (s, 6H), 1.87 (s, 3H), 2.63 (t, *J* = 7.2, 2H), 2.78-2.85 (m, 3H), 2.94 (dd, *J* = 13.7, 5.5, 1H), 3.65 (s, 3H), 4.46-4.50 (m, 1H), 7.30-7.36 (m, 2H), 7.56 (dd, *J* = 7.1, 1.4, 1H), 7.63 (dd, *J* = 8.1, 1.1, 1H), 7.71 (s, 4H), 7.82-7.85 (m, 2H), 7.87 (d, *J* = 7.9, 1H), 8.40 (d, *J* = 7.8, 1H), 10.08 (s, 1H).
^{13}C NMR (150 MHz, DMSO-d_6): 22.3, 26.8, 27.3, 32.7, 36.6, 46.5, 52.0, 119.4, 120.1, 120.5, 120.6, 122.7, 125.2, 126.9, 127.0, 127.2, 135.1, 137.4, 138.2, 138.4, 138.9, 153.6, 154.0, 169.4, 171.3.
MS (ESI): m/z 539.1 [M+H$^+$].

3.7.2 Photophysical and photochemical properties

Freshly prepared solutions at approximately 1x10^{-5} M in DCM were used for photophysical characterization studies. UV-Vis absorption spectra were performed using an Agilent Cary 60 spectrophotometer. PL spectra were obtained with a Cary Eclipse

Fluorescence Spectrophotometer. The irradiation experiments involving the diadduct derivative **(*E*,*E*)-34** were carried out with a tunable source Zolix (TLS2-X300PU-G, 300W UV Xenon Light Source with monochromator Omni-λ2047i).

[2+2] Photocycloaddition reaction of diadduct derivative (*E*,*E*)-34.

A solution of diadduct derivative **(*E*,*E*)-34** (12 mg, 0.013 mmol) was dissolved in deuterated dichloromethane (1.0 mL) in a 5 mm NMR Pyrex tube. The solution was exposed to a monochromatic light centered at 327 nm generated by means of a tunable source Zolix, and ^{1}H NMR spectra were recorded at regular time intervals (0, 2, 4, 8, 16, 24, and 42 hours).

Dimethyl 3-((*S*)-5-acetamido-6-methoxy-6-oxohexyl)-6,7-bis(4-(9,9-dimethyl-9*H*-fluoren-2-yl)phenyl)-3-azabicyclo[3.2.0]heptane-1,5-dicarboxylate (38).

The solution contained in the NMR tube was concentrated, and the crude product was purified by flash chromatography using petroleum ether-ethyl acetate (1:1) as the eluent to give compound **38** (10 mg, yield 83%) as a colorless glassy solid. Figure 17 shows the comparison of the ^{1}H NMR spectra of the isolated compound **38** with reference compounds **20** and **21** (see Research Article 2.8 and 2.9), highlighting spectral similarities and structural correlation. The presence of characteristic signals corresponding to protons of the azabicyclo[3.2.0]heptane scaffold confirmed the successful occurrence of the [2+2] photocycloaddition reaction.

MS (ESI): m/z 935.2 [M + H^{+}].

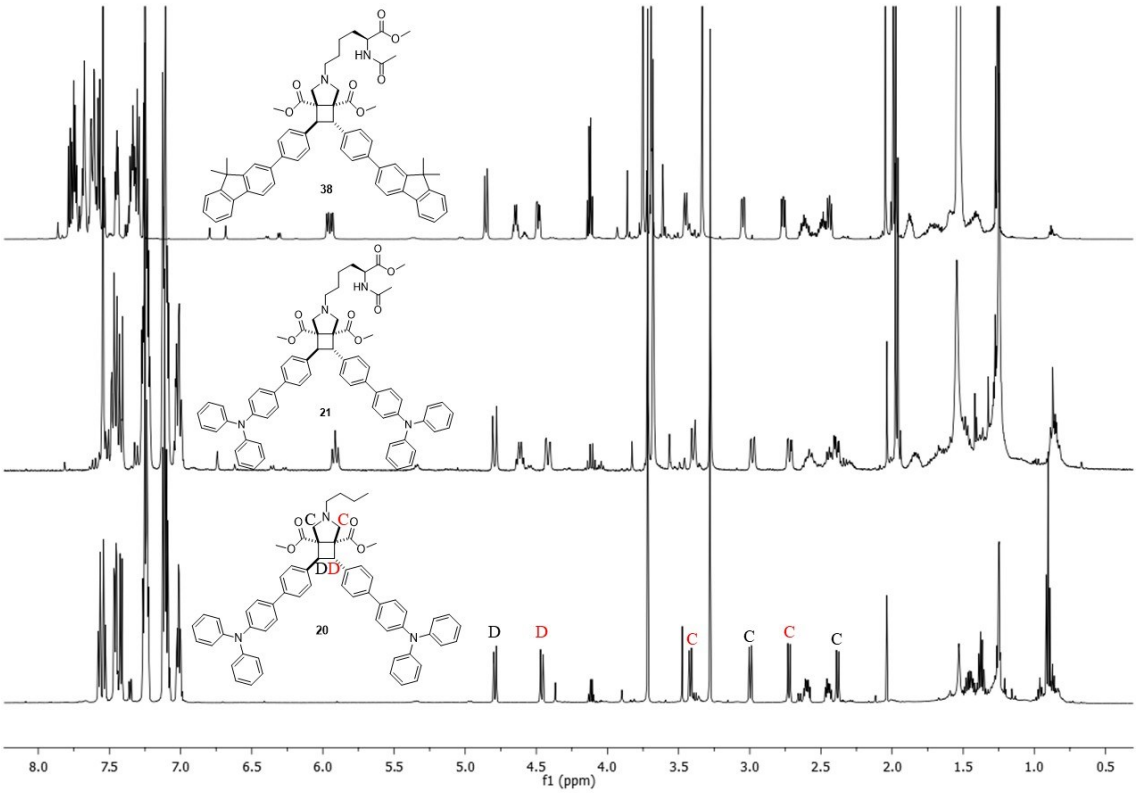

Figure 17. Comparison of the ^{1}H NMR spectra (600 MHz, $CDCl_3$) of the isolated compound **38** with reference compounds **20** and **21** bearing the triphenylamine moiety.

Reaction of MBHA derivative 24 with Human Serum Albumin (HSA)

To a solution of HSA (Human Ricombinant Serum Albumin Expressed in Pichia Pastoris, Aldrich A7736, 67 mg, 1.0 μmol) in deuterium oxide (1.4 mL), buffered at pH 7.4 with Phosphate Buffered Saline (PBS, 14 mg), MBHA derivative **24** (0.43 mg, 1.0 μmol) was added as a (20 mM) solution in DMSO-d_6 (50 μL). The reaction mixture was divided into two 5 mm NMR Pyrex tubes and heated at 37 °C and 50 °C, respectively. ^{1}H NMR spectra were recorded at regular time intervals (0, 1, 2, 4, 8, and 24 h).

3.8 REFERENCES

1. Zhang, Y.; Park, K.Y.; Suazo, K.F.; Di Stefano, M. Recent progress in enzymatic protein labelling techniques and their applications. *Chem. Soc. Rev.*, **2018**, *47*, 9106-9136.
2. Zimmer, M. Green Fluorescent Protein (GFP): Applications, Structure, and Related Photophysical Behavior. *Chem. Rev.*, **2002**, *102*, 3, 759-782.
3. Wang, Y.; Wang, G.; O'Kane, D.J.; Szalay, A.A.; A study of protein-protein interactions in living cells using luminescence resonance energy transfer (LRET) from *Renilla* luciferase to *Aequorea* GFP. *Mol. Gen. Genet.*, **2001**, *264*, 578-587.
4. Park, S.H.; Raines, R.T. Green Fluorescent protein as a signal for protein-protein interactions. *Protein Sci.*, **1997**, *6*, 2344-2349.
5. Schneider, A.F.L.; Hackenberger, C.P.R. Fluorescent labelling in living cells. *Curr. Opin. Biotechnol.*, **2017**, *48*, 61-68.
6. Guignet, E.G.; Hovius, R.; Vogel, H. Reversible site-selective labeling of membrane proteins in live cells. *Nat. Biotechnol.*, **2004**, *22*, 440-444.
7. Tsukiji, S.; Miyagawa, M.; Takaoka, Y.; Tamura, T.; Hamachi, I. Ligand-directed tosyl chemistry for protein labeling *in vivo*. *Nat. Chem. Biol.*, **2009**, *5*, 341-343.
8. Puliti, D.; Warther, D.; Orange, C.; Specht, A.; Goeldner, M. Small photoactivatable molecules for controlled fluorescence activation in living cells. *Bioorg. Med. Chem.*, 2011, 19, 1023-1029.
9. Teoh, C.L.; Su, D.; Sahu, S.; Yun, S.W.; Drummond, E.; Prelli, F.; Lim, S.; Cho, S.; Ham, S.; Wisniewski, T.; Chang, Y.T. Chemical Fluorescent Probe for Detection of Aβ Oligomers. *J. Am. Chem. Soc.*, **2015**, *137*, 42, 13503-13509.
10. Fernandez-Suarez, M.; Ting, A.Y. Fluorescent probes for super-resolution imaging in living cells. *Nat. Rev. Mol. Cell. Biol*., **2008**, *9*, 929-943.
11. Vendrell, M.; Zhai, D.; Cheng Er, J.; Chang, Y.T. Combinatorial Strategies in Fluorescent Probe Development. *Chem. Rev.*, **2012**, *112*, 8, 4391-4420.
12. Meimetis, L.G.; Carlson, J.C.T.; Giedt, R.J.; Kohler, R.H.; Weissleder, R. Ultrafluorogenic Coumarin–Tetrazine Probes for Real-Time Biological Imaging. *Angew. Chem.*, **2014**, *126*, 7661-7664.
13. Kozma, E.; Kele, P. Fluorogenic probe for super-resolution microscopy. *Org. Biomol. Chem.*, **2019**, *17*, 215-233.

14. Lukinavičius, G.; Reymond, L.; Umezawa, K.; Sallin, O.; D'Este, E.; Göttfert, F.; Ta, H.; Hell, S.W.; Urano, Y.; Johnsson, K. Fluorogenic Probes for Multicolor Imaging in Living Cells. *J. Am. Chem. Soc.*, **2016**, *138*, 30, 9365-9368.
15. Krall, N.; da Cruz, F.P.; Boutureira, O.; Bernardes, G.J.L. Site-selective protein-modification chemistry for basic biology and drug development. *Nature Chem.*, **2016**, *8*, 103-113.
16. Ma, D.L.; Wong, W.L.; Chung, W.H.; Chan, F.Y.; So, P.K.; Lai, T.S.; Zhou, Z.Y.; Leung, Y.C.; Wong, K.Y. A Highly Selective Luminescent Switch-On Probe for Histidine/Histidine-Rich Proteins and Its Application in Protein Staining. *Angew. Chem.*, **2008**, *120*, 3795-3799.
17. Leitner, A.; Lindner, W. Functional Probing of Arginine Residues in Proteins Using Mass Spectrometry and an Arginine-Specific Covalent Tagging Concept. *Anal. Chem.*, **2005**, *77*, 14, 4481-4488.
18. Seki, Y.; Ishiyama, T.; Sasaki, D.; Abe, J.; Sohma, Y.; Oisaki, K.; Kanai, M. Transition Metal-Free Tryptophan-Selective Bioconjugation of Proteins. *J. Am. Chem. Soc.*, **2016**, *138*, 34, 10798-10801.
19. Chalker, J.M.; Bernardes, J.L., Lin, Y.A.; Davis, B.G. Chemical Modification of Proteins at Cysteine: Opportunities in Chemistry and Biology. *Chem. Asian J.*, **2009**, *4*, 630-640.
20. Singh, J. The Ascension of Targeted Covalent Inhibitors. *J. Med. Chem.*, **2022**, *65*, 8, 5886-5901.
21. Kim, G.; Grams, R.J.; Hsu, K.L. Advancing Covalent Ligand and Drug Discovery beyond Cysteine. *Chem. Rev.*, **2025**, *125*, 14, 6653-6684.
22. Koul, D.; Shen, R.; Kim, Y.W.; Kondo, Y.; Lu, Y.; Bankson, J.; Ronen, S.M.; Kirkpatrick, D.L.; Powis, G.; Yung, W.K.A. Cellular and in vivo activity of a novel PI3K inhibitor, PX-866, against human glioblastoma. *Neuro-Oncol.*, **2010**, *12*, 559-569.
23. Vazquez-Rodriguez, S.; Wright, M.; Rogers, C.M.; Cribbs, A.P.; Velupillai, S.; Philpott, M.; Lee, H.; Dunford, J.E.; Huber, K.V.M.; Robers, M.B.; Vasta, J.D.; Thezenas, M.L.; Bonham, S.; Kessler, B.; Bennett, J.; Fedorov, O.; Raynaud, F.; Donovan, A.; Blagg, J.; Bavetsias, V.; Oppermann, U.; Bountra, C.; Kawamura, A.; Brennan, P.E. Design, Synthesis and Characterization of Covalent KDM5 Inhibitors. *Angew. Chem. Int. Ed.*, **2018**, *58*, 515-519.

24. Schwartz, P.A.; Kuzmic, P.; Solowiej, J.; Bergqvist, S.; Bolanos, B.; Almaden, C.; Nagata, A.; Ryan, K.; Feng, J.; Dalvie, D.; Kath, J.C.; Xu, M.; Wani, R.; Murray, B.W. Covalent EGFR inhibitor analysis reveals importance of reversible interactions to potency and mechanisms of drug resistance. *PNAS*, **2013**, *111*, 173-178.
25. Kalkhof, S.; Sinz, A. Chances and pitfalls of chemical cross-linking with amine-reactive *N*-hydroxysuccinimide esters. *Anal. Bioanal. Chem.*, **2008**, *392*, 305-312.
26. Patel, M.K.; Vijayakrishnan, B.; Koeppe, J.R.; Chalker, J.M.; Doores, K.J.; Davis, B.G. Analysis of the dispersity in carbohydrate loading of synthetic glycoproteins using MALDI-TOF mass spectrometry. *Chem. Commun.*, **2010**, *46*, 9119-9121.
27. Nakamura, T.; Kawai, Y.; Kitamoto, N.; Osawa, T.; Kato, Y. Covalent Modification of Lysine Residues by Allyl Isothiocyanate in Physiological Conditions: Plausible Transformation of Isothiocyanate from Thiol to Amine. *Chem. Res. Toxicol.*, **2009**, *22*, 3, 536-542.
28. Kathman, S.G.; Span, I.; Smith, A.T.; Xu, Z.; Zhan, J.; Rosenzweig, A.C.; Statsyuk, A.V. A Small Molecule That Switches a Ubiquitin Ligase From a Processive to a Distributive Enzymatic Mechanism. *J. Am. Chem. Soc.*, **2015**, *137*, 39, 12442-12445.
29. Jakob, C.G.; Upadhyay, A.K.; Donner, P.L.; Nicholl, E.; Addo, S.N.; Qiu, W.; Ling, C.; Gopalakrishan, S.M.; Torrent, M.; Cepa, S.P.; Shanley, J.; Shoemaker, A.R.; Sun, C.C.; Vasudevan, A.; Woller, K.R.; Shotwell, J.B.; Shaw, B.; Bian, Z.; Hutti, J.E. Novel Modes of Inhibition of Wild-Type Isocitrate Dehydrogenase 1 (IDH1): Direct Covalent Modification of His315. *J. Med. Chem.*, **2018**, *61*, 15, 6647-6657.
30. He, X.; Carter, D. Atomic structure and chemistry of human serum albumin. *Nature*, **1992**, *358*, 209-215.
31. Krantz, A.; Hanel, A. M.; Strug, I.; Wilczynski, A.; Wolff, J. J.; Huang, W.; Huang, L. H.; Settineri, T.; Holmes, D. L.; Hardy, M. C.; Bridon, D. P. SITE-SPECIFIC LABELING OF A PROTEIN LYSINE RESIDUE BY NOVEL KINETIC LABELING COMBINATORIAL LIBRARIES. *Comput. Struct. Biotechnol. J.*, **2014**, *9*, e201431001.
32. Szekeres, G. P.; Kneipp, J. Different binding sites of serum albumins in the protein corona of gold nanoparticles. *Analyst*, **2018**, *143*, 6061-6068.

33. Sugio, S.; Kashima, A.; Mochizuki, S.; Noda, M.; Kobayashi, K. Crystal structure of human serum albumin at 2.5 Å resolution. *PEDS*, **1999**, *12*, 439-446.
34. Fanali, G.; di Masi, A.; Trezza, V.; Marino, M.; Fasano, M.; Ascenzi, P. Human serum albumin: From bench to bedside. *Mol. Aspects Med.*, **2012**, *33*, 209-290.
35. Guex, N.; Peitsch, M.C. SWISS-MODEL and the Swiss-Pdb Viewer: An environment for comparative protein modeling. *Electrophoresis*, **2005**, *18*, 2714-2723.
36. Wardell, M.; Wang, Z.; Ho, J.X.; Robert, J.; Ruker, F.; Ruble, J.; Carter, D.C. The Atomic Structure of Human Methemalbumin at 1.9 Å. *Biochem. Biophys. Res. Commun.*, **2002**, *291*, 813-819.
37. Sudlow, G.; Birkett, D.J.; Wade, D.N. The Characterization of Two Specific Drug Binding Sites on Human Serum Albumin. *Mol. Pharmacol.*, **1975**, *11*, 824-832.
38. Sudlow, G.; Birkett, D.J.; Wade, D.N. Further Characterization of Specific Drug Binding Sites on Human Serum Albumin. *Mol. Pharmacol.*, **1976**, *12*, 1052-1061.
39. Spada, A.; Emami, J.; Tuszynski, J.A.; Lavasanifar, A. The Uniqueness of Albumin as a Carrier in Nanodrug Delivery. *Mol. Pharmaceutics*, **2021**, *18*, 5, 1862-1894.
40. Asano, S.; Patterson, J.T.; Gaj, T.; Barbas III, C.F. Site-Selective Labeling of a Lysine Residue in Human Serum Albumin. *Angew. Chem. Int. Ed.*, **2014**, *53*, 11783-11786.
41. Chen, S.; Yu, G.; Zhang, B.; Wang, Y.; Zhang, N.; Chen, Y. Human serum albumin (HSA) coated liposomal indocyanine green for *in vivo* tumor imaging. *RSC Adv.*, **2016**, *6*, 15220-15225.
42. Langiu, M.; Dadparvar, M.; Kreuter, J.; Ruonala, M.O. Human Serum Albumin-Based Nanoparticle-Mediated *In Vitro* Gene Delivery. *PLoS ONE*, **2013**, *9*, e107603.
43. Miele, E.; Spinelli, G.P.; Miele, E.; Tomao, F.; Tomao, S. Albumin-bound formulation of paclitaxel (Abraxane® ABI-007) in the treatment of breast cancer. *Int. J. Nanomed.*, **2009**, *4*, 99-105.
44. Yi, X.; Lian, X.; Dong, J.; Wan, Z.; Xia, C.; Song, X.; Fu, Y.; Gong, T.; Zhang, Z. Co-delivery of Pirarubicin and Paclitaxel by Human Serum Albumin Nanoparticles to Enhance Antitumor Effect and Reduce Systemic Toxicity in Breast Cancers. *Mol. Pharmaceutics*, **2015**, *12*, 11, 4085-4098.

45. Paolino, M.; Tassone, G.; Governa, P.; Saletti, M.; Lami, M.; Carletti, R.; Sacchetta, F.; Pozzi, C.; Orlandini, M.; Manetti, F.; Olivucci, M.; Cappelli, A. Morita–Baylis–Hillman Adduct Chemistry as a Tool for the Design of Lysine-Targeted Covalent Ligands. *ACS Med. Chem. Lett.*, **2025**, *16*, 3, 397-405.
46. Paolino, M.; Reale, A.; Razzano, V.; Giorgi, G.; Giuliani, G.; Villafiorita-Monteleone, F.; Botta, C.; Coppola, C.; Sinicropi, A.; Cappelli, A. Design, synthesis, structure, and photophysical features of highly emissive cinnamic derivatives. *New J. Chem.*, **2020**, *44*, 13644-13653.
47. Xu, J.; Zong, Q.; Peng, S.; Liao, J.; Zhao, H.; Kong, H.; Xu, J. Design, Synthesis and Properties of Novel BODIPY Dyes With Styryl as π-Bridge at 3,5-Positions. *ChemistrySelect*, **2020**, *5*, 9330-9335.
48. Wang, M.; Gaj, X.; Li, J.; Wei, Y.; Shi, Y.; Cao, X.; Yin, G. Isomeric intramolecular charge-transfer complexes: the effect of relative positions of the donor and acceptor on photophysical and mechanochromic properties. *J. Mater. Chem. C*, **2025**, *13*, 13474-13481.
49. Chen, L.; Uwamizu, A.; Sayama, M.; Kano, K.; Otani, Y.; Kondo, S.; Inoue, A.; Aoki, J.; Ohwada, T. Exploration of LPS_2 agonist binding modes using the combination of a new hydrophobic scaffold and homology modeling. *Eur. J. Med. Chem*., **2023**, *252*, 115271.
50. Kumar, V.; Banerjee, M.; Chatterjee, A. A reaction based turn-on type fluorogenic and chromogenic probe for the detection of trace amount of nitrite in water. *Talanta*, **2012**, *99*, 610-615.
51. Prentice, J.A.; Kasivisweswaran, S.; van de Weerd, R.; Bridges, A.A. Biofilm dispersal patterns revealed using far-red fluorogenic probes. *PLoS Biol.*, **2024**, *22*, e3002928.
52. Li, S.; Peng, Z.; Leblanc, R. M. Method To Determine Protein Concentration in the Protein–Nanoparticle Conjugates Aqueous Solution Using Circular Dichroism Spectroscopy. *Anal. Chem.*, **2015**, *87*, 6455-6459.

3.9 RESEARCH ARTICLE: **"A Facile Access to Green Fluorescent Albumin Derivatives"**

Authors: Mario Saletti, Marco Paolino, Jacopo Venditti, Claudia Bonechi, Germano Giuliani, Stefania Lamponi, Giusy Tassone, Antonella Caterina Boccia, Chiara Botta, Lluís Blancafort, Federica Poggialini, Chiara Vagaggini, and Andrea Cappelli

Publication: ChemBioChem

Publisher: Wiley-VCH GmbH

DOI: doi.org/10.1002/cbic.202300862

Supporting information: cbic202300862-sup-0001-misc_information.pdf

Contribution: The Ph.D. candidate conducted reactivity studies involving the MBHA acetyl derivative and Human Serum Albumin. In this context, kinetic investigations were performed using ^{1}H NMR spectroscopy (400 MHz), alongside evaluation of emission properties shifts upon excitation of the reaction mixture under UV light (365 nm).

Check for updates

ChemBioChem

Research Article
doi.org/10.1002/cbic.202300862

Chemistry Europe
European Chemical Societies Publishing

www.chembiochem.org

A Facile Access to Green Fluorescent Albumin Derivatives

Mario Saletti,[a] Marco Paolino,[a] Jacopo Venditti,[a] Claudia Bonechi,[a] Germano Giuliani,[a] Stefania Lamponi,[a] Giusy Tassone,[a] Antonella Boccia,[b] Chiara Botta,[b] Lluís Blancafort,[c] Federica Poggialini,[a] Chiara Vagaggini,[a] and Andrea Cappelli*[a]

A Morita-Baylis-Hillman Adduct (MBHA) derivative bearing a triphenylamine moiety was found to react with human serum albumin (**HSA**) shifting its emission from the blue to the green-yellow thus leading to green fluorescent albumin (**GFA**) derivatives and enlarging the platform of probes for aggregation-induced fluorescent-based detection techniques. A possible interaction of MBHA derivative **7** with a lipophilic pocket within the **HSA** structure was suggested by docking studies. DLS experiments showed that the reaction with **HSA** induce a conformational change of the protein contributing to the aggregation process of **GFA** derivatives. The results of investigations on the biological properties suggested that **GFA** retained the ability of binding drug molecules such as warfarin and diazepam. Finally, cytotoxicity evaluation studies suggested that, although the MBHA derivative **7** at 0.1 μg/mL affected the percentage of cell viability in comparison to the negative control, it cannot be considered cytotoxic, whereas at all the other concentrations ≥ 0.5 μg/mL resulted cytotoxic at different extent.

Introduction

In the past decades, protein labeling has been widely used in research and industry for biosensing, diagnostic imaging, targeted drug delivery, and other applications.[1] For example, most of the recent works have focused attention on the functionalization of proteins or antibodies, which can be used as drugs against cancer or infections.[2] The developed strategies are usually based on the reactivity of side chain residues of lysine and cysteine containing amino or thiol groups, respectively.[1] In particular, *N*-hydroxysuccinimide (NHS) esters,[3] isocianate (or thioisocianate),[4] and aldehydes for reductive amination[5] represent the most relevant functional groups exploited in the attack of the amino residue of lysine, while maleimides,[6] and α-halocarbonyls[7] are the main electrophiles used for the functionalization of the nucleophilic group of cysteines.[8] In addition, novel synthetic procedures involving selective metal-catalysed or metal-directed reactions, have been optimized.[9] However, these methods require the modification of the native protein (by chemical reactions or via genetic expressions) before its functionalization, which may involve complex synthetic steps and the possibility of chemo-functional alterations of the protein structure. Therefore, great efforts have been made to develop strategies to functionalize proteins at precisely defined sites while preserving their native functions and studying their structure-function relationships.[10–13]

In recent years, particular attention has been dedicated to the design of probes capable of tagging proteins in complex environments.[14–16]

Fluorescence-based detection techniques represent important tools in the study of protein interactions and function,[17] and fluorescent dyes are certainly at the bases of these techniques. However, in recent years, fluorogenic labeling strategies have demonstrated some important advantages such as the higher signal-to-noise ratio due to the fluorescence activation after its reaction/attachment to the desired site.[18–20] Furthermore, the fluorogens showing aggregation induced emission (AIE) features (i.e. emission intensities higher in the solid state than in solution)[21] display higher sensitivity, accuracy, and photostability when compared to traditional fluorescence probes, which are emissive in solution but often undergoes to aggregation caused quenching (ACQ) processes at high concentration.[22,23]

Some Morita-Baylis-Hillman derivatives (i.e. **1**, Figure 1) have been recently developed in our laboratories to react with imidazole[24] or *n*-butylammine[25] leading to cinnamic derivatives (i.e. **2**). showing fluorogenic properties. Although, these cinnamic derivatives displayed very weak emission in solution, methoxy and dimethoxy derivatives showed AIE features. In particular, compound **2** featured a bright blue emission with photoluminescence quantum yields (PL QY) around two orders of magnitude higher in the solid state with respect to the

[a] M. Saletti, M. Paolino, J. Venditti, C. Bonechi, G. Giuliani, S. Lamponi, G. Tassone, F. Poggialini, C. Vagaggini, A. Cappelli
Dipartimento di Biotecnologie, Chimica e Farmacia (Dipartimento di Eccellenza 2018–2022), Università degli Studi di Siena, Via Aldo Moro 2, 53100 Siena, Italy
Tel: +39 0577 232416
E-mail: andrea.cappelli@unisi.it

[b] A. Boccia, C. Botta
Istituto di Scienze e Tecnologie Chimiche "G. Natta" - SCITEC (CNR), Via A. Corti 12, 20133 Milano, Italy

[c] L. Blancafort
Institute of Computational Chemistry and Catalysis and Department of Chemistry, University of Girona, C/M. A. Capmany 69, 17003 Girona, Spain

Supporting information for this article is available on the WWW under https://doi.org/10.1002/cbic.202300862

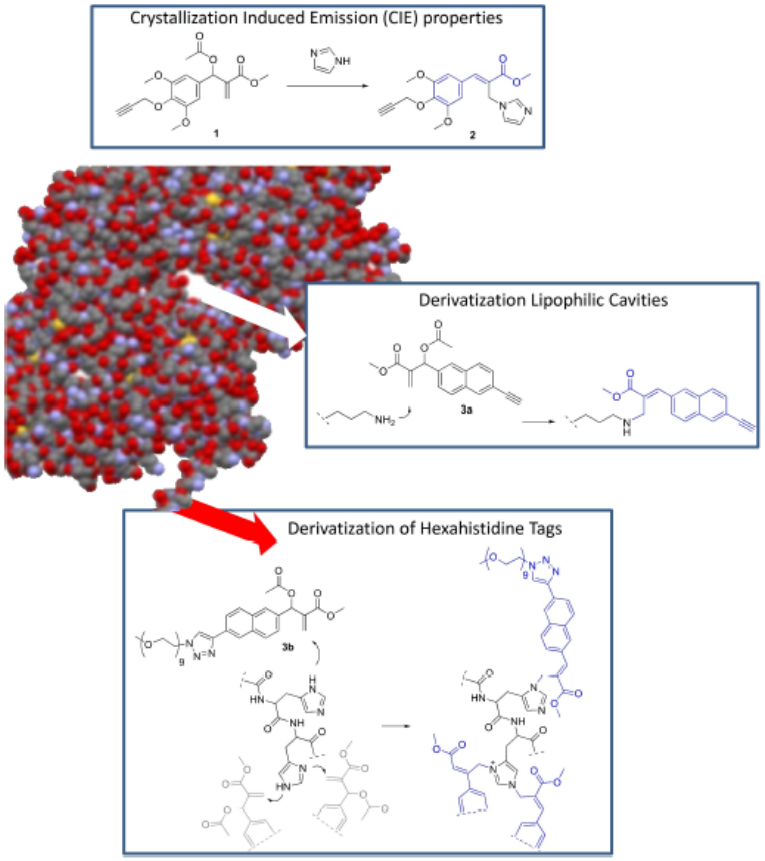

Figure 1. Structures of MBHA derivatives **1** leading to **2**, and MBHA derivatives **3 a,b** involved in site-specific protein derivatization.

corresponding values measured in solution, with the apparent presence of crystallization induced emission (CIE) phenomenon.[24]

In order to extend the π electron system, the phenyl group of these compounds (i.e. **1** and **2**) was then converted into the naphthalene nucleus (i.e. in compounds **3 a,b**), preparing fluorogenic molecules capable of generating monoadducts or diadducts compounds endowed with AIE properties.[26]

The reactivity of some naphthalene MBHA derivatives (i.e. **3 a,b**) was then studied in model proteins, and **3 a** was found to show a potential in the functionalization of lysine residues embedded in lipophilic pockets,[27] whereas **3 b** in the site-specific PEGylation of engineered proteins bearing poly-histidine tags.[28,29]

Very recently, we were successful in identifying cinnamic derivatives **4**, **5**, and **6** (Figure 2) as interesting fluorogenic

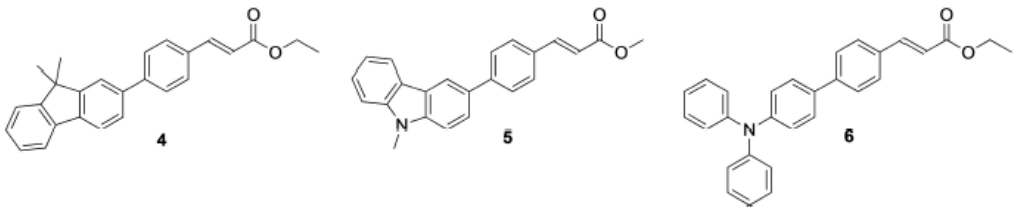

Figure 2. Structure of fluorescent cinnamic derivatives **4**, **5**, and **6**.

compounds showing photoluminescence quantum yield in the order of 57–80% and emission maxima in the range of 407–540 nm.[30]

The very promising photophysical features shown by triphenylamine cinnamic derivative **6** led to the development of the new fluorogenic probe **7**[31] potentially useful in the labeling of basic amino acid residues through an addition-elimination mechanism involving zwitterionic intermediates **8** and leading to cinnamic derivatives **9** (Figure 3).

Very intriguingly, the characterization of the photophysical and the photochemical features of MBHA derivative **7** provided us with very interesting results, confirming the promising photophysical features of the fluorophore contained in cinnamic derivatives **6**, **11**, and **12**.[31] In particular, these studies demonstrated that the shift of the double bond from the acrylic structure of **7** and **10** to the cinnamic one of **6**, **11**, and **12** produced a significant (130-150 nm) red shift in the emission of these compounds with photoluminescence quantum yield (PLQY) values around 58–80%.[31]

Thus, in the present work we investigated the reactivity features of MBHA derivative **7** in interacting with human serum albumin (**HSA**), which represents one of the most interesting proteins of human body. In fact, **HSA** is the most abundant protein in human plasma playing key roles in regulating the oncotic pressure and in carrying important endogenous (i.e. fatty acids, hormones, bilirubin etc.) and exogenous (i.e. drugs) substances. Moreover, **HSA** has been used in the development of drug delivery systems such as abraxane, a nanoparticle formulation of paclitaxel-loaded **HSA** used in the clinical treatment of metastatic breast cancer, small cell lung cancer, and advanced pancreatic cancer.[32,33]

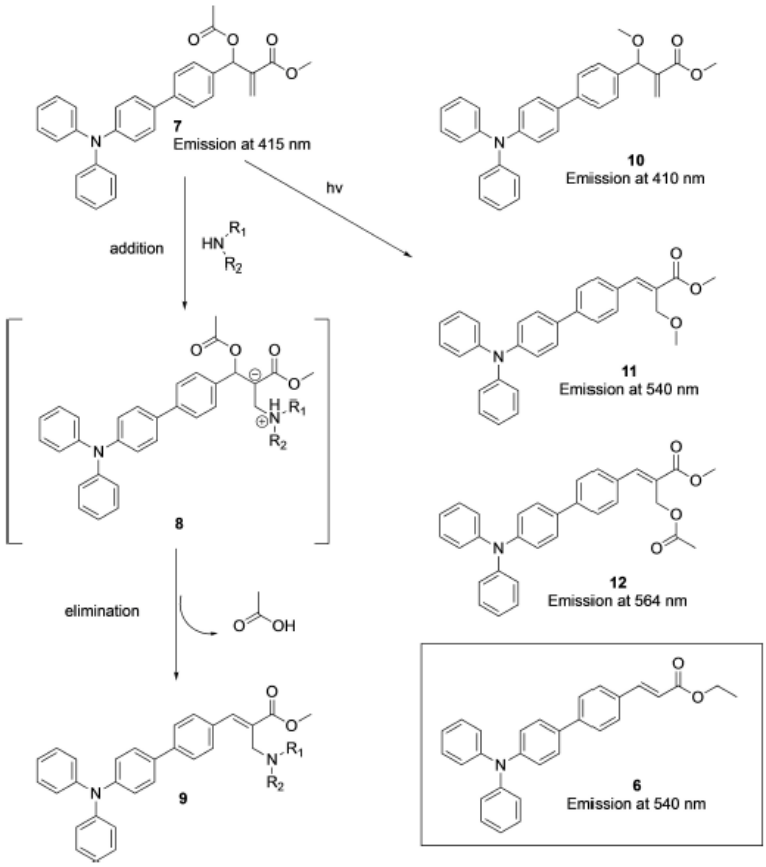

Figure 3. Structure of reactive MBHA derivative **7** leading to acrylic derivative **10** and cinnamic derivatives **9–12**.

Results and Discussion

Interaction of MBHA derivative 7 with HSA

The interaction of compound **7** with **HSA** was investigated by means of a range of different techniques such as Nuclear Magnetic Resonance (NMR) spectroscopy, absorption and emission spectroscopy, and computational docking simulations.

NMR. First, we started with a series of ^{1}H NMR experiments focused to detect the release of acetate during the elimination step following the initial addition step of the addition-elimination reaction involving a nucleophilic amino acid residue and MBHA derivative **7**. In particular, **HSA** (67 mg, 1.0 micromol) was dissolved in deuterium oxide (1.4 mL) containing phosphate buffered saline (PBS, 14 mg) at pH 7.4 into a 5 mm NMR tube and **7** (0.48 mg, 1.0 micromol) was added as a (50 mM) solution in deuterated dimethylsulfoxide (DMSO-d_6, 0.020 mL). The resulting reaction mixture was promptly analyzed by recording a ^{1}H NMR spectrum to obtain the information on the starting conditions (t = 0). The tube was then heated into an oil bath a 50 °C and ^{1}H NMR spectra were recorded at regular time intervals (i.e. 0, 1, 2, 4, 8, 24 h). The obtained spectra were elaborated all in the same manner and staked as shown in Figure 4.

The comparative analysis of the spectra showed that the shape of the **HSA** spectrum was stable in agreement with the reported stability of **HSA** solutions during prolonged heating at 60 °C.[34] Conversely, some visible differences can be easily attributed to the presence of MBHA derivative **7** and the small amount of DMSO added. In particular, while the apparent intensity of the signal at 2.66 ppm (assigned to DMSO added) was stable during the prolonged heating at 50 °C, the one of the signal at 1.88 ppm (assigned to acetate protons) increased progressively during the heating suggesting a progress of the addition-elimination reaction.

Very interestingly, all these events were paralleled by clear-cut changes in the fluorescence emission, which could be easily visualized by exposing the NMR tube-reactor to the UV lamp commonly used for TLC revelation at (365 nm) (Figure 5). In fact, the initial (t = 0) blue emission of MBHA derivative **7** (probably in aggregate form as suggested by its bright emission) progressively turned to the green-yellow during the prolonged heating at 50 °C, supporting the occurrence of the addition-elimination reaction leading to Green Fluorescent Albumin (**GFA**).

Absorption and emission spectroscopy. In Figure 6a the normalized absorption spectra of PBS and **HSA**-PBS in H_2O are compared with the absorption spectra of **7** in DMSO, **7** in DMSO-H_2O, and **7-HSA**-PBS in DMSO-H_2O. In Figure 6b the emission properties of **7** in DMSO and **7** in DMSO-H_2O solutions are shown. In Figure 6c and 6d the pictures of the solutions of **7**

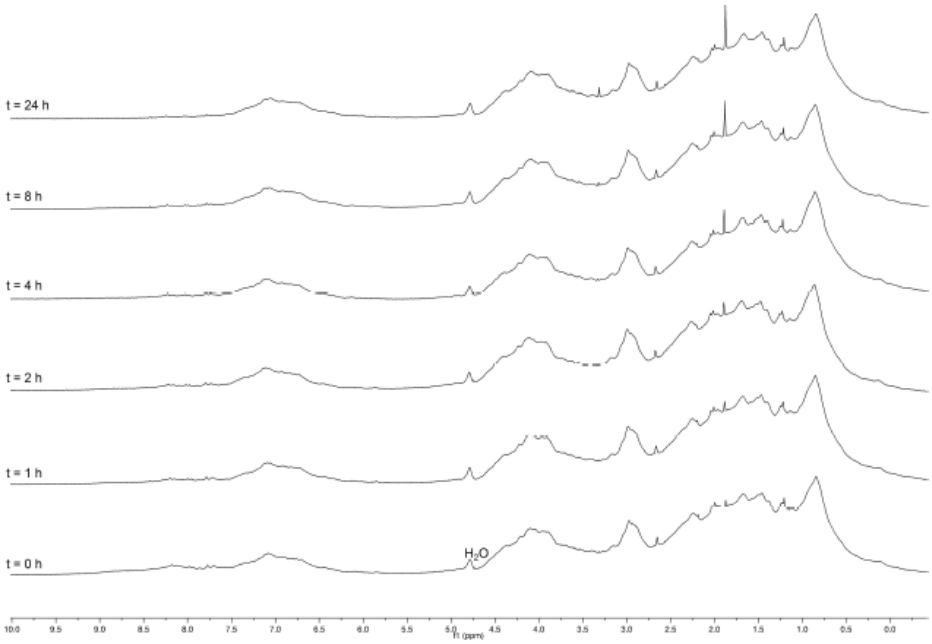

Figure 4. Comparison of the ^{1}H NMR (400 MHz) spectra of the reaction mixtures obtained with **HSA** (67 mg, 1.0 micromol) in D_2O (1.4 mL) containing solid PBS (Aldrich, 14 mg) at pH 7.4 and compound **7** (0.48 mg, 1.0 micromol), which was added as a (50 mM) solution in DMSO-d_6 (0.020 mL). The reaction mixtures contained into a 5 mm NMR tube were heated at 50 °C and ^{1}H NMR spectra were recorded at regular time intervals (0, 1, 2, 4, 8, and 24 h). The bottom trace was obtained with an **HSA** solution in D_2O.

Figure 5. Comparison of the fluorescence emission of the reaction mixtures obtained with **HSA** (67 mg, 1.0 micromol) in D_2O (1.4 mL) containing PBS (Aldrich) at pH 7.4 and compound **7** (0.48 mg, 1.0 micromol), which was added as a (50 mM) solution in DMSO-d_6 (0.020 mL). The reaction mixtures contained into a 5 mm NMR tube were heated at 50 °C and were photographed at regular time intervals (0, 1, 2, 4, 8, and 24 h, from left to right in the sequence) under excitation at 365 nm.

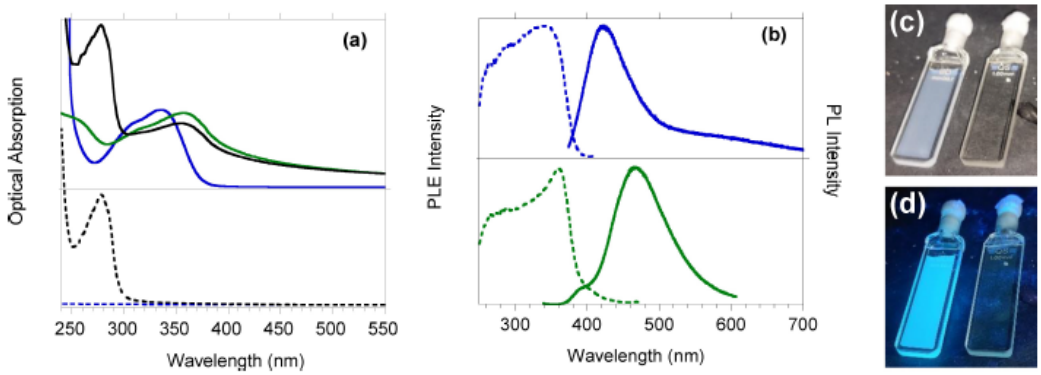

Figure 6. (a) Top: Absorption spectra of solutions of **7** in DMSO (blue solid line, [**7** (0.48 mg, 1.0 micromol) in DMSO (0.620 mL)]), **7** in DMSO-H_2O, (green solid line, [**7** (0.48 mg, 1.0 micromol) in DMSO (0.620 mL) and water (1.4 mL)]), **7-HSA**-PBS in DMSO-H_2O (black solid line, [**7** (0.48 mg, 1.0 micromol), **HSA** (67 mg, 1.0 micromol), PBS (14 mg) in DMSO (0.020 mL) and water (1.4 mL)]); Bottom: Absorption spectra of solutions of PBS in H_2O (blue dashed line, [PBS (14 mg) in water (1.4 mL)]), **HSA**-PBS in H_2O, (black dashed line, [**HSA** (67 mg, 1.0 micromol) and PBS (14 mg) in water (1.4 mL)]); (b) Top: PL and PLE spectrum of **7** in DMSO ([**7** (0.48 mg, 1.0 micromol) in DMSO (0.620 mL)]); Bottom: PL and PLE spectrum of **7** in DMSO-H_2O mixture [0.10 mL of [**7** (0.48 mg, 1.0 micromol) in DMSO (0.620 mL) and water (1.4 mL)] diluted in water (0.500 mL)]; $\lambda_{exc} = 330$ nm; $\lambda_{em} = 423$ nm (top); $\lambda_{em} = 480$ nm (bottom). (c,d) Photo of **7** in DMSO (right) [**7** (0.48 mg, 1.0 micromol) in DMSO (0.620 mL)] and DMSO-H_2O mixture (left) [**7** (0.48 mg, 1.0 micromol) in DMSO (0.620 mL) and water (1.4 mL)] in ambient light (c) and under UV lamp exposure (d).

in DMSO and **7** in DMSO-H_2O are shown both under ambient light and by UV lamp exposure.

The absorption spectrum of **7** red-shifted (from 336 nm to 356 nm) by adding water to the DMSO solution (see Figure 6a). This red-shift was a consequence of the formation of aggregates in the solution when the non-solvent (water) was added to the good solvent (DMSO). The formation of microaggregates was also responsible of light diffusion, giving the observed upshift of the absorption spectrum baseline (Figure 6a) and the opalescent aspect of the solution (Figure 6c). The red-shift observed in the absorption spectrum was very probably associated to the variation of the molecular conformation and/or to inter-molecular interactions occurring upon microaggregation. In fact, molecular planarization induces a red-shift in the absorption spectra and intermolecular interactions rigidify the molecular structure. The emission properties of rigidified molecules are enhanced thanks to the deactivation of intramolecular motions that in solution reduces radiative emission. This behavior is typical of AIE molecules with restricted intramolecular motions (RIM) properties in the solid state.[35,36]

Compound **7** displayed a very weak deep-blue emission (420 nm) when molecularly dissolved in a good solvent (DMSO) while its emission was strongly enhanced in intensity and shifted to 478 nm by adding water (bad solvent), as shown in Figure 6b. A similar behaviour was observed when a DMSO solution of **7** was added to the water solution of **HSA** (1.0 micromol) containing PBS (leading to **7-HSA**). The absorption spectrum of **7-HSA** (see Figure 6a) well corresponded to the absorptions of the different components (i.e. **HSA** shows a sharp peak at 277 nm while PBS did not absorb in the UV-Vis range). When excited at 360 nm, its PL spectrum was identical to that of **7** dissolved in a DMSO-water mixture while, upon exciting **HSA** at 277 nm, the emission of **HSA** was also observed at 332 nm (Figure ESI-1 and ESI-2).

The reaction of compound **7** with **HSA** was then monitored with a photoluminescence analysis of **7-HSA** solution during the heating process, in comparison with a reference solution of **7** in DMSO-H_2O subjected to the same heating treatment.

As shown in Figure 7, by heating the **7-HSA** solution, its PL spectrum showed a progressive red-shift from 480 nm to 525 nm and the solution became transparent (Figure 8a and

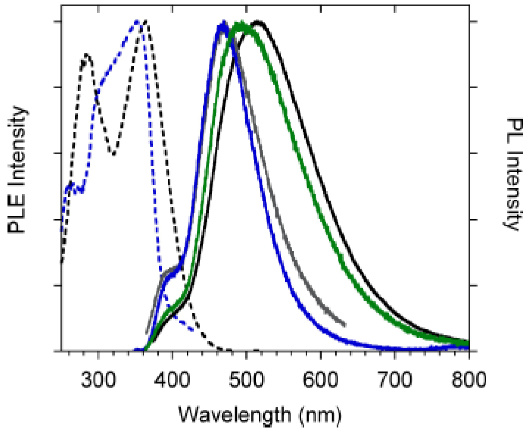

Figure 7. Normalized PL (solid lines, $\lambda_{exc}=330$ nm) spectra of **7-HSA** solution during the heating treatment at 50 °C at different times (blue, pristine solution; grey, 2 h; green, 4 h; black, 8 h). Normalized PLE spectra (dashed lines) of the pristine solution (blue, $\lambda_{em}=480$ nm) and after 8 h treatment at 50 °C (black, $\lambda_{em}=525$ nm, [**7** (0.48 mg, 1.0 micromol), **HSA** (67 mg, 1.0 micromol), PBS (14 mg) in DMSO (0.020 mL) and water (1.4 mL)]).

(a) (b)

Figure 8. Photo of **7-HSA** solution heated at 50 °C for 8 h (left), pristine **7-HSA** solution (middle) and **7** DMSO-H_2O reference solution (right) heated at 50 °C for 8 h, in ambient light (a) and under UV irradiation (b). left and center: [**7** (0.48 mg, 1.0 micromol), **HSA** (67 mg, 1.0 micromol), PBS (14 mg) in DMSO (0.020 mL) and water (1.4 mL)]; right: [**7** (0.48 mg, 1.0 micromol) in DMSO (0.620 mL) and water (1.4 mL)].

Figure ESI-4) while no changes were observed for the reference solution (see Figure 7 and 8). This observation indicated that the thermal treatment of **7-HSA** modified the extent of micro-aggregation in solution, while no effects were observed for the reference solution of **7**. More interestingly, in Figure 7 a clear variation is observed after the thermal treatment in the PL excitation profiles (PLE) of **7-HSA** solution, showing a sharp peak at 280 nm that well corresponds to the absorption of **HSA** (see Figure 6a). This observation demonstrates that, in the **7-HSA** solution, **HSA** is able to transfer energy to **7** only after thermal treatment, indicating that the thermal treatment activates energy transfer by reducing the average distance between the two chromophores. By further dilution of the solution, energy transfer was observed to be independent on solution concentration. This fact, together with the red-shift of the emission, well supports the reaction between **HSA** and **7** leading to green fluorescent albumin (**GFA**). On the other hand, the persistence of **HSA** emission at 330 nm after the thermal treatment (see Figure ESI-2), showed the presence of **HSA** macromolecules non-coupled to **7**.

Docking simulations. Owing to the complexity of the **HSA** structure, the reactivity of MBHA derivative **7** could be rationalized by assuming initial non-covalent interactions with eventual binding sites on the **HSA** surface (or possibly with the pockets known to transport fatty acids and drugs) followed by the occurrence of the addition-elimination reaction with histidine, lysine, or arginine residues leading to the formation of covalent conjugates and to liberation of acetate ions. Thus, the interaction of MBHA derivative **7** with **HSA** was studied in silico by computational docking simulations to evaluate the possible existence of preferential non-covalent interaction sites, which could accommodate **7** allowing the reaction with the suitable nucleophilic amino acid residues. Our first step in this direction was to evaluate the accessible conformations of the protein through Molecular Dynamics (MD) simulations. Following this preliminary approach, molecular docking of **7** was then performed and the results obtained are shown in Figure 9.

The best pose of **7** was locate in the middle of the three I–II–III domains of the protein itself,[37] as showed in Figure 9. Analyzing the conformation clusters obtained, a versatile fitting of the ligand in this pocket was observed. This can be related to the relatively large size of the **HSA** pocket that allows the binding of **7** in many different manners. Comparing our results with the crystal structure of **HSA** complexed with warfarin (see Figure ESI-5),[38] we immediately notice similar (but not perfectly overlapping) poses of the two ligands within site I (of domain II) of **HSA**, as defined by Sudlow.[39] In fact, this high affinity binding site appears to be very large and adaptable, capable of binding bulky molecules such as bilirubin or different molecules in independent ways.[40] Considering the potential energy of ligand-protein complex obtained, the results showed a grid score of −46.5 kcal/mol,[41] suggesting a good accommodation of **7** within **HSA** structure. In particular, the contribution of the van der Waals energy is considerably greater (−45.7 kcal/mol) when compared to the value of the electrostatic energy (−0.8 kcal/mol). Similar results were observed for binding simulations in hydrophobic environment, where the entropic contribution appears to dominate the biomolecular associations mechanism.[42]

More in detail, compound **7** seems to fit perfectly into the pocket, placing the acrylic part inside the pocket and keeping the aromatic portion near the surface. This hydrophobic part of the molecule seems to interact with other aromatic residues present at the edge of the pocket (see Figure ESI-6 of the Supporting Information). Furthermore, confirming the hydrophobic nature of the pocket, no migration of water molecules within the binding site was observed in our 70 ns of simulation. The hydrogen bond (1.97 Å) between Arginine 257 and the carbonyl of the acrylic group is also shown in Figure 9. It seems to be a stable interaction between ligand and **HSA** but other nucleophilic residues, such as Lysine 199 and Histidine 242, are

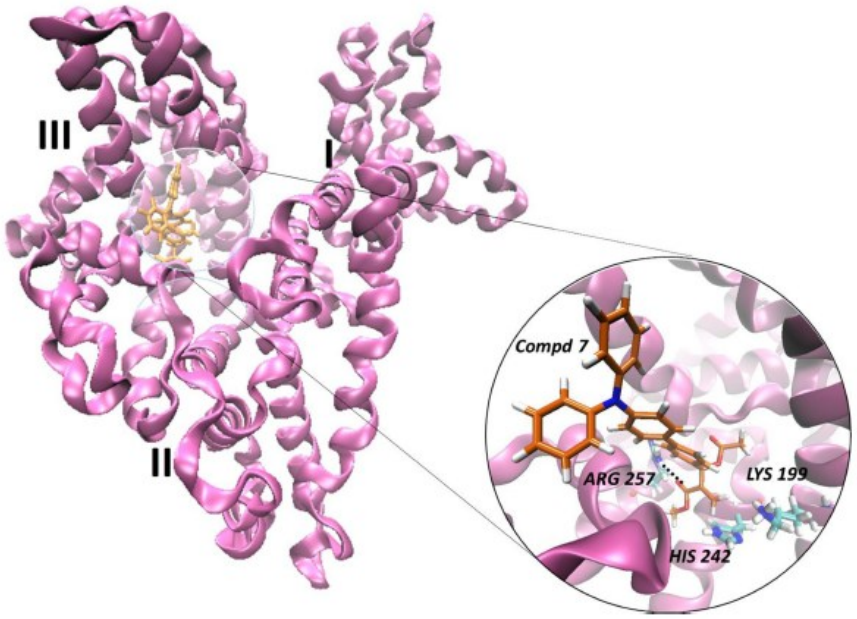

Figure 9. The most significant docking pose of MBHA derivative **7** within **HSA** structure.

also close to **7**. These residues do not yet appear to interact with the ligand but, proceeding with the MDs, they could determine alternative binding ways within the protein pocket. We refer particularly to the activated double bond of **7**, where the polarization of the electron cloud (the partial charges of **7** are reported in the Supporting Information), could promoting the addition-elimination reaction with the nearby residue Lys 199 (distance between C28 and N is 3.4 Å). It is noteworthy that Lys 199 was reported to be capable of reacting with aspirin by accepting the acetyl group of the drug molecule, suggesting a strong nucleophilic character.[43] This interesting feature could be determinant in the conjugation reaction following the initial recognition step. In other words, several important features appeared to suggest a potentially selective conjugation reaction of **7** with **HSA**: the affinity for the putative binding site, the strong nucleophilic character of Lys 199 and the correct orientation of the reacting groups.

Protein characterization

The product of the addition-elimination reaction (i.e. **GFA**) was characterized in comparison with the starting **HSA** by SDS page experiments and dynamic light scattering (DLS) measurements to ascertain the eventual existence of significant differences between **GFA** and starting **HSA** induced by the interaction with MBHA derivative **7**. Furthermore, the biological properties of **GFA** were evaluated in terms of the potential ability of binding drug molecules with respect to native **HSA**.

SDS page experiments. The high purity of the starting **HSA** protein sample and of the reaction product between **HSA** and MBHA derivative **7** after 24 h of incubation at 50 °C were confirmed through SDS-PAGE analysis (Figure 10). Both the

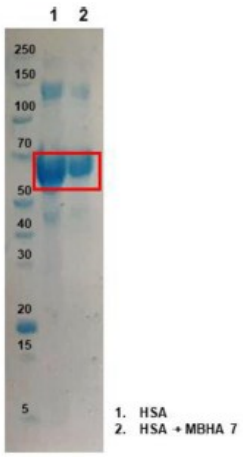

Figure 10. SDS-PAGE analysis (Bis-TRIS gel 4–12% NuPAGE, Thermo Fisher Scientific) of **HSA** (molecular weight 66472 Da) and the reaction product between **HSA** and MBHA derivative **7** after 24 h of incubation at 50 °C. The bands relating to both samples are highlighted in red. The marker used was the PageRuler Broad Range Unstained Protein Ladder (Thermo Fisher Scientific).

samples contained only one species as demonstrated by the presence of a single protein band after SDS-PAGE separation. This result confirmed the **HSA** stability in the mild reaction conditions. The small differences between the native protein and the derivatized sample **GFA** appeared to confirm the occurrence of derivatization reaction, but they could be not truly significant owing to the small value (i.e. 418 Da) of the chromophore with respect to the **HSA** molecular mass.

To verify the occurrence of derivatization, the resulting gel was exposed to the UV lamp (365 nm). However, no bands were discernible due to potential interference from the protein visualization dye (SimplyBlue™ SafeStain - Thermo Fisher). We assumed that the **GFA** emission (around 525 nm) could be quenched by the dye (i.e. comassie brilliant blue, absorption maximum at 595 nm) used in the SDS page experiments. To overcome this issue, electrophoretic analysis was performed again by loading the samples (**HSA** and the reaction product between **HSA** and MBHA derivative **7** after 24 hours of incubation at 50 °C) in duplicate. A section of the gel containing both samples was run following the previously described protocol, while the samples loaded as duplicates were loaded in the absence of the loading buffer (which contains the bromophenol blue as a dye, in its formulation). The first section of the gel was stained to allow the visualization of the samples, while the second section remained unstained and was subsequently exposed to UV lamp. The exclusion of dyes during sample preparation and visualization enabled the detection of an emissive band of green-yellow staining at the position (height) corresponding to the band of the derivatized protein, by comparison with the position of the band in the stained section of the gel.

Dynamic Light Scattering. DLS is a powerful technique that provides essential structural information about biological macromolecules in solution. In particular, DLS experiments allow the measurement of hydrodynamic diameter, polydispersity, and the presence of protein aggregates in solutions to be made. As reported in Table 1 and in Figure 11, the tendency

Table 1. Mean size, polydispersity index, and ζ-potential values of **GFA** compared to those of starting **HSA**.

Sample	Concentration	Size ± SD (nm)	Size ± SD (nm)	Size ± SD (nm)	PDI ± SD	ζ -potential ± SD (mv)
HSA	HSA (67 mg, 1.0 micromol) and PBS (14 mg) in water (1.4 mL)	8.91 ± 0.65	–	–	0.30 ± 0.13	-11.47 ± 0.64
GFA (Conc-Sol)	0.425 mL of [7 (0.48 mg, 1.0 micromol), HSA (67 mg, 1.0 micromol), PBS (14 mg) in DMSO (0.020 mL) and water (1.4 mL)] diluted in 1.0 mL of water	8.71 ± 0.75	50.0 ± 2.5	420.2 ± 6.3	0.40 ± 0.15	-19.05 ± 0.15
GFA (Dil-Sol)	0.275 mL [7 (0.48 mg, 1.0 micromol), HSA (67 mg, 1.0 micromol), PBS (14 mg) in DMSO (0.020 mL) and water (1.4 mL)] diluted in 1.0 mL of water	8.38 ± 0.87	91.8 ± 4.1	424.1 ± 7.1	0.46 ± 0.17	-18.37 ± 0.30

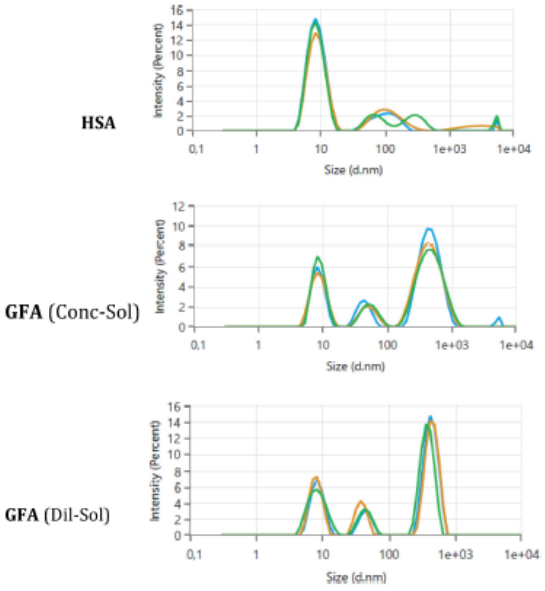

Figure 11. Size distribution profiles obtained by DLS experiments. The concentrations are reported in Table 1.

towards aggregation of **HSA** increases in **GFA** derivatives and this behavior was stable also to dilution.

In fact, DLS revealed in the **GFA** solution the presence of two populations of aggregates with dimension values of 50–92 nm and 420–424 nm, respectively. These results suggest that the reaction of **7** with **HSA** led to a conformational change of the protein.

The polydispersity index is a measure of the width of unimodal size distributions. The PDI of the **GFA** samples was generally low (~0.40), indicating good dispersion homogeneity and suggesting that the reaction of **7** with **HSA** does not modify the degree of uniformity of the size distribution of the protein system.

The ζ-potential value was not subject to variations due to the reaction of **7** with **HSA**. The surface charge of the aggregate systems retained the properties of a neutral or zwitterionic dispersion.

All these experimental results suggest that the reaction of **7** with **HSA** leads to a conformational change in **HSA** that contributes to the aggregation process of **GFA** derivatives.

Biological properties. The biological properties of **GFA** were investigated in terms of the potential ability of binding drug molecules. Thus, warfarin and diazepam were selected because these drugs are generally recognized as the gold standard molecules in such investigations. In particular, warfarin is generally recognized to bind Sudlow's site I (known also warfarin site), whereas diazepam was demonstrated to bind with high affinity to a different site (site II or diazepam site).[44] Thus, **GFA** was incubated with these drug molecules, and the fraction of the drug bound to the macromolecule was used as a measure of the binding affinity (Table 2).

Moreover, to evaluate the potential effects of the prolonged heating in the **HSA**'s ability to bind drug molecules, warfarin and diazepam were incubated in presence of native **HSA**, both before and after the treatment at 50 °C for 8 h. As reported in the Table 2, both the reaction of **HSA** with MBHA derivative **7** and the thermal treatment at 50 °C (for 8 h) of **HSA** alone appeared to produce only negligible changes in the affinity of **HSA** for the drug molecules. Thus, **GFA** appeared to retain the biological properties of native **HSA** as drug carrier and potential drug delivery system.

In vitro cytotoxicity of MBHA derivative 7

Finally, non-confluent adhered fibroblasts were incubated with increasing concentrations of MBHA derivative **7** for 24 h and then membrane integrity was evaluated by quantifying the uptake of the vital dye Neutral Red into the cells.

As shown in Figure 12, the cell toxicity of MBHA derivative **7** increased by increasing its concentration. In particular, the sample demonstrated no toxic effect toward fibroblasts for the concentration of 0.01 μg/mL as the percentage of live cells was not statistically different ($p < 0.05$) in comparison to the negative control but differed significantly from those of the positive control which had a strong cytotoxic effect. By increasing the test compound concentration at 0.1 μg/mL a reduction of cell viability of about 20% in comparison to the negative control was detected. Concerning the cytotoxicity, the standard ISO 10993–5 claims that a material can be considered as not cytotoxic if allows for a cell viability of over 70% after an exposure for 24 h. So, although the MBHA derivative **7** at 0.1 μg/mL sample affected the percentage of cell viability in comparison to the negative control, it cannot be considered cytotoxic.

At all the other concentrations ≥ 0.5 μg/mL, the test sample resulted cytotoxic but with a different extent with an IC_{50} at 1 μg/mL and a percentage of vital cells non statistically different from positive control at 5 μg/mL, i.e. the highest tested value.

Conclusions

In the aim of obtaining new fluorogenic probes potentially useful in basic amino acid labelling, the very promising optical features of previously published cinnamic derivative **6** stimulated the design of Morita-Baylis–Hillman acetate derivative **7** bearing a triphenylamine moiety. This MBHA derivative was found to show interesting AIE properties with a bright blue emission (478 nm) of its microaggregates in DMSO-water dispersions. Moreover, MBHA derivative **7** was found to react with human serum albumin (**HSA**) shifting its emission from the blue to the green-yellow (525 nm) thus leading to green fluorescent albumin (**GFA**) derivatives. Very intriguingly, **HSA** was able to transfer energy to the newly-formed cinnamic fluorophore emitting at 525 nm in **GFA** only after the thermal treatment. This result was strongly suggestive that the thermal treatment activates energy transfer by reducing the average distance between the chromophores of **HSA** and the newly-formed cinnamic fluorophore in **GFA**. In other words, the thermal treatment appeared to play a crucial role in promoting the reaction of MBHA derivative **7** that allowed the close proximity between the newly-formed cinnamic fluorophore and the tyrosine (and/or tryptophan) residues of **HSA**.

Table 2. Binding affinities of drug molecules (warfarin and diazepam) for **GFA** in comparison with native **HSA** and **HSA** after the thermal treatment at 50 °C.

	Fraction of bound drug (% ± SD)		
	GFA	HSA	HSA-50 °C
Warfarin	94.75 ± 3.87	93.59 ± 3.71	94.90 ± 4.19
Diazepam	84.09 ± 4.21	83.31 ± 3.98	83.60 ± 3.46

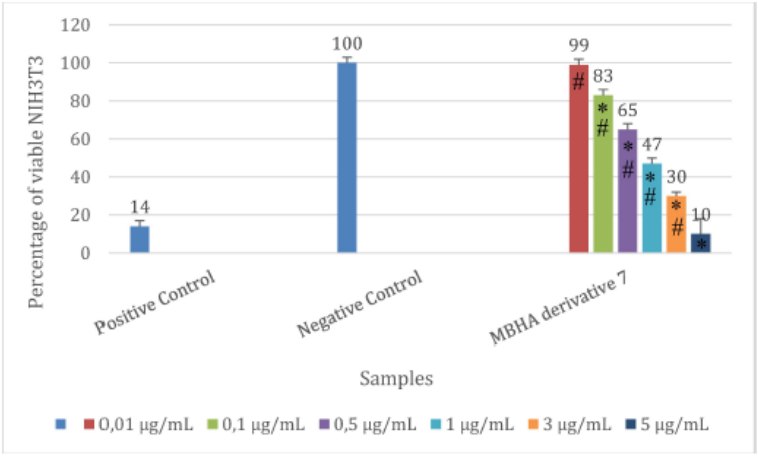

Figure 12. Percentage of viable NIH3T3 fibroblasts evaluated by the NRU assay after 24, h of contact with increasing concentrations of MBHA derivative **7**. Data are means ± SD of three experiments run in six replicates. * Value is statistically different in comparison to negative control (complete medium), $p < 0.05$. # Values are statistically different in comparison to positive control SDS, $p < 0.05$.

Docking studies suggested a possible interaction of MBHA derivative **7** with a lipophilic pocket within the **HSA** structure that could induce Lys199 to interact with the activated double bond of **7** in the addition-elimination reaction.

Characterization studies performed with **GFA** sample (i.e. SDS page experiments) demonstrated the stability of **HSA** to the reaction conditions, and DLS measurements revealed an increased propensity of **GFA** to form aggregates of well-established dimensions probably because of possible conformational changes produced by the reaction of MBHA derivative **7** with **HSA**.

The biological properties of **GFA** were investigated in terms of the potential ability of binding drug molecules such as warfarin and diazepam, which are generally recognized as standard molecules in such investigations. The results suggested that **GFA** retained the biological properties of native **HSA** as drug carrier and potential drug delivery system.

Finally, MBHA derivative **7** at 0.1 µg/mL was found to affect the cell viability in comparison to the negative control, but it cannot be considered cytotoxic at this concentration. On the other hand, at all the other tested concentrations ≥0.5 µg/mL resulted cytotoxic at a different extent with an IC_{50} at 1 µg/mL.

Experimental Section

Chemicals. Reagents, reference drugs and solvents were purchased from Sigma-Aldrich Srl (Milan. Italy). Milli-Q quality water (Millipore. Milford. MA. USA), acetonitrile (ACN) and formic acid (FA) were used for the chromatographic analyses.

Synthesis. NMR spectra were recorded with a Bruker DRX-400 AVANCE III or a Bruker DRX-600 AVANCE spectrometer in the indicated solvents: the values of the chemical shifts are expressed in ppm.

Reaction of MBHA derivative 7 with HSA. HSA (67 mg, 1.0 micromol) was dissolved in deuterium oxide (1.4 mL) containing phosphate buffered saline (PBS, 14 mg) at pH 7.4 into a 5 mm NMR tube and **7** (0.48 mg, 1.0 micromol) was added as a (50 mM) solution in deuterated dimethylsulfoxide (DMSO-d_6, 0.020 mL). The resulting reaction mixture was promptly analyzed by recording a ^{1}H NMR spectrum to obtain the information on the starting conditions (t = 0). The tube was then heated into an oil bath a 50 °C and ^{1}H NMR spectra were recorded at regular time intervals (i.e. 1, 2, 4, 8, 24 h).

Photophysical properties. UV-vis absorption spectra are obtained with a Perkin Elmer Lambda 900 spectrometer. PL spectra are obtained with a NanoLog composed by a iH320 spectrograph equipped with a Synapse QExtra charge-coupled device by exciting with a monochromated 450 W Xe lamp. The spectra are corrected for the instrument response.

Molecular Dynamics and Docking simulations. The crystal structure of the Human Serum Albumin, **HSA** (PDB ID 1UOR)[45] was used as a starting point for the simulations. To generate the model, we first checked the ionizable residues to determine their protonation, then the entire system was solvated with explicit water molecules and the energy minimized. To avoid excessive fluctuations of the system, initial constraints on the solute were used. The procedure using the SHAKE algorithm was employed to fix hydrogens and constrain all bonds involving hydrogen. Before the docking simulation, the protein was subjected to 20 ns of Molecular Dynamics (MD) to obtain a better sampling of the conformations. These MD simulations were executed using AMBER16 program[46] with ff14SB as the force field, at constant temperature (300°K) and pressure (1 atm) with a step size of 2 fs. Next, the lowest energy binding pose of the fully optimized compound **7** within HAS, was simulated using the DOCK6.9 algorithm.[47] The results were carefully checked, then the most representative ligand-protein complex was selected among the conformation clusters based on the lowest energy scores obtained. Further details of the procedure are reported in the Supporting Information. Thereafter, to better highlight the ligand interactions within the protein, an additional 50 ns of MD was performed.

Table 3. Chromatographic parameters adopted for the LC/UV-MS method.

Time (min)	% Eluent A H_2O (FA 0.1 %v/v)	% Eluent B ACN (FA 0.1 %v/v)	Flow (mL/min)	Wavelength (nm)	Scan Range (m/z)[a]
0–1	100				
15–19	20	80	0.6	254	100–2000
20	100				

[a]The detection was conducted both in positive and negative modes of ionization.

SDS page experiments. The purity of the protein samples was studied by SDS-PAGE analysis (NuPAGE 4–12% Bis-Tris protein gels; Thermo Fisher Scientific, Waltham, Massachusetts, USA).

DLS measurements. DLS measurements were performed using a Malvern Zetasizer Pro-Red (Worcestershire, UK) equipped with a 632.8 nm He–Ne laser. Samples were analyzed as synthesized without prior filtration.

Experimental measurements were performed in backscattering mode with a fixed scattering angle of 173 ° at 25 °C, after an equilibration step of 2 min. Each sample was recorded in triplicate. The correlation function was analyzed using the general purpose method to derive the intensity-weighted particle size distribution and polydispersity index.

The ζ -potential was determined at 25 °C. Electrophoretic mobility data were converted to ζ -potential (mV) using the Smoluchowski approximation. The average values of three consecutive measurements are given.

HPLC-UV/MS method. The chromatographic analyses were performed using an Agilent 1260 LC/MSD VL system (G1946 C) (Agilent Technologies. Palo Alto. CA) constituted by a vacuum solvent degassing unit, a binary high-pressure gradient pump, a 1260 series UV detector, and an 1100 MSD model VL benchtop mass spectrometer. The Agilent 6130 series mass spectra detection (MSD) single-quadrupole instrument was equipped with the orthogonal spray API-ES (Agilent Technologies. Palo Alto. CA). Nitrogen was used as nebulizing and drying gas. Chromatographic separation was performed using a Phenomenex Kinetex EVO C18–100 Å (150 mm×4.6 mm, 5 µm particle size) at room temperature (RT) and gradient elution with a binary solution was conducted as reported in Table 3.

Binging affinity to HSA, HSA-50 °C, and GFA. Warfarin and diazepam have been selected as reference compounds due to their well-known high affinity to **HSA** site I and II, respectively. The binding affinity was evaluated for both compounds by incubating in presence of a PBS 1 mM (pH 7.4) solution of **HSA** (batch n° 068 K7538 V), **HSA-50 °C**, and **GFA**. The working concentration of **HSA**, **HSA-50 °C**, and **GFA** was of 50 µM, while warfarin and diazepam were tested at the final concentration of 100 µM to ensure the affinity towards proteins and allow a suitable chromatographic response. Samples were incubated at 37 °C for 30 min, and then centrifuged at 5000 rpm for 15 minutes using centrifugal filters (Amicon Ultra®, regenerated cellulose, membrane pore size 30,000 NMWL). Filtered volumes were collected and analyzed applying the HPLC-UV/MS method described above. The percentages of bound compounds were calculated by comparison with reference solutions.

Cell Culture and in vitro Cytotoxicity Test. Cytotoxicity is defined as the degree to which a test sample induces toxicity (damage) to cells. This may occur by one or more mechanisms including damage to cell membranes. In order to evaluate the in vitro cytotoxicity of MBHA derivative **7**, the direct contact tests, proposed by ISO 10995–5 was used [ISO 10995–5:2009; Biological Evaluation of Medical Devices-Part 5: Tests for Cytotoxicity: In Vitro Methods. ISO: Geneva, Switzerland, 2009]. As the evaluation of in vitro acute toxicity does not depend on the final use for which the product is intended, the document ISO 10995–5:2009 recommends many cell lines from the American Type Collection. Among them, to test MBHA derivative **7** cytotoxicity, NIH3T3 mouse fibroblasts were chosen American Type Culture Collection (USA).

Fibroblasts NIH3T3 were propagated in DMEM supplemented with 10% fetal calf serum, 1% L-glutamine-penicillin-streptomycin solution, and 1% MEM non-essential amino acid solution, and then incubated at 37 °C in a humidified atmosphere containing 5% CO_2. Once at confluence, the cells were washed with 0.1 M PBS, separated with trypsin-EDTA solution, and centrifuged at 1000 r.p.m. for 5 min. The pellet was re-suspended in complete medium (dilution 1:15).

Cells (1.5×10^4) suspended in 1 mL of complete medium were seeded in each well of a 24 well round multidish and incubated at 37 °C in an atmosphere of 5% CO_2. After 24 h of culture, the culture medium was discharged and the MBHA derivative **7** solubilized in DMSO and diluted in complete medium, was added to each well to test increasing concentration ranging from 0.01 to 5 µg/mL. The experiment was repeated three times and each concentration was set up in six replicates. Complete medium was used as negative control and Sodium Dodecyl Sulphate (SDS) was used as positive control.

Cell toxicity, in terms of membrane integrity, of increasing concentrations of MBHA derivative **7** after 24 h of incubation towards fibroblasts NIH3T3 was evaluated by the uptake of the vital dye Neutral Red into the cells following the procedure previously reported.[48]

Acknowledgements

M.P. and A.C. acknowledge the MUR for the financial support under the project CN00000041 – "National Center for Gene Therapy and Drugsbased on RNA Technology" – CUP B63C2200061 0006 Mission 4 Component 2 (M4C2) – investment 1.4 [CN3] of the National Recovery and Resilience Plan (PNRR) funded by the European Union "Next Generation EU". M.P. acknowledge the University of Siena for the financial support of the project Chromo-GEnUP through the F-CUR2022 funding line (2265-2022-PM-CONRICMIUR_PC-FCUR2022_003). Open Access publishing facilitated by Università degli Studi di Siena, as part of the Wiley - CRUI-CARE agreement.

Conflict of Interests

The authors declare no conflict of interest.

Data Availability Statement

The data that support the findings of this study are available from the corresponding author upon reasonable request.

[1] V. K. Kadambar, A. Melman, *Adv. Exp. Med. Biol.* **2019**, *1140*, 237–250.
[2] J. Maneesh, N. Kamal, S. K. Batra, *Trends Biotechnol.* **2007**, *25*, 307–316.
[3] C. C. Ward, J. I. Kleinman, D. K. Nomura, *ACS Chem. Biol.* **2017**, *12*, 1478–1483.
[4] P. Rosa-Neto, B. Wängler, L. Iovkova, G. Boening, A. Reader, K. Jurkschat, E. Schirrmacher, *ChemBioChem* **2009**, *10*, 1321–1324.
[5] V. Raindlová, R. Pohl, M. Hocek, *Chem. Eur. J.* **2012**, *18*, 4080–4087.
[6] K. Pagano, M. Paolino, S. Fusi, V. Zanirato, C. Trapella, G. Giuliani, A. Cappelli, S. Zanzoni, H. Molinari, L. Ragona, M. Olivucci, *J. Phys. Chem. Lett.* **2019**, *10*, 2235–2243.
[7] Smith, B. D. Higgin, J. J. Raines, *Bioorg. Med. Chem. Lett.* **2011**, *21*, 5029–5032.
[8] S. B. Gunnoo, A. Madder, *ChemBioChem* **2016**, *17*, 529–553.
[9] P. G. Isenegger, B. G. Davis, *J. Am. Chem. Soc.* **2019**, *141*, 8005–8013.
[10] E. A. Hoyt, P. M. S. D. Cal, B. L. Oliveira, G. J. L. Bernardes, *Nat. Chem. Rev.* **2019**, 147–171.
[11] S. J. Walsh, S. Omarjee, W. R. J. D. Galloway, T. T.-L. Kwan, H. F. Sore, J. S. Parker, M. Hyvönen, J. S. Carroll, D. R. Spring, *Chem. Sci.* **2019**, *10*, 694–700.
[12] X. Chen, K. Muthoosamy, A. Pfisterer, B. Neumann, T. Weil, *Bioconjugate Chem.* **2012**, *23*, 500–508.
[13] M. J. Matos, B. L. Oliveira, N. Martínez-Sáez, A. Guerreiro, P. M. S. D. Cal, J. Bertoldo, M. Maneiro, E. Perkins, J. Howard, M. J. Deery, J. M. Chalker, F. Corzana, G. Jimenez-Oses, G. J. L. Bernardes, *J. Am. Chem. Soc.* **2018**, *140*, 4004–4017.
[14] E. G. Guignet, R. Hovius, H. Vogel, *Nat. Biotechnol.* **2004**, *4*, 440–444.
[15] B. A. Griffin, S. R. Adams, R. Y. Tsien, *Science* **1998**, *281*, 269–272.
[16] B. Krishnan, A. Szymanska, L. M. Gierasch, *Chem. Biol. Drug Des.* **2007**, *69*, 31–40.
[17] Z. Wang, X. Ding, S. Li, J. Shi, Y. Li, *RSC Adv.* **2014**, *4*, 7235–7245.
[18] L. Rong, C. Zhang, Q. Lei, S.-. Y. Qin, J. Feng, X.-. Z. Zhang, *Adv. Sci.* **2016**, *3*, 1500211.
[19] Z. Wang, X. Ding, S. Li, J. Shi, Y. Li, *RSC Adv.* **2014**, *4*, 7235–7245.
[20] L. D. Lavis, T. -Y Chao, R. T. Raines, *ACS Chem. Biol.* **2006**, *1*, 252–260.
[21] J. Mei, N. L. C. Leung, R. T. K. Kwok, J. W. Y. Lam, B. Z. Tang, *Chem. Rev.* **2015**, *115*, 11718–11940.
[22] D. Ding, K. Li, B. Liu, B. Z. Tang, *Acc. Chem. Res.* **2013**, *46*, 2441–2453.
[23] W. C. Wu, C. Y. Chen, Y. Tian, S. H. Jang, Y. Hong, Y. Liu, R. Hu, B. Z. Tang, Y. T. Lee, C. T. Chen, W. C. Chen, A. K. Y. Jen, *Adv. Funct. Mater.* **2010**, *20*, 1413–1423.
[24] V. Razzano, M. Paolino, A. Reale, G. Giuliani, R. Artusi, G. Caselli, M. Visintin, F. Makovec, A. Donati, F. Villafiorita-Monteleone, C. Botta, A. Cappelli, *ACS Omega* **2017**, *2*, 5453–5459.
[25] M. Saletti, J. Venditti, M. Paolino, A. Zacchei, G. Giuliani, G. Giorgi, C. Bonechi, A. Donati, A. Cappelli, *RSC Adv.* **2023**, *13*, 35773–35780.
[26] V. Razzano, M. Paolino, A. Reale, G. Giuliani, A. Donati, G. Giorgi, R. Artusi, G. Caselli, M. Visintin, F. Makovec, S. Battiato, F. Samperi, F. Villafiorita-Monteleone, C. Botta, A. Cappelli, *RSC Adv.* **2018**, *8*, 8638–8656.
[27] G. Tassone, M. Paolino, C. Pozzi, A. Reale, L. Salvini, G. Giorgi, M. Orlandini, F. Galvagni, S. Mangani, X. Yang, B. Carlotti, F. Ortica, L. Latterini, M. Olivucci, A. Cappelli, *ChemBioChem* **2022**, *23*, e202100449.
[28] M. Paolino, M. Visintin, E. Margotti, M. Visentini, L. Salvini, A. Reale, V. Razzano, G. Giuliani, G. Caselli, F. Tavanti, M. C. Menziani, A. Cappelli, *New J. Chem.* **2019**, *43*, 17946.
[29] M. Paolino, A. Reale, V. Razzano, G. Giuliani, A. Donati, C. Bonechi, G. Caselli, M. Visintin, F. Makovec, C. Scialabba, M. Licciardi, E. Paccagnini, M. Gentile, L. Salvini, F. Tavanti, M. C. Menziani, A. Cappelli, *New J. Chem.* **2019**, *43*, 6834–6837.
[30] M. Paolino, A. Reale, V. Razzano, G. Giorgi, G. Giuliani, F. Villafiorita-Monteleone, C. Botta, C. Coppola, A. Sinicropi, A. Cappelli New, *J. Chem.* **2020**, *44*, 13644–13653.
[31] M. Saletti, M. Paolino, J. Venditti, C. Bonechi, G. Giuliani, A. Boccia, C. Botta, A. Cappelli, *Dyes Pigm.* **2023**, *219*, 111571.
[32] W. J. Gradishar, D. Krasnojon, S. Cheporov, A. N. Makhson, G. M. Manikhas, A. Clawson, P. Bhar, *J. Clin. Oncol.* **2009**, *27*, 3611–3619.
[33] M. J. Hawkins, P. Soon-Shiong, N. Desai, *Adv. Drug Delivery Rev.* **2008**, *60*, 876–885.
[34] A. Spada, J. Emami, J. A. Tuszynski, A. Lavasanifar, *Mol. Pharm.* **2021**, *18*, 1862–1894.
[35] J. D. Luo, Z. L. Xie, J. W. Y. Lam, L. Cheng, H. Y. Chen, C. F. Qiu, H. S. Kwok, X. W. Zhan, Y. Q. Liu, D. B. Zhu B. Z Tang, *Chem. Commun.* **2001**, 1740–1741.
[36] E. Cariati, V. Lanzeni, E. Tordin, R. Ugo, C. Botta, A. Giacometti Schieroni, A. Sironi, D. Pasini, *Phys. Chem. Chem. Phys.* **2011**, *13*, 18005–18014.
[37] M. M. Salim, M. E. El Sharkasy, F. Belal, M. Walash, *Spectrochim. Acta Part A* **2021**, *252*, 119495.
[38] https://www.rcsb.org/structure/2BXD.
[39] G. Sudlow, D. J. Birkett, D. N. Wade, *Mol. Pharmacol.* **1975**, *11*, 824–832.
[40] U. Kragh-Hansen, *Dan. Med. Bull.* **1990**, *37*, 57–84.
[41] E. C. Meng, D. A. Gschwend, J. M. Blaney, I. D. Kuntz, *Proteins Struct. Funct. Genet.* **1993**, *17*, 266–278.
[42] E. Barratt, R. J. Bingham, D. J. Warner, C. A. Laughton, S. E. V. Phillips, S. W. Homans, *J. Am. Chem. Soc.* **2005**, *127*, 11827–11834.
[43] F. Yang, C. Bian, L. Zhu, G. Zhao, Z. Huang, M. Huang, *J. Struct. Biol.* **2007**, *157*, 348–355.
[44] G. Dargó, D. Bajusz, K. Simon, J. Müller, G. T. Balogh, *J. Med. Chem.* **2020**, *63*, 1763–1774.
[45] X. M. He, D. C. Carter, *Nature* **1993**, *364*, 362.
[46] D. A. Case, R. M. Betz, D. S. Cerutti, T. E. Cheatham, III, T. A. Darden, R. E. Duke, T. J. Giese, H. Gohlke, A. W. Goetz, N. Homeyer, S. Izadi, P. Janowski, J. Kaus, A. Kovalenko, T. S. Lee, S. LeGrand, P. Li, C. Lin, T. Luchko, R. Luo, B. Madej, D. Mermelstein, K. M. Merz, G. Monard, H. Nguyen, H. T. Nguyen, I. Omelyan, A. Onufriev, D. R. Roe, A. Roitberg, C. Sagui, C. L. Simmerling, W. M. Botello-Smith, J. Swails, R. C. Walker, J. Wang, R. M. Wolf, X. Wu, L. Xiao and P. A. Kollman (**2016**), AMBER 2016, University of California, San Francisco.
[47] https://onlinelibrary.wiley.com/doi/epdf/10.1002/jcc.23905.
[48] S. Lamponi, M. C. Baratto, E. Miraldi, G. Baini, M. Biagi, *Plants* **2021**, *10*, 97.

Manuscript received: February 24, 2024
Revised manuscript received: January 24, 2024
Accepted manuscript online: February 18, 2024
Version of record online: March 13, 2024

CHAPTER 4

MBHA-BASED MACROCYCLIC CROWN ETHER-PARACYCLOPHANE HYBRID COMPOUNDS

4.1 CROWN ETHER: A GENERAL INTRODUCTION

Macrocycles represent a captivating class of large-ring molecules that have become central to modern chemistry due to their distinctive structural characteristics and broad range of applications. Among them, crown ethers stand out as the most extensively studied and widely utilized macrocyclic compounds. These latter molecules, composed of repeating ether units, were first discovered and described by Charles J. Pedersen in 1967, a breakthrough that later earned him the Nobel Prize in Chemistry in 1987.[1] Crown ethers are generally categorized into two main types: aliphatic crown ethers, consisting solely of ether linkages, and aromatic crown ethers, which incorporate aromatic moieties, such as benzo- or dibenzo- units, alongside ether functionalities.[2] A further subclass, known as aza crown ethers, arises when one or more oxygen atoms are replaced by nitrogen atoms within the macrocyclic ring.[3] The defining feature of crown ethers lies in their remarkable ability to form stable complexes with metal cations. This property is attributed to the presence of electron-rich heteroatoms that create a central cavity suitable for ion coordination.[4] Such host-guest interaction supports their pivotal role in supramolecular chemistry, particularly in the selective binding of alkali and alkaline earth metals. The resulting complexes often exhibit amphiphilic character, possessing a hydrophilic core that surrounds the bound cation and a hydrophobic exterior.[5,6] The structural versatility of these macrocycles, defined by ring size, donor atom type, and substitution patterns, enables fine-tuning of their binding properties, making them indispensable tools in analytical chemistry, catalysis, molecular recognition, and drug delivery.[7]

In this regard, crown ethers have proven particularly valuable in drug delivery, primarily because of their ionophoric properties, which facilitate efficient membrane transport and modulate interactions with biological systems. Their ability to complex metal cations allows for the design of responsive delivery systems, including vesicular structures such as liposomes and niosomes, capable of encapsulating both hydrophilic and lipophilic drugs.[8,9] For example, Echegoyen and co-workers developed cholesterol-linked crown ethers forming functional vesicles.[10] Whilst niosomes are defined as non-ionic liposomes, they can be engineered to respond to specific cations and enhance drug release. For instance, Darwish and Uchegbu demonstrated that crown ether-based niosomes composed of *N*-hexadecanoyl-2-aminomethyl-15-crown-5 enhanced the release of rhodamine B in the presence of Ca^{2+} ions.[11] Similarly, the Muzzalupo group designed niosomal formulations of 5-fluorouracil (5-FU) that improved drug stability and reduced

cytotoxic effects.[12] Building on such evidence, crown ether-based drug-targeting systems have emerged as promising tools in cancer therapy, improving drug permeability and cellular uptake through stable cation-complexation mechanisms. For example, Borrel et al. demonstrated that various crown ethers can act as effective carriers for pirarubicin, an anticancer agent with limited cellular permeability due to its high polarity.[13] Crown ethers have also been employed in the design of nanocarrier systems. Lee and collaborators reported a series of core-shell nanoparticles bearing dibenzo-crown ethers. These multifunctional systems were used for the delivery and imaging of doxorubicin in tumor cells, optimizing the drug release through different approaches.[14]

Beyond their use in drug delivery, crown ethers have attracted growing interest as ion transport carriers and synthetic ion channels, owing to their amphiphilic nature and strong cation-complexing capacity. Cellular membranes are composed of an external hydrophilic surface and an internal hydrophobic core. These structures serve as selective barriers that protect the intracellular environment against the external environment and regulate essential physiological functions such as osmotic pressure, homeostasis, metabolism, pH balance, and intercellular communication and signaling processes.[15,16] Crown ether-based systems that mimic these natural mechanisms have emerged as innovative tools to design artificial transmembrane channels.[17,18] Natural ion channels are dynamic systems that respond to external stimuli, such as pH changes, ligand binding, enzymatic activity, or voltage fluctuations, to regulate ion flow. Designing artificial channels with stimuli-responsive gating mechanisms is therefore essential. In this regard, crown ethers have demonstrated the ability to interact with lipid membranes, particularly monolayer lipid membranes (MLMs), forming membrane pores whose gating properties can be synthetically tuned to respond to voltage, pH, or light stimuli.[19] At the same time, supramolecular chemistry, which relies on noncovalent intramolecular interactions such as hydrogen bonding, van der Waals force, electrostatic interactions, and π-π stacking, provides the framework for assembling these functional systems.[20] Cazacu et al. exploited these principles to investigate cellular processes using crown ether-based membrane systems, underscoring their potential in membrane biophysics and bioengineering.[21] In recent years, a notable advancement in this field has been the development of hydraphiles, synthetic ion channels composed of three crown ether macrocycles linked by alkyl spacers of variable lengths.[22] Voyer and his research group designed hydraphile systems incorporating peptide α-helical moieties that adopted conformational alignments ideal for Na^+ transport, with precise spacing between crown ether units.[23-25] Alternatively, Zeng et

al. engineered polypeptide-based hydraphiles that self-assemble into K^+-selective channels,[26] while Zhu and collaborators developed light-responsive ion channels utilizing azobenzene moieties capable of reversible cis/trans isomerization to control ion transport.[27]

In addition to the earlier-mentioned applications, crown ethers can interact directly with cellular membranes, influencing permeability and thereby altering ionic balance and structural integrity. This property underlies their moderate cytotoxicity effects against tumor and bacterial cells.[22,28] Importantly, these systems offer new therapeutic perspectives for the treatment of channelopathies, including cardiac arrhythmias, cystic fibrosis, and neuropsychiatric disorders.[19] Detailed studies have revealed that the molecular length of hydrophilic crown ether derivatives strongly correlates with their ion transport efficiency across bilayer membranes. Specifically, compounds that were too short to extend over the bilayer exhibited no activity, while those significantly longer than the bilayer thickness showed only marginal activity. These findings suggest the existence of an optimal molecular length for effective antibacterial performance.[29] Moreover, crown ethers have been shown to enhance the efficacy of classical antibiotics such as erythromycin, kanamycin, and rifampicin, acting as a synergistic agent. This enhancement is likely attributable to their ability to disrupt membrane integrity, thereby facilitating the intracellular uptake of antibiotic compounds.[22] Notably, the cytotoxicity properties of dialkylated lariat ether derivatives have also been linked to membrane destabilization mechanisms.[30] In both 2011 and 2013, independent research groups led by Marjanovic and Smithrud, respectively, reported that a diverse array of crown ethers, aza crown ethers, and crown ether-host rotaxane (CEHR) derivatives exhibited antiproliferative activities against five distinct tumor-cell lines.[28,31] In particular, Smithrud et al. demonstrated that CEHRs induced apoptosis via necrotic pathways, attributed to elevated intracellular concentrations of cations such as Mg^{2+} and Ca^{2+}.[32]

Owing to their structural adaptability and unique ion-complexing capabilities, crown ethers remain essential molecular architectures in supramolecular chemistry and advanced biotechnology applications, offering promising prospects for future developments in drug design, delivery, and therapeutic innovation.

4.2 AIMS OF THE CHAPTER

Over recent years, the research activity of the group to which I belong has primarily focused on the design, synthesis, and application-oriented evaluation of a broad range of MBHA acetyl derivatives, as outlined in **Chapter 2**. Briefly, these MBHA compounds were found to react with various nucleophilic models, including *n*-butylamine, lysine derivatives, imidazole, and histidine derivatives, thereby enhancing their reactivity toward more complex biological systems.[33-39] Notably, MBHA derivative **38** exhibited intrinsic reactivity toward a single-chain Fv antibody bearing a hexahistidine tag, leading to the formation of multi-PEGylated species.[36,37] In addition, other MBHA derivatives **39-40** were found to selectively react with a lysine residue situated within a lipophilic pocket of a retinoic acid binding protein (Figure 1).[37,39] These findings, together with the results presented in the preceding chapters of this thesis, provided the rationale for further developing studies centered on MBHA derivatives.

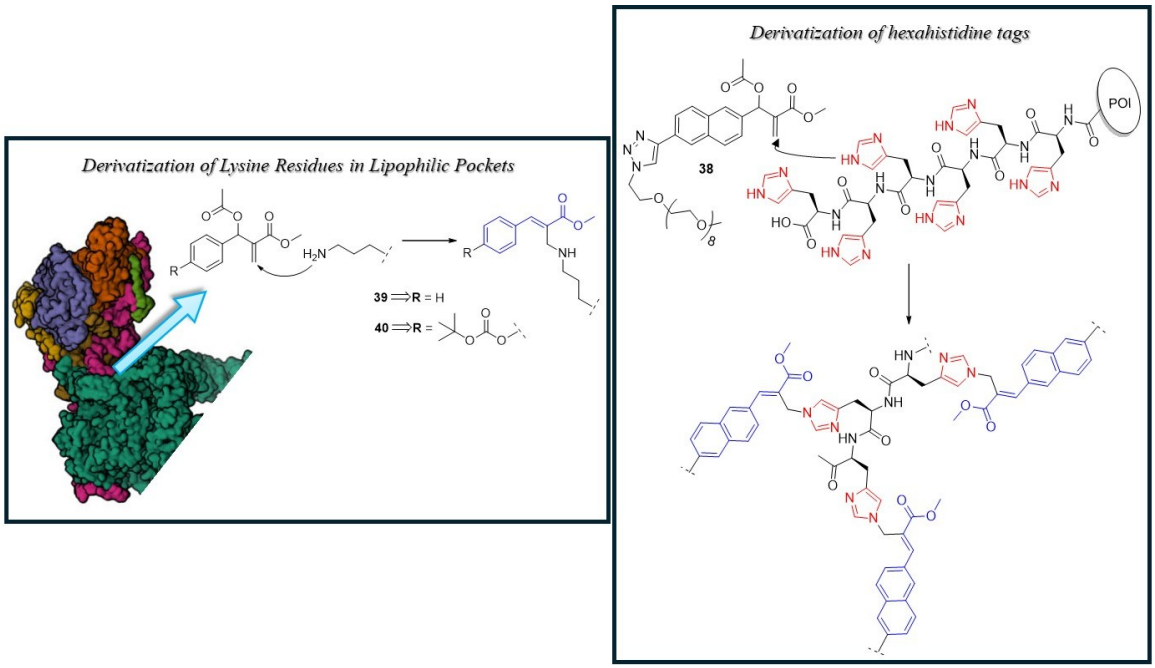

Figure 1. Application of MBHA acetyl derivatives in protein functionalization.[36-39]

In this Chapter, the use of MBHA derivatives is directed toward the formation of symmetric dimers, designed to incorporate two electrophilic functionalities capable of interacting with systems bearing reactive basic groups, such as primary amino groups or imidazole. This interaction can promote the formation of looped structures with amphiphilic character, endowing the resulting systems with intriguing properties reminiscent of both crown ethers and paracyclophane derivatives. Specifically, MBHA acetyl derivative **41** could be employed as a synthon in the convergent synthesis of

oligo(ethylene glycol)-tethered MBHA dimers **42a-d** via the well-established Copper(I)-Catalyzed Azide-Alkyne Cycloaddition (CuAAC) (Figure 2). The mild and chemoselective nature of CuAAC represents a key advantage in practice. In this context, this reaction has played a central role in the synthesis of numerous supramolecular architectures, as exemplified by Goldup's work on the synthesis of novel rotaxanes and catenanes.[40] To simulate such nucleophilic groups found in more complex biological systems, the reactivity of the OEG-tethered MBHA dimers **42a-d** could be investigated using *n*-butylamine as the simplest model, leading to the formation of macrocyclic crown ether-paracyclophane hybrid structures **43a-d** (Figure 2).

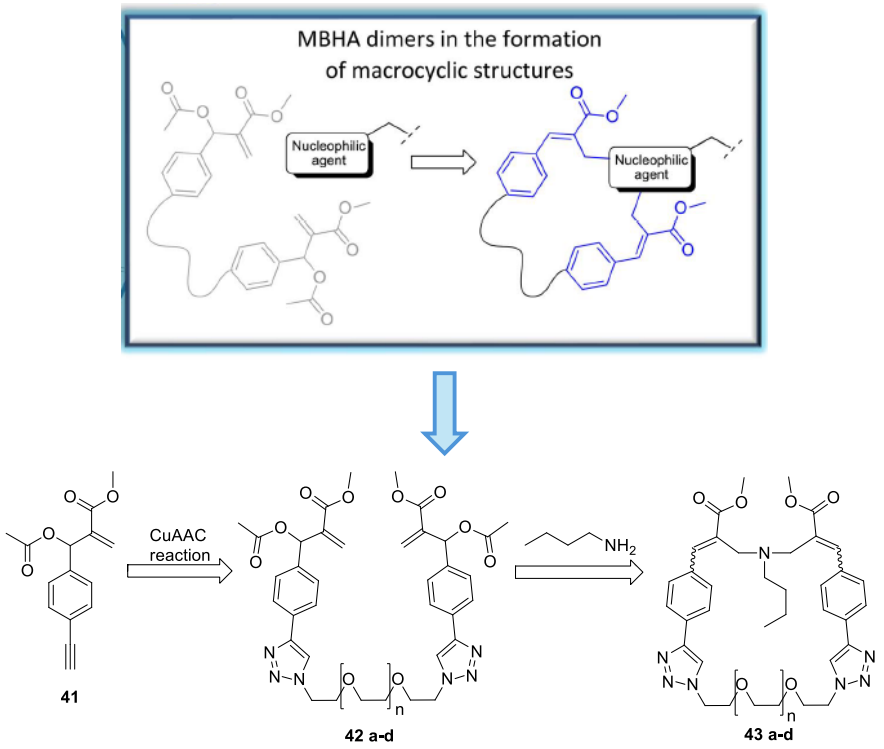

Figure 2. Design of MBHA dimers **42a-d**, developed for the formation of macrocyclic structures. Their reactivity was evaluated using *n*-butylamine as a model nucleophile. The compounds differ by the length of the OEG spacer: **42-43a** (n = 1), **42-43b** (n = 2), **42-43c** (n = 3), and **42-43d** (n = 4).

Furthermore, the presence of two cinnamic moieties in compounds **43a-d** prompted an investigation into their photochemical behavior, for which the simplest tri(ethylene glycol)-based compound **43a** was selected. Finally, considering the previously reported cytotoxic activities of crown ethers, the macrocyclic derivatives **43a-d** could be evaluated for their biological properties to identify their potential as anticancer agents.

4.3 SYNTHESIS OF MACROCYCLIC CROWN ETHER-PARACYCLOPHANE HYBRID COMPOUNDS FROM MBHA ACETYL DERIVATIVE SCAFFOLDS.

4.3.1 Synthesis procedures

The synthetic pathway was developed from two key synthons, each obtained through a series of straightforward synthetic steps (**Scheme 1**).

Scheme 1. Convergent synthetic procedure of dimeric MBHA derivatives 42a-d.

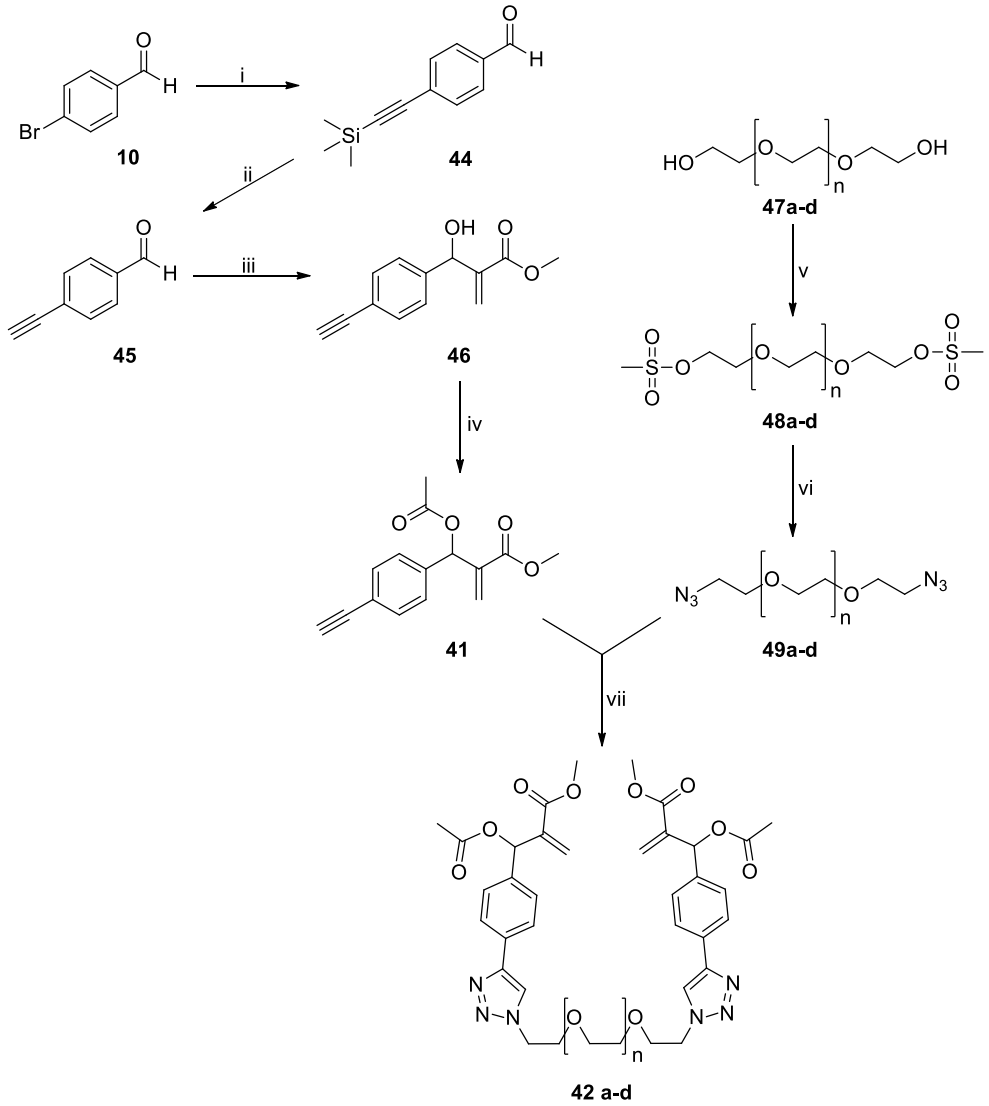

Scheme 1. (***i***) Trimethylsilylacetylene, $Pd(PPh_3)_2Cl_2$, CuI, TEA, dry THF; (***ii***) K_2CO_3, CH_3OH; (***iii***) DABCO, methyl acrylate, CH_3OH; (***iv***) CH_3COCl, TEA, CH_2Cl_2; (*v*) CH_3SOCl, TEA, CH_2Cl_2; (***vi***) NaN_3, DMF, CH_3CN; (***vii***) CuBr(I), DIPEA, CH_3CN. The compounds differ by the length of the OEG spacer: **42a** (n = 1), **42b** (n = 2), **42c** (n = 3), and **42d** (n = 4).

The commercially available 4-bromobenzaldehyde **10** underwent a Sonogashira coupling reaction with trimethylsilylacetylene in the presence of TEA as a base and a catalytic system composed of $Pd(PPh_3)_2Cl_2$ and CuI, yielding compound **44**. This intermediate was subsequently desilylated using potassium carbonate to afford the corresponding terminal alkyne-aldehyde **45**. Next, an MBH reaction was performed between aldehyde **45** and methyl acrylate in the presence of DABCO and catalytic amounts of methanol, resulting in the formation of alcohol derivative **46**. This compound was then acetylated using acetyl chloride in the presence of TEA to obtain the corresponding MBHA acetyl derivative **41**. In parallel, the diazide synthons **49a-d** were synthesized starting from the commercially available OEG **47a-d**. These were first activated via reaction with mesyl chloride to yield the corresponding mesylated intermediates **48a-d**, which were then converted into diazide derivatives **49a-d** by means of nucleophilic substitution with sodium azide in a DMF-ACN mixture. Finally, the MBHA acetyl derivative **41** was subjected to a CuAAC reaction with the relative diazide derivatives **49a-d** in dry acetonitrile, using CuBr(I) as a catalyst and DIPEA as a base, to afford the corresponding symmetric dimers **42a-d**. These dimeric MBHA derivatives **42a-d** were subsequently reacted with *n*-butylamine in refluxing chloroform, leading to the formation of macrocyclic crown ether-paracyclophane hybrid structures **43a-d** (**Scheme 2**) as mixtures of diastereomers.

Scheme 2. Reaction between MBHA dimers Xa-d with *n*-butylamine.

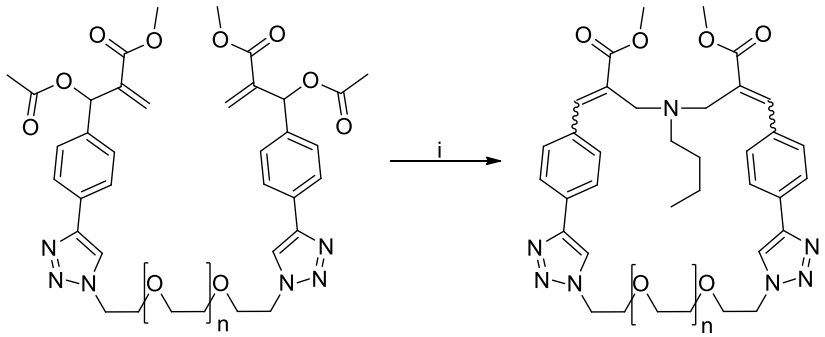

Scheme 2. (i) *n*-Butylamine, CH_3Cl. The compounds differ by the length of the OEG spacer: **42-43a** (n = 1), **42-43b** (n = 2), **42-43c** (n = 3), and **42-43d** (n = 4).

Among the diastereomeric pairs obtained, only the mixture of macrocyclic compound **43a** proved suitable for purification by flash chromatography. This process yielded **(*E*,*Z*)-43a**

as the least polar fraction with 17% yield, and **(*E*,*E*)-43a** as the most polar fraction with 35% yield (Figure 3). The symmetric isomer **(*E*,*E*)-43a** was successfully crystallized from ethyl acetate, affording crystals suitable for X-ray diffraction analysis. The resulting structural data confirmed the geometry of the compound and enabled its complete characterization by means of NMR spectroscopy.

In contrast, the separation of the diastereomeric mixtures of macrocycle derivatives **43b-d** was considerably more challenging due to their increased polarity. Nevertheless, using the ^{1}H NMR spectra of **(*E*,*Z*)-43a** and **(*E*,*E*)-43a** as reference standards, it was possible to assign the diastereomeric ratio of (*E*,*Z*) and (*E*,*E*) forms in derivatives **43b-d** as approximately 2:1.

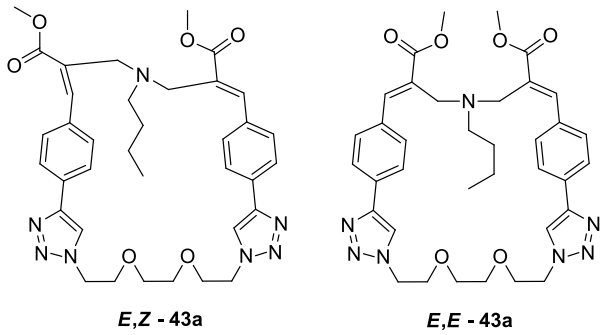

Figure 3. Structures of compounds **(*E*,*Z*)-43a** and **(*E*,*E*)-43a**.

4.3.2 Photophysical and photochemical studies

The presence of two cinnamic moieties in the structure of these macrocycle compounds, structurally related to the diadduct derivatives **17**, **19**, and **34** previously seen in **Chapter 2** and **Chapter 3**, prompted an investigation into their photophysical and photochemical properties. UV-Vis absorption spectra of **(*E*,*Z*)-43a** and **(*E*,*E*)-43a** revealed low-energy absorption maxima, approximately 300 nm for the symmetric derivative **(*E*,*E*)-43a** and a slightly blue-shifted maximum around 290 nm for the **(*E*,*Z*)-43a** isomer. The presence of two photoisomerizable double bonds suggested a propensity for both photoisomerization and [2+2] photocycloaddition processes (**Scheme 3**).

Scheme 3. Photochemical behavior of **(*E*,*E*)-43a** under 305 nm irradiation.

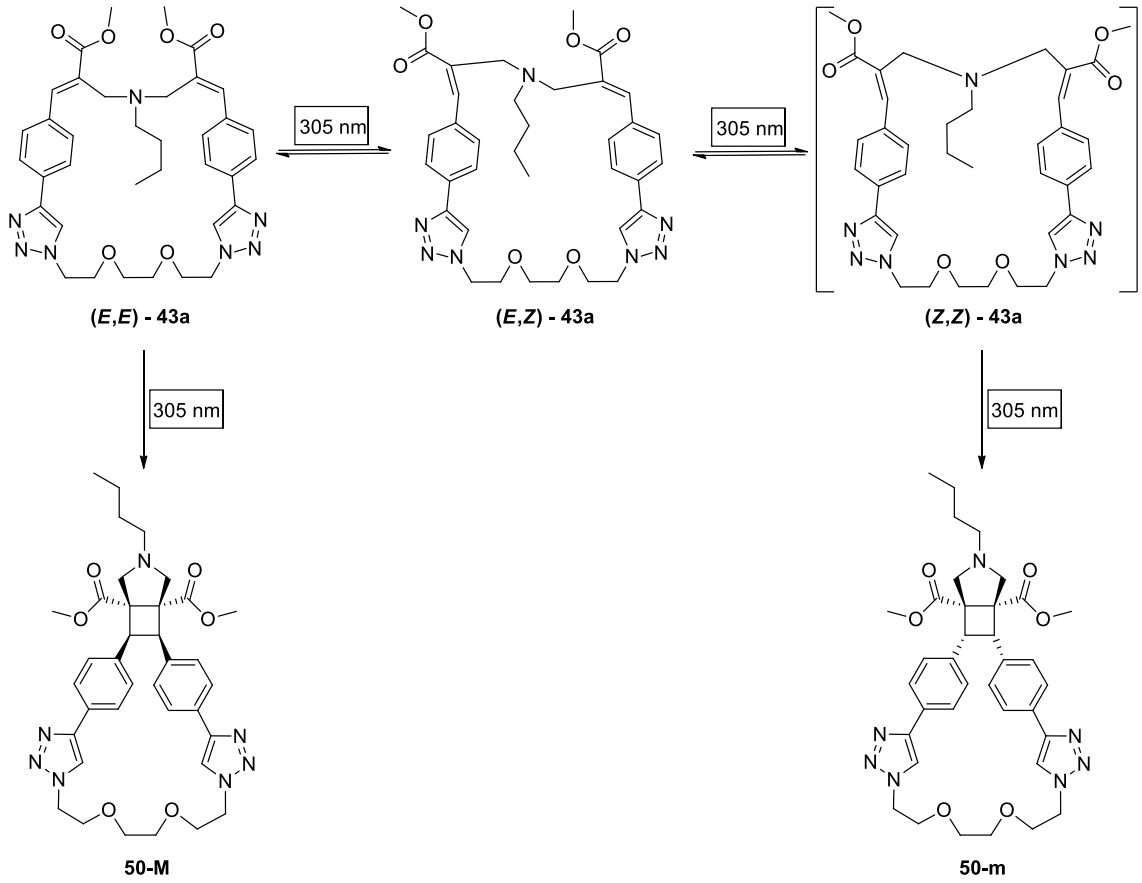

To explore these behaviors, a series of photochemical studies was conducted. The **(*E*,*E*)-43a** isomer was selected due to its symmetric structure, which provided a simplified ^{1}H NMR spectrum and good solubility in deuterated solvents such as methanol and DMSO. In a 5 mm NMR Pyrex tube, both solutions were irradiated with monochromatic light centered at 305 nm, yielding distinct outcomes. Irradiation in methanol-d_4 resulted in the gradual formation of a white precipitate. Nevertheless, ^{1}H NMR spectra, recorded at regular time intervals (Figure 4), showed the progressive conversion of **(*E*,*E*)-43a** in solution into the corresponding symmetric cyclobutane derivative **X**. The precipitate was separated from the reaction mixture and analyzed in DMSO-d_6, identifying the **(*E*,*Z*)-43a** isomer.

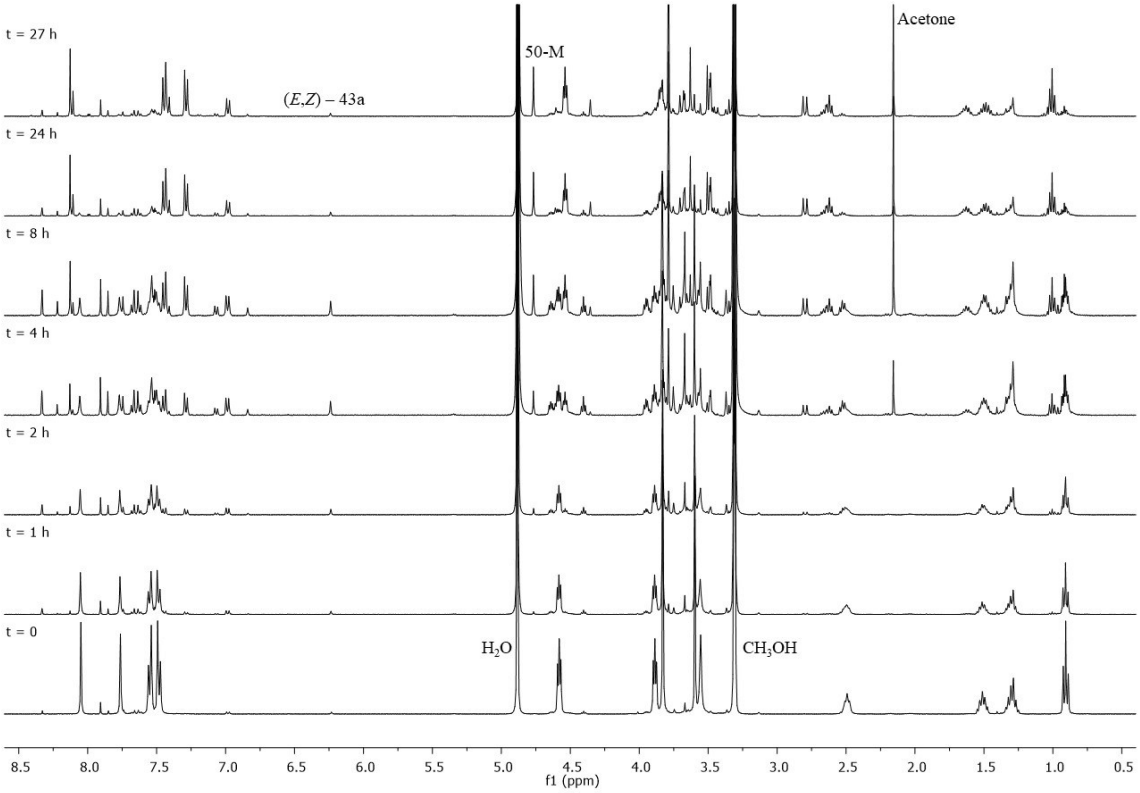

Figure 4. Comparison of ^{1}H NMR spectra (400 MHz) obtained by irradiating compound **(*E*,*E*)-43a** (10 mg, 0.015 mmol) in CD_3OD (1.5 mL) with a monochromatic light centered at 305 nm at room temperature. The monochromatic wavelength was selected using a tunable light source Zolix (TLS2-X300PU-G, 300W UV Xenon Light Source with monochromator Omni-λ2047i). ^{1}H NMR spectra were registered at regular time intervals (0, 1, 2, 4, 8, 24, and 27 hours).

To prevent precipitation of asymmetric isomer **(*E*,*Z*)-43a**, DMSO-d_6 was selected as a more suitable solvent. Under these conditions, similar photochemical behavior was observed, with the absence of precipitate formation being the only notable difference. Spectral analysis indicated the formation of two products with symmetric geometry in an approximate 2:1 ratio (Figure 5).

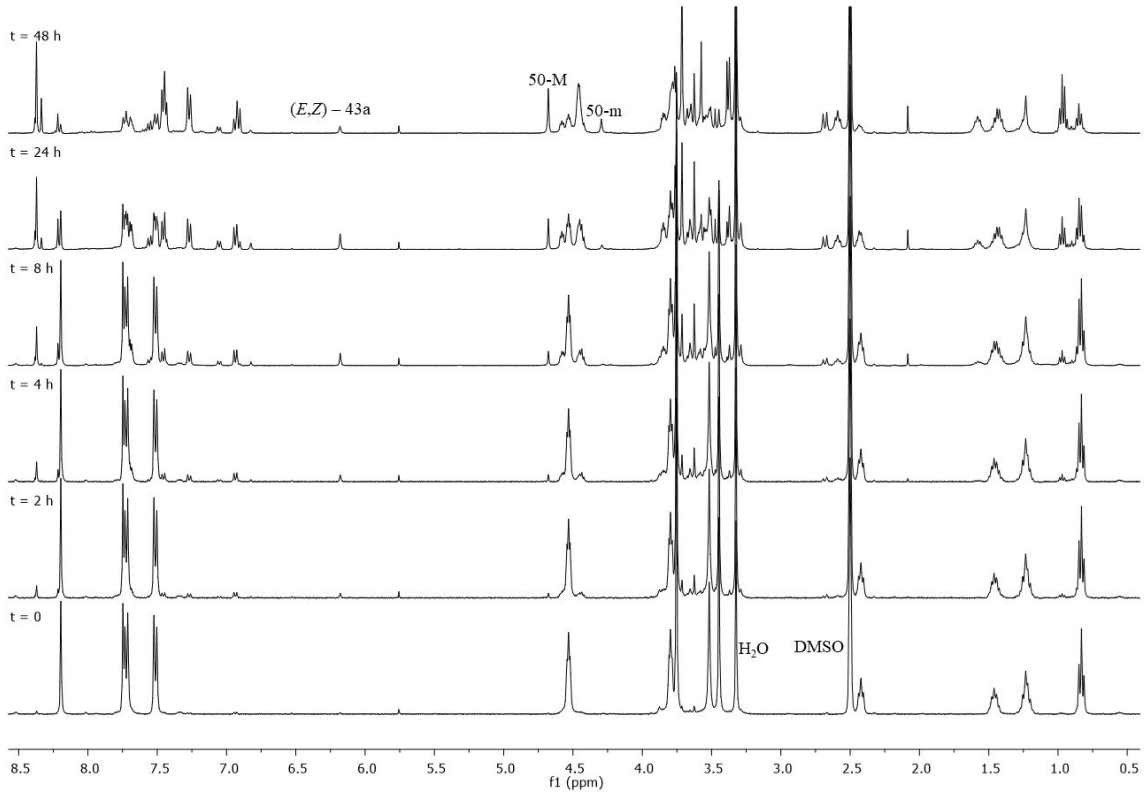

Figure 5. Comparison of ^{1}H NMR spectra (400 MHz) obtained by irradiating compound **(*E*,*E*)-43a** (10 mg, 0.015 mmol) in DMSO-d_6 (1.0 mL) with a monochromatic light centered at 305 nm at room temperature. The monochromatic wavelength was selected using a tunable light source Zolix (TLS2-X300PU-G, 300W UV Xenon Light Source with monochromator Omni-λ2047i). ^{1}H NMR spectra were registered at regular time intervals (0, 2, 4, 8, 24, and 48 hours).

Particularly, hypothesizing that diastereomer **(*E*,*E*)-43a** could undergo [2+2] photocycloaddition reaction to afford compound **50-M**, at the same time, the photoisomerization process yielded asymmetric diastereomer **(*E*,*Z*)-43a**. The latter, unable to participate in [2+2] photocycloaddition reaction due to geometric constraints, may undergo a second photoisomerization to regenerate **(*E*,*E*)-43a** or form **(*Z*,*Z*)-43a** isomer. Consequently, the minor formation of compound **50-m** was attributed to the [2+2] photocycloaddition of the **(*Z*,*Z*)-43a** diastereomer (see **Scheme 3**).

Dimethyl (1^{4}*Z*,5^{4}*Z*)-3^{3}-butyl-1^{1}*H*,5^{1}*H*-8,11-dioxa-3^{3}-aza-1,5(4,1)-ditriazola-3(6,7) bicyclo[3.2.0]eptane-2,4(1,4)-dibenzenecyclotridecaphane-3^{1},3^{5}-dicarboxylate (50-M)

The irradiated solution in DMSO-d_6 of **(*E*,*E*)-Xa** was concentrated, and the resulting residue was purified by flash chromatography using ethyl acetate-methanol (95:5) as the eluent to afford compound **50-M** (4.0 mg, yield 40%) as an off-white solid.

^{1}H NMR (600 MHz, DMSO-d_6): 0.97 (t, J = 7.4 Hz, 3H), 1.39-1.48 (m, 2H), 1.54-1.61 (m, 2H), 2.59 (t, J = 7.3 Hz, 2H), 2.68 (d, J = 10.7 Hz, 2H), 3.35-3.40 (m, 4H), 3.66 (d, J = 10.7 Hz, 2H), 3.71 (s, 6H), 3.73-3.83 (m, 4H), 4.43-4.48 (m, 4H), 4.68 (s, 2H), 7.27 (d, J = 8.4 Hz, 4H), 7.45 (d, J = 8.4 Hz, 4H), 8.37 (s, 2H).
^{13}C NMR (150 MHz, DMSO-d_6): 173.4, 146.0, 136.2, 130.9, 128.4, 123.5, 121.7, 69.9, 69.1, 59.0, 57.9, 54.9, 52.3, 50.0, 45.7, 29.9, 20.4, 13.9.

4.3.3 Cytotoxicity activity evaluation

The cytotoxic activities of compounds **(*E*,*Z*)-43a**, **(*E*,*E*)-43a**, and **43b-d** were evaluated against non-confluent, adherent human breast cancer MDA-MB-231 and human melanoma A375 cells using Doxorubicin as the positive control. The outcomes were summarized in **Table 1**.

Table 1. IC_{50} value (μM) of the tested samples towards MDA-MB-231 and A375 cells.

Compounds	**IC_{50} (μM)**	
	MDA-MB-231 Cells	**A375 Cells**
Doxorubicin	1.5	0.5
(*E*,*Z*)-43a	0.8	0.8
(*E*,*E*)-43a	1.0	0.8
43b	1.0	0.8
43c	0.8	0.8
43d	1.0	1.0

Overall, the slight differences in cytotoxic potency observed among macrocyclic derivatives **43a-d** suggested that the underlying cytotoxic mechanism may be attributed to a structurally non-specific interaction between the macrocyclic compounds and key cellular components, such as the cell membrane. This assumption appeared to be in full agreement with the current literature.[28,30]

The data collected allowed us to publish two journal articles in RSC Advances and Pharmaceuticals. For more details, see the Research Article in **Paragraph 4.5** and the Research Article in **Paragraph 4.6**.

4.4 REFERENCES

1. Pedersen, C. J. The Discovery of Crown Ethers (Noble Lecture). *Angew. Chem., Int. Ed. Engl.*, **1988**, *27*, 1021-1027.
2. Pedersen, C. J. Cyclic polyethers and their complexes with metal salts. *J. Am. Chem. Soc.*, **1967**, *89*, 26, 7017-7036.
3. Krakowiak, K. E.; Bradshaw, J. S.; Zamecka-Krakowiak, D. J. Synthesis of aza-crown ethers. *Chem. Rev.*, **1989**, *89*, 4, 929-972.
4. Izatt, R. M.; Bradshaw, J. S.; Nielsen, A. A.; Lamb, J. D.; Christensen, J. J.; Sen, D. Thermodynamic and kinetic data for cation-macrocycle interaction. *Chem. Rev.*, **1985**, *85*, 4, 271-339.
5. Ikeda, I.; Emura, H.; Yamamura, S.; Okahara, M. Contribution of lipophilicity to the performance of crown ethers. Effect of bulk and shape of the lipophylic substituents. *J. Org. Chem.*, **1982**, *47*, 26, 5150-5153.
6. Chen, L.; Zhang, H. Y.; Liu, Y. High Affinity Crown Ether Complexes in Water: Thermodynamic Analysis, Evidence of Crystallography and Binding of NAD^+. *J. Org. Chem.*, **2012**, *77*, 21, 9766-9773.
7. Chehardoli, G.; Bahmani, A. The role of crown ethers in drug delivery. *SupMOL CHEM*, **2019**, *31*, 221-238.
8. Baillie, A. J.; Coombs, G. H.; Dolan, T. F.; Laurie, J. Non-ionic surfactant vesicles, niosomes, as a delivery system for the anti-leishmanial drug, sodium stibogluconate. *J. Pharm. Pharmacol.*, **1986**, *38*, 502-505.
9. Uchegbu, I. F.; Florence, A. T. Non-ionic surfactant vesicles (niosomes): Physical and pharmaceutical chemistry. *Adv. Colloid Interface Sci.*, **1995**, *58*, 1-55.
10. Echegoyen, L. E.; Hernandex, J. C.; Kaifer, A. E.; Gokel, G. W.; Echegoyen, L. Aggregation of steroidal lariat ethers: the first example of nonionic liposomes (niosomes) formed from neutral crown ether compounds. *J. Chem. Soc., Chem. Commun.*, **1988**, 836-837.
11. Darwish, I. A.; Uchegbu, I. F. The evaluation of crown ether based niosomes as cation containing and cation sensitive drug delivery systems. *Int. J. Pharm.*, **1997**, *159*, 207-213.
12. Muzzalupo, R.; Nicoletta, F. P.; Trombino, S.; Cassano, R.; Iemma, F.; Picci, N. A new crown ether as vesicular carrier for 5-fluoruracil: Synthesis, characterization and drug delivery evaluation. *Colloids Surf. B Biointerfaces*, **2007**, *58*, 197-202.

13. Borrel, M. N.; Fiallo, M.; Veress, I.; Suillerot, A. G. The effect of crown ethers, tetraalkylammonium salts, and polyoxyethylene amphiphiles on pirarubicin incorporation in K562 resistant cells. *Biochem. Pharmacol.*, **1995**, *50*, 2069-2076.
14. Lee, S. F.; Zhu, X. M.; Wang, Y. X. J.; Xuan, S. H.; You, Q.; Chan, W. H.; Wong, C. H.; Yu, J. C.; Cheng, C. H. K.; Leung, K. C. F. Ultrasound, pH, and Magnetically Responsive Crown-Ether-Coated Core/Shell Nanoparticles as Drug Encapsulation and Release Systems. *ACS Appl. Mater. Interfaces*, **2013**, *5*, 1566-1574.
15. Flood, E.; Boiteux, C.; Lev, B.; Vorobyov, I.; Allen, T. W. Atomistic Simulations of Membrane Ion Channel Conduction, Gating, and Modulation. *Chem. Rev.*, **2019**, *119*, 13, 7737-7832.
16. Cho, W.; Stahelin, R. V. Membrane-Protein Interactions in Cell Signaling and Membrane Trafficking. *Annu. Rev. Biophys.*, **2005**, *34*, 119-151.
17. Gokel, G. W.; Carasel, I. A. Biologically active, synthetic ion transporters. *Chem. Soc. Rev.*, **2007**, *36*, 378-389.
18. Tsukube, H. Highly selective transport of biogenetic amines and drugs by using functionalized “acyclic crown ether”. *Tetrahedron Lett.*, **1982**, *23*, 2109-2112.
19. He, L.; Zhang, T.; Zhu, C.; Yan, T.; Liu, J. Crown Ether-Based Ion Transporters in Bilayer Membranes. *Chem. Eur. J.*, **2023**, *29*, e202300044.
20. Dergham, M.; Lin, S.; Geng, J. Supramolecular Self-Assembly in Living Cells. *Angew. Chem.*, **2022**, *134*, e202114267.
21. Cazacu, A.; Tong, C.; van der Lee, A.; Fyles, T. M.; Barboiu, M. Columnar Self-Assembled Ureido Crown Ethers: An Example of Ion-Channel Organization in Lipid Bilayers. *J. Am. Chem. Soc.*, **2006**, *128*, 29, 9541-9548.
22. Negin, S.; Smith, B. A.; Unger, A.; Leevy, W. M.; Gokel, G. W. Hydraphiles: A Rigorously Studied Class of Synthetic Channel Compounds with *In Vivo* Activity. *Int. J. Biomedical Imaging*, **2013**, *2013*, 803579.
23. Otis, F.; Auger, M.; Voyer, N. Exploiting Peptide Nanostructures To Construct Functional Artificial Ion Channels. *Acc. Chem. Res.*, **2013**, *46*, 12, 2934-2943.
24. Meillon, J. C.; Voyer, N. A Synthetic Transmembrane Channel Active in Lipid Bilayers. *Angew. Chem., Int. Ed. Engl.*, **1997**, *36*, 967-969.
25. Otis, F.; Racine-Berthiaume, C.; Voyer, N. How Far Can a Sodium ion Travel within a Lipid Bilayer?. *J. Am. Chem. Soc.*, **2011**, *133*, 17, 6481-6483.

26. Ren, C.; Shen, J.; Zeng, H. Combinatorial Evolution of Fast-Conducting Highly Selective K^+-Channels via Modularly Tunable Directional Assembly of Crown Ethers. *J. Am. Chem. Soc.*, **2017**, *139*, 36, 12338-12341.
27. Liu, T.; Bao, C.; Wang, H.; Lin, Y.; Jia, H.; Zhu, L. Light-controlled ion channels formed by amphiphilic small molecules regulate ion conduction via cis-trans photoisomerization. *Chem. Commun.*, **2013**, *49*, 10311-10313.
28. Marjanovic, M.; Kralj, M.; Supek, F.; Frkanec, L.; Piantanida, I.; Smuc, T.; Tusek-Bozic, L. Antitumor Potential of Crown Ethers: Structure-Activity Relationships, Cell Cycle Disturbances, and Cell Death Studies of a Series of Ionophores. *J. Med. Chem.*, **2007**, *50*, 5, 1007-1018.
29. Weber, M.; Schlesinger, P. H.; Gokel, G. W. Dynamic Assessment of Bilayer Thickness by Varying Phospholipid and Hydraphile Synthetic Channel Chain Lenghts. *J. Am. Chem. Soc.*, **2005**, *127*, 2, 636-642.
30. Carrasquel-Ursulaez, W.; Reeves, R. D.; Dehghany, M.; Jones, C.; Schomaker, J. M.; Chanda, B. Re-evaluation of the mechanism of cytotoxicity of dialkylated lariat ether compounds. *RSC adv.*, **2020**, *10*, 40391-40394.
31. Smithrud, D. B.; Wang, X.; Tarapore, P.; Ho, S. Crown Ether Host-Rotaxanes as Cytotoxic Agents. *ACS Med. Chem. Lett.*, **2013**, *4*, 1, 27-31.
32. Wang, X.; Zhu, J.; Smithrud, D. B. Synthesis and Investigation of Host-[2]Rotaxanes That Bind Metal Cations. *J. Org. Chem.*, **2010**, *75*, 10, 3358-3370.
33. Razzano, V.; Paolino, M.; Reale, A.; Giuliani, G.; Artusi, R.; Caselli, G.; Visintin, M.; Makovec, F.; Donati, A.; Villafiorita-Monteleone, F.; Botta, C.; Cappelli, A. Development of Imidazole-Reactive Molecules Leading to a New Aggregation-Induced Emission Fluorophore Based on the Cinnamic Scaffold. *ACS Omega*, **2017**, *2*, 9, 5453-5459.
34. Razzano, V.; Paolino, M.; Reale, A.; Giuliani, G.; Donati, A.; Giorgi, G.; Artusi, R.; Caselli, G.; Visintin, M.; Makovec, F.; Battiato, S.; Samperi, F.; Villafiorita-Monteleone, F.; Botta, C.; Cappelli, A. Ploy-histidine grafting leading to fishbone-like architectures. *RSC Adv.*, **2018**, *8*, 8638-8656.
35. Paolino, M.; Visintin, M.; Margotti, E.; Visintini, M.; Salvini, L.; Reale, A.; Razzano, V.; Giuliani, G.; Caselli, G.; Tavanti, F.; Menziani, M. C.; Cappelli, A. Functionalization of protein hexahistidine tags by functional nanoreactors. *New J. Chem.*, **2019**, *43*, 17946-17953.

36. Paolino, M.; Reale, A.; Razzano, V.; Giuliani, G.; Donati, A.; Bonechi, C.; Caselli, G.; Visintin, M.; Makovec, F.; Scialabba, C.; Licciardi, M.; Paccagnini, E.; Gentile, M.; Salvini, L.; Tavanti, F.; Menziani, M. C.; Cappelli, A. Nanoreactors for the multi-functionalization of poly-histidine fragments. *New J. Chem.*, **2019**, *43*, 6834-6837.
37. Tassone, G.; Paolino, M.; Pozzi, C.; Reale, A.; Salvini, L.; Giorgi, G.; Orlandini, M.; Galvagni, F.; Mangani, S.; Yang, X.; Carlotti, B.; Ortica, F.; Latterini, L.; Olivucci, M.; Cappelli, A. Xanthopsin-Like Systems via Site-Specific Click-Functionalization of a Retinoic Acid Binding Protein. *ChemBioChem*, **2021**, *23*, e202100449.
38. Lami, M.; Barneschi, L.; Saletti, M.; Olivucci, M.; Cappelli, A.; Paolino, M. Preparation of Light-responsive Unnatural RNA Bases via a Chromogenic Morita-Baylis-Hillman Adduct Path. *ChemPhotoChem*, **2024**, *8*, e202400093.
39. Paolino, M.; Tassone, G.; Governa, P.; Saletti, M.; Lami, M.; Carletti, R.; Sacchetta, F.; Pozzi, C.; Orlandini, M.; Manetti, F.; Olivucci, M.; Cappelli, A. Morita–Baylis–Hillman Adduct Chemistry as a Tool for the Design of Lysine-Targeted Covalent Ligands. *ACS Med. Chem. Lett.*, **2025**, *16*, 3, 397-405.
40. Saady, A.; Goldup, S. M. Triazole formation and the click concept in the synthesis of interlocked molecules. *Perspective*, **2023**, *9*, 2110-2127.

4.5 RESEARCH ARTICLE: "A tri(ethylene glycol)-tethered Morita-Baylis-Hillman dimer in the formation of macrocyclic crown ether-paracyclophane hybrid structures"

Authors: Mario Saletti, **Jacopo Venditti**, Marco Paolino, Arianna Zacchei, Germano Giuliani, Gianluca Giorgi, Claudia Bonechi, Alessandro Donati, Andrea Cappelli

Publication: RSC Advances

Publisher: Royal Society of Chemistry

DOI: doi.org/10.1039/D3RA06792K

Supporting Information: doi.org/10.1039/D3RA06792K

Contribution: Ph.D. candidate performed the synthesis of the compound, followed by the characterization studies by means of ^{1}H NMR spectroscopy, photophysical, and photochemical properties.

RSC Advances

PAPER

View Article Online
View Journal | View Issue

Cite this: *RSC Adv.*, 2023, **13**, 35773

A tri(ethylene glycol)-tethered Morita–Baylis–Hillman dimer in the formation of macrocyclic crown ether-paracyclophane hybrid structures†

Mario Saletti, Jacopo Venditti, Marco Paolino, Arianna Zacchei, Germano Giuliani, Gianluca Giorgi, Claudia Bonechi, Alessandro Donati and Andrea Cappelli *

Received 6th October 2023
Accepted 27th November 2023

DOI: 10.1039/d3ra06792k

rsc.li/rsc-advances

A Morita–Baylis–Hillman acetate was dimerized by a click-chemistry Copper(I)-Catalysed Azide–Alkyne Cycloaddition (CuAAC) reaction employing a tri(ethylene glycol) diazide derivative to obtain a dimeric MBHA derivative. The reaction of this dimeric MBHA derivative with *n*-butylamine afforded a photoisomerizable macrocyclic crown ether-paracyclophane hybrid architecture that is potentially useful in a large variety of applications as well as those already well-known for crown ethers.

Introduction

Crown ethers are macrocyclic compounds of poly(ethylene glycol) (PEG) that can exist in two forms: aliphatic ones, formed from four to ten ethylene oxide units, and the aromatic ones, in which we can find one or two benzene rings (benzocrown and dibenzocrown ethers respectively). Their name comes from the studies conducted by Charles J. Pedersen who in 1967 observed the aspect of host–guest complexes formed with metal cations. This ability is due to the conformational and chemical features of the system, which allow the creation of an electron rich cavity whose dimensions are crucial to confer a coordination selectivity of alkali, alkaline earth ions and, as recently demonstrated, non-metallic species. For these reasons, crown ethers have many applications: as phase transfer catalysts, for creating chiral stationary phases and in the construction of mechanically interlocked structures such as rotaxanes, pseudorotaxanes and catenanes. This has led to their use in the development of synthetic molecular devices activated by light, pH and redox. They also have applications in the biological field as parts of artificial intramembrane canals and to allow the translocation of ionic species.[1–3]

The ability to control the functions of crown ethers by an on–off light switch was investigated by Shinkai and coworkers in 1987. They synthesized photoresponsive crown ethers having an intra-annular azo substituent that could interact with a metal only following photoisomerization of the intra-annular azo substituent from *trans* to *cis*.[4] Also Vicens and coworkers explained an interesting system where the binding activity of the calix[4]crown ether is photosensitive: Na^+ is favorably extracted by the *trans*-isomer of the structure, while the *cis* form extracts better the Rb^+ and Cs^+.[5]

In the field of the synthesis and study of mechanically interlocked molecules (MIMs), the concept of "click" chemistry is very relevant. In 2001 Sharpless, Finn, and Kolb, proposed that chemists could generate substances by linking small modular units in reactions with high yield, high chemoselectivity and stereospecificity, high thermodynamic driving force that could lead to the formation of irreversible bonds and ultimately under mild reaction conditions with few or no by-products. For these reasons, the best-known click reaction, the Copper(I)-Catalised Azide–Alkyne Cycloaddition (CuAAC) was quickly embraced by the MIM community as soon as it appeared. Many syntheses of MIMs are based on click-type reactions, such as the formation of amide, ureidic, carbamate, or S_N2-type bonds and cycloaddition reactions to stop the interlocked structure.

The mild and chemoselective nature of the CuAAC reaction was the first quality to be highlighted in practice: Stoddart described the synthesis of rotaxanes and catenanes using the CuAAC reaction together with their iconic "blue box" viologen macrocycle.[6]

The Morita–Baylis–Hillman (MBH) reaction is very important in the field of organic chemistry because it afford to create new C–C bonds. In particular, MBH Adducts (MBHA) arise from a reaction between a carbon electrophile (for example an aldehyde) and an activated alkene, catalysed by a tertiary amine or phosphine, to provide an allylic alcohol.[7] This can be processed into a great leaving group by acetylation. In case an activated imine reacts instead of the aldehyde, it is called aza-Morita–Baylis–Hillman reaction. These reactions allow to obtain versatile and chiral products using chiral substrates or organic

Dipartimento di Biotecnologie, Chimica e Farmacia, Università di Siena, Via A. Moro 2, 53100 Siena, Italy. E-mail: andrea.cappelli@unisi.it; Tel: +39 0577 232416

† Electronic supplementary information (ESI) available: Experimental details for the synthesis and the characterization of compounds **1**, **2a,b** and their intermediates. CCDC 2286050. For ESI and crystallographic data in CIF or other electronic format see DOI: https://doi.org/10.1039/d3ra06792k

chiral catalysts; this makes them an excellent example of organocatalysis for green chemistry.[8]

Some years ago, we have developed MBHA derivatives capable of reacting with imidazole to afford cinnamic derivatives showing fluorogenic properties.[9] Moreover, the structures of these compounds were subsequently elaborated to obtain a number of MBHA derivatives potentially useful in a wide range of different applications in protein functionalization (Fig. 1).[10–14]

In the present work, the structure of our MBHA derivatives was manipulated in the aim of obtaining a tri(ethylene glycol)-tethered MBHA dimer **1** (Fig. 2) potentially useful in the functionalization of materials containing reactive basic (*i.e.* amino or imidazole) groups with the formation of amphiphilic loops potentially provided with a wide range of intriguing properties such as those shown by both crown ethers and paracyclophane derivatives. We found that the tri(ethylene glycol)-tethered MBHA dimer **1** was capable of reacting with primary amines (*i.e.* *n*-butylamine) leading to the formation of macrocyclic crown ether-paracyclophane hybrid structures **2** that could be modulated by light.

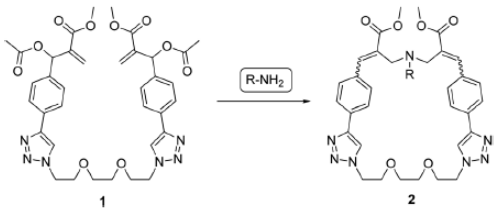

Fig. 2 Reaction of MBHA dimer **1** with primary amines leading to macrocyclic crown ether-paracyclophane hybrid structures **2**.

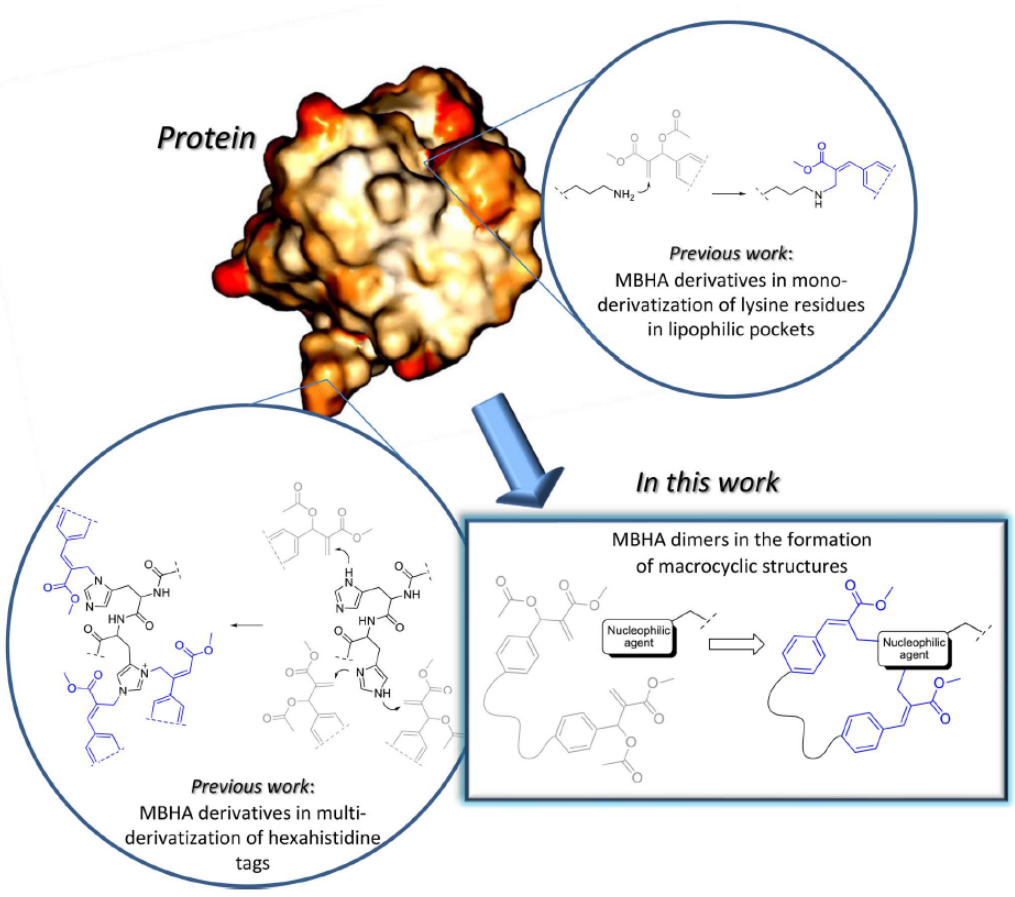

Fig. 1 Applications of MBHA derivatives to protein functionalization.

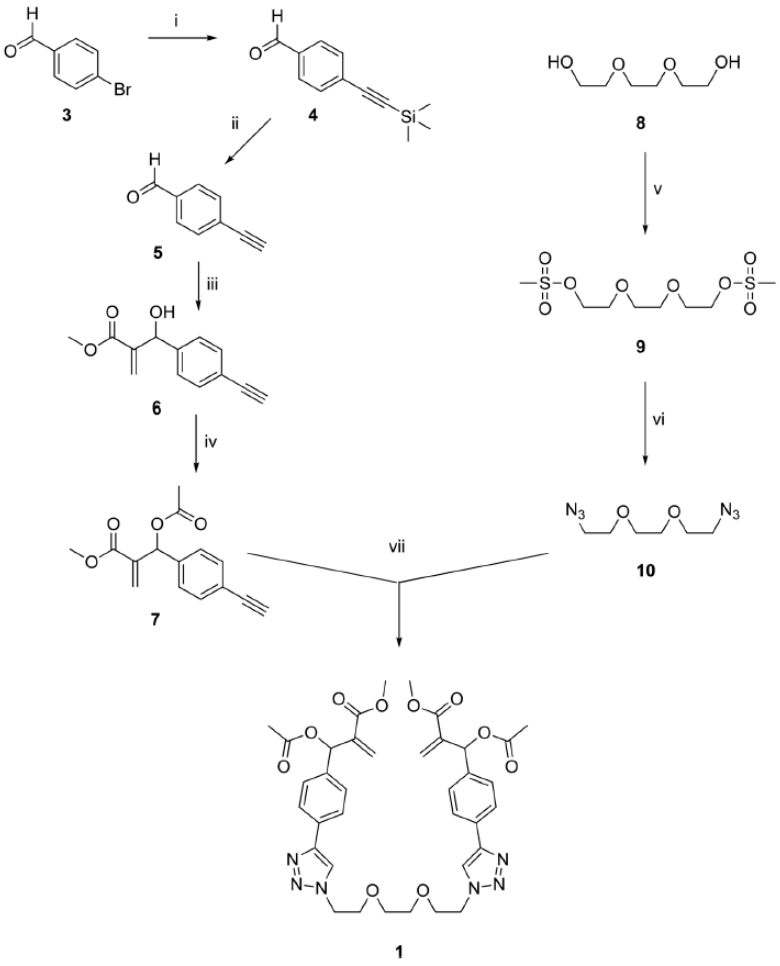

Scheme 1 Convergent procedure for the preparation of dimeric MBHA derivative **1**. Reagents: (i) trimethylsilylacetylene, $Pd(PPh_3)_2Cl_2$, CuI, TEA, THF; (ii) K_2CO_3, MeOH; (iii) DABCO, methyl acrylate, MeOH; (iv) CH_3COCl, TEA, CH_2Cl_2; (v) CH_3SO_2Cl, TEA, CH_2Cl_2; (vi) NaN_3, DMF, CH_3CN; (vii) CuBr(I), DIPEA, CH_3CN.

Results and discussion

Synthesis and structural characterization

The synthesis of dimeric MBHA derivative **1** was carried out by the convergent procedure shown in Scheme 1.

The MBHA component **7** of the convergent synthesis was prepared from 4-bromobenzaldehyde **3**, which was used in a Sonogashira reaction with trimethylsilylacetylene in the presence of $Pd(PPh_3)_2Cl_2$, CuI, and TEA in THF as the solvent to obtain trimethylsilyl derivative **4**,[15] which was promptly desilylated with potassium carbonate in methanol. The resulting aldehyde **5** (ref. 16) was used in a Morita–Baylis–Hillman reaction with methyl acrylate in the presence of DABCO and methanol to afford MBHA derivative **6**, which was promptly acetylated with acetyl chloride in the presence of triethylamine as the base in dry DCM, with a satisfactory yield of **7** (*i.e.* 82%). The diazide component **10** of the convergent synthesis was prepared starting from the commercially available tri(ethylene glycol) **8**, which was activated by reaction with mesyl chloride to the corresponding mesylate **9** and then made to react with sodium azide in DMF-acetonitrile. The final coupling step was performed in the conditions of a click chemistry Copper(I)-Catalised Azide–Alkyne Cycloaddition (CuAAC) reaction in acetonitrile in the presence of CuBr(I) as the catalyst and DIPEA as the base to obtain the tri(ethylene glycol)-tethered MBHA dimer **1**.

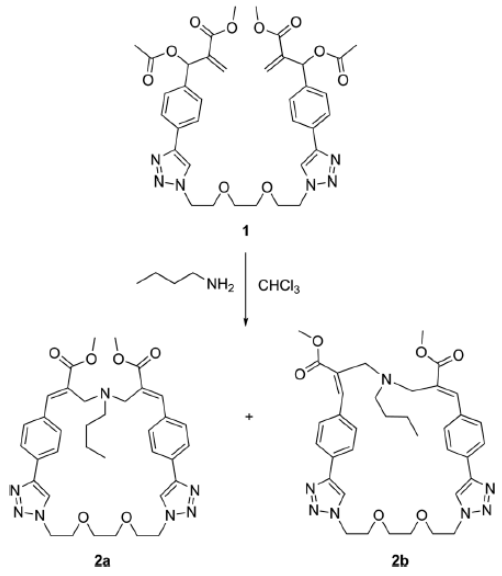

Scheme 2 Reaction of MBHA dimer **1** with *n*-butylamine leading to macrocyclic crown ether-paracyclophane hybrid structures **2a,b**.

Dimeric MBHA derivative **1** was found to react with *n*-butylamine in refluxing chloroform to afford the mixture of macrocyclic diastereomers **2a,b** in good yield (Scheme 2).

Fortunately, these isomers showed suitable physicochemical features to be easily separated by flash chromatography with ethyl acetate–methanol (95 : 5) as the eluent. In particular, compound **2b** was obtained as a white crystalline solid (yield 17%) as the least polar fraction of the chromatographic purification, whereas compound **2a** was obtained as a yellowish-white crystalline solid (yield 35%) as the most polar fraction of the chromatographic purification. Moreover, after purification by flash chromatography, compound **2a** was recrystallized from ethyl acetate by slow evaporation to obtain single crystals suitable for X-ray diffraction studies, which allowed the structure to be confirmed by crystallographic studies (Fig. 3).

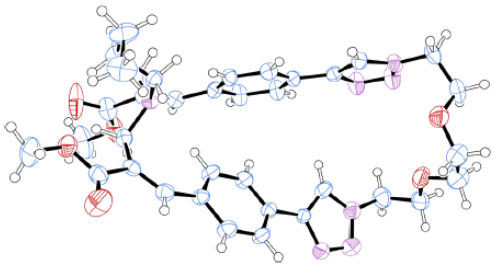

Fig. 3 Structure of compound **2a** obtained by crystallographic studies. Ellipsoids enclose 50% probability.

The crystallographic structure of (*E*,*E*) diastereomer **2a** was considered to constitute a good starting point for the structural characterization of **2b**. Thus, the ^{1}H and ^{13}C NMR spectra of **2a** were assigned and compared with those of the corresponding (*E*,*Z*) diastereomer **2b** (Fig. 4 and 5).

The comparison stressed the symmetric structure of **2a** (as supported by the crystallographic studies) with respect to the relative lack of symmetry of (*E*,*Z*) diastereomer **2b**, which showed two distinct sets of signals in almost all the regions of its NMR spectra with the exception if the signals of the butylamine moiety. Thus, these results supported the structure of diastereomer **2b**.

The structures of macrocyclic compounds **2a,b** were investigated also by several different mass spectrometry techniques such as trapped ion mobility mass spectrometry (TIMS), tandem mass spectrometry (MSn), and energy resolved tandem mass spectrometry. The results of TIMS characterization suggested the presence of two different ion populations due to different protonation sites in the amine and triazole nitrogen atoms or to two different conformations. However, the MS/MS spectra of the two ion populations were superimposable, thus supporting the latter hypothesis rather than the former one. For both compounds fragmentation pathways show the loss of 28 u, due to N_2 from the triazole moiety, and of C_4H_9N from the butylamine moiety. Moreover, energy resolved tandem mass spectrometry showed that diastereomer (*E*,*E*) **2a** appeared to be more stable than the corresponding (*E*,*Z*) diastereomer **2b** in agreement with the most abundant formation in the reaction of **1** with *n*-butylamine.

Photophysical and photochemical characterizations

The photophysical features of compounds **2a,b** were investigated in terms of absorption spectra in methanol (see ESI†). The absorption spectra of these two cinnamic derivatives showed very similar low energy peaks in the UV-B range, with absorption maximum at *ca.* 300 nm for the (*E*,*E*) diastereomer **2a** and a slight blue shifted peak at *ca.* 290 nm for the (*E*,*Z*) diastereomer **2b**. The photochemical features of the macrocyclic compounds were investigated by ^{1}H NMR spectroscopy studies starting from (*E*,*E*) diastereomer **2a** owing to its well-established (*i.e.* by crystallography) symmetric structure, the simplicity of its ^{1}H NMR spectrum, and its solubility in deuterated solvents such as methanol and DMSO. Thus, compound **2a** was dissolved in deuterated methanol into a 5 mm NMR tube and the resulting solutions were exposed to UV-B light into an appropriate photoreactor (Multirays, Helios Quartz). ^{1}H NMR spectra were registered at regular time intervals, elaborated, and compared (see ESI†). The comparison of the ^{1}H NMR spectra recorded with the solution of **2a** in deuterated methanol exposed to UV-B irradiation for increasing times (*i.e.* from 5 to 30 min) supported the liability of this (*E*,*E*) diastereomer to undergo photoisomerization with the formation of an almost insoluble compound, which precipitated from the reaction mixture. In

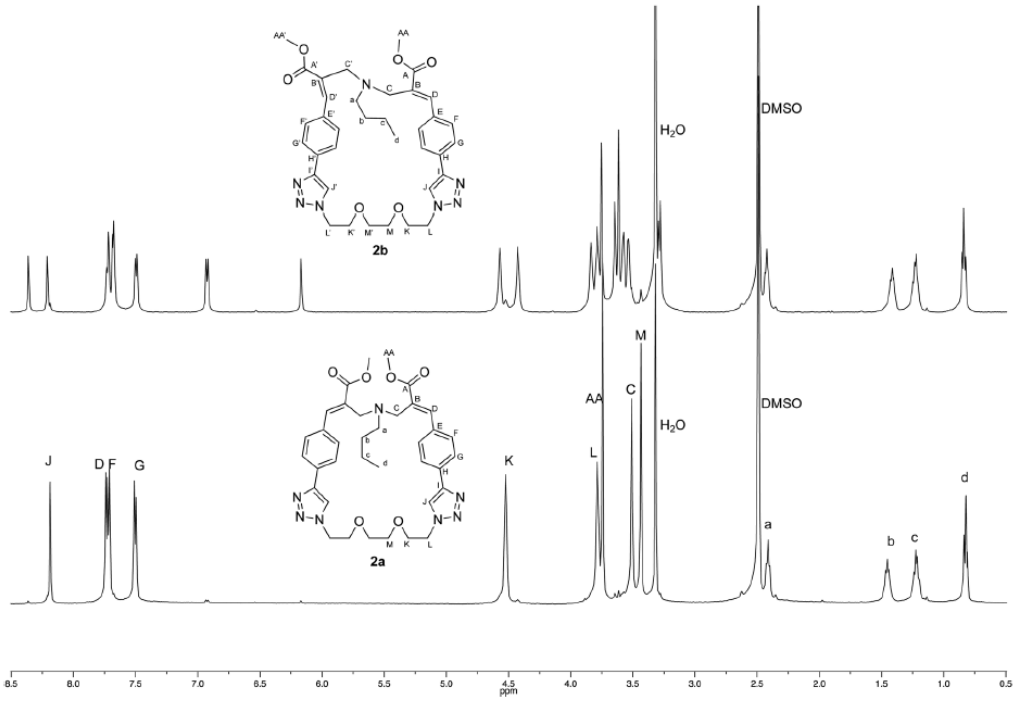

Fig. 4 Comparison of the ^{1}H NMR spectra recorded (500 MHz, DMSO-d_6) with crystalline samples of **2a** and **2b**.

fact, after 15 min exposition to UV-B irradiation, the formation of a white precipitate was observed, and the amount of this material appeared to increase in the time with the UV-B exposition. After storing the NMR tube containing the mixture at room temperature for three weeks, the spectrum suggested that negligible amounts of materials remained in the solution. Thus, a spectrum was recorded after dissolving the white precipitate with deuterated DMSO, and this spectrum supported the formation of (*E*,*Z*) diastereomer **2b** by photoisomerization with UV-B light of (*E*,*E*) diastereomer 2a in methanol. Apparently, the low solubility of the light-induced (*E*,*Z*) diastereomer **2b** in methanol could affect this photoisomerization reaction, but further experiments in different solvents are granted to explore the potential existence of different reaction pathways.

Computational studies

To further support the experimental data obtained, we calculated the relative energies of the two isomers using density functional theory (DFT) methodology (Fig. 6). Calculations were performed using B3LYP as functional and 6-31G* as basis set of the GAUSSIAN package (version 16).[17] The Polarized Continuum Model (PCM) simulating the solvent environment and Grimme dispersion D3 correction for long range (van der Waals) interactions were used. The two diastereomers were fully optimized in DMSO as implicit solvent ($\varepsilon = 46.826$), calculating the energy gap (at 298 K) between the conformations. The results confirm the higher stability of the (*E*,*E*) diastereomer 2a compared to the (*E*,*Z*) one **2b**, with an energy gap of 6.2 kcal mol^{-1}. Further computational studies are in progress in order to rationalize the photoisomerization features of these interesting macrocyclic derivatives.

Conclusions

In conclusion, a tri(ethylene glycol)-tethered MBHA dimer (**1**) was synthesized and found to react with *n*-butylamine leading to the formation of macrocyclic crown ether-paracyclophane hybrid structures **2** that could be modulated by light. Thus, reactive MBHA dimer **1** could find applications in the functionalization of materials containing reactive basic groups with the formation of amphiphilic loops provided with a wide range of intriguing properties such as those shown by both crown ethers and paracyclophane derivatives. Deeper investigations are in progress to characterize the complex photoisomerization features of this interesting new family of macrocyclic derivatives, also in light of the little information on similar structures reported in the literature.[18]

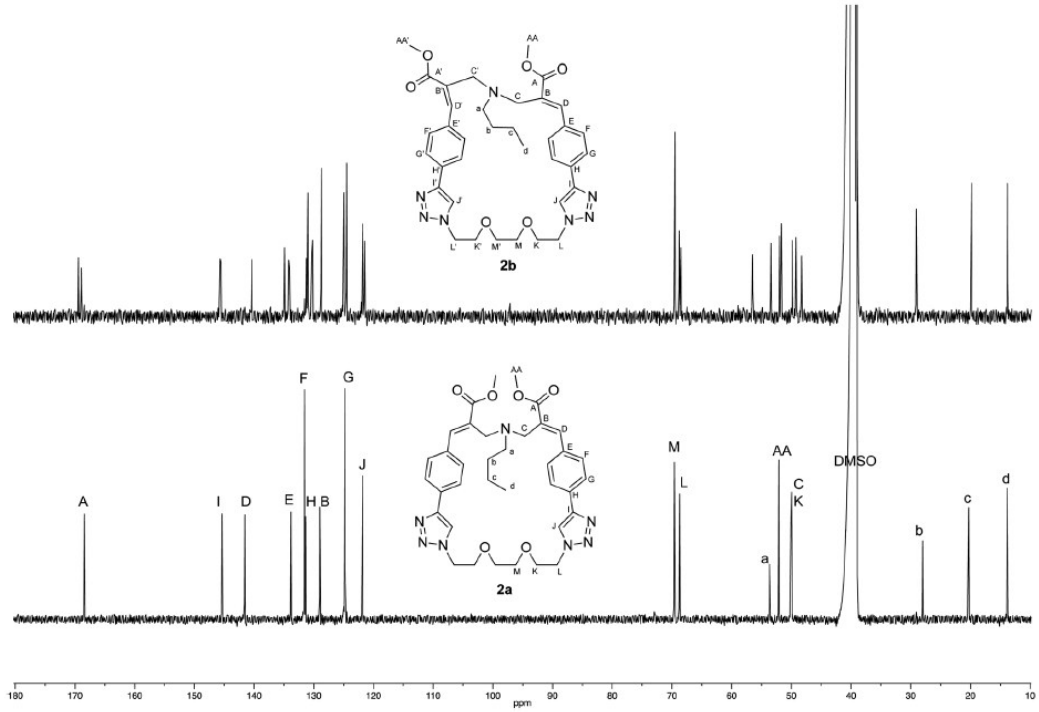

Fig. 5 Comparison of the ^{13}C NMR spectra recorded (125 MHz, DMSO-d_6) with crystalline samples of **2a** and **2b**.

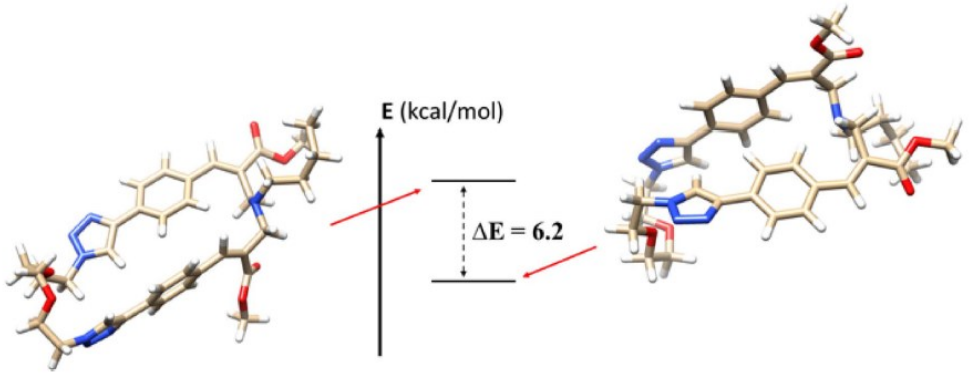

Fig. 6 Comparison of the 3D structures of **2a** (right) and **2b** (left).

Experimental section

Chemistry

All chemicals used were of reagent grade. Yields refer to purified products and are not optimized. Melting points were determined in open capillaries on a Gallenkamp apparatus and are uncorrected. Merck silica gel 60 (230–400 mesh) was used for flash chromatography purifications. Merck TLC plates, silica gel 60 F_{254} were used for TLC. NMR spectra were recorded with a Bruker DRX-400 AVANCE or a Bruker DRX-500 AVANCE spectrometer in the indicated solvents (TMS as internal standard): the values of the chemical shifts are expressed in ppm

and the coupling constants (J) in Hz. Mass spectra were recorded on an Agilent 1100 LC/MSD operating with an electrospray source.

X-ray crystallography

A single crystal of 2a was submitted to X-ray data collection on an Oxford-Diffraction Xcalibur Sapphire 3 diffractometer with a graphite monochromated Mo-Kα radiation ($\lambda = 0.71073$ Å) at 293 K. The structure was solved by direct methods implemented in SHELXS-97 program.[19] The refinement was carried out by full-matrix anisotropic least-squares on F2 for all reflections for non-H atoms by means of the SHELXL-97 program.[20] The structure crystallizes in the monoclinic crystal system and space group $P2_1/a$ with cell parameters: $a = 10.9638(9)$ $b = 22.3683(18)$ $c = 14.3096(13)$Å, $\beta = 102.531(8)°$. Crystallographic data for this structure have been deposited with the Cambridge Crystallographic Data Centre as supplementary publication no. CCDC 2286050. Copies of the data can be obtained, free of charge, on application to CCDC, 12 Union Road, Cambridge CB2 1EZ, UK; (fax: + 44 (0) 1223 336 033; or e-mail: deposit@ccdc.cam.ac.uk).

Mass spectrometry measurements

Each compound was dissolved in methanol (Sigma, HPLC Grade) to obtain a final concentration of about 1×10^{-5} M and injected in the electrospray source *via* flow injection at a flow rate of 5 µL min^{-1}.

Two different mass spectrometers have been used: an LCQ-Deca ion trap (IT, Thermo Finnigan, Bremen, D) and a timsTOF trapped ion mobility QTOF (Bruker, Bremen, D), both of them operating with an electrospray ionization source (ESI) in positive ion mode.

Operating conditions for the ESI sources were as follows: IT: spray voltage 4.5 kV; capillary temperature 200 °C; sheath gas (nitrogen) flow rate *ca.* 0.75 L min^{-1}; tims TOF: end plate offset 500 V; spray voltage 4.5 kV; capillary temperature 180 °C; sheath gas (nitrogen) flow pressure 5.8 psi; dry gas flow rate 4.0 L min^{-1}.

The calibration of the timsTOF mass spectrometer was carried out using Na Formate: 10 mM NaOH in a solution of isopropanol/H_2O (50/50) with 0.2% of formic acid.

MS^n product ion experiments carried out inside the ion trap were done by isolating the precursor ion and then by applying a supplementary potential for collision induced dissociations; collision gas: He; collision energy: 20–40% arbitrary units.

MS^2 product ion experiments carried out inside the timsTOF were done by isolating the precursor ion, by the quadrupole analyzer, and submitting it to collision induced dissociation reactions inside the collision cell with nitrogen and making production ion analysis in high resolution mode inside the time of flight analyzer.

In all MS^n experiments the isolation window of the precursor ion was 1 or 2 u.

For ion mobility MS experiments, the timsTOF instrument has been used: gas inside the TIMS cell was N_2, and the temperature of the cell was 305 K. The TIMS mode was set on "custom" with $1/K_0$ starting on 1.23 V·s cm^{-2} and $1/K_0$ ending on 1.27 V·s cm^2; ramp time was set on 600.0 ms with lock duty cycle at 100%. The calibration was carried out manually for each calibrant, using ESI-L Low Concentration Tuning Mix (Agilent Technologies). Before the calibration, the calibrant ion at m/z 622 was set on 132.0 ± 1.0 V through the setting of the gas flow on the instrument.

Optical properties

UV-vis absorption spectra are obtained with a Specord 210 Analytik Jena spectrometer.

Author contributions

The manuscript was written through the contributions of all authors. In particular: Mario Saletti, Jacopo Venditti, Marco Paolino, Arianna Zacchei, and Germano Giuliani were involved in the synthesis and the preliminary characterization; Claudia Bonechi and Alessandro Donati performed the NMR studies; Gianluca Giorgi performed the crystallographic studies and the mass spectrometry characterization; Andrea Cappelli designed the compounds and organized the research activities. All authors have given approval to the final version of the manuscript.

Conflicts of interest

The authors declare no competing financial interest.

Acknowledgements

M. P. and A. C. acknowledge the MUR for the financial support under the project CN00000041 – "National Center for Gene Therapy and Drugsbased on RNA Technology" – CUP B63C2200061 0006 Mission 4 Component 2 (M4C2) – investment 1.4 [CN3] of the National Recovery and Resilience Plan (PNRR) funded by the European Union "Next Generation EU". M. P. acknowledge the University of Siena for the financial support of the project Chromo-GEnUP through the F-CUR2022 funding line (2265-2022-PM-CONRICMIUR_PC-FCUR2022_003). Thanks are due also to Prof. Lluis Blancafort for providing access to computational resources.

References

1 F. Nicoli, M. Baroncini, S. Silvi, J. Groppi and A. Credi, Direct synthetic routes to functionalised crown ethers, *Org. Chem. Front.*, 2021, 8, 5531–5549.
2 D. B. Amabilino and J. Fraser Stoddart, Interlocked and intertwined structures and superstructures, *Chem. Rev.*, 1995, 95, 2725–2828.
3 J. Y. Sung, S.-M. Jin, S. Lee, S.-Y. An and J. S. Jin, Unusual enantiomeric separation due to residual amines in chiral crown ether stationary phase linked by long alkyl chain, *Talanta*, 2021, 235, 122739.
4 S. Shinkai, K. Miyazaki and O. Manabe, Photoresponsive crown ethers. Part 18. Photochemically 'switched-on' crown ethers containing an intra-annular azo substituent and

their application to membrane transport, *J. Chem. Soc., Perkin Trans. 1 (1972–1999)*, 1987, 449–456.
5 R. H. El Halabieh, O. Mermut and C. J. Barrett, Using light to control physical properties of polymers and surfaces with azobenzene chromophores, *Pure Appl. Chem.*, 2004, 76(7–8), 1445–1465.
6 A. Saady and S. M. Goldup, Triazole formation and the click concept in the synthesis of interlocked molecules, *Chem*, 2023, 9, 2110–2127.
7 W. P. Juma, D. Nyoni, D. Brady and M. L. Bode, The Application of biocatalysis in the preparation and resolution of Morita-Baylis-Hillman Adducts and their derivatives, *ChemBioChem*, 2022, 23.
8 H. Pellissier, Recent developments in the asymmetric organocatalytic Morita–Baylis–Hillman reaction, *Tetrahedron*, 2017, 73, 2831–2861.
9 V. Razzano, M. Paolino, A. Reale, G. Giuliani, R. Artusi, G. Caselli, M. Visintin, F. Makovec, A. Donati, F. Villafiorita-Monteleone, C. Botta and A. Cappelli, Development of imidazole-reactive molecules leading to a new aggregation-induced emission fluorophore based on the cinnamic scaffold, *ACS Omega*, 2017, 2, 5453–5459.
10 V. Razzano, M. Paolino, A. Reale, G. Giuliani, A. Donati, G. Giorgi, R. Artusi, G. Caselli, M. Visintin, F. Makovec, S. Battiato, F. Samperi, F. Villafiorita-Monteleone, C. Botta and A. Cappelli, Poly-histidine grafting leading to fishbone-like architectures, *RSC Adv.*, 2018, 8, 8638–8656.
11 M. Paolino, A. Reale, V. Razzano, G. Giuliani, A. Donati, C. Bonechi, G. Caselli, M. Visintin, F. Makovec, C. Scialabba, M. Licciardi, E. Paccagnini, M. Gentile, L. Salvini, F. Tavanti, M. C. Menziani and A. Cappelli, Nanoreactors for the multi-functionalization of poly-histidine fragments, *New J. Chem.*, 2019, 43, 6834–6837.
12 M. Paolino, M. Visintin, E. Margotti, M. Visentini, L. Salvini, A. Reale, V. Razzano, G. Giuliani, G. Caselli, F. Tavanti, M. C. Menziani and A. Cappelli, Functionalization of protein hexahistidine tags by functional nanoreactors, *New J. Chem.*, 2019, 43, 17946.
13 G. Tassone, M. Paolino, C. Pozzi, A. Reale, L. Salvini, G. Giorgi, M. Orlandini, F. Galvagni, S. Mangani, X. Yang, B. Carlotti, F. Ortica, L. Latterini, M. Olivucci and A. Cappelli, Xanthopsin-like systems via site-specific click-functionalization of a retinoic acid binding protein, *ChemBioChem*, 2022, 23, e202100449.
14 M. Saletti, M. Paolino, J. Venditti, C. Bonechi, G. Giuliani, A. Boccia, C. Botta and A. Cappelli, Synthesis, Photophysical and Photochemical features of a Morita-Baylis-Hillman Adduct Derivative Bearing a Triphenylamine Moiety, *Dyes Pigm.*, 2023, 219, 111571.
15 K. Worm-Leonhard and M. Meldal, Green Catalysts: Solid-phase peptide carbene ligands in aqueous transition-metal catalysis, *Eur. J. Org Chem.*, 2008, 31, 5244–5253.
16 G. Pelletier, W. S. Bechara and A. B. Charette, Controlled and chemoselective reduction of secondary amides, *J. Am. Chem. Soc.*, 2010, 132, 12817–12819.
17 M. J. Frisch, G. W. Trucks, H. B. Schlegel, G. E. Scuseria, M. A. Robb, J. R. Cheeseman, G. Scalmani, V. Barone, G. A. Petersson, H. Nakatsuji, X. Li, M. Caricato, A. V. Marenich, J. Bloino, B. G. Janesko, R. Gomperts, B. Mennucci, H. P. Hratchian, J. V. Ortiz, A. F. Izmaylov, J. L. Sonnenberg, D. Williams-Young, F. Ding, F. Lipparini, F. Egidi, J. Goings, B. Peng, A. Petrone, T. Henderson, D. Ranasinghe, V. G. Zakrzewski, J. Gao, N. Rega, G. Zheng, W. Liang, M. Hada, M. Ehara, K. Toyota, R. Fukuda, J. Hasegawa, M. Ishida, T. Nakajima, Y. Honda, O. Kitao, H. Nakai, T. Vreven, K. Throssell, J. A. Montgomery Jr, J. E. Peralta, F. Ogliaro, M. J. Bearpark, J. J. Heyd, E. N. Brothers, K. N. Kudin, V. N. Staroverov, T. A. Keith, R. Kobayashi, J. Normand, K. Raghavachari, A. P. Rendell, J. C. Burant, S. S. Iyengar, J. Tomasi, M. Cossi, J. M. Millam, M. Klene, C. Adamo, R. Cammi, J. W. Ochterski, R. L. Martin, K. Morokuma, O. Farkas, J. B. Foresman and D. J. Fox, *Gaussian 16, Revision C.01*, Gaussian, Inc., Wallingford CT, 2016.
18 S. Akabori and S. Tsuchiya, The Preparation of crown ethers containing dicinnamoyl groups and their complexing abilities, *Bull. Chem. Soc. Japan*, 1990, 63, 1623–1628.
19 G. M. A. Sheldrick, Short History of SHELX, *Acta Crystallogr., Sect. A: Found. Crystallogr.*, 2008, 64, 112–122.
20 G. M. Sheldrick, Crystal Structure Refinement with SHELXL, *Acta Crystallogr., Sect. C: Struct. Chem.*, 2015, 71, 3–8.

4.6 RESEARCH ARTICLE: "Synthesis and Reactivity of Oligo(ethylene glycol)-Tethered Morita-Baylis-Hillman Dimers in the Formation of Macrocyclic Structures Showing Remarkable Cytotoxicity"

Authors: Marco Paolino, Mario Saletti, **Jacopo Venditti**, Arianna Zacchei, Alessandro Donati, Claudia Bonechi, Germano Giuliani, Stefania Lamponi, Andrea Cappelli

Publication: Pharmaceuticals

Publisher: MDPI

DOI: doi.org/10.3390/ph18040473

Supporting information: N. A.

Contribution: Ph.D. candidate performed the synthesis and the purification of the compounds, followed by their characterization by means of ^{1}H NMR spectroscopy.

pharmaceuticals

MDPI

Article

Synthesis and Reactivity of Oligo(ethylene glycol)-Tethered Morita–Baylis–Hillman Dimers in the Formation of Macrocyclic Structures Showing Remarkable Cytotoxicity

Marco Paolino *, Mario Saletti, Jacopo Venditti, Arianna Zacchei, Alessandro Donati, Claudia Bonechi, Germano Giuliani, Stefania Lamponi and Andrea Cappelli

Dipartimento di Biotecnologie, Chimica e Farmacia, Università degli Studi di Siena, Via Aldo Moro 2, 53100 Siena, Italy; andrea.cappelli@unisi.it (A.C.)
* Correspondence: paolino3@unisi.it

Abstract: Background/Objectives: Crown ethers have received increasing interest owing to their ability to form stable complexes with cations. This molecular feature has been successfully exploited in the development of biologically relevant ionophores. **Methods**: In order to obtain innovative crown ethers derivatives, a Morita–Baylis–Hillman adduct (MBHA) acetate (**4**) bearing a phenylacetylene moiety was dimerized via the click-chemistry CuAAC reaction with oligo(ethylene glycol) diazide derivatives to build-up a small series of dimeric MBHA derivatives (**5a-d**). These dimeric MBHA derivatives were reacted with n-butylamine to afford tunable macrocyclic crown ether-paracyclophane hybrid architectures (**6a-d**). **Results**: Compounds (*E*,*Z*)-**6a**, (*E*,*E*)-**6a**, **6b-d** showed, in human breast cancer MDA-MB-231 and human melanoma A375 cells, IC_{50} values comparable with those of reference anticancer agent Doxorubicin. **Conclusions**: This exploration approach provides original new macrocyclic architectures potentially useful as anticancer agents.

Keywords: macrocyclic compounds; crown ethers; paracyclophane derivatives; cytotoxicity; anticancer agents

Academic Editor: Thierry Besson

Received: 3 February 2025
Revised: 20 March 2025
Accepted: 21 March 2025
Published: 27 March 2025

Citation: Paolino, M.; Saletti, M.; Venditti, J.; Zacchei, A.; Donati, A.; Bonechi, C.; Giuliani, G.; Lamponi, S.; Cappelli, A. Synthesis and Reactivity of Oligo(ethylene glycol)-Tethered Morita–Baylis–Hillman Dimers in the Formation of Macrocyclic Structures Showing Remarkable Cytotoxicity. *Pharmaceuticals* **2025**, *18*, 473. https://doi.org/10.3390/ph18040473

1. Introduction

Crown ethers are macrocyclic oligomers of ethylene oxide that exist in two forms: aliphatic and aromatic [1–3]. They were named on the bases of the evidence on the formation of host–guest complexes with metal cations [3,4]. In fact, the unique conformational and chemical characteristics of crown ethers allow them to create an electron-rich cavity, making them selective for alkali, alkaline-earth ions, and even non-metallic species. As a result, in the biological field, crown ethers can play a role in artificial intramembrane channels and enable the translocation of ionic species [2,5–7]. For example, a study reported the potential cytotoxicity of hydraphile compounds to bacterial [8] and mammalian cells presumably due to the unregulated ion flux through the plasma membrane [9] and even as discussed by Cai and Arenaz some crown ethers can show antiproliferative activity [10]. These assumptions together with the awareness that some ionophores, such as valinomycin [11,12], have been reported to display antitumor effects, led Marjanovic and co-workers to check the possible antiproliferative/antitumor ability of crown ethers [13]. Their findings support the hypothesis that the powerful antiproliferative activity of several crown ether compounds tested is the outcome of their activity as membrane-active potassium ion transporters, which can promote K^+ efflux [13].

Then, the cell membrane can be targeted by cationic ionophores (including crown ethers) [14], causing an imbalance in major physiological cations homeostasis and toxic consequences even in normal tissues [15]. Indeed, past studies have shown that these cationic ionophores can cause reversible toxic effects in several species, such as neurobehavioral effects, eye and skin irritation, and testicular atrophy [16]. Because of that the authors believe that crown ethers (or other membrane-active drugs) could be used as alternative anticancer drugs since they should induce different toxicity than conventional drugs and could complement existing therapy also thanks to their demonstrated ability to inhibit the efflux of anticancer drugs through P-glycoprotein (P-gp) [17].

The results of the study mentioned above also indicate that crown ethers show significant inhibition of cancer cell growth that is closely related to the composition of the hydrophilic cavity and the characteristics of the surrounding hydrophobic ring. The most effective compounds proved to be di-*tert*-butyldicyclohexano-18-crown-6, and di-*tert*-butyldibenzo-18-crown-6, which showed significant cytotoxicity. Additionally, these compounds significantly affected the distribution of cell cycle phases, causing an arrest in the G1 phase followed by the induction of apoptosis [18]. The importance of molecular structure, orientation of hydrophobic groups, and distribution of polarizable elements for interaction, presumably, with cell membranes, has been highlighted. Therefore, their results support the hypothesis that crown ethers may inhibit cancer cell growth through the perturbation of potassium ion homeostasis, which, in turn, leads to cell cycle perturbations and apoptosis, but further in vitro and in vivo studies are needed to confirm it and evaluate their potential clinical use [13,18].

For the synthesis of the crown ethers described below, we have applied the concept of "click" chemistry that involves linking small modular units in reactions with specific characteristics like high yield, chemoselectivity and stereospecificity, high thermodynamic driving force, irreversible bond formation, and mild conditions with few or no by-products [19,20]. The Copper(I)-Catalyzed Azide-Alkyne Cycloaddition (CuAAC) is the best-known "click" reaction, and it is commonly used in mechanically interlocked molecule (MIM) synthesis, including the creation of rotaxanes and catenanes [21,22].

On the other hand, the Morita–Baylis–Hillman reaction is essential in organic chemistry as it allows the formation of new C-C bonds, involving a carbon electrophile, an activated alkene, and catalysts such as tertiary amine or phosphine [23]. It results in the formation of an allylic alcohol that can be acetylated to become an excellent starting group. This reaction allows the creation of versatile and chiral products demonstrating the effectiveness of organocatalysis for green chemistry [24,25].

Several Morita–Baylis–Hillman adduct (MBHA) derivatives were designed and synthesized in our laboratories to react with imidazole, histidine derivatives, n-butylamine, lysine derivatives, and proteins [26–35], and the reactivity of some MBHA compounds was evaluated in protein models. Very interestingly, the results obtained with a single chain Fv antibody suggested that MBHA derivative **1a** (Figure 1) reacted with the hexahistidine tag producing multi-PEGylated species [28,29].

On the other hand, MBHA derivatives **1b**, **2a**,**b** (Figure 1) were found to react with a lysine residue embedded in a lipophilic pocket of a retinoic acid binding protein [30,36]. Finally, MBHA derivative **3** was found to react with human serum albumin (HSA) producing a significant shift in the emission from the blue to the green-yellow, thus leading to green fluorescent albumin (GFA) derivatives [33]. Since docking studies suggested a possible interaction between the acrylic activated moiety of compound **3** (Figure 1) with a lysine residue located into a lipophilic pocket in the HSA structure [33], the reactivity of MBHA derivative **3** was evaluated with n-butylamine, Nα-acetyl-*L*-lysine methyl ester, and a poly-(*L*-lysine) derivative as models of the lysine amino acid residues [35]. In the reaction

of compound **3** with n-butylamine, or with Nα-acetyl-*L*-lysine methyl ester we observed the formation of the corresponding diadduct derivatives along with the monoadduct ones in variable proportions depending on the reaction conditions. In particular, compound **3** showed the tendency to produce diadducts especially in polar solvents systems where stacking interactions between the extended aromatic moieties may play a major role in stabilizing the diadduct structure [35].

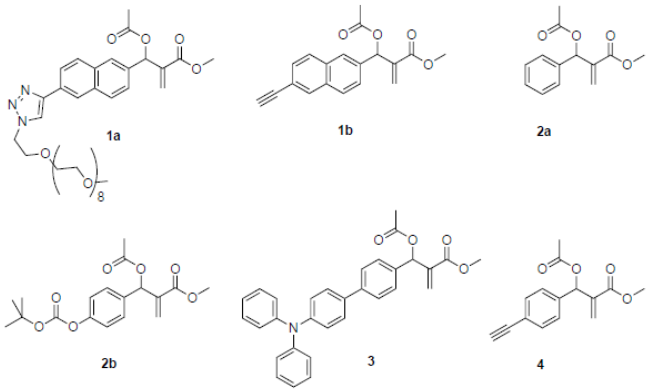

Figure 1. Structure of MBHA derivatives **1a,b**, **2a,b**, **3**, and **4**.

Very recently, MBHA derivative **4** was used as a synthon in the convergent synthesis of tri(ethylene glycol)-tethered MBHA dimer **5a** (Scheme 1), which was designed to be used in the functionalization of materials containing reactive basic groups such as amino or imidazole moieties [32]. The reactivity of tri(ethylene glycol)-tethered MBHA dimer **5a** was studied with n-butylamine as the simplest model of a lysine residue, and this reaction lead to the formation of macrocyclic crown ether-paracyclophane hybrid structures **6a** that could be modulated by light [32].

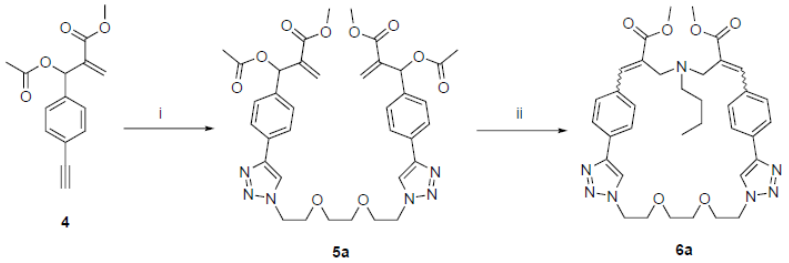

Scheme 1. Synthesis of MBHA dimer **5a** and reaction with n-butylamine leading to macrocyclic crown ether-paracyclophane hybrid structures **6a**. Reagents: (i) N_3-CH_2CH_2O-CH_2CH_2O-CH_2CH_2-N_3, CuBr(I), DIPEA, CH_3CN; (ii) $CH_3CH_2CH_2CH_2NH_2$, $CHCl_3$.

In the present work, the tri(ethylene glycol) component of the synthesis was replaced with the higher three homologues [i. e. tetra(ethylene glycol), penta(ethylene glycol), and hexa(ethylene glycol) derivatives] to obtain the MBHA dimers **5b-d**, and their reactivity towards n-butylamine was evaluated in the same conditions used for lower homologue **5a**. The evaluation of the biological properties of the resulting crown ether-paracyclophane hybrid structures revealed a remarkable cytotoxicity in cancer cell lines, providing original new macrocyclic architectures potentially useful as anticancer agents.

2. Results and Discussion

2.1. Synthesis

The synthesis of dimeric MBHA derivatives **5b-d** (Scheme 2) was accomplished by the same convergent procedure previously developed for the preparation of lower homologue **5a** [32].

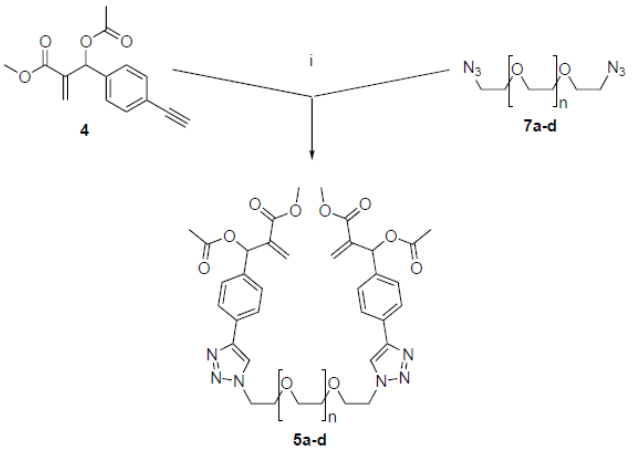

Scheme 2. Procedure for the preparation of dimeric MBHA derivatives **5a-d**. Reagents: (i) CuBr(I), DIPEA, CH_3CN. **5a** and **7a**: n = 1; **5b** and **7b**: n = 2; **5c** and **7c**: n = 3, **5d**, and **7d**: n = 4.

The MBHA component **4** of the convergent synthesis was re-prepared from 4-bromobenzaldehyde as previously described [32]. Similarly, the diazide components **7b-d** [37–39] were prepared starting from the commercially available oligo(ethylene glycol) by using the same procedure employed for the preparation of lowest homologue **7a** [32]. The final CuAAC coupling reaction was carried out at room temperature for two hours in acetonitrile in the presence of CuBr(I) as the catalyst and DIPEA as the base to obtain in good yields the oligo(ethylene glycol)-tethered MBHA dimers **5b-d**.

As already performed with **5a**, compounds **5b-d** were then made to react with n-butylamine (Scheme 3) to obtain the mixtures of macrocyclic diastereomers **6b-d** in good (i.e., 38–62%) yields.

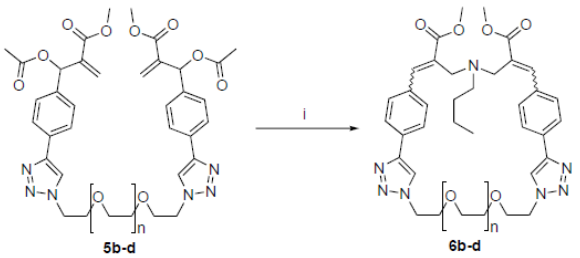

Scheme 3. Reaction of oligo(ethylene glycol)-tethered MBHA dimers **5b-d** with n-butylamine. Reagents: (i) $CH_3CH_2CH_2CH_2NH_2$; $CHCl_3$.

The (*E*,*E*) and (*E*,*Z*) diastereomers of the smallest member **6a** of the series were easily separated by flash chromatography and were obtained in a ratio of 2:1 in the pure crystalline form as white solids [32]. Furthermore, (*E*,*E*)-**6a** was recrystallized from ethyl

acetate by slow evaporation, and its structure was confirmed by crystallography [32]. The crystallographic structure of (*E*,*E*)-**6a** was used as the starting point for the structural characterization of the whole set of macrocyclic derivatives **6a-d**. In particular, the ^{1}H NMR spectra of (*E*,*E*)-**6a** was assigned and compared with those of the corresponding (*E*,*Z*)-diastereomer (Figure 2) [32].

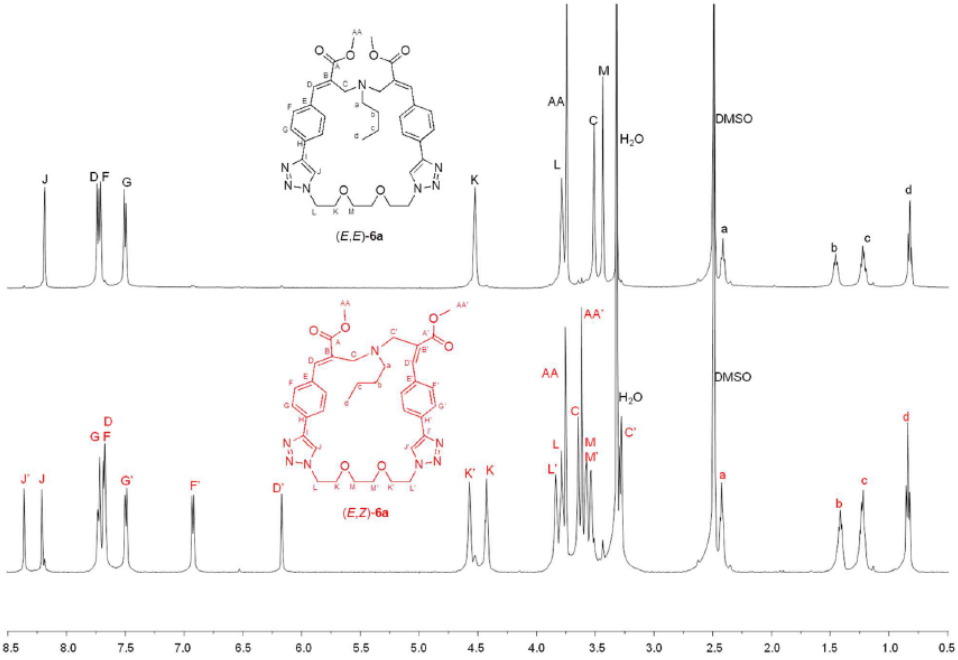

Figure 2. Comparison of the ^{1}H NMR spectra recorded (500 MHz, DMSO-d_6) with crystalline samples of (*E*,*E*)-**6a** and (*E*,*Z*)-**6a**. The signal assignment is reported in red for (*E*,*Z*)-**6a** and in black for (*E*,*E*)-**6a**.

The comparison of the ^{1}H NMR spectra highlights the lack of symmetry of (*E*,*Z*)-**6a** with respect to the symmetric structure of (*E*,*E*)-**6a** as supported by the crystallographic studies [32]. In fact, two distinct sets of signals are visible in almost all the regions of (*E*,*Z*)-**6a** spectra with the exception of the signals of the butylamine moiety. This configurational effect is due to the presence in the unsymmetrical diastereomer molecule of two cinnamic moieties showing opposite E/Z configurations, which could affect also the conformational preferences. It should be noted the great differences in the chemical shift values observed for the signals attributed to protons G′, F′, and D′ with respect to those assigned to the corresponding G, F, and D belonging to the cinnamic moiety in (*E*)-configuration.

On the other hand, the separation of the diastereomeric mixtures of macrocycle derivatives **6b-d** obtained by the reaction of n-butylamine with MBHA dimers **5b-d** bearing longer oligo(ethylene glycol) tethers was rather difficult, owing to the increasing polarity of the compounds. Thus, ^{1}H NMR spectra were performed on the diastereomeric mixtures, and the spectra obtained were compared with the corresponding spectrum obtained with the (2:1) mixture of diastereomers (*E*,*E*)-**6a** and (*E*,*Z*)-**6a** (Figure 3).

The comparison of the spectra shows that the samples were composed by two diastereomers (*E*,*E*) and (*E*,*Z*) of macrocycle derivatives **6b-d** in the ratio of 2:1. These results confirmed that the symmetric (*E*,*E*) diastereomers of **6a-d** were more stable than the corresponding (*E*,*Z*)-diastereomers, and the length of the oligo(ethylene glycol) chain appeared

to play a negligible role in affecting the relative stability of the diastereomers. On the other hand, the length of the oligo(ethylene glycol) chain appeared to affect the chemical shift values of the signals in the aromatic regions of ^{1}H NMR spectra (Figure 4).

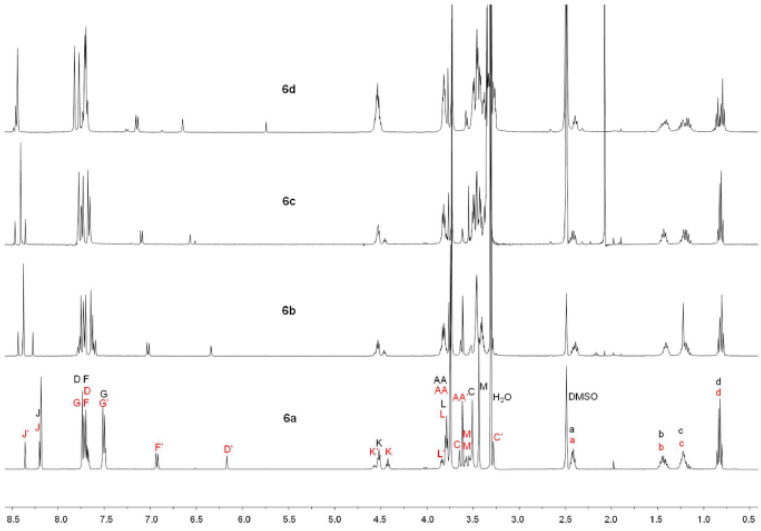

Figure 3. Comparison of the ^{1}H NMR spectra recorded (400 MHz, DMSO-d_6) with the samples obtained from the reaction of dimeric MBHA derivatives **5b-d** with n-butylamine. The ^{1}H NMR spectrum in the bottom trace was obtained with the (2:1) mixture of (*E*,*E*)-**6a** (the assignment is reported in black) and (*E*,*Z*)-**6a** (the assignment is reported in red) and is reported as the reference spectrum.

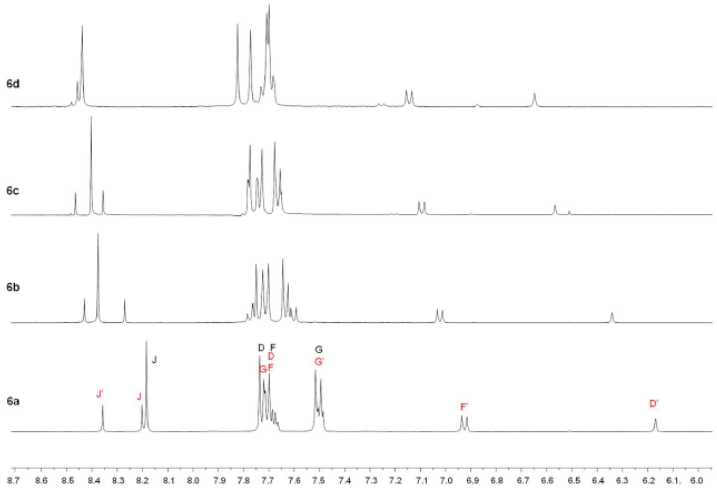

Figure 4. Comparison of the aromatic regions of the ^{1}H NMR spectra recorded (400 MHz, DMSO-d_6) with the samples obtained from the reaction of dimeric MBHA derivatives **5b-d** with n-butylamine. The ^{1}H NMR spectrum in the bottom trace was obtained with the (2:1) mixture of (*E*,*E*)-**6a** (the assignment is reported in black) and (*E*,*Z*)-**6a** (the assignment is reported in red) and is reported as the reference spectrum.

In fact, a progressive down-field shift was observed for all the signals attributed to aromatic protons. This observation appeared to suggest the existence of differences in the relative orientations of the aromatic moieties induced by the macrocycle dimensions.

In order to evaluate this assumption, molecular modeling calculations were performed on the symmetric (*E*,*E*) diastereomers of compounds **6a**,**d** that represented the most abundant species in the (2:1) mixtures. In particular, the geometries of the symmetric diastereomers were fully optimized by using density functional theory (DFT) methodology [40] in DMSO as implicit solvent (ε = 46.826). Calculations were performed using B3LYP as functional and 6–31G* as basis set of the GAUSSIAN package (version 16) [41]. The polarized continuum model (PCM) simulating the solvent environment and Grimme dispersion D3 correction for long range (van der Waals) interactions were used [42,43]. The results confirm the differences in the relative orientations of the aromatic moieties induced by the macrocycle dimensions in (*E*,*E*) diastereomers of **6a**,**d** (Figure 5).

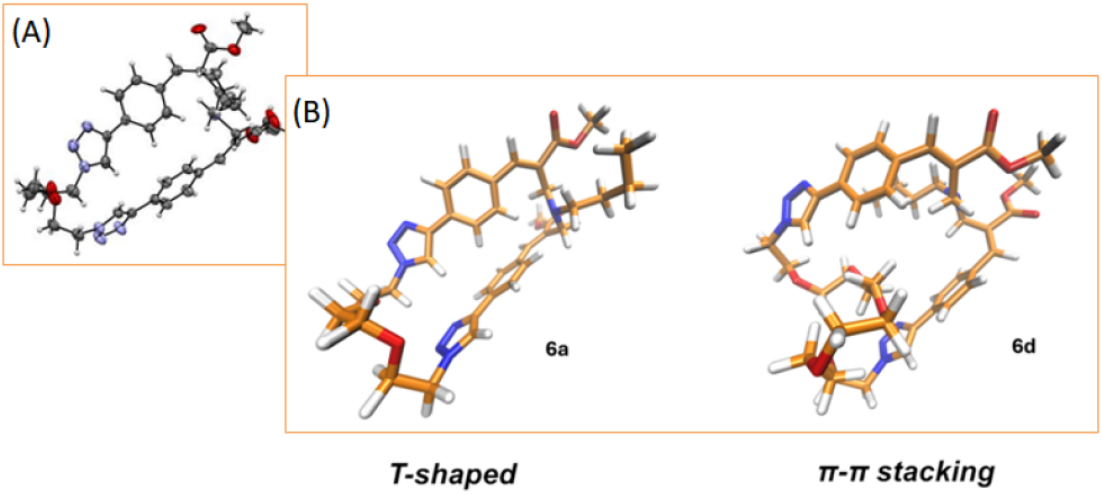

Figure 5. Comparison of (**A**) the X-ray structure of (*E*,*E*)-**6a** [32] with the computed 3D structures (**B**) of (*E*,*E*)-**6a** (**left**) and (*E*,*E*)-**6d** (**right**).

In fact, the aromatic moieties of (*E*,*E*)-**6a** were characterized by a compact T-shaped orientation [44] as the one observed in the crystal structure [32], whereas a more relaxed π-π stacked orientation was observed in (*E*,*E*)-**6d** structure. This observation appeared to be fully consistent with the progressive down-field shift in the signal (i.e., the most intense singlet in the aromatic region visible in Figure 4) attributed to the triazole proton (H-J in Figure 2). We assumed that T-shaped interaction of the triazole proton observed in (*E*,*E*)-**6a** structure was capable of shielding the protons and therefore producing an up-field shift with respect to (*E*,*E*)-**6d**. Interestingly, a similar effect was observed also for the aromatic protons (H-G in Figure 2) of the phenyl groups closest to the triazole ring that appeared to share the same orientation of H-J in Figure 5.

Further computational studies are in progress in order to evaluate the conformational features of these interesting macrocyclic derivatives.

2.2. Biological Evaluation of Macrocycle Derivatives **6a-d**: *In Vitro Cytotoxicity Assay*

Non-confluent, adhered human breast cancer MDA-MB-231 and human melanoma A375 cells were incubated with increasing concentrations of (*E*,*Z*)-**6a**, (*E*,*E*)-**6a**, **6b**, **6c**, **6d**, and Doxorubicin (used as positive control) [45], ranging from 0.1 to 3.0 μM. Cells were

analyzed after 24 h, and the results (Figure 6) showed that both exponentially growing human tumor cell lines exhibited characteristic dose–response trends for all six tested compounds [46,47].

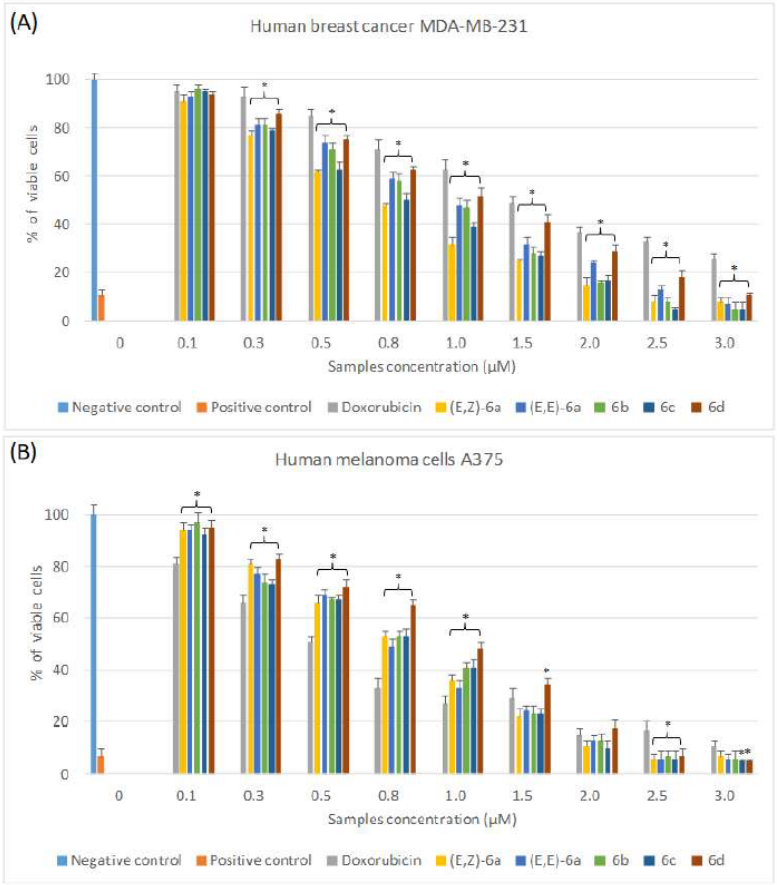

Figure 6. Percentage of viable (**A**) human breast cancer MDA-MB-231 and (**B**) human melanoma cells A375 after 24 h of contact with different concentrations of test compounds, as determined by the Neutral Red Uptake. Negative control: complete medium; positive control: 4 µL of Lysis Solution (a 1:250 dilution of 9% wt:vol Triton X-100) per 100 µL of cells in culture medium. Data are mean ± SD of three experiments run in six replicates. * Values are statistically different versus Doxorubicin, $p < 0.05$.

In particular, as reported in Figure 6A, the cytotoxic effect of all tested samples towards MDA-MB-231 cells increased with increasing concentrations, but to varying degrees [48,49]. Doxorubicin and compound **6d** demonstrated a lower cytotoxic effect compared to (*E*,*Z*)-**6a**, (*E*,*E*)-**6a**, **6b**, and **6c** at concentrations ≥ 0.3 µM. Compounds (*E*,*Z*)-**6a** and **6c** were the most cytotoxic at concentrations ranging from 0.3 to 1.5 µM; (*E*,*E*)-**6a** and **6b** were more cytotoxic than Doxorubicin but less than (*E*,*Z*)-**6a** and **6c** from 0.3 to 2.5 µM.

The IC_{50} value for MDA-MB-231 cells was 1.5 µM for Doxorubicin, 1.0 µM for (*E*,*E*)-**6a**, **6b**, **6d**, and 0.8 µM for both (*E*,*Z*)-**6a** and **6c** (Table 1).

Table 1. IC_{50} value (μM) of the tested samples towards MDA-MB-231 and A375IC50 cells.

Compounds	IC_{50} (μM)	
	MDA-MB-231 Cells	A375 Cells
Doxorubicin	1.5	0.5
(*E*,*Z*)-**6a**	0.8	0.8
(*E*,*E*)-**6a**	1.0	0.8
6b	1.0	0.8
6c	0.8	0.8
6d	1.0	1.0

Similarly to MDA-MB-231 cells, the cytotoxic effect of all tested samples towards human melanoma A375 cells increased with increasing concentrations, but to varying degrees [50]. As reported in Figure 6B, at concentrations ranging from 0.1 to 1.0 μM Doxorubicin demonstrated a higher cytotoxic effect compared to (*E*,*Z*)-**6a**, (*E*,*E*)-**6a**, **6b**, and **6c** towards human melanoma A375 cells, while, at concentrations higher than 1.5 μM, the latter was found to be more cytotoxic. The least cytotoxic sample was compound **6d**, which showed minimal ability to interfere with cell viability at concentrations ranging from 0.3 to 2.0 μM. No significant differences were found among the other tested compounds, (*E*,*Z*)-**6a**, (*E*,*E*)-**6a**, **6b**, and **6c**.

This trend was also demonstrated by the IC_{50} values for A375 cells: 0.5 μM for Doxorubicin (the most cytotoxic compound), 1.0 μM for sample **6d** (the least cytotoxic), and 0.8 μM for (*E*,*Z*)-**6a**, (*E*,*E*)-**6a**, **6b**, and **6c**, which all showed the same degree of cytotoxicity.

Overall, the slight differences (see Table 1) observed in the cytotoxicity potency of macrocyclic derivatives **6a-d** led us to assume that the cytotoxicity mechanism could be linked to a structurally non-specific interaction of the macrocyclic compounds with some key cellular components such as membrane. This assumption appeared to be in full agreement with the current literature. In fact, evidence has been reported that crown ethers are capable of inhibiting tumor-cell growth through the disruption of potassium ion homeostasis leading to cell cycle perturbations and apoptosis [13]. On the other hand, an alternative hypothesis is that the interaction of macrocyclic derivatives **6a-d** with cellular membranes could lead to loss of membrane integrity [51]. However, specifically designed experiments are required in order to gain experimental evidence supporting this hypothesis.

3. Conclusions

In the aim of obtaining a small series of new macrocyclic crown ether-paracyclophane hybrid architectures, a Morita–Baylis–Hillman acetate bearing a clickable phenylactylene moiety was dimerized by click-chemistry CuAAC reaction employing oligo(ethylene glycol) diazide derivatives with the formation of a small series of dimeric MBHA. The reaction of these dimeric MBHA derivatives with n-butylamine afforded the designed macrocyclic crown ether-paracyclophane hybrid architectures, which were evaluated for their potential cytotoxicity in human breast cancer MDA-MB-231 and human melanoma A375 cells. Very interestingly, tested compounds (*E*,*Z*)-**6a**, (*E*,*E*)-**6a**, **6b-d** showed remarkable cytotoxicity with IC_{50} values comparable with reference anticancer agent Doxorubicin. Thus, this exploration approach provides original new macrocyclic architectures potentially useful as anticancer agents. The versatility of our synthetic approach can rapidly lead to the expansion of this family of compounds by exploiting different nucleophilic agents, such as amino acids or peptides, often exploited in anticancer drugs to increase cell penetration and cell targeting [52–60].

4. Experimental Section

4.1. Synthesis

Column chromatography was carried out using a Merck (Darmstadt, Germany) silica gel 60 (230–400 mesh). Merck TLC plates, silica gel 60 F_{254} were used for TLC. NMR spectra were recorded with a Bruker DRX-500 AVANCE (Billerica, MA) or a Bruker DRX-400 AVANCE III spectrometer in the indicated deuterated solvents (TMS as internal standard): the values of the chemical shifts are expressed in ppm and the coupling constants (*J*) in Hz. Mass spectrometry experiments were carried out using an Agilent (Santa Clara, CA) 1100 LC/MSD operating with an electrospray source.

General procedure for the synthesis of compounds **5b-d**.

To a mixture of **4** (2 equivalents) and the appropriate diazide derivative **7b-d** (1 equivalent) in anhydrous acetonitrile, DIPEA (0.75 equivalents) and CuBr(I) (0.75 equivalents) were added in the sequence. The resulting mixture was stirred at r.t. under a nitrogen atmosphere for 2 h. Then, the reaction mixture was concentrated under reduced pressure, and the resulting residue was dissolved in dichloromethane and washed with NH_4OH. The organic phase was dried over Na_2SO_4 and concentrated under reduced pressure. The purification of the residue by flash chromatography with the indicated eluent furnished the desired MBHA dimer **5b-d**.

Dimethyl 2,2′-((((((oxybis(ethane-2,1-diyl))bis(oxy))bis(ethane-2,1-diyl))bis(1*H*-1,2,3-triazole-1,4-diyl))bis(4,1-phenylene))bis(acetoxymethylene))diacrylate (**5b**).

The title compound was obtained starting from **7b** (57 mg, 0.23 mmol) as a thick light-yellow oil (66 mg, yield 37%) using ethyl acetate-methanol 95:5 *v*/*v* as the eluent. ^{1}H NMR (400 MHz, $CDCl_3$): 2.11 (s, 6H), 3.53 (s, 8H), 3.70 (s, 6H), 3.80 (t, *J* = 5.0, 4H), 4.49 (t, *J* = 5.0, 4H), 5.90 (s, 2H), 6.40 (s, 2H), 6.67 (s, 2H), 7.42 (d, *J* = 8.2, 4H), 7.78 (d, *J* = 8.2, 4H), 7.89 (s, 2H). MS (ESI): *m*/*z* 783.3 [M + Na^+].

Dimethyl 2,2′-((((3,6,9,12-tetraoxatetradecane-1,14-diyl)bis(1*H*-1,2,3-triazole-1,4-diyl))bis(4,1-phenylene))bis(acetoxymethylene))diacrylate (**5c**).

The title compound was obtained starting from **7c** (83.5 mg, 0.29 mmol) as a thick yellow oil (0.123 mg, yield 53%) using ethyl acetate-methanol 95:5 *v*/*v* as the eluent. ^{1}H NMR (400 MHz, $CDCl_3$): 2.11 (s, 6H), 3.46–3.62 (m, 12H), 3.70 (s, 6H), 3.87 (t, *J* = 4.9, 4H), 4.57 (t, *J* = 4.9, 4H), 5.90 (s, 2H), 6.41 (s, 2H), 6.67 (s, 2H), 7.45 (d, *J* = 8.2, 4H), 7.89 (d, *J* = 8.2, 4H), 8.15 (s, 2H). MS (ESI): *m*/*z* 827.3 [M + Na^+].

Dimethyl 2,2′-((((3,6,9,12,15-pentaoxaheptadecane-1,17-diyl)bis(1*H*-1,2,3-triazole-1,4-diyl))bis(4,1-phenylene))bis(acetoxymethylene))diacrylate (**5d**).

The title compound was obtained starting from **7d** (87 mg, 0.26 mmol) as a pale-yellow oil (0.137 mg, yield 62%) using ethyl acetate-methanol 95:5 *v*/*v* as the eluent. ^{1}H NMR (400 MHz, $CDCl_3$): 2.10 (s, 6H), 3.56 (m, 16H), 3.69 (s, 6H), 3.87 (t, *J* = 4.9, 4H), 4.55 (t, *J* = 4.9, 4H), 5.88 (s, 2H), 6.40 (s, 2H), 6.68 (s, 2H), 7.41 (d, *J* = 8.1, 4H), 7.80 (d, *J* = 8.1, 4H), 7.96 (s, 2H). MS (ESI): *m*/*z* 871.3 [M + Na^+].

Reaction of homodimer **5b** with n-butylamine.

Dimethyl (1^4Z,11^4Z)-6-butyl-1^1H,11^1H-14,17,20-trioxa-6-aza-1,11(4,1)-ditriazola-2,10(1,4)-dibenzenacyclodocosaphane-3,8-diene-4,8-dicarboxylate (**6b**).

Compound **5b** (66 mg, 0.087 mmol) was solubilized in $CHCl_3$ (11 mL), and then, n-butylamine (17 µL, 0.174 mmol) was added. The resulting mixture was refluxed for 24 h. Subsequently, this mixture was concentrated under reduced pressure and the organic residue obtained was purified by flash chromatography with ethyl acetate-methanol (8:2) as the eluent to obtain **6b** as white solid (35.5 mg, yield 57%). The ^{1}H NMR spectrum showed the presence of (*E*,*E*) and (*E*,*Z*) diastereomers as a (2:1) mixture (Figures 3 and 4). MS (ESI): *m*/*z* 714.3 [M + H^+]. MS (ESI): *m*/*z* 736.3 [M + Na^+].

Reaction of homodimer **5c** with n-butylamine.

Dimethyl (1^4Z,11^4Z)-6-butyl-1^1H,11^1H-14,17,20,23-tetraoxa-6-aza-1,11(4,1)-ditriazola-2,10(1,4)-dibenzenacyclopentacosaphane-3,8-diene-4,8-dicarboxylate (**6c**).

Compound **5c** (0.114 g, 0.14 mmol) was solubilized in $CHCl_3$ (17 mL), and then, n-butylamine (28 µL, 0.28 mmol) was added. The resulting mixture was refluxed for 24 h. Subsequently, this mixture was concentrated under reduced pressure, and the organic residue obtained was purified by flash chromatography with ethyl acetate-methanol (85:15) as the eluent to obtain **6c** as waxy white solid (66 mg, yield 62%). The ^{1}H NMR spectrum showed the presence of (*E*,*E*) and (*E*,*Z*) diastereomers as a (2:1) mixture (Figures 3 and 4). MS (ESI): *m*/*z* 758.3 [M + H^+]. MS (ESI): *m*/*z* 780.3 [M + Na^+].

Reaction of homodimer **5d** with n-butylamine.

Dimethyl (1^4Z,11^4Z)-6-butyl-1^1H,11^1H-14,17,20,23,26-pentaoxa-6-aza-1,11(4,1)-ditriazola-2,10(1,4)-dibenzenacyclooctacosaphane-3,8-diene-4,8-dicarboxylate (**6d**).

Compound **5d** (0.137 g, 0.16 mmol) was solubilized in $CHCl_3$ (20 mL) and then n-butylamine (32 µL, 0.32 mmol) was added. The resulting mixture was refluxed for 24 h. Subsequently, this mixture was concentrated under reduced pressure. The organic residue obtained was purified by flash chromatography with ethyl acetate-methanol (9:1) as the eluent to obtain **6d** as yellow waxy oil (49 mg, yield 38%). The ^{1}H NMR spectrum showed the presence of (*E*,*E*) and (*E*,*Z*) diastereomers as a (2:1) mixture (Figures 3 and 4). MS (ESI): *m*/*z* 802.4 [M + H^+]. MS (ESI): *m*/*z* 824.4 [M + Na^+].

4.2. Biological Evaluation of Macrocycle Derivatives **6a-d**

4.2.1. Materials

Dulbecco's Modified Eagle's Medium, trypsin solution, and all the solvents used for cell culture were purchased from Merck. Human breast cancer MDA-MB-231 cells and human melanoma cells A375 were purchased from American Type Culture Collection (Manassas, VA, USA).

4.2.2. In Vitro Cytotoxicity Assay

Both human breast cancer MDA-MB-231 and human melanoma cells A375 cells were maintained in DMEM at 37 °C in a humidified atmosphere containing 5% CO_2. The culture medium was supplemented with 10% fetal calf serum (FCS), 1% L-glutamine-penicillin-streptomycin solution, and 1% MEM Non-Essential Amino Acid Solution. Once at confluence, cells were washed with PBS 0.1M, detached with trypsin-EDTA solution, and then centrifuged at 1000 rpm for 5 min. The pellet was re-suspended in the medium solution (dilution 1:15).

Cells (1.5×10^4) suspended in 1 mL of complete medium were seeded in each well of a 24 well round multidish and incubated at 37 °C in an atmosphere of 5% CO_2. Once reached 50% of confluence (i.e., after 24 h of culture), the culture medium was discharged and the test compounds, properly diluted in completed medium, were added to each well.

The stock solutions of test compounds (*E*,*Z*)-**6a**, (*E*,*E*)-**6a**, **6b**, **6c**, **6d**, and Doxorubicin were prepared in DMSO. The following concentrations of each sample were tested: 0.1; 0.3; 0.5; 0.8; 1.0; 1.5; 2.0; 2.5; 3.0 µM.

Each experiment was repeated three times, and all samples were set up in six replicates. Complete medium was used as negative control and 4 µL of Lysis Solution (a 1:250 dilution of 9% wt:vol Triton X-100) per 100 µL of cells in culture medium, as positive control [61]. After 24 h of incubation, cell viability was evaluated by Neutral Red uptake, as previously reported [62].

4.2.3. Statistical Analysis

Multiple comparison was performed by one-way ANOVA using GraphPad version 10.4 [63]. Differences with $p < 0.05$ were considered significant.

Author Contributions: Conceptualization, A.C.; Formal analysis, M.S., J.V., A.Z., A.D., C.B., G.G., S.L. and A.C.; Investigation, M.P., M.S., J.V., A.Z., A.D., C.B., G.G., S.L. and A.C.; Data curation, M.P.; Writing—original draft, M.P., A.Z. and A.C.; Supervision, A.C. and M.P.; Funding acquisition, M.P. All authors have read and agreed to the published version of the manuscript.

Funding: This research was funded by CN00000041—"National Center for Gene Therapy and Drugs-based on RNA Technology"—CUP B63C2200061 0006 Mission 4 Component 2 (M4C2)—investment 1.4 [CN3] of the National Recovery and Resilience Plan (PNRR) funded by the European Union "Next Generation EU" and by the University of Siena, project Chromo-GEnUP through the F-CUR2022 funding line (2265-2022-PM-CONRICMIUR_PC-FCUR2022_003).

Institutional Review Board Statement: Not applicable.

Informed Consent Statement: Not applicable.

Data Availability Statement: The data presented in this study are contained within the article. Requests for further details can be directed to the corresponding author.

Acknowledgments: M.P. and A.C. acknowledge the MUR for the financial support under the project CN00000041—"National Center for Gene Therapy and Drugsbased on RNA Technology"—CUP B63C2200061 0006 Mission 4 Component 2 (M4C2)—investment 1.4 [CN3] of the National Recovery and Resilience Plan (PNRR) funded by the European Union "Next Generation EU". M.P. acknowledge the University of Siena for the financial support of the project Chromo-GEnUP through the F-CUR2022 funding line (2265-2022-PM-CONRICMIUR_PC-FCUR2022_003).

Conflicts of Interest: The authors declare no conflict of interest.

References

1. Pedersen, C.J. Cyclic polyethers and their complexes with metal salts. *J. Am. Chem. Soc.* **1967**, *89*, 7017–7036.
2. Pedersen, C.J. The Discovery of Crown Ethers (Noble Lecture). *Angew. Chem. Int. Ed. Engl.* **1988**, *27*, 1021–1027.
3. Bradshaw, J.S.; Izatt, R.M. Crown Ethers: The Search for Selective Ion Ligating Agents. *Acc. Chem. Res.* **1997**, *30*, 338–345. [CrossRef]
4. Gokel, G.W.; Leevy, W.M.; Weber, M.E. Crown Ethers: Sensors for Ions and Molecular Scaffolds for Materials and Biological Models. *Chem. Rev.* **2004**, *104*, 2723–2750.
5. Nicoli, F.; Baroncini, M.; Silvi, S.; Groppi, J.; Credi, A. Direct synthetic routes to functionalised crown ethers. *Org. Chem. Front.* **2021**, *8*, 5531–5549. [PubMed]
6. Ullah, F.; Khan, T.A.; Iltaf, J.; Anwar, S.; Khan, M.F.; Khan, M.R.; Ullah, S.; Fayyaz ur Rehman, M.; Mustaqeem, M.; Kotwica-Mojzych, K.; et al. Heterocyclic Crown Ethers with Potential Biological and Pharmacological Properties: From Synthesis to Applications. *Appl. Sci.* **2022**, *12*, 1102. [CrossRef]
7. Gokel, G.W.; Ferdani, R.; Liu, J.; Pajewski, R.; Shabany, H.; Uetrecht, P. Hydraphile Channels: Models for Transmembrane, Cation-Conducting Transporters. *Chem. A Eur. J.* **2001**, *7*, 33–39.
8. Leevy, W.M.; Gokel, M.R.; Hughes-Strange, G.B.; Schlesinger, P.H.; Gokel, G.W. Structure and medium effects on hydraphile synthetic ion channel toxicity to the bacterium *E. coli*. *New J. Chem.* **2005**, *29*, 205–209.
9. Leevy, W.M.; Gammon, S.T.; Levchenko, T.; Daranciang, D.D.; Murillo, O.; Torchilin, V.; Piwnica-Worms, D.; Huettner, J.E.; Gokel, G.W. Structure–activity relationships, kinetics, selectivity, and mechanistic studies of synthetic hydraphile channels in bacterial and mammalian cells. *Org. Biomol. Chem.* **2005**, *3*, 3544–3550. [CrossRef]
10. Cai, M.-Y.; Arenaz, P. Antimutagenic effect of crown ethers on heavy metal-induced sister chromatid exchanges. *Mutagenesis* **1998**, *13*, 27–32.
11. Su, Z.; Ran, X.; Leitch, J.J.; Schwan, A.L.; Faragher, R.; Lipkowski, J. How Valinomycin Ionophores Enter and Transport K+ across Model Lipid Bilayer Membranes. *Langmuir* **2019**, *35*, 16935–16943.
12. Huang, S.; Liu, Y.; Liu, W.-Q.; Neubauer, P.; Li, J. The Nonribosomal Peptide Valinomycin: From Discovery to Bioactivity and Biosynthesis. *Microorganisms* **2021**, *9*, 780. [CrossRef] [PubMed]
13. Marjanović, M.; Kralj, M.; Supek, F.; Frkanec, L.; Piantanida, I.; Šmuc, T.; Tušek-Božić, L. Antitumor Potential of Crown Ethers: Structure−Activity Relationships, Cell Cycle Disturbances, and Cell Death Studies of a Series of Ionophores. *J. Med. Chem.* **2007**, *50*, 1007–1018.
14. Roy, A.; Talukdar, P. Recent Advances in Bioactive Artificial Ionophores. *ChemBioChem* **2021**, *22*, 2925–2940. [CrossRef] [PubMed]

15. Pang, L.; Feng, H.; Zhong, W.; Dong, H.; Shen, Y.; Yu, B.; Cong, H. Design of crown ether based micelles and their anti-tumor properties by perturbing potassium ion homeostasis. *Mater. Des.* **2021**, *211*, 110159. [CrossRef]
16. Gad, S.C.; Reilly, C.; Siino, K.; Gavigan, F.A.; Witz, G. Thirteen Cationic I0n0ph0res: Their Acute Toxicity, Neurobehavioral and Membrane Effects. *Drug Chem. Toxicol.* **1985**, *8*, 451–468.
17. Guberović, I.; Marjanović, M.; Mioč, M.; Ester, K.; Martin-Kleiner, I.; Šumanovac Ramljak, T.; Mlinarić-Majerski, K.; Kralj, M. Crown ethers reverse P-glycoprotein-mediated multidrug resistance in cancer cells. *Sci. Rep.* **2018**, *8*, 14467.
18. Kralj, M.; Tušek-Božić, L.; Frkanec, L. Biomedical Potentials of Crown Ethers: Prospective Antitumor Agents. *ChemMedChem* **2008**, *3*, 1478–1492.
19. Devaraj, N.K.; Finn, M.G. Introduction: Click Chemistry. *Chem. Rev.* **2021**, *121*, 6697–6698. [CrossRef]
20. Hein, C.D.; Liu, X.-M.; Wang, D. Click Chemistry, A Powerful Tool for Pharmaceutical Sciences. *Pharm. Res.* **2008**, *25*, 2216–2230.
21. Saady, A.; Goldup, S.M. Triazole formation and the click concept in the synthesis of interlocked molecules. *Chem* **2023**, *9*, 2110–2127.
22. Khodadadi Yazdi, M.; Sajadi, S.M.; Seidi, F.; Rabiee, N.; Fatahi, Y.; Rabiee, M.; Dominic, C.D.M.; Zarrintaj, P.; Formela, K.; Saeb, M.R.; et al. Clickable polysaccharides for biomedical applications: A comprehensive review. *Prog. Polym. Sci.* **2022**, *133*, 101590.
23. Basavaiah, D.; Naganaboina, R.T. The Baylis–Hillman reaction: A new continent in organic chemistry—our philosophy, vision and over three decades of research. *New J. Chem.* **2018**, *42*, 14036–14066.
24. Juma, W.P.; Nyoni, D.; Brady, D.; Bode, M.L. The Application of Biocatalysis in the Preparation and Resolution of Morita-Baylis-Hillman Adducts and Their Derivatives. *ChemBioChem* **2022**, *23*, e202100527.
25. Pellissier, H. Recent developments in the asymmetric organocatalytic Morita−Baylis−Hillman reaction. *Tetrahedron* **2017**, *73*, 2831–2861.
26. Razzano, V.; Paolino, M.; Reale, A.; Giuliani, G.; Artusi, R.; Caselli, G.; Visintin, M.; Makovec, F.; Donati, A.; Villafiorita-Monteleone, F.; et al. Development of Imidazole-Reactive Molecules Leading to a New Aggregation-Induced Emission Fluorophore Based on the Cinnamic Scaffold. *ACS Omega* **2017**, *2*, 5453–5459.
27. Razzano, V.; Paolino, M.; Reale, A.; Giuliani, G.; Donati, A.; Giorgi, G.; Artusi, R.; Caselli, G.; Visintin, M.; Makovec, F.; et al. Poly-histidine grafting leading to fishbone-like architectures. *RSC Adv.* **2018**, *8*, 8638–8656.
28. Paolino, M.; Visintin, M.; Margotti, E.; Visentini, M.; Salvini, L.; Reale, A.; Razzano, V.; Giuliani, G.; Caselli, G.; Tavanti, F.; et al. Functionalization of protein hexahistidine tags by functional nanoreactors. *New J. Chem.* **2019**, *43*, 17946–17953.
29. Paolino, M.; Reale, A.; Razzano, V.; Giuliani, G.; Donati, A.; Bonechi, C.; Caselli, G.; Visintin, M.; Makovec, F.; Scialabba, C.; et al. Nanoreactors for the multi-functionalization of poly-histidine fragments. *New J. Chem.* **2019**, *43*, 6834–6837.
30. Tassone, G.; Paolino, M.; Pozzi, C.; Reale, A.; Salvini, L.; Giorgi, G.; Orlandini, M.; Galvagni, F.; Mangani, S.; Yang, X.; et al. Xanthopsin-Like Systems via Site-Specific Click-Functionalization of a Retinoic Acid Binding Protein. *ChemBioChem* **2022**, *23*, e202100449.
31. Saletti, M.; Paolino, M.; Venditti, J.; Bonechi, C.; Giuliani, G.; Boccia, A.; Botta, C.; Cappelli, A. Synthesis, photophysical and photochemical features of a Morita-Baylis-Hillman adduct derivative bearing a triphenylamine moiety. *Dye. Pigment.* **2023**, *219*, 111571. [CrossRef]
32. Saletti, M.; Venditti, J.; Paolino, M.; Zacchei, A.; Giuliani, G.; Giorgi, G.; Bonechi, C.; Donati, A.; Cappelli, A. A tri(ethylene glycol)-tethered Morita–Baylis–Hillman dimer in the formation of macrocyclic crown ether-paracyclophane hybrid structures. *RSC Adv.* **2023**, *13*, 35773–35780. [CrossRef] [PubMed]
33. Saletti, M.; Paolino, M.; Venditti, J.; Bonechi, C.; Giuliani, G.; Lamponi, S.; Tassone, G.; Boccia, A.; Botta, C.; Blancafort, L.; et al. A Facile Access to Green Fluorescent Albumin Derivatives. *ChemBioChem* **2024**, *25*, e202300862. [CrossRef] [PubMed]
34. Lami, M.; Barneschi, L.; Saletti, M.; Olivucci, M.; Cappelli, A.; Paolino, M. Preparation of Light-responsive Unnatural RNA Bases via a Chromogenic Morita-Baylis-Hillman Adduct Path. *ChemPhotoChem* **2024**, *8*, e202400093. [CrossRef]
35. Venditti, J.; Saletti, M.; Paolino, M.; Contena, S.; Bonechi, C.; Giuliani, G.; Giorgi, G.; Boccia, A.C.; Botta, C.; Blancafort, L.; et al. Reactivity of a Morita–Baylis–Hillman Adduct Derivative Bearing a Triphenylamine Moiety with Lysine Models. *Chem. Asian J.* **2024**, *19*, e202400617. [CrossRef]
36. Paolino, M.; Tassone, G.; Governa, P.; Saletti, M.; Lami, M.; Carletti, R.; Sacchetta, F.; Pozzi, C.; Orlandini, M.; Manetti, F.; et al. Morita–Baylis–Hillman Adduct Chemistry as a Tool for the Design of Lysine-Targeted Covalent Ligands. *ACS Med. Chem. Lett.* **2025**, *16*, 397–405. [CrossRef]
37. Payne, C.M.; Baltos, J.-A.; Langiu, M.; Sinh Lu, C.; Tyndall, J.D.A.; Gregory, K.J.; May, L.T.; Vernall, A.J. Development of Putative Bivalent Dicovalent Ligands for the Adenosine A1 Receptor. *ChemBioChem* **2024**, *25*, e202400242. [CrossRef]
38. Bonger, K.M.; van den Berg, R.J.B.H.N.; Heitman, L.H.; IJzerman, A.P.; Oosterom, J.; Timmers, C.M.; Overkleeft, H.S.; van der Marel, G.A. Synthesis and evaluation of homo-bivalent GnRHR ligands. *Bioorg. Med. Chem.* **2007**, *15*, 4841–4856. [CrossRef]
39. Goswami, L.N.; Houston, Z.H.; Sarma, S.J.; Jalisatgi, S.S.; Hawthorne, M.F. Efficient synthesis of diverse heterobifunctionalized clickable oligo(ethylene glycol) linkers: Potential applications in bioconjugation and targeted drug delivery. *Org. Biomol. Chem.* **2013**, *11*, 1116–1126. [CrossRef]

40. van Mourik, T.; Bühl, M.; Gaigeot, M.-P. Density functional theory across chemistry, physics and biology. *Philos. Trans. R. Soc. A Math. Phys. Eng. Sci.* **2014**, *372*, 20120488. [CrossRef]
41. Frisch, M.J.; Trucks, G.W.; Schlegel, H.B.; Scuseria, G.E.; Robb, M.A.; Cheeseman, J.R.; Scalmani, G.; Barone, V.; Petersson, G.A.; Nakatsuji, H.; et al. Gaussian 2016.
42. Mennucci, B. Polarizable continuum model. *WIREs Comput. Mol. Sci.* **2012**, *2*, 386–404.
43. Brandenburg, J.G.; Grimme, S. *Dispersion Corrected Hartree–Fock and Density Functional Theory for Organic Crystal Structure Prediction BT—Prediction and Calculation of Crystal Structures: Methods and Applications*; Atahan-Evrenk, S., Aspuru-Guzik, A., Eds.; Springer International Publishing: Cham, Switzerland, 2014; pp. 1–23. ISBN 978-3-319-05774-3.
44. Reuter, K.; Maas, R.G.M.; Reuter, A.; Kilgenstein, F.; Asfaha, Y.; von Hänisch, C. Synthesis of heteroatomic bridged paracyclophanes. *Dalt. Trans.* **2017**, *46*, 4530–4541. [CrossRef] [PubMed]
45. Kulikova, L.N.; Purgatorio, R.; Beloglazkin, A.A.; Tafeenko, V.A.; Reza, R.G.; Levickaya, D.D.; Sblano, S.; Boccarelli, A.; de Candia, M.; Catto, M.; et al. Chemical and Biological Evaluation of Novel 1H-Chromeno[3,2-c]pyridine Derivatives as MAO Inhibitors Endowed with Potential Anticancer Activity. *Int. J. Mol. Sci.* **2023**, *24*, 7724. [CrossRef] [PubMed]
46. Majellaro, M.; Stefanachi, A.; Tardia, P.; Vicenti, C.; Boccarelli, A.; Pannunzio, A.; Campanella, F.; Coluccia, M.; Denora, N.; Leonetti, F.; et al. Investigating Structural Requirements for the Antiproliferative Activity of Biphenyl Nicotinamides. *ChemMedChem* **2017**, *12*, 1380–1389. [CrossRef] [PubMed]
47. Nevskaya, A.A.; Matveeva, M.D.; Borisova, T.N.; Niso, M.; Colabufo, N.A.; Boccarelli, A.; Purgatorio, R.; de Candia, M.; Cellamare, S.; Voskressensky, L.G.; et al. A New Class of 1-Aryl-5,6-dihydropyrrolo[2,1-a]isoquinoline Derivatives as Reversers of P-Glycoprotein-Mediated Multidrug Resistance in Tumor Cells. *ChemMedChem* **2018**, *13*, 1588–1596.
48. Gurunathan, S.; Han, J.W.; Eppakayala, V.; Jeyaraj, M.; Kim, J.-H. Cytotoxicity of Biologically Synthesized Silver Nanoparticles in MDA-MB-231 Human Breast Cancer Cells. *Biomed. Res. Int.* **2013**, *2013*, 535796.
49. Bashi, M.; Madanchi, H.; Yousefi, B. Investigation of cytotoxic effect and action mechanism of a synthetic peptide derivative of rabbit cathelicidin against MDA-MB-231 breast cancer cell line. *Sci. Rep.* **2024**, *14*, 13497.
50. Zheng, M.; Priebe, W.; Walch, E.T.; Roth, K.G.; Han, M.; Tang, C.-H.; Lee, S.; Poindexter, N.J.; Fokt, I.; Grimm, E.A. WP760, a melanoma selective drug. *Cancer Chemother. Pharmacol.* **2007**, *60*, 625–633.
51. Carrasquel-Ursulaez, W.; Reeves, R.D.; Dehghany, M.; Jones, C.; Schomaker, J.M.; Chanda, B. Re-evaluation of the mechanism of cytotoxicity of dialkylated lariat ether compounds. *RSC Adv.* **2020**, *10*, 40391–40394.
52. Schneider, T.; Brüssow, N.; Yuvanc, A.; Budisa, N. Synthesis of New Aza- and Thia-Crown Ether Based Amino Acids. *ChemistrySelect* **2020**, *5*, 2854–2857. [CrossRef]
53. Awasthi, A.; Kumar, N.; Mishra, A.; Ravi, R.; Dalal, A.; Shankar, S.; Chandra, R. Noscapine–Amino Acid Conjugates Suppress the Progression of Cancer Cells. *ACS Pharmacol. Transl. Sci.* **2022**, *5*, 1292–1304. [PubMed]
54. Maeng, H.-J.; Kim, E.-S.; Chough, C.; Joung, M.; Lim, J.W.; Shim, C.-K.; Shim, W.-S. Addition of amino acid moieties to lapatinib increases the anti-cancer effect via amino acid transporters. *Biopharm. Drug Dispos.* **2014**, *35*, 60–69.
55. Heh, E.; Allen, J.; Ramirez, F.; Lovasz, D.; Fernandez, L.; Hogg, T.; Riva, H.; Holland, N.; Chacon, J. Peptide Drug Conjugates and Their Role in Cancer Therapy. *Int. J. Mol. Sci.* **2023**, *24*, 829. [CrossRef]
56. Hou, L.; Hou, Y.; Liang, Y.; Chen, B.; Zhang, X.; Wang, Y.; Zhou, K.; Zhong, T.; Long, B.; Pang, W.; et al. Anti-tumor effects of P-LPK-CPT, a peptide-camptothecin conjugate, in colorectal cancer. *Commun. Biol.* **2022**, *5*, 1248.
57. Dean, T.T.; Jelú-Reyes, J.; Allen, A.C.; Moore, T.W. Peptide–Drug Conjugates: An Emerging Direction for the Next Generation of Peptide Therapeutics. *J. Med. Chem.* **2024**, *67*, 1641–1661. [PubMed]
58. Wang, M.; Rakesh, K.P.; Leng, J.; Fang, W.-Y.; Ravindar, L.; Channe Gowda, D.; Qin, H.-L. Amino acids/peptides conjugated heterocycles: A tool for the recent development of novel therapeutic agents. *Bioorg. Chem.* **2018**, *76*, 113–129. [PubMed]
59. Vadevoo, S.M.P.; Gurung, S.; Lee, H.-S.; Gunassekaran, G.R.; Lee, S.-M.; Yoon, J.-W.; Lee, Y.-K.; Lee, B. Peptides as multifunctional players in cancer therapy. *Exp. Mol. Med.* **2023**, *55*, 1099–1109.
60. Hoppenz, P.; Els-Heindl, S.; Beck-Sickinger, A.G. Peptide-Drug Conjugates and Their Targets in Advanced Cancer Therapies. *Front. Chem.* **2020**, *8*, 571.
61. Riss, T.; Niles, A.; Moravec, R.; Karassina, N.; Vidugiriene, J. *Cytotoxicity Assays: In Vitro Methods to Measure Dead Cells*; Markossian, S., Grossman, A., Arkin, M., Auld, D., Austin, C., Baell, J., Brimacombe, K., Chung, T.D.Y., Coussens, N.P., Dahlin, J.L., et al., Eds.; Bethesda: Rockville, Maryland, 2004.

62. Lamponi, S. Preliminary In Vitro Cytotoxicity, Mutagenicity and Antitumoral Activity Evaluation of Graphene Flake and Aqueous Graphene Paste. *Life* **2022**, *12*, 242. [CrossRef]
63. Ross, A.; Willson, V.L. *One-Way Anova BT—Basic and Advanced Statistical Tests: Writing Results Sections and Creating Tables and Figures*; Ross, A., Willson, V.L., Eds.; SensePublishers: Rotterdam, The Netherlands, 2017; pp. 21–24. ISBN 978-94-6351-086-8.

OTHER PUBLICATIONS

1. Simone Pepi, Marco Paolino, Mario Saletti, Jacopo Venditti, Luigi Talarico, Marco Andreassi, Germano Giuliani, Gianfranco Caselli, Roberto Artusi, Andrea Cappelli, Gemma Leone, Agnese Magnani, Lucio Rovati. Ferulated Poly(vinyl alcohol) based hydrogels. *Heliyon*, **2023**, *e22330*.
2. Francesca Terracina, Mario Saletti, Marco Paolino, Jacopo Venditti, Germano Giuliani, Claudia Bonechi, Mariano Licciardi, Andrea Cappelli. Cross-Linked Hyaluronan Derivatives in the Delivery of Phycocyanin. *Gels*, **2024**, *91.*
3. Marco Paolino, Mario Saletti, Jacopo Venditti, Federica Castriconi, Germano Giuliani, Samuele Maramai, Alessandra Toti, Carla Ghelardini, Rosanna Matucci, Narcy Alcazar Villalobos, Maurizio Anzini, Andrea Cappelli. Use of imidazo[1,5-α]quinoline scaffold as the pharmacophore in the design of bivalent ligands of central benzodiazepine receptors. *Bioorg. Med. Chem.*, **2025**, *118006*.
4. Mario Saletti, Simone Pepi, Marco Paolino, Jacopo Venditti, Germano Giuliani, Claudia Bonechi, Gemma Leone, Agnese Magnani, Claudio Rossi, Andrea Cappelli. Crosslinking by Click Chemistry of Hyaluronan Graft Copolymers Involving Resorcinol-Based Cinnamate Derivatives Leading to Gel-like Materials. *Gels*, **2024**, 10, *751*.
5. Mario Saletti, Marco Paolino, Jacopo Venditti, Germano Giuliani, Antonietta Rossi, Danilo D'Avino, Sara Perna, Ina Varfaj, Roccaldo Sardella, Antonio Macchiarulo, Samuele Maramai, Stefania Lamponi, Andrea Cappelli, Maurizio Anzini. Design, Synthesis, and Biological Characterization of Macromolecular Ester Prodrugs of a Selective Cyclooxygenase-2 Inhibitor. *ChemMedChem*, **2025**, *e202500691*.
6. Fabrizia Fabrizi de Biani, Maddalena Corsini, Annalisa Reale, Marco Paolino, Jacopo Venditti, Mario Saletti, Germano Giuliani, Claudio Bonechi, Alessandro Doanti, Marco Consumi, Claudio Rossi, Chiara Botta, Andrea Cappelli. Oxidative Dimerization of Thiophene-Substituted Indenone Derivatives. *Chemistry – An Asian Journal*, **2026**, *21:e70630*.